



UNIVERSITI PUTRA MALAYSIA

**SYNTHESIS AND CHARACTERIZATION OF NEW
TETRAETHYLAMMONIUM-BASED CHIRAL IONIC LIQUIDS FOR
BIOCATALYSIS APPLICATION**

**KHAIRULAZHAR BIN JUMBRI
FS 2009 43**



Abstract of thesis presented to the Senate of Universiti Putra Malaysia in fulfilment of the requirement for the Degree of Master of Science

**SYNTHESIS AND CHARACTERIZATION OF NEW
TETRAETHYLAMMONIUM-BASED CHIRAL IONIC LIQUIDS FOR
BIOCATALYSIS APPLICATION**

By

KHAIRULAZHAR BIN JUMBRI

November 2009

Chairman : Mohd Basyaruddin Abdul Rahman, PhD

Faculty : Science

Chiral ionic liquids (CILs), molten salts at temperature below than 100 °C are unique liquids having different characteristics from ordinary liquids. Since these CILs are prepared by coupling various organic ions, there are many chances to create novel functionalities by changing structure of components ions. These liquids combine with their ability to perform a task with their “green” character, which makes them environmental friendly solvents. Lately, researchers focused to synthesize CILs for their potential applications in many reactions such as chiral discrimination.

In this study, eleven new CILs derived from chiral amino acids and plant acid have been synthesized and characterized. They are tetraethylammonium L-serinate, tetraethylammonium L-prolinate, tetraethylammonium L-threoninate, tetraethylammonium L-isoleucinate, tetraethylammonium L-asparaginate, tetraethylammonium L-glutamate, tetraethylammonium L-glutamate, tetraethylammonium L-methioninate, tetraethylammonium L-histidinate, tetraethylammonium L-lysinate and



tetraethylammonium L-malate. Meanwhile, one compound derived from chiral plant acids (tetraethylammonium L-tartrate) can't be classified as ILs due to high melting point above 100 °C.

All of these salts were prepared using simple neutralization reaction which gave good overall yield (>85 % yields for CILs derived from amino acids and 98 % for tetraethylammonium L-malate) at room temperature. ¹H NMR and elemental analysis were carried out to identify the molecular structure and purity of CILs produced. Colour of each CILs's produced depending on the anions used. All CILs were hygroscopic and easily dissolved in water and polar organic solvents. The new CILs synthesized from plant acid have higher melting point (T_m 87.7 ± 0.4 °C) compared to CILs derived from amino acids (T_m 54.3 ± 1.0 °C for tetraethylammonium L-histidinate and T_m 58.7 ± 1.0 °C for tetraethylammonium L-asparaginate).

The thermal properties were studied by using differential scanning calorimetry (DSC) and thermogravimetric analysis (TGA). DSC analysis showed that CILs in a liquid form had no melting point (T_m) and glass transition temperature (T_g). Meanwhile, in the TGA study, it was found that CILs derived from amino acids have a slightly low decomposition temperature (T_{onset} 168 to 210 °C) compared to tetraethylammonium L-malate (T_{onset} 210 °C), but all CILs were stable up to 160 °C.

Single crystal X-ray diffraction was used to solve the crystal structures of tetraethylammonium L-malate and tetraethylammonium L-tartrate. The crystal systems for both compounds were monoclinic. Analysis also carried out in order to reveal an extensive series of hydrogen bonds between H-atoms on the cation and the anion meanwhile each CILs' optical polarity was measured using polarimeter. Their viscosity



and ionic conductivity for CILs in a liquid form were also determined and observed by using viscometer and conductivity meter. The strong correlation between viscosity and ionic conductivity was observed.

In biocatalysis application, chiral ionic liquid-coated enzyme (CILCE) was employed in the esterification of oleyl alcohol with various fatty acids. CILCE was prepared by simple method involving coating of *Candida rugosa* lipase with tetraethylammonium L-asparaginate and was found to give a better percentage of conversion of ester (60 – 81 %) compared to native enzyme (36 – 70 %) for all fatty acids from short, medium and long alkyl chains.

Abstrak tesis yang dikemukakan kepada Senat Universiti Putra Malaysia sebagai memenuhi keperluan Ijazah Master Sains

**SINTESIS DAN PENCIRIAN CECAIR IONIK KIRAL YANG BAHARU
BERASASKAN TETRAETILAMONIUM UNTUK APLIKASI BIOMANGKIN**

Oleh

KHAIRULAZHAR BIN JUMBRI

November 2009

Pengerusi : Mohd Basyaruddin Abdul Rahman, Ph.D

Fakulti : Sains

Cecair ionik kiral (CILs), garam lebur pada suhu di bawah 100 °C adalah cecair unik yang mempunyai ciri yang berbeza daripada cecair biasa. Disebabkan cecair ini disediakan melalui pepadanan pelbagai ion organik, terdapat banyak kemungkinan untuk mencipta fungsi CILs yang baharu dengan menukar struktur komponen ion. Cecair ini digabungkan dengan kemampuannya untuk melakukan tugas dengan ciri “hijaunya” yang mana membuatkan cecair ini pelarut yang mesra alam. Kebelakangan ini, ramai penyelidik menumpukan perhatian terhadap sintesis CILs untuk melihat potensi kegunaannya di dalam banyak tindak balas seperti diskriminasi kiral.

Dalam kajian ini, sebelas cecair ionik kiral baharu yang berasal dari kiral asid amino dan asid tumbuhan telah disintesis dan dicirikan. Sebatian tersebut adalah tetraetilamonium L-serinat, tetraetilamonium L-prolinat, tetraetilamonium L-threoninat, tetraetilamonium L-iso-leucinat, tetraetilamonium L-sasparaginat, tetraetilamonium L-glutaminat, tetraetilamonium L-glutamat, tetraetilamonium L-methinonat, tetraetilamonium L-histidinat, tetraetilamonium L-lysinat dan tetraetilamonium L-malat. Sementara itu, satu



sebatian lain yang disintesis daripada kiral asid tumbuhan (tetraetilamonium L-tartarate) tidak diklasifikasikan sebagai cecair ionic kiral kerana mempunyai takat lebur melebihi 100 °C.

Kesemua garam CILs ini telah disediakan menggunakan tindak balas penulenan mudah yang memberikan hasil keseluruhan yang baik (>85 % hasil untuk CILs yang berasal daripada kiral asid amino dan 98 % hasil untuk tetraetilamonium L-malat) pada suhu bilik. ¹H resonan magnetic nuklear (RMN) dan analisis elemen dilakukan untuk mengenalpasti struktur molekul dan ketulenan CILs yang dihasilkan. Warna untuk setiap CILs yang terhasil adalah bergantung kepada anion yang digunakan. Semua CILs didapati bersifat higroskopik dan mudah larut di dalam air dan pelarut organik polar. Satu CILs baharu yang disintesis daripada kiral asid tumbuhan mempunyai takat lebur yang tinggi (T_m 87.7 ± 0.4 °C) berbanding CILs yang berasal daripada kiral asid amino (T_m 54.3 ± 1.0 °C untuk tetraetilamonium L-histidinat dan T_m 58.7 ± 1.0 °C untuk tetraetilamonium L-asparaginat).

Sifat termal telah dipelajari menggunakan kalorimeter pengimbasan kebezaan (DSC) dan analisis thermogravimetrik (TGA). Analisis DSC menunjukkan CILs dalam bentuk cecair tidak mempunyai takat lebur (T_m) dan suhu peralihan gelas (T_g). Sementara itu, dalam kajian TGA, didapati bahawa CILs yang berasal daripada kiral asid amino mempunyai suhu penguraian yang sedikit rendah (T_{onset} 168 hingga 210 °C) berbanding tetraethylammonium L-malate (T_{onset} 210 °C), tetapi kesemua CILs stabil sehingga suhu 160 °C.

Penyerakkan sinar-X kristal tunggal telah digunakan untuk membuktikan struktur sebatian tetraetilammonium L-malat dan tetraetilammonium L-tartarat. Didapati bahawa sistem kristal bagi kedua-dua sebatian ini adalah monoklinik. Analisis juga telah dilakukan untuk

menunjukkan rangkaian ikatan hidrogen di antara atom hidrogen kation dan anion manakala polariti optik bagi setiap CILs ditentukan dengan menggunakan polarimeter. Kepekatan dan konduktiviti ionik untuk CILs dalam bentuk cecair juga ditentukan dan diamati menggunakan alat kepekatan dan meter konduktiviti. Perhubungan yang kuat di antara kepekatan dan konduktiviti ionik telah diamati.

Dalam aplikasi biomangkin, enzim bersalut cecair ionic kiral (CILCE) telah digunakan dalam tindakbalas pengeksteran olil alkohol dengan pelbagai asid lemak. CILCE telah disediakan melalui kaedah yang mudah dengan menyalut lipase daripada *Candida rugosa* dengan tetraetilamonium L-asparaginat dan penggunaan CILCE telah dikaji dan memberikan peratus penukaran ester yang lebih baik (60 – 81 %) berbanding enzim asli (36 – 70 %) bagi semua asid lemak daripada asid lemak berantai pendek, sederhana dan panjang.

ACKNOWLEDGEMENTS

Alhamdulillah, praise to ALLAH s.w.t., for giving me the strength to endure all challenges and complete this research. Firstly, I would like to thank my supervisor, Prof. Dr. Mohd Basyaruddin Abdul Rahman, who gave me the opportunity to conduct this research, for the help, advice and directed me through nearly two years of thesis work. His supportive discussions and enthusiasm for chemistry always replenished my energy to work. I'm also indebted to my co-supervisor, Prof. Dr. Mahiran Basri and Dr. Kamaliah Sirat for their invaluable guidance, encouragement and criticism, which kept me in a right track. Without these people, this thesis would not have been possible.

To my research group, Enzyme and Microbial Technology Research Group UPM, especially thanks to Prof. Dato Dr. Abu Bakar Salleh and Prof. Dr. Raja Noor Zaliha Raja Abd Rahman for their valuable advice and suggestions during weekly meeting. I would like also thanks to Dr. Emilia Abdul Malek and Dr. Bimo Ario Tejo for their opinion, support and discussion during completion of this thesis.

I want to thanks all of my lab mates in lab 401 especially to Kak Emmy, Kak Nora, Casey, Salwa, Naz, Intan, Azlan, Alif, Fairuz, Rizal, Asrul, Peter, Zati and Naimah that participated in their own way during my research. Without all of you, I would not have made it this far.

To all my housemates, thank you for the support during my thesis period.



Special thank to my family, especially my mom and dad, there is no way I can adequately express my gratitude in words, for the support, love and encouragement you have shown me throughout the years and for many sacrifices that you have made for me. Last but not least, thank to Ministry of Science, Technology and Innovation Malaysia (MOSTI) for scholarship *National Science Fellowship* (NSF) and Universiti Putra Malaysia for financial support and facilities.



I certify that a Thesis Examination Committee has met on 17th November 2009 to conduct the final examination of Khairulazhar Jumbri on his thesis entitled “Synthesis and Characterization of New Chiral Ionic Liquids for Biocatalysis Application” in accordance with the Universities and University College Act 1971 and the Constitution of the Universiti Putra Malaysia [P.U.(A) 106] 15 March 1998. The Committee recommends that the student be awarded the Master of Science Degree

Members of the Thesis Examination Committee were as follows:

Irmawati Ramli, PhD

Associate Professor
Faculty of Science
Universiti Putra Malaysia
(Chairman)

Nor Azah Yusuf, PhD

Associate Professor
Faculty of Science
Universiti Putra Malaysia
(Internal Examiner)

Tan Yeng Peng, PhD

Associate Professor
Faculty of Science
Universiti Putra Malaysia
(Internal Examiner)

Yatimah Alias, PhD

Associate Professor
Department of Chemistry
Faculty of Science
Universiti Malaya
Malaysia
(External Examiner)

BUJANG KIM HUAT, Ph.D

Professor/Deputy Dean
School of Graduate Studies
Universiti Putra Malaysia

Date: 12 February 2010



The thesis submitted to the Senate of Universiti Putra Malaysia has been accepted as fulfilment of the requirement for the degree of Master of Science. The members of the Supervisory Committee were as follows:

Mohd. Basyaruddin Abdul Rahman, PhD

Professor
Faculty of Science
Universiti Putra Malaysia
(Chairman)

Mahiran Basri, PhD

Professor
Faculty of Science
Universiti Putra Malaysia
(Member)

Kamaliah Sirat, PhD

Lecturer
Faculty of Science
Universiti Putra Malaysia
(Member)

HASANAH MOHD GHAZALI, PhD

Professor and Dean
School of Graduate Studies
Universiti Putra Malaysia

Date: 17 March 2010



DECLARATION

I hereby declare that the thesis is my original work except for quotations and citations which have been acknowledged. I also declare that it has not been previously, and is not concurrently, submitted for any other degree at Universiti Putra Malaysia or at any other institutions.

KHAIRULAZHAR JUMBRI

Date: 18 January 2010



TABLE OF CONTENTS

ABSTRACT	Page
	i
ABSTRAK	iv
ACKNOWLEDGEMENTS	vii
APPROVAL	ix,x
DECLARATION	xi
LIST OF TABLES	xv
LIST OF FIGURES	xvi
LIST OF SCHEMES	xvii
LIST OF ABBREVIATIONS	xviii
OVERVIEW OF THE CHEMICAL STRUCTURES	xx

CHAPTER	Page
1 INTRODUCTION	1
1.1 Objectives of the Research	3
2 LITERATURE REVIEW	4
2.1 History of Ionic Liquids (ILs)	4
2.2 Introduction to ILs	6
2.3 Physico-chemical Properties of ILs	7
2.3.1 Wide Liquid Range and Thermal Stability	8
2.3.2 Melting Points	8
2.3.3 Viscosity of ILs	10
2.3.4 Polarity	11
2.3.5 Water Miscibility	12
2.3.6 Density and Surface Tension	12
2.4 Preparation of ILs	13
2.5 Purification and Impurities in ILs	14
2.6 Chiral Ionic Liquids (CILs)	16
2.7 Previous Related Chiral Ionic Liquids (CILs)	18
2.8 Application of ILs	21
2.8.1 Ionic Liquids (ILs) as Solvents for Extraction	21
2.8.2 Biocatalytic Reaction in ILs	22
2.8.3 Lipases in ILs	23
2.9 Ionic Liquid-Coated Enzyme (ILCE)	25



3	MATERIALS AND METHODS	27
3.1	Materials	27
3.1.1	Solvents	27
3.1.2	Chemicals	27
3.1.3	Enzyme	28
3.1.4	Equipments/Instruments	28
3.2	Methods	30
3.2.1	Preparation of CILs Derived from Amino Acids	30
3.2.2	Preparation of CILs Derived from Plant Acids	31
3.2.3	Crystallization of Solid CILs	32
3.2.4	Preparation of Chiral Ionic Liquid-Coated Enzyme (CILCE)	32
3.2.5	Esterification Reaction of Oleyl Alcohol with Various Fatty Acids	33
3.3	Analytical Methods	35
3.3.1	Nuclear Magnetic Resonance (NMR) Spectroscopy	35
3.3.2	CHNS/O-Element Analysis	35
3.3.3	Differential Scanning Calorimetry (DSC)	36
3.3.4	Thermogravimetric Analysis (TGA)	36
3.3.5	Single X-ray Crystallography	37
3.3.6	Optical Rotation	38
3.3.7	Viscosity Determination	39
3.3.8	Ionic Conductivity	39
4	RESULTS AND DISCUSSIONS	40
4.1	Nuclear Magnetic Resonance (NMR) spectrum of CILs	40
4.1.1	Tetraethylammonium L-serinate	41
4.1.2	Tetraethylammonium L-prolinate	41
4.1.3	Tetraethylammonium L-threoninate	42
4.1.4	Tetraethylammonium L-isoleucinate	42
4.1.5	Tetraethylammonium L-asparaginate	43
4.1.6	Tetraethylammonium L-glutamate	43
4.1.7	Tetraethylammonium L-glutamate	44
4.1.8	Tetraethylammonium L-methioninate	44
4.1.9	Tetraethylammonium L-histidinate	45
4.1.10	Tetraethylammonium L-lysinate	46
4.1.11	Tetraethylammonium L-tartrate	46
4.1.12	Tetraethylammonium L-malate	47



4.2	Elemental Analysis (CHNS/O)	48
4.3	Colour of CILs	50
4.4	Melting Temperature (T_m)	51
4.5	Solubility in Organic Solvents	53
4.6	Thermogravimetric Analysis (TGA)	55
4.7	Single Crystal X-ray Crystallography	63
4.7.1	Crystal Structure Tetraethylammonium L-tartrate ([N ₂₂₂₂][tar])	63
4.7.2	Crystal Structure Tetraethylammonium L-malate ([N ₂₂₂₂][mal])	68
4.8	Optical Rotation, ($[\alpha]_D^{25}$)	73
4.9	Viscosity and Ionic Conductivity	74
4.10	Application of CILs	80
4.10.1	Esterification of Oleyl Alcohol with Various Fatty Acids	80
5	CONCLUSIONS	84
5.1	Recommendation for Further Studies	87
	REFERENCES	88
	APPENDIX A	101
	APPENDIX B	102
	APPENDIX C	126
	APPENDIX D	132
	APPENDIX E	141
	LIST OF PUBLICATIONS	153
	BIODATA OF STUDENT	190



LIST OF TABLES

Table		Page
1	The effect of cation size on the melting point.	9
2	Effect of anion size on the melting point of [emim]X ILs.	10
3	Starting material and abbreviation names for CILs synthesized using neutralization method	31
4	Starting materials and ratios of oleyl alcohol with various fatty acids in esterification reaction.	34
5	Element analysis data for all CILs synthesized.	49
6	Physical properties, percentage yield (%), melting temperature (T_m) and solubility data of CILs.	50
7	The start temperature (T_{start}) and onset temperature (T_{onset}) for tetraethylammonium-based chiral ionic liquids.	55
8	Structure of 'R' amino acid, functional group present and T_{onset} for ten amino acids used in this work.	59
9	Crystal data and structure refinement for tetraethylammonium L-tartrate.	64
10	Hydrogen-bond geometry (\AA) for tetraethylammonium L-tartrate.	68
11	Crystallographic details of the presented crystal structures for tetraethylammonium L-malate.	69
12	Hydrogen-bond geometry (\AA) for tetraethylammonium L-malate.	72
13	Optical rotation value for starting acid and CILs ($[\alpha]_D^{25}$) at 25 °C.	73
14	Molecular weight (Mw), viscosity (cP) and ionic conductivity (mS/cm) data for CILs produced at 25 °C.	75



LIST OF FIGURES

Figure		Page
1	Examples of some typical cations and anions of ILs.	7
2	Different anions responsible for water immiscibility and miscibility of ILs.	12
3	Structure of chiral ionic liquids (CILs)	18
4	The structure of tetraethylammonium cation (a) and imidazolium cation (b).	53
5	The structure of L(-)-malic acid contained two carboxylic acids moiety and one hydroxyl group	57
6	Basic structure of amino acids.	59
7	Structure of L-glutamic acid (glu) (a), L-glutamine (gln) (b) and L-asparagine (asn) (c).	60
8	Structure of L-serine (ser) (a) and L-threonine (thr) (b).	61
9	Structure of L-lysine (lys) (a) and L-methionine (met) (b).	62
10	Structure of L-histidine (his) (a), L-proline (pro) (b) and L-isoleucine (ile) (c).	63
11	Molecular structure of tetraethylammonium L-tartrate determined by single crystal X-ray diffraction. Hydrogen bonds between anion cation are shown as dashed lines.	66
12	The crystal packing for tetraethylammonium L-tartrate, view down the c-axis. Hydrogen bonds are shown as dashed lines.	67
13	The molecular structure of tetraethylammonium L-malate with atoms label and 40 % probability ellipsoids for non-H atoms. The hydrogen atoms of the cations were omitted for clarity. Intramolecular interactions are shown as dashed lines.	70
14	The crystal packing for tetraethylammonium L-malate, view down the c-axis showing infinite 1-D chain along the a- and b-axes of the unit cell. Intermolecular interactions are shown as dashed lines.	71
15	Symmetry properties of tetraethylammonium used to synthesize CILs.	76
16	Relationship between ionic conductivity and viscosity at 25 °C.	78
17	Percentage of conversion of various esters in hexane. Reaction was performed at 40 °C for 1 hour.	81



LIST OF SCHEMES

Scheme		Page
1	Platinum catalyzed hydroformylation of ethylene.	5
2	Dimerization of propene in weakly acidic chloroaluminate ILs.	5
3	Example of neutralization reaction method involved -onium hydroxide with free acids.	14
4	Transtesterification reaction of N-acetyl-1-phenylalanine ethyl ester and Nacetyl-1-tryosine ethyl ester into corresponding propyl esters.	23
5	1-Methoxyethyl-3-methylimidazolium ([moemim][BF ₄]) dissolves ~5 mg/ml glucose at 55 °C yield 99 %; selectivity: 93 % 6-O-acetyl D-glucose.	25
6	General route to synthesis of tetraethylammonium-based CILs derived from amino acids.	30
7	General route to synthesis of tetraethylammonium-based CILs derived from plant acids.	32
8	Deuterium exchange between D ₂ O solvent and –OH hydrogen (a) and amino hydrogen (b).	40
9	Deprotonation of carboxylic acid residue by hydroxide ion to form carboxylate ion and water as by-product.	54
10	Schematic presentation of the Hoffman degradation reaction.	56



LIST OF ABBREVIATIONS

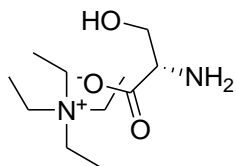
ILs	ionic liquids
RTILs	room temperature ionic liquids
CILs	chiral ionic liquids
MeOH	methanol
T_m	melting temperature
T_g	glass transition
T_{start}	start temperature
T_{onset}	onset temperature
EtOH	ethanol
dd	doublet of doublets
t	triplet
s	singlet
q	quartet
m	multiplet
asn	asparagine
gln	glutamine
glu	glutamic acid
his	histidine
ile	isoleucine
lys	lysine
mal	malic acid
met	methionine
pro	proline
ser	serine
thr	threonine
$[BF_4]^-$	tetrafluoroborate
$[PF_6]^-$	hexafluorophosphate
$[Tf_2N]^-$	bis(trifluoromethylsulfonyl)imide



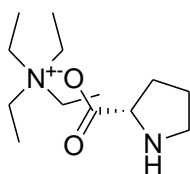
[N ₂₂₂₂]	tetraethylammonium
VOCs	volatile organic compounds
VOSs	volatile organic solvents
CILCE	chiral ionic liquid-coated enzyme
ILCE	ionic liquid-coated enzyme
CRL	<i>Candida rugosa</i> lipase
CHNS/O	carbon hydrogen nitrogen sulphur/oxygen
DSC	Differential Scanning Calorimetry
TGA	Thermogravimetric Analysis

OVERVIEW OF THE CHEMICAL STRUCTURES

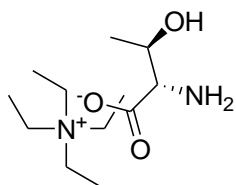
1. [N₂₂₂₂][ser]: tetraethylammonium L-serinate



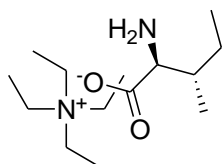
2. [N₂₂₂₂][pro]: tetraethylammonium L-prolinate



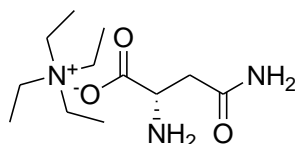
3. [N₂₂₂₂][thr]: tetraethylammonium L-threoninate



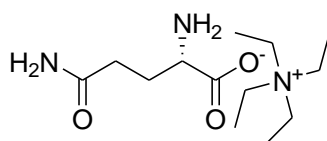
4. [N₂₂₂₂][ile]: tetraethylammonium L-isoleucinate



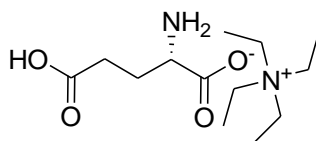
5. [N₂₂₂₂][asn]: tetraethylammonium L-asparaginate



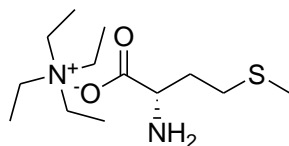
6. [N₂₂₂₂][gln]: tetraethylammonium L-glutamate



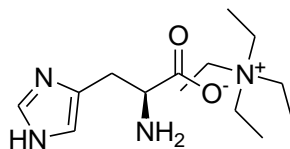
7. [N₂₂₂₂][glu]: tetraethylammonium L-glutamate



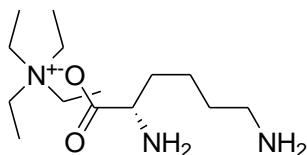
8. [N₂₂₂₂][met]: tetraethylammonium L-methioninate



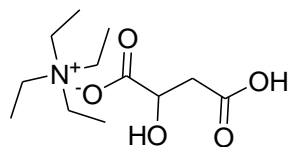
9. [N₂₂₂₂][his]: tetraethylammonium L-histidinate



10. [N₂₂₂₂][lys]: tetraethylammonium L-lysinate



11. [N₂₂₂₂][mal]: tetraethylammonium L-malate



CHAPTER 1

INTRODUCTION

Lately, ionic liquids (ILs) are attracting a number of overwhelmed science and industrial communities as a reaction media, extraction solvents, electrolytes and in life sciences (Kagimoto *et al.*, 2007). These liquids that contain ions show good and tunable solubility properties with negligible vapor pressure and excellent thermal stability have rapidly found as valuable substitutes for many volatile solvents (Welton, 1999 and van Rantwijk *et al.*, 2003).

ILs are a new class of solvents that currently receiving much attention for their wide range of applications especially in catalysis and biocatalysis, dissolving polar to non-polar substrates and almost anything including coal, plastics, metal and even rock (Obliosca *et al.*, 2007). They are not as flammable as the volatile organic solvents (VOSs) therefore, making process safety and environmental concerns less of an issue. The thermodynamics and kinetics of reactions carried out in ILs can possibly varied to those in traditional VOSs and therefore creating great interests amongst chemists in their potential as solvents, co-solvents and catalysts.

A wide range of ILs consisted of inorganic/organic cations and anions have been successfully synthesized. In view of the emerging importance of ILs as reaction media in organic synthesis, researchers have turn their attraction on the synthesis of chiral ionic liquids (CILs) for their particularly potential applications to chiral discrimination, including asymmetric synthesis and optical resolution of racemates (Wang *et al.*, 2005). Several examples of CILs were mentioned in the literature and partial information can be



found in some reviews reported by Baudequin *et al.* (2005) and Tran *et al.* (2006). Due to their ease of synthesis and their particular chiral properties, these new CILs should play a central role in enantioselective research and expand the scope of chiral solvents. A significant transfer of chirality in these solvents can be expected due to their high degree of organization.

The specific properties of CILs should perform the classical chiral solvents for asymmetric induction. Studies about the application of CILs in asymmetric synthesis are not only an opportunity but also a challenge for researchers. It is interesting, meaningful and necessary to synthesize different kinds of CILs from different starting materials, especially from the chiral pool. Good chemical and configurational stability, are some of the most important criteria for synthesis of CILs and necessary properties for their application to chiral discrimination.

Another great property of ILs is their insolubility in most organic solvents which led us to envisage that they might be suitable as coating materials for immobilizing enzymes or cells. Interestingly, van Rantwijk *et al.* (2003) observed that ILs can enhance the selectivity of an enzyme. It was also demonstrated that they are useful as a media for the enzymatic reaction of polar substrates, which are difficult to dissolve in conventional organic solvents (Park and Kazlauskas, 2003). The very first ionic liquid coated enzyme (IL-CE) was reported by Lee and Kim (2002), which is easily prepared and exhibits markedly enhanced enantioselectivity and stability.

The aim of the study was to synthesis and characterizes a series of new CILs, and used the suitable CILs as biocatalysts in esterification reactions. To do this, the selected CILs, tetraethylammonium L-asparaginate was coated onto *Candida rugosa* lipase to form chiral



ionic liquid-coated enzyme (CILCE). CILCE was later tested for esterification reactions of oleyl alcohol with various fatty acids in order to figure out their amazing properties.

1.1 Objectives of the Research

This research embarks on the following objectives:

- 1) To synthesize twelve new tetraethylammonium-based chiral ionic liquids (CILs) derived from amino acids and chiral plant acids.
- 2) To characterize the physico-chemical properties of CILs.
- 3) To identify the suitable CILs for coating with *Candida rugosa* lipase (CRL) to form chiral ionic liquid-coated enzyme (CILCE).
- 4) To determine the enzymatic activity of CILCE in esterification reactions.



CHAPTER 2

LITERATURE REVIEW

2.1 History of Ionic Liquids (ILs)

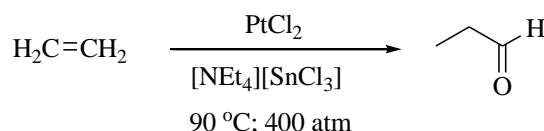
ILs may be considered as a new class of remarkable solvents, but they have been around for many years dating back to the 1900s (Seddon, 2002). There has been an increased interest in them due to their capability of being used as reaction solvents. The first recorded ILs, ethylammonium nitrate $[\text{EtNH}_3][\text{NO}_3]$, is a liquid form at room temperature. It was developed by the military for use in liquid propellants. It is now widely used in the structuring of surfactants and the study of protein folding (Summers and Flowers II, 2000).

One of the first alkyimidazolium room temperature ionic liquids (RTILs), 1-ethyl-3-methylimidazolium tetrachloroaluminate, which was obtained through the mixing of 1-ethyl-3-methylimidazolium chloride with aluminium trichloride, was reported by Wilkes *et al.* (1982). This chloroaluminate ILs act as both catalyst and solvent in many processes (Boon *et al.*, 1986). Chemical reactions in the chloroaluminate ILs, including Friedel-Crafts (Boon *et al.*, 1986) and oligomerization reactions (Ellis *et al.*, 1999) have been tested successfully. However they suffered a major drawback. They found to be moisture-sensitive and reactive towards various organic compounds, consequently limiting their range of applications (Brauer *et al.*, 2001).

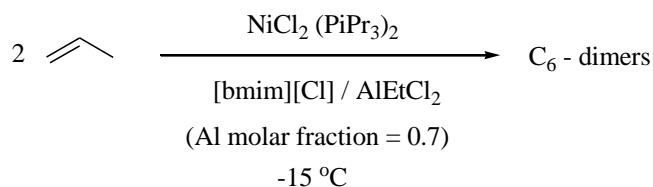


The air and water-stable ILs based on dialkylimidazolium cations were discovered in 1992 by combining the cation with water-stable anions (Wilkes and Zaworotko, 1992). These ILs were based on anions such as halide, tetrafluoroborate, hexafluorophosphate, nitrate, sulfate and trifluoromethanesulfonate. The tetrafluoroborate and hexafluorophosphate ILs are the common “workhorses” for transition metal catalysis using ILs. The hexafluorophosphate ILs are, however, less stable to moisture and are known to hydrolyze in the presence of water and heat to form HF and/or phosphoric acid.

ILs were used for the first time as a solvent for homogeneous transition metal catalysis in which, platinum catalyzed hydroformylation of ethylene was performed in tetraethylammonium trichlorostannate (m.p. 78 °C) (Scheme 1) (Parshall, 1972). ILs were later used as solvents for homogeneous metal catalysts by Chauvin *et al.* (1990) and Carlin and Wilkes, (1990). The dimerization of propene in weakly acidic chloroaluminate ILs (Scheme 2) was investigated by Chauvin *et al.* (1990).



Scheme 1: Platinum catalyzed hydroformylation of ethylene.



Scheme 2: Dimerization of propene in weakly acidic chloroaluminate ILs.

2.2 Introduction to ILs

Molten salts at ambient temperature that contain only ions without the presence of solvent are referred to as “Ionic liquids” (Wilkes and Zaworotko, 1992, Wassercheid and Welton, 2003 and Ohno, 2005). ILs possess different properties from molecular liquids, making them promising substances for use in a variety of fields. Commonly, ILs are divided into two main categories:

1. Binary ILs (also referred to first-generation ILs) consisting of several different ionic species in equilibrium. For example mixtures of aluminium (III) chloride and 1,3-dialkylimidazolium chlorides (Sun *et al.*, 1988).
2. Simple ILs (also referred to second-generation ILs) consists of a single anion and a single cation (Wilkes and Zaworotko, 1992).

Some typical structures of ILs are shown in Figure 1. Heteroatom cations such as alkylimidazolium, alkylpyridinium, alkylammonium and alkylphosphonium ions are the most widely used cations in the ILs family. The possible variability of the associated anions, in theory, possible to generate a large number of ILs possessing a wide range of physical characteristics. There are about one trillion (10^{18}) possible cation/anion combinations to produce RTILs (Holbrey and Seddon, 1999).



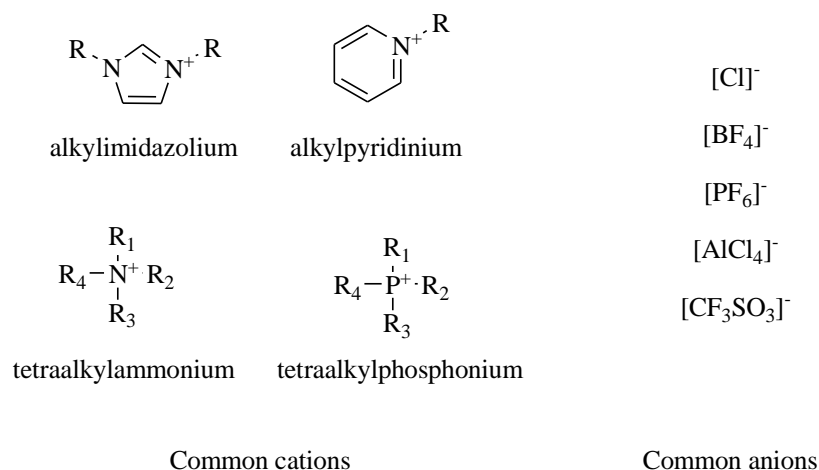


Figure 1: Examples of some typical cations and anions of ILs.

2.3 Physico-chemical Properties of ILs

ILs has been dubbed “designer solvents” because the properties of them that can be fine-tuned to favour certain needs of a respective reaction (Earle and Seddon, 2000). As a solvent, they can be designed to optimize a reaction with the control over both yield and selectivity (Earle *et al.*, 2004). Varying the cations or anions, or both, could alter the properties of the ILs such as melting point, solubility, acidity, density, viscosity, hydrophobicity and refractive index to fit the needs of a specific reaction. The unique properties of ILs are determined based on its structure and interactions between the ions present in ILs. The anions of ILs determine the chemical properties to a large extent (Tokuda *et al.*, 2005). The purity of ILs is an extremely important factor when measuring their physical properties (Seddon *et al.*, 2000).

2.3.1 Wide Liquid Range and Thermal Stability

An interesting feature of ILs that common molecular solvents do not possess is their exceptionally wide liquid range. For example, water has a liquid range of 100 °C (0 to 100 °C) and dichloromethane of 145 °C (-95 to 40 °C) at ambient pressure. In comparison, [bmim][BF₄] and [bmim][PF₆] has a liquids range of 400 °C. They also possess a high thermal stability, which is dependent on both the anion and cation (Fredlake *et al.*, 2004).

The upper limit of the liquid range normally signifies thermal decomposition rather than vaporization since ILs are non-volatile. The decomposition temperature of an ILs varies with the type of anions. For example, [emim][BF₄] has been reported to be stable to about 300 °C and [emim][N(SO₂CF₃)₂] is stable to more than 400 °C (Bonhôte *et al.*, 1996). The thermal stability of ILs therefore depends on the nucleophilicity of the anion. The weaker coordinating anions are more susceptible to high temperature decomposition (Ngo *et al.*, 2000).

2.3.2 Melting Points

Both the cation and anion affects the melting point of ILs. The main factors that influence the melting points are the charges, sizes, the distribution of charges on the ions, the symmetry of the ions, hydrogen bonding (H-bonding) ability and van der Waals interactions (Wasserscheid and Welton, 2003). Increasing the size of the anion or the cation results in a decrease in the melting point of ILs. Large cations tend to reduce the melting points of ILs. The cation symmetry is also important in determining the melting point. The more unsymmetrical the cation, the more difficult it is to have efficient ion-ion packing onto a solid thereby decreasing the melting point of ILs (Ajam, 2005). Additions

of other functionalities such as ether groups around the ions increases the melting points due to an increase in the number of interactions between the ions.

Furthermore, an increase in alkyl chain length on the imidazolium cation initially causes a decrease in melting point of ILs. Increasing the alkyl chain length beyond a certain point (*e.g.* 8-10 carbons for 1-alkyl-3-methylimidazolium cations), the melting point tends to increase due to an effect on the efficiency of ion packing (Ajam, 2005). For example, the effect of changes in the cation for different chloride salts is shown in Table 1. Alkaline metal salts are known to have high melting points and these melting points are reduced to temperatures at or below the room temperature by replacing the simple inorganic cations with unsymmetrical organic cations (Lide, 1992).

Table 1: The effect of cation size on the melting point

Cation	Melting Point (°C)	Reference
NaCl	803	(Lide, 1992)
KCl	772	(Lide, 1992)
[mmim][Cl]	125	(Wasserscheid and Keim, 2000)
[emim][Cl]	87	(Wasserscheid and Keim, 2000)
[bmim][Cl]	65	(Wasserscheid and Keim, 2000)

Similarly, an increase in anions size reduces the melting point of ILs. However, not all ILs follow this rule of decreasing melting point with increasing anion size (example [emim][PF₆]). The effect of anion size on the melting point of [emim][X] ILs is showed in Table 2.



Table 2: Effect of anion size on the melting point of [emim]X ILs

Anion (X)	Melting Point (°C)	Reference
[Cl] ⁻	87	(Wasserscheid and Keim, 2000)
[BF ₄] ⁻	15	(Holbrey and Seddon, 1999)
[PF ₆] ⁻	62	(Fuller <i>et al.</i> , 1994)
[CF ₃ SO ₃] ⁻	-9	(Bonhôte <i>et al.</i> , 1996)
[N(SO ₂ CF ₃) ₂] ⁻	-3	(Bonhôte <i>et al.</i> , 1996)

2.3.3 Viscosity of ILs

ILs are generally more viscous (comparable to the viscosities of oils) than most common molecular solvents, varying over a range of <10 to >1000 cP at room temperature. For example, water and ethylene glycol have viscosity values of 0.89 cP and 16.10 cP respectively. The viscosity of ILs is strongly dependent on the temperature, their tendency to form hydrogen bonds and the strength of their van der Waals interactions (Bonhôte *et al.*, 1996). An increase in the formation of hydrogen bonds between cation-anion resulted to a higher viscosity of ILs. The influence of H-bonding can be diminished by fluorinating the ILs (Pomaville and Poole, 1990). A stronger van der Waals interaction between ions also contributed to the increment in the viscosity. The purity of ILs is an important factor when determining accurate values for viscosity. Small amounts of impurities present in ILs have a dramatic effect on the viscosity. Water tends to decrease the viscosity of ILs while high chloride impurities increase their viscosity (Seddon *et al.*, 2000).

The viscosity also increases when using longer or fluorinated alkyl chains on the cations due to stronger van der Waals interactions for ILs with the same anion (Bonhôte *et al.*, 1996). Other than that, the more asymmetrical the cation, the lower viscosity of ILs (Jiang

et al., 2008). It has been shown that the viscosity of imidazolium-based ILs can be reduced by using highly branched and compact alkyl chains (Swartling *et al.*, 2000). As an example, phosphonium-based ILs tend to have higher viscosities than imidazolium-based ILs. Also, the addition of co-solvents to ILs can dramatically decrease the viscosity without changing the cations or anions (Fannin *et al.*, 1984). Higher temperatures will also result in a dramatic reduction in the viscosity of ILs (Liao and Hussey, 1996).

2.3.4 Polarity

ILs is considered to be highly polar due to their ionic character. ILs has a polarity that lies between those of water and chlorinated organic solvents (Wasserscheid and Welton, 2003). Due to the presence of the cation and the anion in ILs, there are most likely to be a much wider range of solvent-solute interactions than with conventional organic solvents. Different solvent-solute interactions in ILs using solvatochromic dyes such as Nile Red and Reichardt's dye have been reported (Aki *et al.*, 2001).

The results reported by Muldoon *et al.* (2001) indicated that the polarities of 1,3-dialkylimidazolium salts based on the $[\text{PF}_6]^-$, $[\text{BF}_4]^-$, $[\text{CF}_3\text{SO}_3]^-$ and $[\text{N}(\text{SO}_2\text{CF}_3)_2]^-$ anions can be compared to those of short chain primary alcohols (such as ethanol and methanol) and other polar, aprotic solvents such as dimethylsulfoxide (DMSO) and dimethylformamide (DMF) and therefore can be regarded as being relatively polar. In addition, the polarity decreases as the alkyl chain length increases. In another study using Reichardt's dye, it was shown that tetraalkylammonium cations are relatively non-polar while the cations of type $[\text{NH}_x\text{R}_{(4-x)}]^+$ ($x \geq 1$) are more polar (Muldoon *et al.*, 2001).



2.3.5 Water Miscibility

The solubility of ILs in water is dependent on the nature of the anion, the length of alkyl chain as well as the temperature (Wasserscheid and Welton, 2003). As an example, Figure 2 showed the anions responsible for water miscibility and immiscibility for 1-butyl-3-methylimidazolium cation. In general, an increase in the organic character of the cation results to a decrease of water solubility in ILs (Wasserscheid and Welton, 2003).

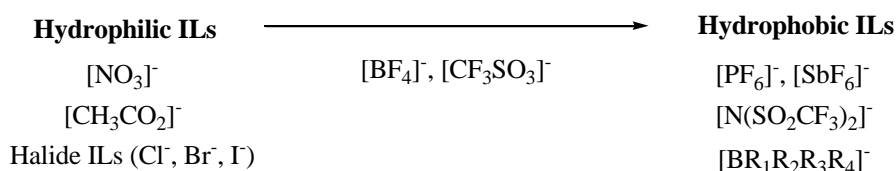


Figure 2: Different anions responsible for water miscibility and immiscibility of ILs.

The solubility of water in ILs increases while using more coordinating anions. Increasing the alkyl chain length cations as well as anions increases the hydrophobicity of the ILs (Seddon *et al.*, 2000). As an example, 1-alkyl-3-methylimidazolium tetrafluoroborate salts with alkyl chain length less than six are miscible with water at 25 °C, but with chain length greater than six, the ILs are immiscible with water (Holbrey and Seddon, 1999).

2.3.6 Density and Surface Tension

Density is one of the most often measured properties of ILs, probably because nearly every application requires knowledge of the density. In general, ILs are denser than water and most of the organic solvents. The molar mass of the anion significantly affects the overall density of ILs. For example, the [Ms₂N]⁻ species have lower densities than the

[Tf₂N]⁻ salts, in agreement with the fact that the molecular volume of the anion is similar but the mass of the fluorine is greater (Pringle *et al.*, 2003). This behaviour has been attributed to the fact that packing may become more compact as the alternating positive and negative species become more even in size.

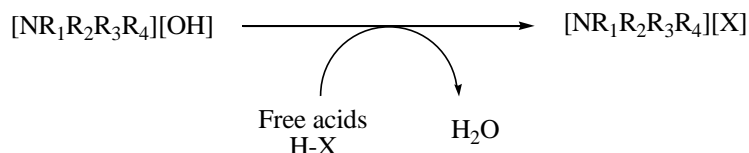
The surface tension of ILs (for example [bmim][PF₆] = 48.8 Nm⁻¹ and [bmim][BF₄] = 46.6 Nm⁻¹) are lower than water (72.2 Nm⁻¹ at 20 °C) but higher than surface tension of alkanes (example, hexane = 18.0 Nm⁻¹) (Huddleston *et al.*, 2001). Increasing the alkyl chains length on the cation resulted in a decrease in the surface tension value (Law and Watson, 2001).

2.4 Preparation of ILs

In some instances, the precursor cation (especially tetraalkylammonium salts) is commercially available, therefore requiring only an anion exchange reaction or a Lewis acid reaction to produce ILs. The preparation of ILs is relatively simple. The anion exchange reaction normally occurs by a metathesis exchange reaction. However, the major problem with the metathesis anion exchange reaction is the stoichiometric amount of metal waste (MX, M = metal) that is formed. Other than that, since halogen anion content is a major issue in the preparation of ILs, these methods are not recommended for the preparation of halogen-free ILs (Ohno and Fukumoto, 2007).

Therefore, the desired ILs can be obtained using various procedures such as the neutralization method. This method is also simple, involving the mixing of -onium hydroxide and free acid to prepare the desired salts (Scheme 3). The advantage of this is that the produced water is the by-product, thus avoiding the use of metal salts and ion-

exchange. The use of silver salts in anion exchange reaction containing amino acids is problematic due to the formation of stable amino acid complexes (Vidugiris *et al.*, 1988). Furthermore, the preparation is relatively easy, just mixing the two components equimolarly.



Scheme 3: Example of neutralization reaction method involved -onium hydroxide with free acids.

As the preparation of water-immiscible ILs is considerably more straightforward to prepare than the water soluble analogues, the method are considered first before the synthesis ILs. With water-immiscible ILs, the free acid or metal salt is washed out with water to give the final ILs product. Meanwhile, water-miscible ILs is normally extracted out of the aqueous phase with dichloromethane (Lancaster *et al.*, 2001).

2.5 Purification and Impurities in ILs

Since the purification of ILs by distillation is not possible due to their negligible vapour pressures, it is important to purify starting materials efficiently, thereby reducing the amount of impurities to be removed in the desired ILs. This protocol resulted in the highest purity possible in the produced ILs. Most ILs based on the common cations and anions should be colorless. The colored impurities present in ILs are probably due to oxidation products, thermal degradation impurities from the starting materials, or traces of compounds from the starting material (Wasserscheid and Welton, 2003). Therefore, it is

important to use freshly distilled starting materials and low temperature synthesis and drying methods to avoid extreme coloration of the ILs. Colored impurities present in ILs normally do not affect most applications using ILs (Seddon, 2000).

The common impurities present in ILs after reaction are halide ions, free acids (protic impurities), water and unreacted starting materials. The presence of these impurities can be extremely detrimental to transition metal catalysts leading to their deactivation (Chauvin *et al.*, 1995). In addition, impurities present in ILs significantly alter their physical properties (Seddon *et al.*, 2000). Purification of ILs is therefore, essential before using it in any application. Water-immiscible ILs is normally much easier to purify than water-miscible ILs by simply washing the ILs with water.

Volatile impurities that present in ILs could be due to unreacted starting materials or organic solvents used. Residual reaction solvents are readily removed by heating the ILs under vacuum condition. These volatile impurities can be easily removed by evaporation from the non-volatile ILs. Unreacted 1-methylimidazole for example is extremely difficult to be removed due to its relatively high boiling point of 198 °C and its strong interaction with the ILs. A colourimetric method implemented by Holbrey *et al.* (2001) allows for the determination of 1-methylimidazole present in the ILs in the 0-3 mole % concentration range. This method is based on the formation of the blue $[\text{Cu}(\text{mim})_4]^{2+}$ ion from the reaction of 1-methylimidazole with copper (II) chloride.

Halide impurities adversely affect the physicochemical properties of ILs. Additionally, they can act as catalyst poisons, as stabilizing ligands and as nucleophiles (Ajam, 2005). The presence of halide ions in the washing solutions can be detected by testing them with a silver nitrate solution which will become white and murky showing the presence of

silver chloride. Halide content in ILs is normally measured using an ion-sensitive electrode or using a wet chemical method (Volhard method) (Vogel, 1961).

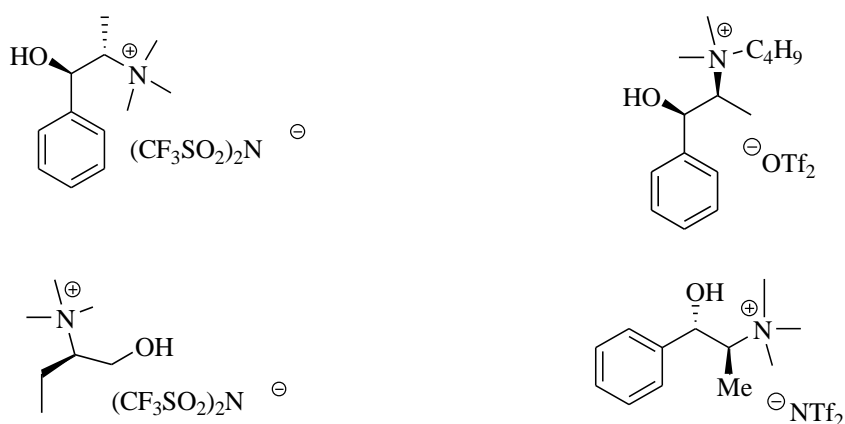
Residual water present in ILs is more problematic to be diminished rather than organic solvents probably due to the existence of H-bonding with ILs. It can normally be removed by heating the ILs under vacuum at 70 to 80 °C for several hours. For example, even hydrophobic ILs such as [bmim][N(SO₂CF₃)₂] can be saturated with about 1.4 wt % water. Hydrophilic ILs tends to contain a more significant amount of water. Water present in the ILs can also affect the physico-chemical properties of ILs, the stability of the ILs and catalyst inhibition (Seddon *et al.*, 2000). The water content in ILs can be determined by Karl-Fischer titration or even IR spectroscopy.

2.6 Chiral Ionic Liquids (CILs)

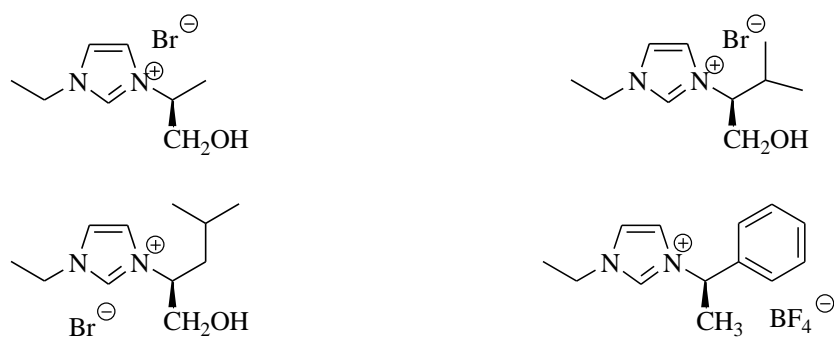
Asymmetric induction is mainly achieved by the use of chiral substrates or reagents, chiral catalysts or enzymes. Chiral solvents were also evaluated even if they have been mainly used for NMR determination of the enantiomeric excess of enantioriched compounds. The first use of a chiral solvent in asymmetric synthesis was reported in 1975 by Seebach (Baudequin *et al.*, 2005). Using a chiral aminoether as solvent, modest enantioselectivity were obtained in the electrochemical reduction of ketones. The study of the application of CILs in asymmetric synthesis is not only an opportunity but also a challenge for researchers. It is interesting, meaningful and necessary to synthesize different kinds of CILs from different starting materials, especially from the chiral pool (Levillain *et al.*, 2003).



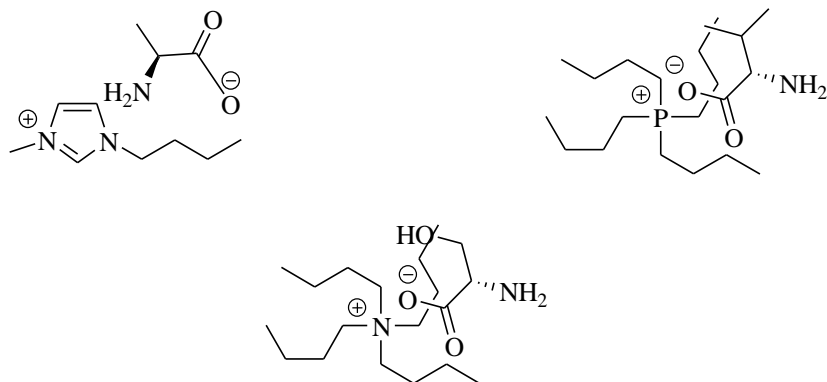
Chiral pool synthesis is defined as synthesis of a complex enantiopure chemical compound from a stock of readily available enantiopure substances. The built-in chirality is then preserved in the remainder of the reaction sequence (Klar *et al.*, 2005). Good chemical stability, especially configurational stability, is one of the most important criteria for synthesis of CILs and a necessary property for their application to chiral discrimination (Wang *et al.*, 2005). The more efficient, economic and simple way to prepare enantiomerically pure ILs is to use precursors derived from the chiral pool either for the generation of the CILs anion, cation or for both. Therefore, CILs are mainly compounds that possess a central chirality. However, some new CILs with an axial or a planar chirality have also been developed (Baudequin *et al.*, 2003). Figure 3 showed a few examples of the structure of CILs that has widely been synthesized.



CILs having chiral cation: Alkylammonium salts



CILs having chiral cation: Alkylimidazolium and Alkylimidazolinium salts



CILs having chiral anion: Amino Acids



Imidazolium with planar chirality

Figure 3: Structure of chiral ionic liquids (CILs)

2.7 Previous Related Chiral Ionic Liquids (CILs)

Chiral ionic liquids (CILs) based on chiral anions such as amino acids (AAs) have received attention during the last few years. Since the AAs contains both an amino group and a carboxylic acid residue in a single molecule, with various side groups and a chiral carbon atom, AAs are suitable candidates to act as a platform for functional ionic liquids (ILs) (Bao *et al.*, 2003, Tao *et al.*, 2005, Fukumoto *et al.*, 2005, Kagimoto *et al.*, 2007, Fukumoto *et al.*, 2006). Since AAs is commercially available and non-expensive starting material, it is easy to obtain pure AAs in large quantities at low cost. They also have an advantage such as biodegradability and biological activity. The availability of AAs as both anions and cations is another advantage.

The first amino acids-ionic liquids (AAILs) were synthesized by Bao *et al.*, (2003). They reported the synthesized of chiral imidazolium ILs derived from natural amino acids. In their work, L-alanine, L-valine, and L-leucine were used as starting material. These CILs were prepared in four steps from optically pure amino acids and the overall yield around 30-33 %.

Meanwhile, two years later Tao *et al.*, (2005) reported the first time two families of a new generation of ILs, in which the chiral cations are directly derived from naturally occurring α -amino acids and α -amino acid ester salts. In their work, halide anion such as PF_6^- , BF_4^- and NTf_2^- were used as anions. The preparation of this ILs using simple protonation reaction carried out by mixing the correct molar ratio of amino acid and relevant strong acid in water, followed by evaporation of the water in air and finally under vacuum. This one-step procedure is a typical atom-economic reaction without any poisonous by-product as compared to the previous method reported by Bao *et al.* (2003).

As mention previously, AAs can be used as anion or cation since it have amino and carboxylic acid residue in a single molecule. Fukumoto *et al.* (2005) have reported the synthesis of room temperature ionic liquids (RTILs) based on alkyimidazolium cation and α -amino acids as anions. Among several -onium cations that they tested, only 1-ethyl-3-methylimidazolium cation ([emim]) exhibit an excellent ability to form RTILs with amino acids. All of the resulting AAILs obtained were transparent and nearly colorless liquids at room temperature. These ILs have been obtained via simple neutralization reaction method.

But, they found that these salts have a high viscosity and low thermal stability. To overcome this problem, they were figure out the new AAILs by change the



alkylimidazolium cation with tetraalkylphosphonium-based (Kagimoto *et al.*, 2007). By using tetrabutylphosphonium-based as a cation ([TBP]), these salts show lower viscosities and higher decomposition temperatures (>300 °C) than previously reported alkylimidazolium-based AAILs.

There are many cations used to prepare AAILs such as pyrrolidinium, pyridinium and alkylammonium. A few article reported the synthesis of AAILs by using alkylammonium-based such as tetramethylammonium ([N₁₁₁₁]), tetraethylammonium ([N₂₂₂₂]) and also tetrabutylammonium cation ([N₄₄₄₄]). Allen *et al.* (2006) has reported the synthesis of 23 new CILs by the reaction of an amino acid or a chiral carboxylic acid with tetrabutylammonium hydroxide ([N₄₄₄₄][OH]) in water. Authors also reported that the choice of tetrabutylammonium in their work was due to the bulky nature of this cation which can reduce the intermolecular attractions in order to obtain a salts being liquid at room temperature.

Recently, Jiang *et al.* (2008) has synthesis and characterize AAILs by using symmetry structure of tetraalkylammonium cation with simple structure of amino acids such as L-valine, L-glycine and L-alanine. Four of nine tetraalkylammonium-based AAILs prepared in their work shows lower viscosities than all AAILs found in the literature. The AAILs with [N₂₂₂₂] cation yielded low viscosity, especially [N₂₂₂₂][L-Ala], the least viscous AAIL ever found and the least viscous IL based on a symmetric [TAA] cation. Although the thermal stability of these AAILs is not improved over typical AAILs, such as [emim][amino acid] and [TBP][amino acid], these newly synthesized AAILs are the first simple amine-functionalized ILs of low viscosity. They also reported that the use of AAILs in reversible CO₂ absorption and approaches 0.5 mol per mol ILs.

2.8 Applications of ILs

2.8.1 Ionic Liquids (ILs) as Solvents for Extraction

Initial reports on utilization of ILs for extraction purposes came from Robin Rogers and his collaborators. In one of the first reports, this group studied the partitioning of substituted benzene derivatives between water and [bmim][PF₆] (Swatloski *et al.*, 2001). The possibility of the fine tuning of the partitioning process by varying ILs structure was also presented. In comparison to traditional solvent extraction behaviour, ILs showed an exceptional behaviour and possibility of significantly complicated partitioning mechanism. It is important to mention that large distribution coefficient has been achieved using ILs as extraction solvents for separation of metal ions by crown ethers (Dai *et al.*, 1999).

Fadeev and Meagher (2001) reported the potential of ILs as extractants in recovery of butyl alcohol from fermentation broth. By measuring the partition coefficient between water and two ILs ($\log P$), Abraham *et al.* (2003) showed that an increase in solute hydrogen bond basicity and solute volume led to a decrease and increase in $\log P$, respectively. Similarly, an increase in solute hydrogen bond acidity also decreased $\log P$. [bmim][PF₆] in concert with dithiazone metal chelator was demonstrated to form neutral metal-dithiazone complexes with heavy metal ions such as to extract heavy metal ions from aqueous solution into [bmim][PF₆]. Distribution ratios of heavy metal complexes between [bmim][PF₆] and water were found to be high and extraction efficiencies pH dependent (Wei and Yang, 2003).

2.8.2 Biocatalytic Reaction in ILs

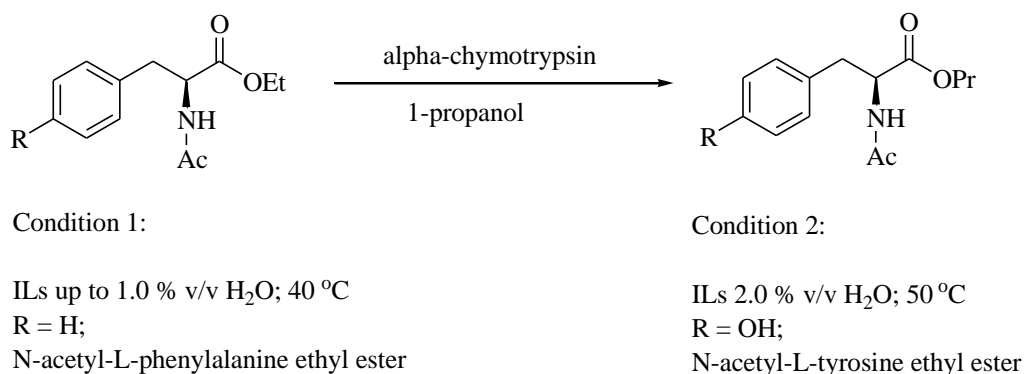
The term ‘biocatalysis’ is the use of natural catalyst such as protein enzyme to perform chemical transformation on organic compounds. This can be achieved by using either the whole cells or partially purified enzymes. ILs seems to be attractive and suitable replacements for commonly used solvents for many applications such as in biocatalysis. ILs has already been used for a large number of organic and catalytic reactions (Welton, 1999). Using ILs as reaction media often affords accelerated activity and improved selectivity when compared to VOSs. In some cases, increased catalyst stability is also observed in the ILs and provides a unique solvent environment.

The main objective using ILs in a reaction is to enhance reaction activity and selectivity. Additional benefits of using ILs in a reaction would be for easy separation of reaction products and recovery of the catalyst due to their nonvolatile nature. An ideal case for the use of ILs in catalytic reactions would be when the catalyst and substrate are soluble in ILs and the reaction product is insoluble in ILs. Additionally, the reaction product should not extract the catalyst, thereby allowing the products to be removed by simple decantation and the catalyst to be recovered and re-used. However, if the reaction products are miscible with the ILs, separation is much more complicated often requiring distillation, which could be facilitated due to the ILs negligible vapour pressure. This method is, however, limited to volatile products and is dependent on the thermal stability of the catalyst. Possible extraction of the product with a co-solvent that is immiscible with the ILs but miscible with the product is possible but often leads to cross contamination.

Many reactions have been successfully tested with ILs and these include oligomerization (Wasserscheid *et al.*, 2001), transesterification reaction (Kim *et al.*, 2001), hydroformylation (Wasserscheid *et al.*, 2002), hydrogenation (Geldbach and Dyson, 2004), carbonylation (Brausch *et al.*, 2004), Diels-Alder reaction (Doherty *et al.*, 2004), oxidation (Yamaguchi *et al.*, 2005), Heck reaction (Mo *et al.*, 2005) and also Suzuki cross-coupling (Xiao and Shreeve, 2005).

2.8.3 Lipases in ILs

In the first publication describing the preparative use of an enzymatic reaction in ILs, protease thermolysin was used for the synthesis of the dipeptide Z-aspartame (Erbeldinger *et al.*, 2000). The reaction rate was comparable to those found in conventional organic solvents such as ethyl acetate. Additionally, the enzyme stability was increased in ILs. The protease α -chymotrypsin has been used for transesterification reaction (Laszlo and Compton, 2001 and Lozano *et al.*, 2001). N-acetyl-1-phenylalanine ethyl ester and N-acetyl-1-tyrosine ethyl ester were transformed into corresponding propyl esters (Scheme 4).



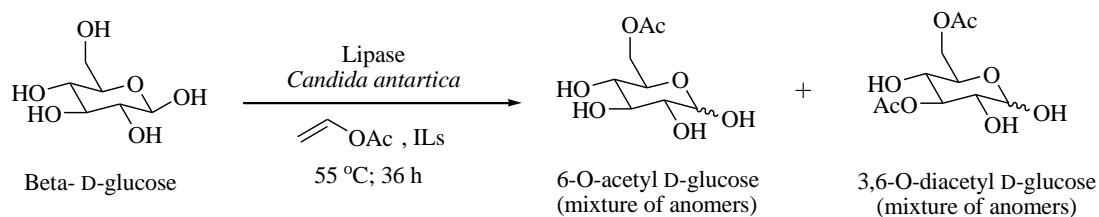
Scheme 4: Transesterification reaction of N-acetyl-1-phenylalanine ethyl ester and N-acetyl-1-tyrosine ethyl ester into corresponding propyl esters.

Laszlo and Compton (2001) used [omim][PF₆] and [bmim][PF₆] and compared their results with conventional VOSs such as acetonitrile or hexane. They also investigated the influence of water content on enzyme activity, as well as the ratio of transesterification and hydrolysis. They found that, as with polar organic solvents, a certain amount of water present in the reaction was necessary to maintain enzyme activity. For both ILs and organic solvents, the rates were of the same order of magnitude.

The majority of enzymes reported so far to be active in ILs belong to the class of lipases, the “work horses” of biocatalyst (Bornscheur and Kazlauskas, 1999). The report from Madeira Lau *et al.* (2000) demonstrated the potential use of enzyme in ILs for alcoholysis, aminolysis and perhydrolysis reactions. They compared the reactivity of *Candida antartica* lipase in ILs such as [bmim][PF₆] and [bmim][BF₄] with conventional VOSs. In all cases, the reaction rates were similar for all the reactions investigated.

The kinetic resolution of 1-phenylethanol was reported by Schöfer *et al.* (2001). They use eight sets of different lipases and two esterases in ten ILs with methyl tert-butyl ether (MTBE) as the reference. Vinyl acetate was used for the transesterification. No activity was observed for the esterases but for the lipases from *Pseudomonas sp.* and *Alcaligenes sp.*, an improved enantioselectivity was observed in [bmim][CF₃SO₂)₂N] as solvent, compare to MTBE. The best result was obtained for *Candida antartica* lipases B in [bmim][CF₃SO₂)₂N] and [omim][PF₆]. Other groups that also investigating the same system observed good activities in these ILs (Park and Kazlauskas, 2001 and Kim *et al.*, 2001).

One particular feature of ILs lies in solvation properties, not only for hydrophobic compounds but also for hydrophilic compounds such as carbohydrates. Park and Kazlauskas (2001) reported the regioselective acylation of glucose in 99 % yield and with 93 % selectivity in [moemim][BF₄] (moe = CH₃OCH₂CH₂), values much higher than those obtained in the VOSs commonly used in this purpose (Scheme 5).



Scheme 5: 1-Methoxyethyl-3-methylimidazolium ([moemim][BF₄]) dissolves ~5mg/ml glucose at 55 °C yield 99 %; selectivity: 93 % 6-O-acetyl D-glucose.

2.9 Ionic Liquid-Coated Enzyme (ILCE)

Non-aqueous biocatalysis provide a useful component of methodology in organic synthesis. However, biocatalysis in non-aqueous media often suffers from reduced activity, selectivity or stability of enzyme (Klibanov, 1997). To overcome these limitations, development of more efficient enzymes has been done. Some recent examples include cross-linked enzyme crystals and aggregates (Cao *et al.*, 2000), ligand co-lyophilized enzymes (Ke and Klibanov, 1998) and enzyme-coated microcrystals (Kreiner *et al.*, 2001).

Although these modified enzymes exhibit better activity, selectivity or stability, the procedures for their preparations in most cases are rather complicated. Until now, the approach using ionic liquid-coated enzyme (ILCE) had been performed and exhibits markedly enhanced enantioselectivity and reliable stability.

According to Lee and Kim (2002), ILCE has been prepared using 1-(3'-phenylpropyl)-3-methylimidazolium hexafluorophosphate, [ppmim][PF₆] and *Pseudomonas cepacia* lipase. ILCE was then tested on transesterification reaction of vinyl acetate. It shows that ILCE still retained 93 % of the activity of its native counterparts even after the fifth run of the reaction. This indicates that, for lipase practically, no significant activity was lost during the coating process and its coated form has satisfactory stability. Accordingly, it is believed that ILCE should be used as a new type of immobilized biocatalyst for biotransformations in organic solvents.

CHAPTER 3

MATERIALS AND METHODS

3.1 Materials

The chemicals listed below were used in this work. All chemicals are commercially available and of analytical grade unless otherwise specified. The chemicals were used without purification unless otherwise stated.

3.1.1 Solvents

Solvents	Manufacturer
Deuterium oxide (for NMR)	Sigma-Aldrich
Ethanol	J.T.Baker
Hexane	J.T.Baker
Methanol	Riedel-de-Haën

3.1.2 Chemicals

Chemicals	Manufacturer
Adipic acid	Merck
Capric acid	Merck
Caprylic acid	Fluka
Hexanoic acid	Merck
Lauric acid	Merck
L-asparagine	Across Organics
L-glutamine	Across Organics



L-glutamic acid	Sigma-Aldrich
L-histidine	Sigma-Aldrich
L-isoleucine	Sigma-Aldrich
L-lysine	Fluka
L-methionine	Sigma-Aldrich
L-proline	Sigma-Aldrich
L-serine	Sigma-Aldrich
L-threonine	Sigma-Aldrich
Myristic acid	Merck
Oleic acid	Merck
Oleyl alcohol	TCI Mark
Palmitic acid	Merck
Stearic acid	Merck
Tetraethylammonium hydroxide	Fisher Scientific
L(-)-malic acid	Across Organics
L(+)-tartaric acid	Sigma-Aldrich

3.1.3 Enzyme

Enzyme

Candida rugosa lipase

Manufacturer

Sigma – Aldrich

3.1.4 Equipment/ Instruments

Equipment/ Instruments

Auto-titrator

Manufacturer

Metrohm, Switzerland

Bruker SMART APEXII CCD Area-Detector
Diffractometer

Bruker Advance



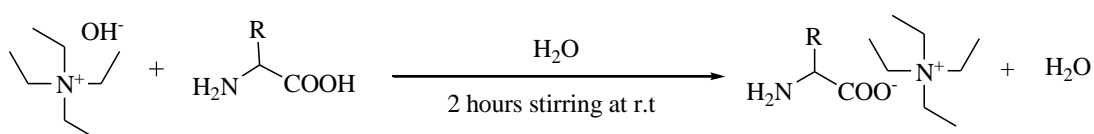
Horizontal Water-Bath Shaker	Hotech Instruments Corp
Jasco P-200 Polarimeter	Jasco, Japan
Leco CHNS-932 Elemental Analyzer	Perkin-Elmer
Magnetic Stirrer – CD 162	Stuart
Magnetic Stirrer – ETS-D4	IKA Labortechnik
Rotary Evaporator – B 480 & R-114	Büchi Waterbath
Vacuum Oven	BINDER GmbH
Vacuum Pump Model 281C-50	Welch, USA



3.2 Methods

3.2.1 Preparation of CILs derived from Amino Acids.

Excess L-asparagine (0.05 mol) were first dissolved in 40 mL of distilled water in a 100 mL beaker. An aqueous solution (20 % in water) of tetraethylammonium hydroxide (36.59 mL, 0.05 mol) was added dropwise into an aqueous solution of L-asparagine and the mixture was stirred with a magnetic stirrer for 2 hours at room temperature. Water was then removed by evaporation at 70 °C for several hours and the crude product was obtained after being dried at 65 °C under vacuum for 2 days. Since tetraethylammonium L-asparaginate ([N₂₂₂₂][asn]) were miscible with ethanol and L-asparagine were nearly insoluble in ethanol, the crude product were added into ethanol (40 mL) to precipitate the excess L-asparagine. After filtration, the solvent was removed by evaporation at 70 °C. Finally, the product appeared as a white solid after being dried in vacuum oven for 2 days at 65 °C. Scheme 6 shows the route to synthesis CILs using neutralization reaction. The same procedure was followed for all CILs derived from chiral amino acids as listed in Table 3.



R = side chain of amino acid

Scheme 6: General route to synthesis of tetraethylammonium-based CILs derived from amino acids (Jiang *et al.*, 2008).

Table 3: Starting materials and abbreviation names for CILs synthesized using neutralization method.

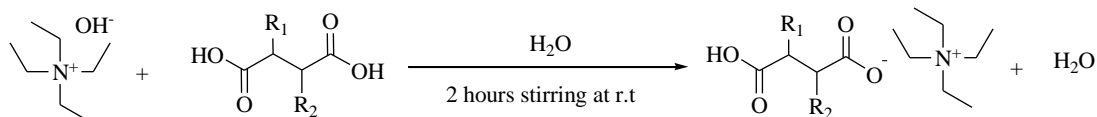
Cation	Anion (Amino acid)	CILs	Abbreviation
[N ₂₂₂₂][OH]	L-serine	Tetraethylammonium L-serinate	[N ₂₂₂₂][ser]
[N ₂₂₂₂][OH]	L-proline	Tetraethylammonium L-prolinate	[N ₂₂₂₂][pro]
[N ₂₂₂₂][OH]	L-threonine	Tetraethylammonium L-threoninate	[N ₂₂₂₂][thr]
[N ₂₂₂₂][OH]	L-isoleucine	Tetraethylammonium L-isoleucinate	[N ₂₂₂₂][ile]
[N ₂₂₂₂][OH]	L-asparagine	Tetraethylammonium L-asparaginate	[N ₂₂₂₂][asn]
[N ₂₂₂₂][OH]	L-glutamine	Tetraethylammonium L-glutamate	[N ₂₂₂₂][gln]
[N ₂₂₂₂][OH]	L-glutamic acid	Tetraethylammonium L-glutamate	[N ₂₂₂₂][glu]
[N ₂₂₂₂][OH]	L-methionine	Tetraethylammonium L-methioninate	[N ₂₂₂₂][met]
[N ₂₂₂₂][OH]	L-histidine	Tetraethylammonium L-histidinate	[N ₂₂₂₂][his]
[N ₂₂₂₂][OH]	L-lysine	Tetraethylammonium L-lysinate	[N ₂₂₂₂][lys]
[N ₂₂₂₂][OH]	L(-)-malic acid*	Tetraethylammonium L-malate	[N ₂₂₂₂][mal]
[N ₂₂₂₂][OH]	L(+)-tartaric acid*	Tetraethylammonium L-tartrate	[N ₂₂₂₂][tar]

[N₂₂₂₂][OH] = tetraethylammonium hydroxide (36.59 mL)

* Plant acid

3.2.2 Preparation of CILs derived from Plant Acids

L(+)-tartaric acid (7.504 g, 0.05 mol) was first dissolved in 20 mL of distilled water in a 100 mL beaker. An aqueous solution (20 % in water) of tetraethylammonium hydroxide (36.59 mL, 0.05 mol) was added dropwise into an aqueous solution of L(+)-tartaric acid and the mixture was stirred with a magnetic stirrer for 2 hours at room temperature. This reaction was slightly exothermic. Water was then removed by evaporation at 70 °C for several hours and white solid product was obtained after being dried at 65 °C under vacuum for 2 days. These procedures were then applied using different anion (L(-)-malic acid) as listed in Table 3. Scheme 7 showed the route to synthesis CILs derived from chiral plant acids.



Scheme 7: General route to synthesis of tetraethylammonium-based CILs derived from plant acids (Allen *et al.*, 2006).

3.2.3 Crystallization of Solid CILs

Two crystals CILs which are [N₂₂₂₂][tar] and [N₂₂₂₂][mal] were synthesized using previous method as mentioned in Section 3.2.2. Suitable crystal [N₂₂₂₂][tar] for X-ray diffraction were obtained by dissolving in methanol and then covered by aluminium foil to allow slow evaporation at room temperature. Clear crystalline solid was obtained after 3 days. For single crystal of [N₂₂₂₂][mal], the synthesis procedure is similar to the previous one. The crystals obtained were sent to Single X-ray Crystallography Unit, School of Physics, Universiti Sains Malaysia for data analyse.

3.2.4 Preparation of Chiral Ionic Liquid-Coated Enzyme (CILCE)

For the preparation of CILCE, *Candida rugosa* lipase (CRL) was chosen because it had been frequently used for biocatalysis, especially esterification and transesterification in organic solvents (Abdul Rahman *et al.*, 2003). In this study, 2.0 g of solid [N₂₂₂₂][asn] was melted (m.p 58.0 ± 1.0 °C) to get a liquid phase. [N₂₂₂₂][asn] was chosen because it has smaller size compare to [N₂₂₂₂][his] (m.p 54.0 ± 1.0 °C). The bigger sizes of CILs form a bulkiness structure of CILCE and therefore make it difficult for the long chain oleyl alcohol and palmitic acid/oleyl acid to enter the active site of enzyme (Gandhi *et al.*, 1995).

Enzyme in powder forms (CRL, 0.2 g mass equivalent) were added to this liquid phase and the mixture was stirred with a glass rod to get a uniform heterogeneous solution. The solution was then allowed to cool to room temperature until the enzyme-CILs mixture solidified. Then, solid phase was grinded to a small size of particles with mortar and pestle to get powder form. Finally, the small CILCE particles were then used without any further treatment in the next experiments to test their activity and selectivity (modified method from Lee and Kim, 2002). CILCE was kept in the freezer to avoid denaturing of the enzyme.

3.2.5 Esterification Reaction of Oleyl Alcohol with Various Fatty Acids

Adipic acid (1.0 mmol, 140 mg) was weighted and placed in 9 sample vials each. Oleyl alcohol (2.0 mmol, 0.63 mL) was added into each vials followed by n-hexane (5 mL) as a solvent. Then, native CRL (15 mg) and CILCE (165 mg (equal amount of CRL)) was added into six out of nine vials (three for native CRL and three fro CILCE) and all vials were closed tightly. The reaction mixture of samples and control (three samples without enzyme) were incubated at 50 °C in a horizontal water bath shaker with shaking speed of 150 rpm continuously for 1 hour.

After 1 hour, the enzyme (native CRL and CILCE) was removed by filtration and the remaining free acid in the reaction mixture was determined using auto-titrator with 0.1 M of NaOH as titrant until an end point of pH 10.0. The activity of CRL/CILCE of each reaction was expressed as a percentage of converted acid. These steps were then applied for various fatty acids as listed in Table 4 (modified from Basri *et al.*, 2005 and Mat Radzi *et al.*, 2005). The percentage of conversion was calculated based on equation in Appendix A.

Table 4: Starting materials and ratios of oleyl alcohol with various fatty acids in esterification reactions.

Entry	Acid	Alcohol	Ratio (mmol)	Ester
1	Adipic acid	Oleyl alcohol	1:2	Di-oleyl adipate
2	Capric acid	Oleyl alcohol	1:1	Oleyl capriate
3	Hexanoic acid	Oleyl alcohol	1:1	Oleyl hexanoate
4	Lauric acid	Oleyl alcohol	1:1	Oleyl laurate
5	Myristic acid	Oleyl alcohol	1:1	Oleyl myristate
6	Oleic acid	Oleyl alcohol	1:1	Oleyl oleate
7	Palmitic acid	Oleyl alcohol	1:1	Oleyl palmitate
8	Stearic acid	Oleyl alcohol	1:1	Oleyl stearate

3.3 Analytical Methods

The instruments used in this project are listed below. All instruments are available in the Department of Chemistry, Faculty of Science, UPM unless otherwise stated.

3.3.1 Nuclear Magnetic Resonance (NMR) Spectroscopy

Nuclear magnetic resonance (NMR) is a technique to determine the structure of organic compounds and provide detail information on the three dimensional structure of molecule in solution. ^1H NMR spectra data were recorded at room temperature on Spectrometer NMR JEOL JNM-ECA 400 MHz and a few of spectra data were record on Varian Unit Inova 500 MHz at Spectroscopy Unit, Laboratory of Natural Product, Institute of Bioscience, UPM. The solvent use was deuteriated oxide (D_2O). ^1H NMR of all presented compounds were available and chemical shift were reported in part per million (ppm). Spectra of CILs were recorded in a 5 mm NMR tube.

3.3.2 CHNS/O Instrument - Element Analysis.

Elemental analysis is a process where a sample of some materials (*e.g.*, soil, waste or chemical compounds) is analyzed for its elemental and sometimes isotopic composition. Elemental analysis can be qualitative (determining elements that present in the sample), and it can be quantitative (determining how much percentage of each elements). Elemental analysis (carbon, hydrogen, nitrogen and sulphur) of powder and liquids samples were performed on a Leco CHNS-932 Elemental Analyzer instrument. About 2 mg of the sample is analyzed and the results in percentages were interpreted allowing a deviation of $\pm 2.0\%$.

3.3.3 Differential Scanning Calorimetry (DSC)

DSC is a thermoanalytical technique in which the difference in the amount of heat required to increase the temperature of a sample and reference are measured as a function of temperature. Both the sample and reference are maintained at very nearly the same temperature throughout the experiment. Generally, the temperature program for a DSC analysis is designed such that the sample holder temperature increases linearly as a function of time. The reference sample should have a well-defined heat capacity over the range of temperatures to be scanned. Melting and glass transition temperature were measured by Mettler-Toledo DSC, model DSC822^e and the data were evaluated using Mettler-Toledo STAR^e software version 9.01.

The DSC instrument was calibrated using indium reference sample provided by Mettler-Toledo. Measurement was carried out at a scan rate of 10 °C/min by cooling the samples from 200 °C to -100 °C, followed by heating from -100 °C to 200 °C. The samples were prepared by placing in a 40 μ L hermetically sealed aluminium pan with a pinhole at the top of the pan. The samples inside the DSC furnace were exposed to a flowing nitrogen atmosphere. The melting point and glass transition temperatures are defined as maximum peak.

3.3.4 Thermogravimetric Analysis (TGA)

TGA is analytical technique used to determine a material's thermal stability and its fraction of volatile components by monitoring the weight changes that occurs as a specimen is heated. The measurement is normally carried out in air or in an inert atmosphere, such as helium or argon and the weight is recorded as a function of increasing

temperature. Mettler-Toledo TGA/SDTA 851^e TGA instrument and Mettler-Toledo STAR^e version 8.10 software were used to determine the onset temperature (T_{onset}). The dried CILs were stored and sampled in a desiccator with a silica gel before analyzing the sample.

All samples were run in alumina pans under nitrogen atmosphere at a heating rate 10 °C/min and temperature was programmed from 25 °C to 600 °C. Flow of nitrogen gas was controlled using TS0800GC1 gas controller and calibration of TGA instruments were done using indium and aluminium references samples. The onset temperature (T_{onset}) is the intersection of the baseline, either from the beginning of the experiment or after the drying step and the tangent of the weight versus temperature curve as decomposition occurs.

3.3.5 Single X-ray Crystallography

Single X-ray crystallography is a technique of determination the arrangement of atoms within a crystal, in which a beam of X-ray strikes a crystal and scatters into many different directions. Different angles and intensities of these scattered beams, can produce a three dimensional picture of the density of electrons within the crystal. From this electron density, the mean positions of the atoms in the crystal can be determined, as well as chemical bonds, disorder and other information.

Main objectives of Single X-ray crystallography techniques are to confirm the structure and to determine the hydrogen bonding interaction in the compounds. Single crystals were mounted in a nylon loop for data collection at 100 K on a Bruker SMART APEXII diffractometer equipped with a CCD area-detector. The images were interpreted and

integrated with the program SAINT from Bruker. The structures were solved and refined by full-matrix least squares on F^2 using SHELXTL program package.

3.3.6 Optical Rotation

Optical rotation or optical activity is the rotation of linearly polarized light as it travels through certain materials. Measurements were carried out on Jasco P-200 Polarimeter equipped with a 100 mm standard glass tube with bulb at 25 °C. The data were recorded on instruments which use the sodium lamp as a radiation source and wavelength for all CILs is constant and standard.

The optical rotation was determined by dissolving a known amount of the CILs into a suitable solvent of known volume. In this procedure, distilled water was used as a solvent and the concentration for all CILs solution was 1 g/100 mL. The sample tube for the machine was then rinsed with CILs solution twice and the tube was then filled with the solution. The optical rotation was then recorded three times and the average was taken as an observed optical rotation value. This value was then used in the following formula (1) to calculate the specific optical rotation value, $[\alpha]_D^{25}$.

$$[\alpha]_D^{25} = \alpha / (lc) \quad (1)$$

Where; $[\alpha]$ = specific optical rotation

α = value of optical rotation observed

l = length of cell (dm)

c = concentration in g/ 100 mL



3.3.7 Viscosity Determination

Viscosities of CILs series were measured using a LVDV –II+Pro Viscometer instrument manufactured by Brookfield Engineering Laboratories, Ins, USA equipped with CPE–52 spindle at 25 °C. Before the reading was taken, the viscometer must be auto zeroed in order to avoid any error. For high viscosity determination, 0.5 mL of each samples were put in the middle of the sample chamber. The instrument was connected to computer with Rheocalc32 software in order to set up the parameters and analyzed the data respectively. All experiments were conducted in duplicate.

3.3.8 Ionic Conductivity

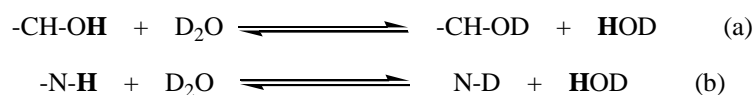
Electrical conductivity or specific conductivity is a measure of a material's ability to conduct an electric current. The electrical conductivity for all CILs were determined using SevenGo Conductivity Meter, manufactured by Mettler-Toledo GmbH, Switzerland. All experiments were conducted at 25 °C and the data were collected after the sample was prepared in triplicate.

CHAPTER 4

RESULTS AND DISCUSSION

4.1 Nuclear Magnetic Resonance (NMR) Spectra

Confirmation of the predicted structures for all new CILs was carried out using ^1H and ^{13}C NMR. In this measurement, D_2O was used as a solvent and there was no peaks observed for hydrogen on the $-\text{OH}$ and $-\text{NH}$ groups. Rapid exchange between $-\text{OH}/-\text{NH}$ with D_2O solvent occurred after a few minutes. The proton was replaced by deuterium, causing it to disappear from the spectrum or its intensity was greatly reduced (Scheme 8). If the exchange takes place, the proton on the adjacent carbon ($\text{CH}-\text{OH}$) will not show any coupling with the $-\text{OH}$ proton.



Scheme 8: Deuterium exchange between D_2O solvent and (a) $-\text{OH}$ hydrogen and (b) amino hydrogen.

The similar trend for tetraethylammonium cation peaks for all CILs were observed in the ranges at δ 3.06 to 3.25 and δ 1.25 to 1.08 ppm for $\text{N}-\text{CH}_2$ and $\text{N}-\text{CH}_2-\text{CH}_3$ peaks integrating eight and twelve protons respectively. $\text{N}-\text{CH}_2$ peak was observed at downfield region due to the protons are deshielded by electronegativity of the nitrogen atom.



4.1.1 Tetraethylammonium L-serinate, ([N₂₂₂₂][ser])

The ¹H NMR spectrum (Appendix B-1) showed one multiplet signal at the downfield region which contributed to the peak HO-CH₂ was observed at the chemical shift δ 3.82–3.77 ppm. This can be explained as the protons were deshielded by the electronegativity of oxygen atom. Meanwhile, the multiplet signals at δ 3.39–3.20 ppm were assigned to O₂C-CH.

¹H NMR (400 MHz, D₂O): δ 3.82–3.77 (m, 2H, HO-CH₂), 3.39–3.20 (m, 1H, O₂C-CH), 3.25 (q, ³J_{HH} = 7.3 Hz, 8H, N-CH₂), 1.25 (t, ³J_{HH} = 7.3 Hz, 12H, N-CH₂-CH₃). ¹³C NMR δ 6.77, 52.03, 57.55, 64.16, 179.02 ppm.

4.1.2 Tetraethylammonium L-prolinate, ([N₂₂₂₂][pro])

The ¹H NMR spectrum (Appendix B-2) showed doublet of doublet (dd) peak containing one proton at the downfield region which attributed to the peak O₂C-CH observed at the chemical shift of δ 3.45 ppm. This was due to the proton adjacent to the carbonyl group were slightly deshielded and shifted downfield in the spectrum. Meanwhile, the multiplet signals at δ 2.99–2.74 ppm containing one proton were assigned to N-CH(β) respectively because the hydrogen was slightly deshielded due to the electronegativity of the attached nitrogen. The multiplet signals at δ 2.17–2.03 ppm integrating for one proton was assigned to HC-CH(α). At δ 1.72–1.61 ppm, one multiplet signal containing three proton was attributed to HC-CH(β) and H₂N-CH₂-CH₂ in the five membered ring respectively.

¹H NMR (400 MHz, D₂O): δ 3.45 (dd, 1H, ³J_{H1Hα} = 7.3 Hz, ³J_{H1Hβ} = 12.12 Hz, O₂C-CH), 3.12–3.09 (m, 1H, N-CH(α)), 3.21 (q, ³J_{HH} = 7.3 Hz, 8H, N-CH₂), 2.99–2.74 (m, 1H, N-CH(β)), 2.17–2.03 (m, 1H, HC-CH(α)), 1.72–1.61 (m, 3H, HC-CH(β) and H₂N-CH₂-



CH_2), 1.14 (t, $^3J_{\text{HH}} = 7.3$ Hz, 12H, N- CH_2 - CH_3). ^{13}C NMR δ 6.75, 25.10, 30.67, 46.19, 51.96, 61.56, 180.28 ppm.

4.1.3 Tetraethylammonium L-threoninate, ($[\text{N}_{2222}][\text{thr}]$)

Appendix B-3 showed the ^1H NMR spectrum of the above compound title. At δ 3.82–3.77 ppm, one multiplet signal was attributed to the OH- CH peak. The proton on the adjacent carbon (CH -OH) was deshielded by the oxygen atom attached. Meanwhile, at downfield region, δ 2.94 ppm was assigned to the O_2C - CH peak. This was due to the proton was slightly deshielded due to the electronegativity of the attached nitrogen atom. The doublet peaks integrating for three protons were assigned to the OH-C- CH_3 signal at δ 1.06 ppm.

^1H NMR (500 MHz, D_2O): δ 3.82–3.77 (m, 1H, OH- CH), 3.14 (q, $^3J_{\text{HH}} = 7.5$ Hz, 8H, N- CH_2), 2.94 (d, $^3J_{\text{HH}} = 5.5$ Hz, 1H, O_2C - CH), 1.13 (t, $^3J_{\text{HH}} = 7.5$ Hz, 12H, N- CH_2 - CH_3), 1.06 (d, $^3J_{\text{HH}} = 6.0$ Hz, 3H, OH-C- CH_3). ^{13}C NMR 6.58, 19.33, 57.73, 68.16, 70.54, 180.32 ppm.

4.1.4 Tetraethylammonium L-isoleucinate, ($[\text{N}_{2222}][\text{ile}]$)

The ^1H NMR spectrum is shown in Appendix B-4. The α -proton was slightly deshielded due to the electronegativity of the nitrogen and appeared at δ 2.96 ppm. The peak at δ 1.65–1.54 ppm was observed for methine proton (H_2N - CH - CH). Another alkanes group was confirmed at δ 1.30–1.28 ppm with multiplet peaks contained two protons (CH - CH_2) and at δ 1.17–1.01 ppm, a multiplet peaks attributed to the CH - CH_3 contained three protons observed respectively. The multiplet peaks at δ 0.82–0.76 ppm were assigned to the CH_2 - CH_3 , confirming the presence of methyl groups.



^1H NMR (500 MHz, D_2O): δ 3.13 (q, $^3J_{\text{HH}} = 7.3$ Hz, 8H, N- CH_2), 2.96 (d, $^3J_{\text{HH}} = 5.0$ Hz, 1H, $\text{O}_2\text{C}-\text{CH}$), 1.65–1.54 (m, 1H, $\text{H}_2\text{N}-\text{CH}-\text{CH}$), 1.30–1.28 (m, 2H, $\text{CH}-\text{CH}_2$), 1.13 (t, $^3J_{\text{HH}} = 7.3$ Hz, 12H, N- CH_2-CH_3), 1.17–1.01 (m, 3H, $\text{CH}-\text{CH}_3$), 0.82–0.76 (m, 3H, CH_2-CH_3). ^{13}C NMR δ 6.63, 11.38, 15.61, 25.19, 39.74, 57.81, 60.43, 179.27 ppm.

4.1.5 Tetraethylammonium L-asparaginate, ($[\text{N}_{2222}]$)[asn]

Appendix B-5 showed the ^1H NMR spectrum for tetraethylammonium L-asparaginate. At δ 3.69–3.57 ppm, a multiplet signal attributed to the $\text{O}_2\text{C}-\text{CH}$ peak was showed. This was due to the proton was slightly deshielded due to the electronegativity of the attached nitrogen atom. Meanwhile, at downfield region, δ 2.64 ppm was assigned to the $\text{OOC}-\text{C}-\text{CH}(\alpha)$ which showed a doublet of doublet (dd) peaks and at δ 2.42 ppm, a similar doublet of doublet peaks, integrating one proton was attributed to $\text{OOC}-\text{C}-\text{CH}(\beta)$.

^1H NMR (400 MHz, D_2O): δ 3.69–3.57 (m, 1H, $\text{O}_2\text{C}-\text{CH}$), 3.25 (q, $^3J_{\text{HH}} = 7.5$ Hz, 8H, N- CH_2), 2.64 (dd, $^2J_{\text{H}\alpha\text{H}\beta} = 12.5$ Hz, $^3J_{\text{HH}} = 5.5$ Hz, 1H, $\text{OOC}-\text{C}-\text{CH}(\alpha)$), 2.42 (dd, $^2J_{\text{H}\alpha\text{H}\beta} = 12.5$ Hz, $^3J_{\text{HH}} = 8.0$ Hz, 1H, $\text{OOC}-\text{C}-\text{CH}(\beta)$), 1.26 (t, $^3J_{\text{HH}} = 7.5$ Hz, 12H, N- CH_2-CH_3). ^{13}C NMR δ 6.75, 40.20, 55.21, 57.10, 176.32, 179.90 ppm.

4.1.6 Tetraethylammonium L-glutamate, ($[\text{N}_{2222}]$)[gln]

The structure of tetraethylammonium L-glutamate was confirmed by the ^1H NMR analysis (Appendix B-6). A triplet signal at downfield region contributed to the peak $\text{O}_2\text{C}-\text{CH}$ at chemical shift δ 3.96 ppm was observed. This downfield region peak was found because the α -hydrogen was slightly deshielded due to the electronegativity of the attached nitrogen. Meanwhile, the multiplet signal ranged from δ 2.35–2.14 ppm was assigned to the $\text{CH}-\text{CH}_2-\text{CH}_2$. The protons were deshielded by the carbonyl group.



Another set of multiplet signal at δ 1.88–1.61 ppm integrating for two protons was assigned to CH-**CH**₂-.

¹H NMR (500 MHz, D₂O): δ 3.96 (t, ³J_{HH} = 7.3 Hz, 1H, O₂C-**CH**), 3.05 (q, ³J_{HH} = 7.3 Hz, 8H, N-**CH**₂), 2.35–2.14 (m, 2H, CH-CH₂-**CH**₂), 1.88–1.61 (m, 2H, CH-**CH**₂-), 1.08 (t, ³J_{HH} = 7.3 Hz, 12H, N-CH₂-**CH**₃). ¹³C NMR δ 6.72, 30.39, 33.84, 56.75, 58.51, 176.43, 181.95 ppm.

4.1.7 Tetraethylammonium L-glutamate, ([N₂₂₂₂][glu])

Proton NMR spectrum for tetraethylammonium L-glutamate (Appendix B-7) showed peaks in the ranged from δ 1.0 to 4.0 ppm. One multiplet signal at downfield region (δ 3.74–3.58 ppm) was attributed to O₂C-**CH** containing one proton. This can be explained because the proton was slightly deshielded due to the electronegativity of the attached nitrogen. Set of multiplet signal at δ 2.57–2.33 ppm, integrating for two protons was assigned to O₂-**CH**₂-. This was due to the hydrogen adjacent to the carbonyl group were slightly deshielded. The multiplet peaks for O₂-CH₂-**CH**₂ was observed between the ranged of δ 2.16–1.99 ppm which containing two protons.

¹H NMR (400 MHz, D₂O): δ 3.74–3.58 (m, 1H, O₂C-**CH**), 3.24 (q, ³J_{HH} = 7.3 Hz, 8H, N-**CH**₂), 2.57–2.33 (m, 2H, O₂-**CH**₂-), 2.16–1.99 (m, 2H, O₂-CH₂-**CH**₂), 1.25 (t, ³J_{HH} = 7.3 Hz, 12H, N-CH₂-**CH**₃). ¹³C NMR δ 6.70, 27.12, 33.62, 51.95, 54.68, 174.40, 180.94 ppm.

4.1.8 Tetraethylammonium L-methioninate, ([N₂₂₂₂][met])

The ¹H NMR spectrum (Appendix B-8) showed the characteristic downfield signal for O₂C-**CH** at δ 3.49–3.36 ppm. The multiplet peaks contained one proton was observed at this downfield signal because the proton was slightly deshielded due to the



electronegativity of the attached nitrogen. Meanwhile, the triplet signals containing two protons at δ 2.51 ppm and singlet signal containing three protons at δ 2.11 ppm was assigned to S-CH₂ and S-CH₃ respectively because the protons was deshielded due to the electronegativity of the attached sulphur. Another set of multiplet peaks at δ 1.82–1.99 ppm, integrating for two protons were assigned to CH-CH₂.

¹H NMR (400 MHz, D₂O): δ 3.49–3.36 (m, 1H, O₂C-CH), 3.25 (q, ³J_{HH} = 7.3 Hz, 8H, N-CH₂), 2.51 (t, ³J_{HH} = 8 Hz, 2H, S-CH₂), 2.11 (s, 3H, S-CH₃), 1.82–1.99 (m, 2H, CH-CH₂), 1.25 (t, ³J_{HH} = 7.3 Hz, 12H, N-CH₂-CH₃). ¹³C NMR δ 6.82, 14.35, 29.87, 33.90, 52.05, 55.30, 181.52 ppm.

4.1.9 Tetraethylammonium L-histidinate, ([N₂₂₂₂][his])

¹H NMR spectrum of the title compound is shown in Appendix B-9. Two singlet signals at downfield region at δ 7.65 and δ 6.91 ppm was attributed to alkenes in the five membered ring. This was due to the hydrogen atoms attached to a double bond were deshielded by the anisotropy of the adjacent double bond and electronegativity of nitrogen atoms. Meanwhile, the triplet signal at δ 3.49 was assigned to O₂C-CH because the hydrogen was deshielded due to the electronegativity of the attached nitrogen. The doublet of doublet (dd) signals contributed to O₂C-CH-CH(α) and O₂C-CH-CH(β) peaks was observed at δ 2.97 ppm and δ 2.83 ppm respectively.

¹H NMR (400 MHz, D₂O): δ 7.65 (s, 1H, N=CH-NH), 6.91 (s, 1H, HN-CH=C), 3.49 (t, ³J_{HH} = 7.3 Hz, 1H, O₂C-CH), 3.19 (q, ³J_{HH} = 7.3 Hz, 8H, N-CH₂), 2.97 (dd, ²J_{H α H β} = 12.5 Hz, ³J_{HH} = 5.5 Hz, 1H, O₂C-CH-CH(α)), 2.83 (dd, ²J_{H α H β} = 12.5 Hz, ³J_{HH} = 7.0 Hz, 1H, O₂C-CH-CH(β)), 1.22 (t, ³J_{HH} = 7.3 Hz, 12H, N-CH₂-CH₃). ¹³C NMR δ 6.64, 31.97, 51.94, 56.16, 118.08, 133.45, 135.84, 181.74 ppm.



4.1.10 Tetraethylammonium L-lysinate, ([N₂₂₂₂][lys])

The structure of tetraethylammonium L-lysinate was confirmed by the ¹H NMR analysis (Appendix B-10). A multiplet signal at downfield region was due to the O₂C-**CH** and tetraethylammonium peak at δ 3.13 ppm integrating nine protons respectively. The triplet signal at δ 2.51 ppm was assigned to the N-**CH**₂ containing two protons. This two downfield region peak was due to the electronegativity of the attached nitrogen. Set of multiplet signal at δ 1.52–1.41 ppm integrating for two protons was assigned to NC-**CH**₂ meanwhile set of multiplet signal at δ 1.36–1.31 ppm was assigned to the NH₂-CH₂-**CH**₂. Another set of multiplet signal at 1.25–1.19 ppm integrating for two protons was assigned to NC-CH₂-**CH**₂.

¹H NMR (400 MHz, D₂O): δ 3.13 (m, 9H, ³J_{HH} = 7.3 Hz, N-**CH**₂ and O₂C-**CH**), δ 2.51 (t, 2H, ³J_{HH} = 7.3 Hz, N-**CH**₂), δ 1.52 to 1.41 (m, 2H, NC-**CH**₂), δ 1.36 to 1.31 (m, 2H, NH₂-CH₂-**CH**₂), δ 1.25 to 1.19 (m, 2H, NC-CH₂-**CH**₂), δ 1.14 (t, 12H, ³J_{HH} = 7.3 Hz, N-CH₂-**CH**₃). ¹³C NMR δ 6.71, 22.43, 30.46, 34.42, 40.23, 52.01, 56.01, 183.45 ppm.

4.1.11 Tetraethylammonium L-tartrate, ([N₂₂₂₂][tar])

Appendix B-11 showed a singlet signal at downfield region. These singlet signals were assigned to the symmetry property of **CH** peak containing one proton at δ 4.50 ppm. This was due to the proton that is deshielded by the electronegative oxygen atom and shifted downfield in the spectrum. This structure was also reconfirmed by using single crystal X-ray diffraction analysis and will be discussed in Section 4.7.1 on page 63.

¹H NMR (400 MHz, D₂O): δ 4.50 (s, 1H, **CH**), δ 3.23 (m, 8H, ³J_{HH} = 7.3 Hz, N-**CH**₂), δ 1.24 (t, 12H, ³J_{HH} = 7.3 Hz, N-CH₂-**CH**₃). ¹³C NMR δ 6.68, 52.01, 73.05, 176.64.



4.1.12 Tetraethylammonium L-malate, ($[N_{2222}][mal]$)

The 1H NMR spectrum, (Appendix B-12) showed a multiplet signal at downfield region. These multiplet signals were assigned to the HO-**CH** peak containing one proton at δ 4.25 ppm. This was due to the proton that is deshielded by the electronegative oxygen atom. Meanwhile, doublet of doublet peaks (dd) and multiplet peaks at δ 2.71 and δ 2.51 ppm were attributed to **CH**₂ peak having two protons respectively. This structure was further confirmed by using single crystal X-ray diffraction analysis and will be discussed in Section 4.7.2 on page 68.

1H NMR (500 MHz, D₂O): δ 4.25 (m, 1H, $^3J_{HH} = 4$ Hz, HO-**CH**), δ 3.13 (q, 8H, $^3J_{HH} = 7.5$ Hz, N-**CH**₂), δ 2.71 (dd, 1H, $^3J_{HH} = 4$ Hz, **CH**₂), δ 2.51 (m, 1H, $^3J_{HH} = 8$ Hz, **CH**₂), δ 1.13 (t, 12H, $^3J_{HH} = 7.5$ Hz, N-CH₂-**CH**₃). ^{13}C NMR δ 6.67, 40.50, 52.01, 68.97, 176.83, 179.56.



4.2 Elemental Analysis (CHNS/O)

As shown in Table 5, the analytical data for all CILs produced were almost in agreement with the theoretical calculations. The percentages of errors were found around $\pm 2.0\%$. This may be due to the impurities present in CILs. Referring to the method for preparing the CILs, during the neutralization reaction, water was produced as a by-product. The small amount of water may still exist in CILs after the drying steps, which was due to the interaction such as H-bonding as the amino acids contain more than one functional groups. H-bonding between molecules of water and CILs is a strong interaction that means it can be very difficult to remove water in CILs.

Other than that, all CILs prepared were hygroscopic which easily absorbed water from air. This might be also the reason why the small amount of water contained in CILs as can be seen from their hydrogen and oxygen percentages. Other impurities could be due to the starting materials such as the slightly excess of amino acids that were used in order to counterion the tetraethylammonium hydroxide. During the filtration of residues, some amino acids might not be well filtered and still remained in CILs. This can be seen from their carbon and nitrogen percentages.

Table 5: Element analysis data for all CILs synthesized.

Entry	CILs	Percentage of element (%)				
		Carbon	Hydrogen	Nitrogen	Sulfur	Oxygen (by difference)
1	[N ₂₂₂₂][ser]	56.00	11.01	11.48	-	21.51
		(56.38)	(11.18)	(11.95)	-	(20.49)
2	[N ₂₂₂₂][pro]	63.53	11.23	11.07	-	14.17
		(63.89)	(11.55)	(11.46)	-	(13.10)
3	[N ₂₂₂₂][thr]	57.90	11.14	10.97	-	19.99
		(58.03)	(11.36)	(11.28)	-	(19.33)
4	[N ₂₂₂₂][ile]	64.25	12.24	9.76	-	13.75
		(64.57)	(12.39)	(9.89)	-	(13.15)
5	[N ₂₂₂₂][asn]	54.93	10.16	15.83	-	19.08
		(55.15)	(10.41)	(16.08)	-	(18.36)
6	[N ₂₂₂₂][gln]	56.38	10.34	15.04	-	18.24
		(56.70)	(10.61)	(15.26)	-	(17.43)
7	[N ₂₂₂₂][glu]	56.27	10.04	9.96	-	23.73
		(56.50)	(10.21)	(10.14)	-	(23.15)
8	[N ₂₂₂₂][met]	55.87	10.64	9.88	11.18	13.03
		(56.07)	(10.86)	(10.06)	(11.52)	(11.49)
9	[N ₂₂₂₂][his]	58.92	9.73	19.45	-	11.09
		(59.12)	(9.92)	(19.70)	-	(11.26)
10	[N ₂₂₂₂][lys]	59.83	10.92	14.38	-	14.87
		(61.05)	(12.08)	(15.26)	-	(11.61)
11	[N ₂₂₂₂][mal]	53.60	8.94	4.91	-	32.55
		(54.73)	(9.57)	(5.32)	-	(30.38)
12	[N ₂₂₂₂][tar]*	50.53	9.09	3.28	-	37.10
		(51.60)	(9.02)	(5.01)	-	(34.37)

Value in bracket from calculated/theory

* Not be considered as ILs due to high m.p (>100 °C)

4.3 Colour of CILs

From Table 6, it can be seen that a series of colour of the new CILs ranges from colourless liquids to orange solid. During the preparation, we observed the colour changes even more obvious when heated at 70 °C while removing traces amount of water. Only [N₂₂₂₂][pro], [N₂₂₂₂][ile] and [N₂₂₂₂][met] showed a yellowish liquids, meanwhile [N₂₂₂₂][ser] showed a orange liquid. Similar results were obtained for amino acid-based ILs synthesized by Allen *et al.* (2006). ILs in their work showed significant darkening when heated to temperatures of 110 °C or more.

Table 6: Physical properties, percentage yield (%), melting temperature (T_m) and solubility data of CILs

CILs	Physical Properties	Yield (%)	Melting Temperature ($T_m/^\circ\text{C}$)	Solubility Test				
				H ₂ O	MeOH	EtOH	Ace	Hex
[N ₂₂₂₂][ser]	Orange liquid	96	-	√	√	√	x	x
[N ₂₂₂₂][pro]	Yellowish liquid	90	-	√	√	√	x	x
[N ₂₂₂₂][thr]	Colourless liquid	94	-	√	√	√	x	x
[N ₂₂₂₂][ile]	Yellowish liquid	87	-	√	√	√	x	x
[N ₂₂₂₂][asn]	White solid	92	58.0 ± 1.0	√	√	√	x	x
[N ₂₂₂₂][gln]	Colourless liquid	91	-	√	√	√	x	x
[N ₂₂₂₂][glu]	Colourless liquid	89	-	√	√	√	x	x
[N ₂₂₂₂][met]	Yellowish liquid	95	-	√	√	√	x	x
[N ₂₂₂₂][his]	Orange solid	86	54.0 ± 1.0	√	√	√	x	x
[N ₂₂₂₂][lys]	Colourless liquid	90	-	√	√	√	x	x
[N ₂₂₂₂][mal]	White solid	99	87.7 ± 0.4	√	√	√	x	x
[N ₂₂₂₂][tar]*	White solid	98	198 ± 1.0	√	√	√	x	x

√ = miscible; X = immiscible

* Not be considered as ILs due to high m.p (> 100 °C)

The different colour of CILs not only caused by the heating procedure, but it can also be explained due to the different anions. Different anions used gave a different colour to the CILs produced. Not all liquid CILs change their colour when heated. [N₂₂₂₂][thr], [N₂₂₂₂][gln], [N₂₂₂₂][glu] and [N₂₂₂₂][lys] maintained their colors when put under vacuum for two days at 65 °C. Meanwhile for solid CILs, only [N₂₂₂₂][his] showed an orange solid compared to the others which observed in white solid. The nature of these colored impurities is yet unknown, as they are not detectable by NMR or other spectroscopic methods.

4.4 Melting Temperature (T_m)

It is well known that the characteristic properties of ILs vary with the choice of anion and cation. The structure of ILs directly impacts upon its properties, in particular the melting point and liquids ranges (Wasserscheid and Welton, 2003). Melting temperature (T_m) of CILs was measured using DSC and the results were presented in Table 6 (page 50). In this work, only four compounds showed a T_m which are two derived from amino acids and another two derived from plant acids.

In comparison, one compound derived from plant acids ([N₂₂₂₂][tar]) showed a highest T_m which was 198 ± 1.0 °C. Because of this compound had T_m above 100 °C, it will not be considered as ILs and will not further explore except for Single X-ray Crystallography analysis. Compound [N₂₂₂₂][tar] did not fulfill the characteristic of ILs with relatively low T_m below 100 °C. On the other hand, [N₂₂₂₂][mal] (T_m 87.7 ± 0.4 °C) have a lower T_m compared to [N₂₂₂₂][tar]. It can be elucidated the non-existence of intermolecular H-bonding between cation and anion in the compound, therefore the ions are most likely to be held together by Coloumbic interactions (Abdul Rahman *et al.*, 2009). Furthermore, the

packing efficiency and T_m were reduced because cation and anion were regarded as two separated units.

Meanwhile, for CILs derived from amino acids, [N₂₂₂₂][his] ($T_m = 54.0 \pm 1.0$ °C) have lower T_m compared to [N₂₂₂₂][asn] ($T_m = 58.0 \pm 1.0$ °C). The increment in anion size in [N₂₂₂₂][his] decreased the T_m of salts through reduction of *Coloumbic* attraction contribution to lattice energy. Similar ILs derived from amino acids has been synthesized by Fukumoto *et al.* (2005). However in their work, alkyimidazolium-based which is 1-ethyl-3-methylimidazolium, ([emim]) was used as a cation with 20 amino acids as a counterion. They reported amino acid ILs based on [emim] cation did not have T_m , but a glass transition temperature (T_g) ranging from -65 to 6 °C. In the measurement, the CILs produced from amino acids had no T_g when the temperature programmed was set up in the range of -60 to 130 °C. According to Jiang *et al.* (2008), they found that the T_g for tetraalkylammonium-based amino acids was in the range of -60 to -80 °C.

In comparison, tetraethylammonium-based CILs synthesized in this work has relatively high T_m compared to alkyimidazolium-based amino acids synthesized by Fukumoto *et al.*, (2005). The high T_m in tetraethylammonium-based CILs was probably due to the charge localization on the nitrogen atom in tetraethylammonium cation (Figure 4a), meanwhile low T_m of alkyimidazolium-based is because the ring is aromatic structure, which facilitates the charge delocalization (Figure 4b). This effect is responsible for lowering the *Coloumbic* forces and reduces the attraction forces between the cation and the anion thus lowering the T_m for alkyimidazolium-based amino acids (Jiang *et al.*, 2008).

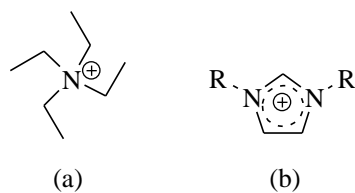


Figure 4: The structure of tetraethylammonium cation (a) and alkyimidazolium cation (b).

Although *Coulombic* forces are one of the factors involved in order to understand T_m , the effect of chains length should also be considered. Increasing the chain length of cations reduced the T_m values. As reported by Wasserscheid and Welton (2003), imidazolium-based ILs decreased the T_m with increasing chain lengths up to C₆-chain. As a comparison with tetrabutylammonium asparaginate ([TBA][asn], T_m 42–44 °C) synthesized by Allen *et al.* (2006), higher T_m was observed for tetraethylammonium L-asparaginate ([N₂₂₂₂][asn], $T_m = 58.0 \pm 1.0$ °C). The value of T_m decreased almost 15 °C between these two ILs because of the side chains of tetraalkylammonium that increased from –ethyl to –butyl.

4.5 Solubility in Organic Solvents

Solubility of the solute, the reaction efficiency as solvent, and the miscibility with other solvents are influenced by the ILs properties (Crowhurst *et al.*, 2004). The solubility of the synthesized CILs in various VOSs has been determined (Table 6, page 50). The results showed that all CILs are miscible with water and some polar organic solvents such as methanol (MeOH) and ethanol (EtOH) but immiscible in non-polar solvents such as acetone and hexane.

For all CILs, they showed a similar pattern which the deprotonation of carboxylic acid residue to form carboxylate during neutralization reaction as shown in Scheme 9. The hydrogen bonds between O–H were broken and the proton became mobile. The interaction of proton and hydroxyl by H–bonding formed water molecules as by-products. The deprotonated carboxylic group has an increase polarity of the CILs (real negative charge) in comparison to the ester group (partial negative charge).



Scheme 9: Deprotonation of carboxylic acid residue by hydroxide ion to form carboxylate ion and water as by-product.

As a conclusion, all new CILs synthesized have a polarity almost similar to polar organic solvents. Additionally, they can be called ‘hydrophilic CILs’ because it was easily dissolved in water (Seddon, 1997). Holbrey and Seddon, (1999) reported that the solubility of ILs in water depends on the nature of the anions and cations. Generally, an increase in the organic character of the cation resulted in a decrease of water solubility of ILs (Wasserscheid and Welton, 2003).

In this work, the same cation was used for all CILs produced but different in the structure of anions. Overall, it can be seen that all anions used have more than one functional groups such as alcohol, carboxylic acid and amine. These functional groups increased the hydrophilic character of the ILs as well as the solubility.

4.6 Thermogravimetric Analysis (TGA)

The thermal stability of ILs is defined by the strength of their heteroatom-carbon and heteroatom-hydrogen bonds (Anouti *et al.*, 2008). The starting temperature (T_{start}) and onset temperature (T_{onset}) for all CILs was summarized in Table 7, meanwhile the thermograms for all CILs produced were showed in Appendix C. For most of CILs, the thermograms showed one major decomposition temperature in the range of 160 to 210 °C. From the results, it was clearly shown that tetraethylammonium-based CILs have lower thermal stability but higher than the minimum 100 °C (Wasserscheid *et al.*, 2002).

Table 7: Starting temperature (T_{start}) and onset temperature (T_{onset}) for tetraethylammonium-based chiral ionic liquids.

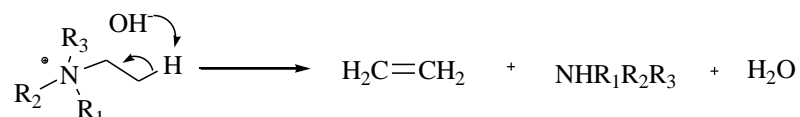
CILs	$T_{\text{start}}/^{\circ}\text{C}$	$T_{\text{onset}}/^{\circ}\text{C}$
[N ₂₂₂₂][ser]	146.67	187.62
[N ₂₂₂₂][pro]	134.69	172.92
[N ₂₂₂₂][thr]	145.72	188.72
[N ₂₂₂₂][ile]	131.61	168.98
[N ₂₂₂₂][asn]	146.63	191.88
[N ₂₂₂₂][gln]	168.27	210.40
[N ₂₂₂₂][lys]	132.97	181.00
[N ₂₂₂₂][glu]	136.46	210.30
[N ₂₂₂₂][met]	133.42	176.15
[N ₂₂₂₂][his]	140.59	174.69
[N ₂₂₂₂][mal]	174.91	210.76

Low thermal stability of tetraethylammonium-based CILs was influenced by the cation. Similar ILs derived from amino acids have been synthesized by Fukumoto *et al.* (2005). They reported that synthesized alkylimidazolium-based ILs (1-ethyl-3-



methylimidazolium, [emim]) have the decomposition temperature (T_d , onset) around 220 °C except for [emim][cys] at 173 °C. As a comparison for both cations, it showed that tetraethylammonium-based ILs have a decomposition temperature at 35 °C lower than alkylimidazolium cation with the same anions.

According to the observation, tetraethylammonium cation has a lower stability than the alkylimidazolium cation. This can be explained that the quaternary ammonium salts in an alkaline environment that are sensitive to the *Hofmann* degradation as reported by Cope and Trumbull, (1960). Alkaline environment in this work came from the ionized amino acids. MacFarlane *et al.* (2006) reported in their work that the ionized amino acids are slightly basic and the mechanism of decomposition is probably related to the *Hoffman* elimination reaction. A schematic presentation of this decomposition path is presented in Scheme 10.



Scheme 10: Schematic presentation of the *Hoffman* degradation reaction

High decomposition temperature of alkylimidazolium-based ILs compared to our synthesized CILs can also be explained due to the pyrolysis of the alkylimidazolium-based salts (Awad *et al.*, 2004). The pyrolysis of alkylimidazolium-based ILs have been reported to proceed most likely via S_N2 process. Therefore, changes in the basicity and/or nucleophilicity of the anions are likely to change the thermal stability (Awad *et al.*, 2004).

Seven new tetraalkylammonium-based amino acids ([TAA][amino acids]) have been synthesized by Jiang *et al.* (2008). They reported that the decomposition values of the ILs in the range of 170 to 200 °C are based on different tetraalkylammonium with three amino acids which are L- and β -alanine, valine and glycine as counterions which was in agreement with our results.

Anions also play an important factor when determining the thermal stability. For CILs derived from chiral plant acid, thermogram showed one major weight losses for [N₂₂₂₂][mal] as shown in Appendix C-11. The first drop which almost 5 % in weight stopped below 100 °C due to moisture adsorbed by the sample and the major weight losses started at temperature \pm 170 °C. Almost 85 % in weight of sample was decomposed and the decomposition curve ended at 261.57 °C.

These CILs derived from plant acid also showed higher decomposition temperature (T_{onset}) compared to amino acids CILs (will be discussed in the next page). This might be due to the presence of hydroxyl group. Hydroxyl group allowed the molecules to form more H-bonding and thus have a strong interaction, therefore more energy (high temperature) was required to break the interaction and as a result, higher temperature decomposition was achieved. Figure 5 shown the structure of L(-)-malic acid.

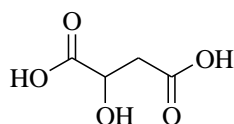


Figure 5: Structure of L(-)-malic acid contained two carboxylic acid moiety and one hydroxyl group.

In case of CILs derived from amino acids, ten different amino acids were employed in order to produce ten different CILs with the same cation which is tetraethylammonium cation ($[N_{2222}]$) as mentioned earlier. All of CILs produced from amino acids showed first drop in weight below 130 °C due to moisture adsorption by the samples except for $[N_{2222}][met]$ (Appendix C-8). Almost of all CILs showed one major weight losses with percentage of sample decomposed in the range of 87 to 98 % except for $[N_{2222}][asn]$, $[N_{2222}][his]$ and $[N_{2222}][gln]$ which showed two major weight losses (Appendix C-5, C-6 and C-9).

Various anions play a significant role in the thermal stability. Fredlake *et al.* (2004) reported that thermal stability depends on both anions and cations. Changing the anions gave a little difference to the decomposition temperature as well as thermal stability. T_{onset} as showed in Table 8 apparently followed the trend: $[N_{2222}][ile] < [N_{2222}][pro] < [N_{2222}][his] < [N_{2222}][met] < [N_{2222}][lys] < [N_{2222}][ser] < [N_{2222}][thr] < [N_{2222}][asn] < [N_{2222}][glu] < [N_{2222}][gln]$.

It is very difficult to explain how different amino acids gave different decomposition temperature for CILs produced, as known that amino acids have more than one functional groups in a single molecule and also different configurational structure. In order to understand the effect of various anions, the amino acids used were separated base on their functional groups present and the structure of amino acids. Figure 6 showed the basic structure of amino acids meanwhile Table 8 depicted their '**R**' structure, functional group present and T_{onset} .

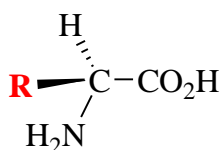


Figure 6: Basic structure of amino acids.

Table 8: Structure of 'R' amino acids, functional group present and T_{onset} for ten amino acids used in this work.

CILs	Structure of 'R'	Functional group presence	$T_{\text{onset}}/^{\circ}\text{C}$
[N ₂₂₂₂][ile]	$\begin{array}{c} \text{---CHCH}_2\text{CH}_3 \\ \\ \text{CH}_3 \end{array}$	Alkane (Neutral amino acid)	168.98
[N ₂₂₂₂][pro]*		Ring (Neutral amino acid)	172.92
[N ₂₂₂₂][his]		Aromatic ring (Imidazole)	174.69
[N ₂₂₂₂][met]	$\text{---CH}_2\text{CH}_2\text{SCH}_3$	Sulphur	176.15
[N ₂₂₂₂][lys]	$\text{---CH}_2\text{CH}_2\text{CH}_2\text{CH}_2\text{NH}_2$	Amine	181.00
[N ₂₂₂₂][ser]	$\text{---CH}_2\text{OH}$	Hydroxyl	187.62
[N ₂₂₂₂][thr]	$\begin{array}{c} \text{---CHOH} \\ \\ \text{CH}_3 \end{array}$	Hydroxyl	188.72
[N ₂₂₂₂][asn]	$\text{---CH}_2\text{CONH}_2$	Amide	191.88
[N ₂₂₂₂][glu]	$\text{---CH}_2\text{CH}_2\text{CO}_2\text{H}$	Carboxylic acid	210.30
[N ₂₂₂₂][gln]	$\text{---CH}_2\text{CH}_2\text{CONH}_2$	Amide	210.40

* The structure of 'R' is a five member ring with N atom (red colour)

From the results in Table 8, it was also found that T_{onset} followed the trend of the functional group present; alkane < ring < sulphur < amine < hydroxyl < amide \approx carboxylic acid. It showed that, the presence of different functional group in the structure of amino acids gave a different thermal stability to CILs produced. However, the other criteria should be considered in order to explain the thermal stability for each CILs because all CILs have different structure. The stereochemistry structure of each amino acid and other interaction such as H-bonding play an important factor when determining the decomposition temperature.

The presence of carboxylic acid (-COOH) and amide (-CONH₂) in the structure of glu and gln gave a better thermal stability for [N₂₂₂₂][glu] and [N₂₂₂₂][gln]. Both of glu (Figure 7a) and gln (Figure 7b) have a similar molecular structures but different in functional group present. The structure of glu have a -COOH meanwhile gln have -CONH₂ functional group. From the results, both of the CILs which were [N₂₂₂₂][glu] (T_{onset} 210.30 °C) and [N₂₂₂₂][gln] (T_{onset} 210.40 °C) have a similar thermal stability. We found that, both functional groups did not showed large effect towards the thermal stability of [N₂₂₂₂][Glu] and [N₂₂₂₂][Gln] while both amino acids structure (gln and glu) have a similar structural properties.

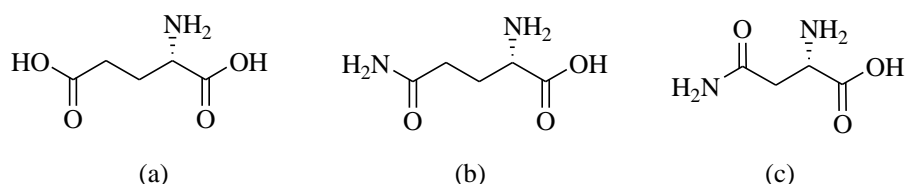


Figure 7: Structure of L-glutamic acid (glu) (a), L-glutamine (gln) (b) and L-asparagine (asn) (c)

Meanwhile, [N₂₂₂₂][asn] (T_{onset} 191.88 °C) have a slightly low thermal stability compared to [N₂₂₂₂][glu] and [N₂₂₂₂][gln]. This is maybe due to size of the molecules. L-asparagine (asn) has a similar functional group with gln, but diversified in number of carbon atom. L-gutamine (gln) (Figure 7b) have five carbon atoms meanwhile asn (Figure 7c) only have four, thus make asn a small molecule compared to gln. It can be concluded that, small molecule ([N₂₂₂₂][asn]) gave a low thermal stability compared to bigger ones ([N₂₂₂₂][gln]).

Figure 8 showed the structure for ser and thr. Both molecules showed similar properties but different in the hydroxyl group they were bonded to. Hydroxyl group in ser (Figure 8a) showed a primary alcohol (1°) meanwhile secondary alcohol (2°) was detected in thr (Figure 8b). Unfortunately, the thermal stability for [N₂₂₂₂][ser] (T_{onset} 187.62 °C) and [N₂₂₂₂][thr] (T_{onset} 188.72 °C) were almost same. This means that, the difference in primary or secondary alcohol place in both structures does not produce any impact towards their thermal stability.

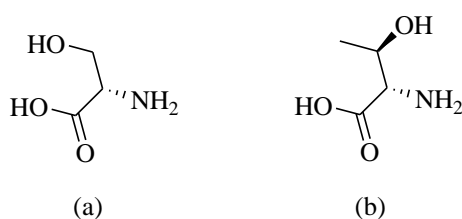


Figure 8: Structure of L-serine (ser) (a) and L-threonine (thr) (b)

As mention earlier, the presence of different functional group affected the thermal stability for all CILs including CILs derived from plant acids. But, others factor such as alkyl chains and configurational structures should be considered in order to understand their thermal stability. The structures of lys (Figure 9a) have a six carbon atoms that form long

alkyl chains compared to others amino acids. As comparison with met (Figure 9b), [N₂₂₂₂][lys] have a T_{onset} of 181.00 °C, a little bit higher than [N₂₂₂₂][met] (T_{onset} , 176.15 °C). This is may be due to the difference in alkyl chains lengths and also functional groups present.

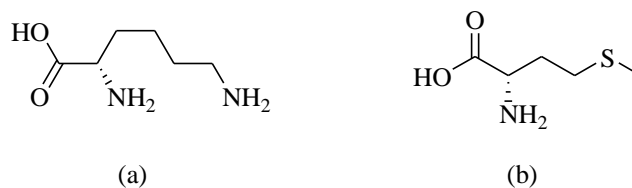


Figure 9: Structure of L-lysine (lys) (a) and L-methionine (met) (b)

From the results, [N₂₂₂₂][his] (T_{onset} 174.69 °C) and [N₂₂₂₂][pro] (T_{onset} 172.92 °C) have almost similar decomposition temperature meanwhile [N₂₂₂₂][ile] have the lowest T_{onset} 168.98 °C compared to all CILs produced. The structure of his (Figure 10a) formed a [N₂₂₂₂][his] and has a slightly high decomposition temperature due to its configurational structure and the presence of imidazole ring.

Meanwhile, without the presence of functional group in the structure of pro (Figure 10b) and ile (Figure 10c) (except for basic functional group for amino acids and alkane group) it was found that both neutral amino acids formed [N₂₂₂₂][pro] and [N₂₂₂₂][ile] have a low decomposition temperature. This might be due to branch alkyl chains or less other interaction such H-bonding.

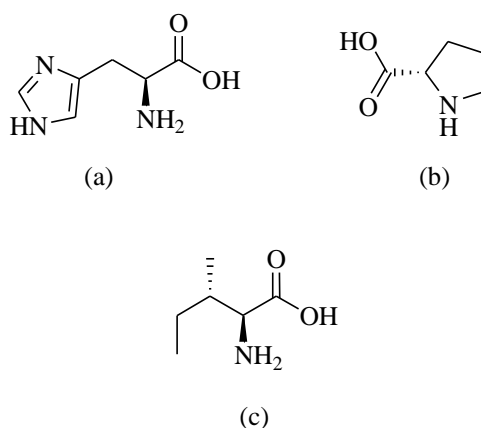


Figure 10: Structure of L-histidine (his) (a), L-proline (pro) (b) and L-isoleucine (ile) (c)

4.7 Single Crystal X-ray Crystallography

Two different crystal structures were obtained depending on the crystallization conditions. Both crystal structures, $[N_{2222}][tar]$ and $[N_{2222}][mal]$ were formed by slow evaporation of methanol after a few days at room temperature. The Single Crystal X-ray structure study was proposed to understand the H-bonding between cation and anion. H-bonding is an important feature in the solid state structure complexes. Publication for both compounds has not been reported yet and we are the first group to publish for these compounds (Abdul Rahman *et al.*, (2008), Abdul Rahman *et al.*, 2009)

4.7.1 Crystal Structure of Tetraethylammonium L-tartrate, ($[N_{2222}][tar]$)

The single crystal of tetraethylammonium L-tartrate contained a monoclinic crystal system with space group $P2_1$, $a = 7.4074(1)\text{\AA}$, $b = 13.8989(2)\text{\AA}$, $c = 8.0546(1)\text{\AA}$ together with $\alpha = 90^\circ$, $\beta = 106.5530(1)^\circ$ and $\gamma = 90^\circ$ respectively. The crystal data for this compound was summarized in Table 9 and the overall data was depicted in Appendix D.

Table 9: Crystal data and structure refinement for tetraethylammonium L-tartrate.

	Data
Empirical formula	C ₁₂ H ₂₉ N O ₈
Formula weight	315.36
Temperature	100.0 (1) K
Wavelength	0.71073 Å
Crystal system, space group	Monoclinic, <i>P</i> 2 ₁
Unit cell dimensions	a = 7.4074(1)Å α = 90° b = 13.8989(2)Å β = 106.5530(1)° c = 8.0546(1)Å γ = 90°
Volume	794.891(19) Å ³
Z, Calculated density	2, 1.318 Mg/m ³
Absorption coefficient	0.110 mm ⁻¹
F(000)	344
Crystal size	0.47 x 0.45 x 0.17 mm
Θ range for data collection	2.64 to 35.00°
Limiting indices	-9 ≤ h ≤ 11, -22 ≤ k ≤ 17, 12 ≤ l ≤ 12
Reflections collected / unique	10518 / 3579 [R(int) = 0.0307]
Completeness to Θ = 35.00	99.40 %
Absorption correction	Semi-empirical from equivalents
Max. and min. transmission	0.9811 and 0.8614
Refinement method	Full-matrix least-squares on F ²
Data / restraints / parameters	3579 / 1 / 218
Goodness-of-fit on F ²	1.049
Final R indices [I > 2σ(I)]	R1 = 0.0371, wR2 = 0.0886
R indices (all data)	R1 = 0.0426, wR2 = 0.0922
Largest diff. peak and hole	0.292 and -0.231 e.Å ⁻³

The asymmetric unit of the title compound contains a tartarate anion as a counterion, a tetraethylammonium cation and two water molecules of crystallization in the structure (Figure 11). Two intermolecular C—H---O hydrogen bonds involving O4 as a bifurcated acceptor link anion and cation in the asymmetric unit to form a seven membered ring, with $R^1_2(7)$ ring motif (Bernstein *et al.*, 1995). These formation of anion-cation pairs connected by two H-bonding was found with C8—H8---O4 distance of 0.96 Å or O---O distance of 3.34 Å and C11—H11---O4 distance of 0.97 Å or O---O distance 3.26 Å, respectively.

No H-bonding could be observed between different anion-cation pairs in the structure of $[N_{2222}][tar]$. In the crystal structure, the ionic units and water molecules are linked via O—H---O and C—H---O hydrogen bonds, forming a two-dimensional network parallel to the (001). Two water molecules are coordinated to tartarate anion. The O1—C1—O2 angle of the carboxylic group is 124.88 °. This is in good agreement with the average bond angle found in *Cambridge Structural Database* (CSD). The molecular structure of a hydrogen-bonded anion-cation pair of $[N_{2222}][tar]$ is shown in Figure 11. In Figure 12, the packing of the molecules in the crystal structure is presented meanwhile H-bonding geometry (Å) was showed in Table 10.

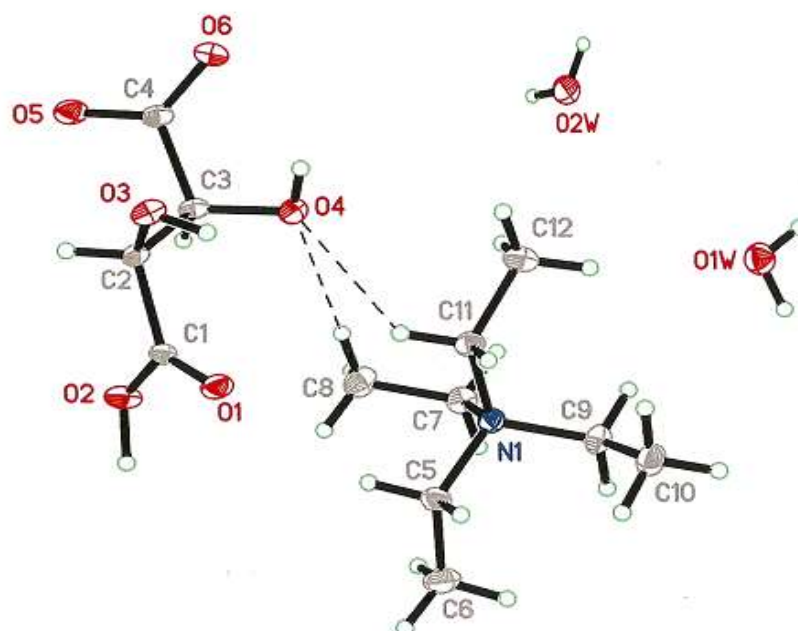


Figure 11: Molecular structure of tetraethylammonium L-tartrate determined by single crystal X-ray diffraction. Hydrogen bonds between anion-cation are shown as dashed lines.

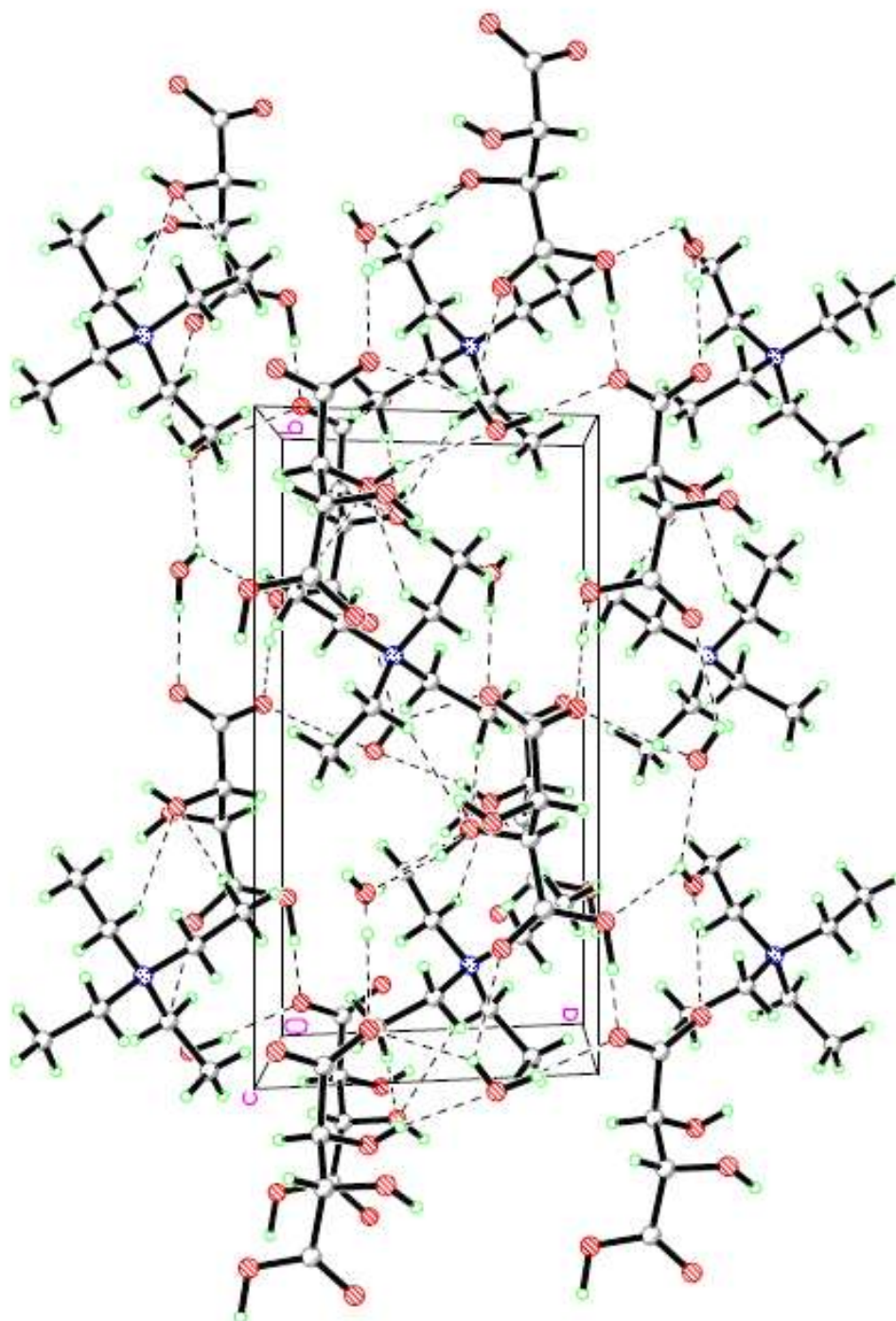


Figure 12: The crystal packing of tetraethylammonium L-tartrate, view down the c-axis.

Hydrogen bonds are shown as dashed lines.

Table 10: Hydrogen-bond geometry (Å) for tetraethylammonium L-tartrate.

D-H---A	D-H	H---A	D---A	D-H---A
O2-H1O2---O5 ⁱ	1.00 (2)	1.52 (2)	2.5108 (13)	173 (2)
O3-H1O3---O1W ⁱⁱ	0.91 (2)	1.85 (2)	2.7191 (14)	162 (2)
O4-H1O4---O2W ⁱⁱⁱ	0.84 (2)	2.18 (2)	2.9780 (16)	160 (2)
O1W-H1W1---O2 ^{iv}	0.82 (2)	2.56 (2)	3.0668 (14)	122 (2)
O1W-H1W1---O2W ^{iv}	0.82 (2)	2.57 (2)	3.2155 (16)	137 (2)
O1W-H2W1---O6 ⁱⁱⁱ	0.88 (3)	2.00 (3)	2.8672 (15)	171 (2)
O2W-H2W2---O1 ^{vi}	0.84 (2)	2.40 (2)	3.0082 (14)	129 (2)
C5-H5A---O3 ^{vii}	0.97	2.56	3.4344 (15)	151
C8-H8B---O4	0.96	2.38	3.3447 (16)	178
C10-H10B---O3 ^{vii}	0.96	2.47	3.4195 (16)	168
C11-H11A---O4	0.97	2.50	3.2693 (15)	136

Symmetry codes: (i) $-x + 2, y - \frac{1}{2}, -z$; (ii) $x, y, z - 1$; (iii) $-x + 1, y - \frac{1}{2}, -z + 1$; (iv) $x - 1, y, z + 1$; (v) $-x + 1, y - \frac{1}{2}, -z + 2$; (vi) $x, y + 1, z + 1$; (vii) $-x + 1, y - \frac{1}{2}, -z$.

4.7.2 Crystal Structure of Tetraethylammonium L-malate, ([N₂₂₂₂][mal])

The crystal structure of tetraethylammonium L-malate contained a monoclinic crystal system with $P2_1$ space group similar to the previous one. This crystal showed a unit cell dimensions, $a = 7.4724(2)\text{Å}$, $b = 19.9721(5)\text{Å}$, $c = 10.2726(3)\text{Å}$, $\gamma = 90^\circ$ $\beta = 92.481(1)^\circ$ and $\alpha = 90^\circ$. The crystal data was summarized in Table 11 and the atomic coordinates, bond lengths and angles, anisotropic displacement parameters, hydrogen coordinates and torsion angles are shown in Appendix E.

Table 11: Crystallographic details of the presented crystal structures for tetraethylammonium L-malate.

	Data
Empirical formula	$C_{24} H_{56} N_2 O_{13}$
Formula weight	580.71
Temperature	100.0(1) K
Wavelength	0.71073 Å
Crystal system, space group	Monoclinic, $P2_1$
Unit cell dimensions	$a = 7.4724(2)\text{Å}$ $\alpha = 90^\circ$ $b = 19.9721(5)\text{Å}$ $\beta = 92.481(1)^\circ$ $c = 10.2726(3)\text{Å}$ $\gamma = 90^\circ$
Volume	$1531.64(7)\text{Å}^3$
Z, Calculated density	2, 1.259 Mg/m ³
Absorption coefficient	0.101 mm^{-1}
F(000)	636
Crystal size	0.45 x 0.35 x 0.32 mm
Θ range for data collection	2.23 to 38.06°
Limiting indices	$-12 \leq h \leq 12$, $-34 \leq k \leq 29$, $-15 \leq l \leq 17$
Reflections collected / unique	36497 / 8479 [R(int) = 0.0291]
Completeness to $\Theta = 35.00$	99.10 %
Absorption correction	Semi-empirical from equivalents
Max. and min. transmission	0.9685 and 0.9560
Refinement method	Full-matrix least-squares on F^2
Data / restraints / parameters	8479 / 1 / 372
Goodness-of-fit on F^2	1.039
Final R indices [$I > 2\sigma(I)$]	R1 = 0.0456, wR2 = 0.1197
R indices (all data)	R1 = 0.0527, wR2 = 0.1247
Largest diff. peak and hole	0.625 and -0.804 e.Å^{-3}

Unlike from previous crystal, the asymmetric unit for this compound was composed of two crystallographically independent ion pairs, with similar conformations and three water molecules of crystallization (Figure 13). One of the water molecules (O1W) was partially occupied with a site-occupancy factor of 0.721 (5). The bond lengths and angles were within normal ranges (Allen *et al.*, 1987). In the crystal structure, there was no intermolecular interaction between cation-anion pair, but it had two intramolecular interactions in anion. Intramolecular O3A—H3OA---O5A and O3B—H3OB---O5B have a similar distance of 0.82 Å (or O—O distance of 2.68 Å) hydrogen bonds form S(5) ring motifs (Bernstein *et al.*, 1995).

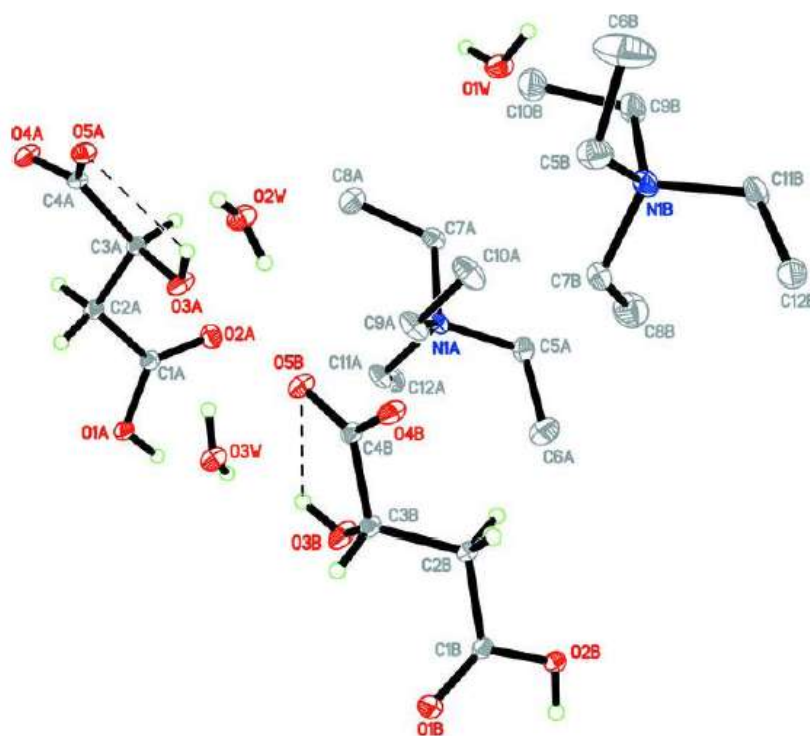


Figure 13: The molecular structure of tetraethylammonium L-malate with atoms label and 40 % probability ellipsoids for non-H atoms. The hydrogen atoms of the cations were omitted for clarity. Intramolecular interactions are shown as dashed lines.

In the crystal structure, the molecules were linked together by water molecules through a direct four membered O—H---O—H---O—H interactions to form one dimension infinite chains along the a-axis. Since the molecules were also linked into one dimension infinite chains along the b-axis, molecular sheets parallel to the (001)-plane were created (Figure 14). The crystal structure was stabilized by two intramolecular O—H---O hydrogen bonds, nine intermolecular O—H---O and ten C—H---O hydrogen bonds. Table 12 showed hydrogen-bond geometry (Å) for tetraethylammonium L-malate.

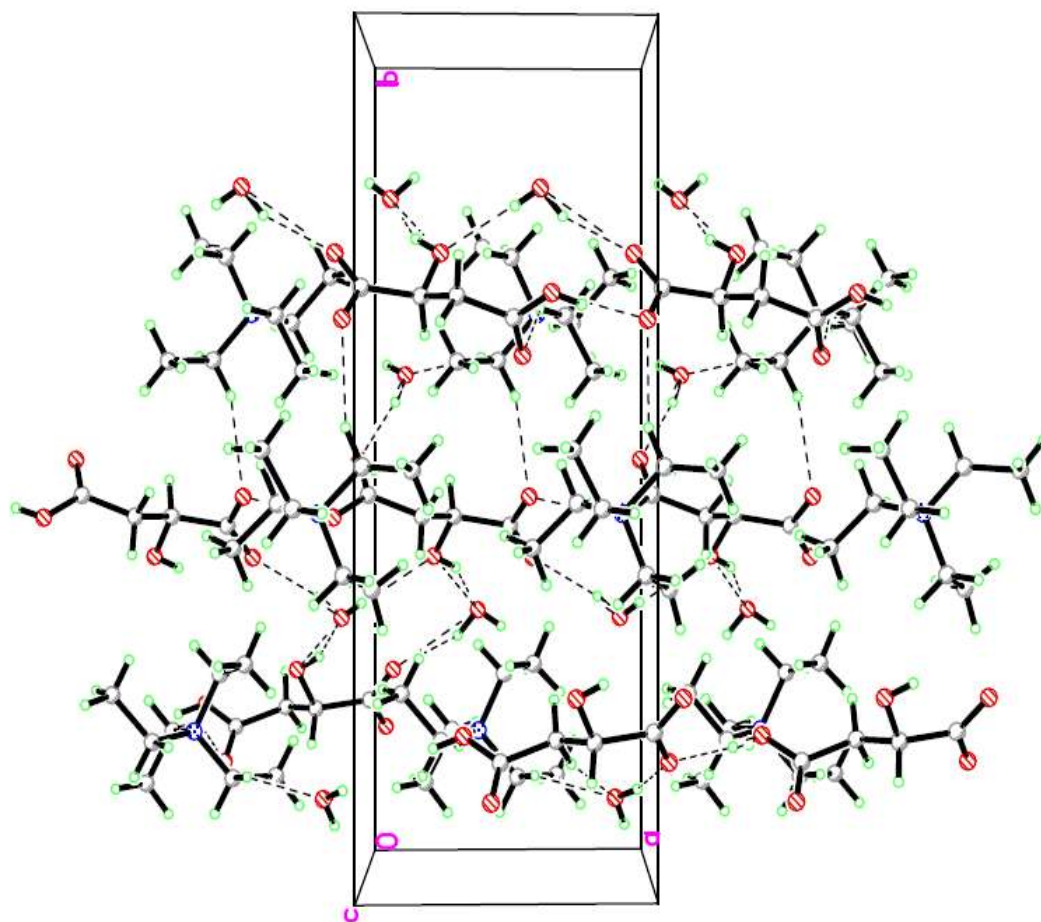


Figure 14: The crystal packing of tetraethylammonium L-malate, view down the c axis showing infinite 1-D chain along the a- and b-axes of the unit cell. Intermolecular interactions are shown as dashed lines.

Table 12: Hydrogen-bond geometry (Å) for tetraethylammonium L-malate

D-H...A	D-H	H...A	D...A	D-H...A
O1A-1OA---O4A ⁱ	0.82	1.68	2.4968 (12)	171.0
O3A-3OA---O2W	0.82	2.00	2.7292 (15)	149.0
O3A-3OA---O5A	0.82	2.24	2.6850 (13)	114.0
O3B-3OB---O3W	0.82	2.00	2.7438 (16)	151.0
O3B-3OB---O5B	0.82	2.26	2.6827 (13)	112.0
O1W-1W1---O4A ⁱⁱ	0.92	2.03	2.9359 (19)	166.0
O1W-2W1---O1B ⁱⁱⁱ	0.92	1.90	2.8020 (2)	165.0
O2W-1W2---O5B	0.84	1.99	2.7962 (14)	162.0
O2W-2W2---O3B ^{iv}	0.65	2.25	2.8969 (14)	175.0
O3W-2W3---O3A	0.75 (3)	2.17 (3)	2.9163 (14)	176.6 (19)
O3W-1W3---O5A ⁱ	0.87 (2)	1.98 (2)	2.7907 (14)	155.0 (2)
C2A-2AB---O1W ^v	0.97	2.44	3.3850 (2)	165.0
C5A-5AA---O1A ⁱⁱ	0.97	2.41	3.2826 (16)	149.0
C7A-7AA---O1W	0.97	2.42	3.2510 (2)	144.0
C11A-11B---O2A	0.97	2.53	3.2863 (16)	135.0
C7A-7AB---O4B ⁱⁱⁱ	0.97	2.46	3.3810 (17)	157.0
C5B-5BB---O4A ^{vi}	0.97	2.50	3.4140 (2)	156.0
C7B-7BB---O2B ^{iv}	0.97	2.47	3.4332 (16)	170.0

Symmetry codes: (i) $x + 1, y, z$; (ii) $x, y, z - 1$; (iii) $-x + 1, y - 1/2, -z + 1$; (iv) $x - 1, y, z$; (v) $x, y, z + 1$; (vi) $-x, y + 1/2, -z + 1$; (vii) $-x, y + 1/2, -z$.



4.8 Optical Rotation, ($[\alpha]_D^{25}$)

In this research, each CILs derived from amino acids and plant acids have a chiral structure. The optical rotation values were measured in aqueous solution with concentration for all CILs and starting acids at 1 g/100 mL. Measurements of optical rotation were performed at 25 °C and the results were tabulated in Table 13. The results showed the magnitudes of optical rotation of CILs which were smaller than starting acids except for [N₂₂₂₂][gln], [N₂₂₂₂][glu], [N₂₂₂₂][met] and [N₂₂₂₂][mal].

Table 13: Optical rotation value ($[\alpha]_D^{25}$) for starting acids and CILs at 25 °C

Compound	Value of Starting Acids	Value of CILs
[N ₂₂₂₂][ser]	- 7.5	- 1.5
[N ₂₂₂₂][pro]	- 84.8	- 42.9
[N ₂₂₂₂][thr]	- 28.6	- 3.8
[N ₂₂₂₂][iso]	+ 11.3	+ 4.9
[N ₂₂₂₂][asn]	- 6.5	- 5.1
[N ₂₂₂₂][gln]	+ 6.3	- 7.4
[N ₂₂₂₂][glu]	+ 11.8	- 2.1
[N ₂₂₂₂][met]	- 7.8	+ 1.1
[N ₂₂₂₂][his]	- 38.9	- 5.2
[N ₂₂₂₂][lys]	+ 12.3	+ 6.9
[N ₂₂₂₂][mal]	-4.8	- 7.4

Interestingly, for [N₂₂₂₂][gln] and [N₂₂₂₂][glu], the direction of optical rotation was different between starting acids and CILs. Both of these starting materials showed a clockwise $[\alpha]_D^{25}$ value, but anti-clockwise $[\alpha]_D^{25}$ value for CILs. From the results, it explained that the direction of plane rotation of the polarized light was at the opposite of the starting acids. Allen *et al.* (2006) reported the optical rotation value for entire



tetrabutylammonium-based amino acids were found to become much smaller than this work except for [TBA][L-met]. This phenomenon also has been previously observed for a variety of amino acids in the presence of an acid or a base (Ding and Armstrong, 2005).

Furthermore, the variation of the optical rotation value of the CILs cannot be compared in any meaningful way to that of the free of amino acids as *ab initio* calculations have shown that variations in conformational structure resulted in variation of the optical rotation value (Pecul, 2006 and Pecul *et al.*, 2004). Meanwhile, for CILs derived from plant acids, the magnitudes of optical rotation for [N₂₂₂₂][mal] was observed much bigger than the starting acid.

4.9 Viscosity and Ionic Conductivity

ILs in general are more viscous than most common solvents. ILs' viscosity at ambient temperature range from around 10 cP to values in excess of 1000 cP. For comparative purposes, the viscosity of water, ethylene glycol and glycerol at room temperature were at 0.89, 16.10 and 934.00 cP. Meanwhile for ionic conductivity properties, ILs also have good ionic conductivities compared to organic solvents/electrolyte systems (up to 10 mS cm⁻¹) (Galinski *et al.*, 2006). Viscosity and ionic conductivity for CILs in room temperature are listed in Table 14. Only CILs in a liquid form have been analyzed.

Table 14: Molecular weight (Mw), viscosity and ionic conductivity data for CILs produced at 25 °C.

CILs	Mw* (g mol ⁻¹)	Viscosity (cP)	Ionic Conductivity (mS/cm)
[N ₂₂₂₂][ser]	234.34	1763	0.16
[N ₂₂₂₂][pro]	244.37	438	0.46
[N ₂₂₂₂][thr]	248.36	1002	0.24
[N ₂₂₂₂][ile]	260.42	526	0.35
[N ₂₂₂₂][asn]	261.36	a	a
[N ₂₂₂₂][gln]	275.39	a	a
[N ₂₂₂₂][lys]	275.43	352	0.54
[N ₂₂₂₂][glu]	276.37	a	a
[N ₂₂₂₂][met]	278.45	462	0.45
[N ₂₂₂₂][his]	284.40	a	a
[N ₂₂₂₂][mal]	263.33	a	a

a = solid or glass at 25 °C, hence the property was not determined; * from calculated/theory

Abbot *et al.*, (2006) reported that viscosity of ILs is dependant on the size of molecules. Large molecules of ILs give a high viscosity compared to small molecules. Conversely, in this study we found that the size of molecule does not influence the viscosity and ionic conductivity. In a series of CILs from amino acids containing the same cation with different anions clearly affects both viscosity and ionic conductivity. The order of increasing viscosity with respect to the anion is: [C₆H₁₃N₂O₂]⁻ (Lys) < [C₅H₈NO₂]⁻ (Pro) < [C₅H₁₀NO₂S]⁻ (Met) < [C₆H₁₂NO₂]⁻ (Ile) < [C₄H₈NO₃]⁻ (Thr) < [C₃H₆NO₃]⁻ (Ser). However, these trends do not exactly correlate with the anions size. This may be due to the effect of anion's property on the viscosity such as their ability to form H-bonding. Meanwhile, the order of increasing ionic conductivity is reversible from the order of increasing viscosity.

The symmetry of cations also affected the slightly changes in viscosity. In this research, tetraethylammonium cation ($[N_{2222}]$) has been used in synthesizing CILs which is large symmetrical molecule. Jiang *et al.* (2008) reported that [TAA][amino acids] composed of asymmetric cations (such as $[N_{1112}]$ and $[N_{1113}]$) and small amino acid anions of simple structure may be expected to have lower viscosity than the symmetric cations with similar amino acid anions. As a general rule, symmetric cations usually cause high viscosity of aliphatic ammonium-based ILs (McFarlane *et al.*, 2004). As described earlier, quaternary ammonium used in this work, have symmetry properties as shown in Figure 15, thus increasing the viscosity of CILs.

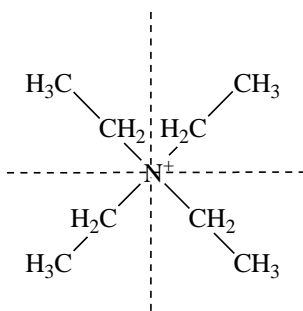


Figure 15: Symmetry properties of tetraethylammonium cation.

From the results in Table 14, the different for viscosity and ionic conductivity was strongly influenced by the different of anion used. In details, the side chains of the corresponding amino acids anions and H-bonding in the structure of CILs were strongly affecting the viscosity and ionic conductivity (Fukumoto *et al.*, 2005). As mention earlier, amino acids have more than one functional groups. This implies that some intra- and intermolecular interactions influenced in the ILs structure. In other words, introduction of a functional group such as H-bonding donor or acceptor increased the viscosity and decreased the ionic conductivity through intra/intermolecular interactions (Ohno and Fukumoto, 2007).

[N₂₂₂₂][ser] and [N₂₂₂₂][thr] have relatively low ionic conductivity, may be due to H-bonding or some other ion interactions which were expected through their side chains. The presence of hydroxyl group (–OH) allowed the molecule to form H-bonding through inter/intramolecular interactions in the structure of CILs, thus the existence of strong H-bonding and cause high viscosities and low ionic conductivities.

Another factor that influences the viscosity and ionic conductivity is the side chains of amino acids itself. The rotation volume in branch side chain of Ile will be decreased if compared to a straight alkyl chain. Thus, it will eventually increase the viscosity and decrease the ionic conductivity of [N₂₂₂₂][ile]. However, the result for viscosity of [N₂₂₂₂][ile] is slightly lower than [N₂₂₂₂][thr] and [N₂₂₂₂][ser], because of no hydroxyl group present in the structure of [N₂₂₂₂][ile].

The difference between met and ile were caused by the presence of the methyl group. Structure of met has only one methyl group compare to ile which has two methyl groups. As reported by Tamar *et al.* (2006), the increase of viscosity also due to the substituted methyl group. Methyl group has a significant effect, observed from the increased of a –CH₂ linkage in the alkyl chain, which is due to the increment of the asymmetry of the molecules.

The relationship between the component ion structures with viscosity and ionic conductivity is not fully understood, probably because there are several parameters, such as shape of ions, charge density, contribution of other interaction forces and conformational change of alkyl chain involved in the structure of ILs (Ohno, 2006).

Meanwhile, Figure 16 showed the strong linear correlation between the ionic conductivity and the viscosity of CILs. When viscosities decrease, the ionic conductivities increase or vice versa. Ionic conductivity in this work showed lower conductivities but slightly higher compared to alkyimidazolium-based amino acids synthesized by Fukumoto *et al.* (2005). This was due to the size of cation. Large cation tends to lower the ionic conductivity, most probably due to the lower mobility of the larger cations (Wassercheid and Welton, 2003).

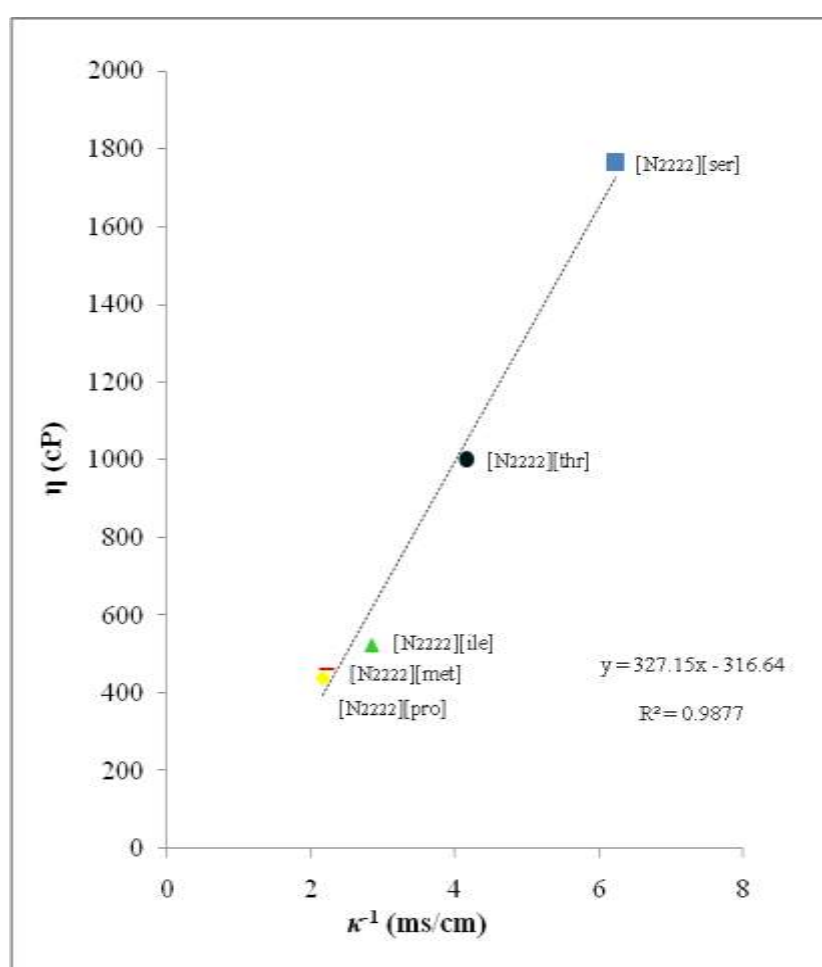


Figure 16: Relationship between ionic conductivity and viscosity at 25 °C.

In the group of alkyimidazolium-based ILs, [emim][gly] has the lowest viscosity of 486 cP at 25 °C. A few of [N₂₂₂₂][amino acids] CILs synthesized in this study had significant lower viscosities compared to [emim][amino acids] ILs. The [emim] cation with protons at

the 2, 4, and 5 positions at imidazolium structure was contribute to H-bonding and it becomes the reason for the high viscosity of the [emim][amino acids] ILs reported by Jiang *et al.* (2008). Meanwhile, Kagimoto *et al.* (2007) found the lowest viscosity for tetrabutylphosponium L-lysinate ([TBP][lys], 277 cP at 25 °C) among tetrabutylphosponium-based ILs. In this work, [N₂₂₂₂][lys] gave 352 cP of viscosity, which was higher than [TBP][lys].

The results for ionic conductivity showed a five CILs synthesized in this work have a high ionic conductivities compared to [emim][amino acids] ILs reported by Fukumoto *et al.* (2005). As an example, [emim][ser] (0.65 mS cm⁻¹) showed the highest conductivity among [emim][amino acids] ILs at 25 °C however in this work, the highest conductivity was observed for [N₂₂₂₂][lys] is 0.54 mS cm⁻¹. As a conclusion, the rest of [N₂₂₂₂][amino acids] CILs showed higher ionic conductivity values compared to [emim][amino acids] ILs excluding [N₂₂₂₂][ser].

4.10 Application of CILs

4.10.1 Esterification of Oleyl Alcohol with Various Fatty Acids

Esterification reactions between oleyl alcohol and various acids was carried out using native lipase and CILCE as a biocatalyst. The chain length varies from short chain adipic acid (C_6 dicarboxylic acid) and hexanoic acid (C_6 carboxylic acid), medium chain capric acid, (C_8 carboxylic acid), lauric acid (C_{12} carboxylic acid) myristic acid (C_{14} carboxylic acid) and palmitic acid (C_{16} carboxylic acid) and long chain stearic acid (C_{18} carboxylic acid) and oleic acid (C_{18} carboxylic acid, one double bond).

The esterification of various acid and alcohol using CILCE showed highest percentage of conversion of ester compared to CRL. Figure 17 showed the percentage of conversion of wax ester in hexane as a reaction media. It is clearly showed that lipase showed enhanced percentage of conversion without losing any significant activity when it is coated with CILs. The conversion of oleyl hexanoate was almost in two folds in CILCE (72.95 %) compared to CRL (40.53 %). For di-oleyl adipate, the different in percentage of conversion is almost 30 % when using CILCE compared to CRL. Similar results also been observed for oleyl caprate and oleyl laurate with the difference between the percentage of conversion of CILCE and CRL was only about 10 %.

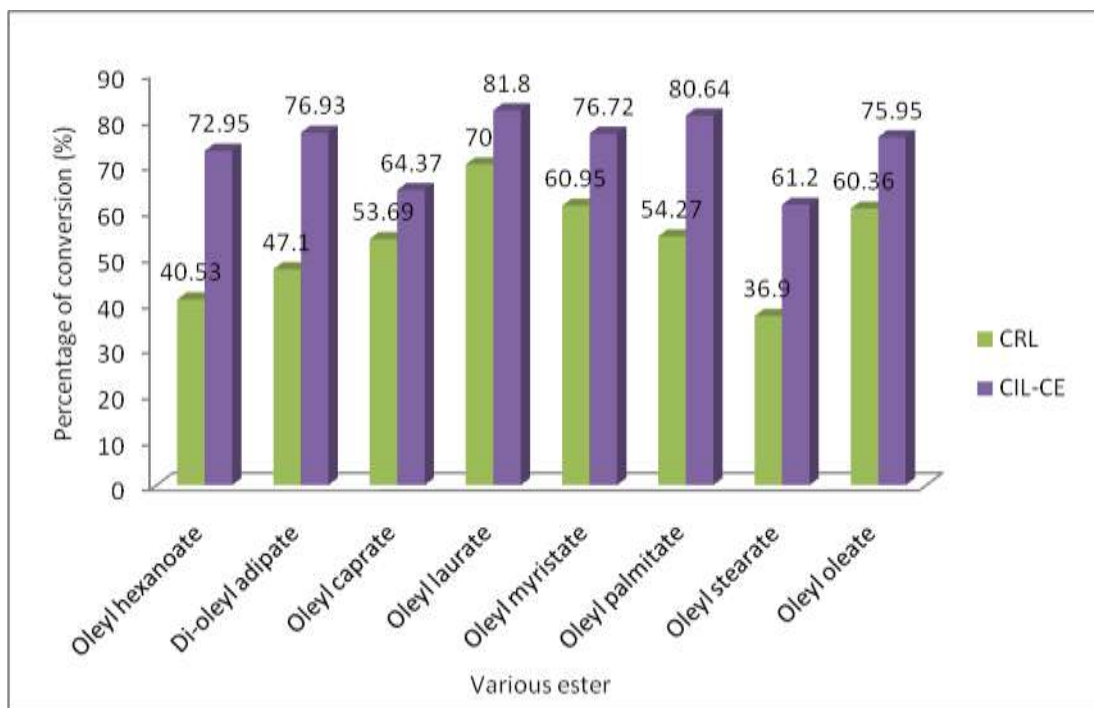


Figure 17: Percentage of conversion of various esters in hexane. Reaction was performed at 40 °C for 1 hour.

Previous study by Ng (2008) reported that the CILCE did not aggregate and the coating ILs are said to be stable and were not removed from the enzyme surface during the reaction. Overall it can be seen that CILCE in most cases are more effective than native CRL for short, medium and long alkyl chain acids. The results of higher percentage of conversion using CILCE can be explained due to the hydrophilicity of CILs itself as previously discussed in Section 4.5 on page 53.

Generally, esterification reaction is a reversible reaction, which means the reaction can produced ester and hydrolysis of ester to form starting material at the same time. During the reaction, water was produced as a by-product with ester. Hydrolysis of ester in the presence of water will reduce the amount of ester, thus lowering the yield. The presence of CILCE in the reaction can act as two functions; as a biocatalyst to increase the percentage of ester and at the same time, absorbed the molecule of water produced. When the amount

of water decreased, possibility of hydrolysis of ester also decreased and the amount of ester increased.

Lipases are easily denatured at high temperature (Wei *et al.*, 2002) where the peptide bonds and amino acid side chains are reactive and can participate in deleterious reactions (Fagain, 1997). This may be one of the reasons why native CRL gave quite a low percentage of conversion as the reactions were carried out at 50 °C. However, for the CILCE, the lipase active conformation was protected against high temperature by CILs, as tetraethylammonium L-asparaginate was thermally stable. Therefore, we found that the conversion were higher in CILCE compared to native CRL. In this context, the coated lipase was able to enhance its performance without losing any significant activity when it is coated with CILs.

Biocatalysis in nonaqueous media often suffers from reduced activity, selectivity or stability of enzyme (Klibanov, 1997). To overcome these limitations, many approaches have focused on the development of more efficient enzymes by enzyme modification, molecular imprinting, additive addition or substrate matching (Lee and Kim, 2002). This new method by coating the enzymes using ILs hopefully would mark the enhancement to enantioselectivity and reliable stability. In the CILCE, the hydrophilic CILs will interact with the hydrophilic enzyme surface (enzyme has a thin essential water layer on its surface).

Okahata and Mori (1997) also observed similar intermolecular H-bonding between the lipid and enzyme in their lipid-coated enzyme. The presence of these hydrogen bonded nano-structures with polar and non-polar regions may be responsible for the stabilization of enzymes coated in CIL that can maintain their functionality under very extreme

denaturative conditions. Thus, both the solvophobic interactions are essential to maintain the native structure and the water shell around the protein molecule which are preserved by the ‘inclusion’ of the aqueous solution of free enzyme into the CILs network. This will promote a clear enhancement of the enzyme stability (Kolle and Dronskowski, 2004).

Although, this is only a preliminary suggestion on how the enzyme and the ILs is bonded during coating process. More research in characterizing its physico-chemical properties will be carried out in near future (for example by using molecular modelling) in order to find out more about this phenomena.

CHAPTER 5

CONCLUSIONS

The main goal of this work is to synthesize a series of tetraethylammonium-based CILs derived from amino acids and plant acid. We have shown that CILs can be synthesized from readily available starting materials and the procedure is very simple and straightforward using neutralization reaction methods. This synthetic pathway showed CILs synthesized in good overall yield (> 85 % yield for CILs from amino acids and > 98 % for CIL derived from plant acids).

By using this simple and reproducible neutralization method, eleven new CILs derived from amino acids and plant acids has been synthesized and characterized meanwhile another one compound (Tetraethylammonium L-tartrate, [N₂₂₂₂][tar]) can't be classified as ILs due to high T_m above 100 °C. The new CILs produced were:

- i) Tetraethylammonium L-serinate ([N₂₂₂₂][ser])
- ii) Tetraethylammonium L-prolinate ([N₂₂₂₂][pro])
- iii) Tetraethylammonium L-threoninate ([N₂₂₂₂][thr])
- iv) Tetraethylammonium L-isooleucinate ([N₂₂₂₂][ile])
- v) Tetraethylammonium L-asparaginate ([N₂₂₂₂][asn])
- vi) Tetraethylammonium L-glutamininate ([N₂₂₂₂][gln])
- vii) Tetraethylammonium L-glutamate ([N₂₂₂₂][glu])
- viii) Tetraethylammonium L-methioninate ([N₂₂₂₂][met])
- ix) Tetraethylammonium L-histidinate ([N₂₂₂₂][his])



- x) Tetraethylammonium L-lysinate ([N₂₂₂₂][lys])
- xi) Tetraethylammonium L-malate ([N₂₂₂₂][mal])

All CILs produced were characterized by ¹H and ¹³C NMR, CHNS/O elemental analysis, DSC, TGA, single crystal X-ray diffraction analysis, optical rotation, viscosity and ionic conductivity.

Single Crystal X-ray data showed that intermolecular H-bonding interaction occurs between cation and anion in [N₂₂₂₂][tar] show a higher melting point compared to intramolecular interaction in the compound of [N₂₂₂₂][mal]. Other than that, the symmetry properties of L(+) tartarate also resulted in high melting point. Meanwhile, the lower melting point of CILs derived from amino acids for [N₂₂₂₂][his] compared to [N₂₂₂₂][asn] could be due to the anion size.

TGA analysis showed that the presence of more than one functional group in a single molecule of anions, different conformational structure and also different alkyl chain clearly affected the thermal stability of each CILs produced. The viscosity and ionic conductivity for liquid CILs were also been determined. Interestingly, it was found that size of molecules did not influence the viscosity and ionic conductivity. The symmetry of cation, different of anions used and other interaction such as H-bonding were affected the viscosity and ionic conductivity. Other than that, the strong relationship between viscosity and ionic conductivity was found. When the viscosity was increased, the ionic conductivity was decreased or vice versa.

In biocatalysis application, tetraethylammonium L-asparaginate was chosen to be coated with *Candida rugosa* lipase (CRL) due to the smaller size compared to tetraethylammonium L-histidinate. This CILCE was then used as biocatalyst in esterification of oleyl alcohol and various fatty acids. It was observed that CILCE showed a better percentage of conversion when compared to native CRL for all alkyl chain of fatty acids from short, medium and long chains. The observation indicated that coated lipase showed enhance activity.

In near future, specific modifications of the chemical and physical properties of the tetraethylammonium-type CILs may assist their presence especially in pharmaceutical industries. For example, tetraethylammonium L-lysinate showed less viscosity as compared to other CILs should find a new solvent for chiral discrimination and CILCE should find uses as a new type of biocatalyst in many chemical reactions.

5.1 Recommendation for Further Studies

Based on this study, several strategies should be further studied for the improvement of CILs in term of the synthesis of CILs and its applications. Among the strategies are:

1. Selecting the appropriate anions for decreasing the viscosity and improving their thermal stabilities of CILs.
2. Study of other suitable combinations of cations and anions to tailor the best ILs for desired applications should be thoroughly researched.
3. Study the physico-chemical properties of CILCE. More research should be done in order to know the interactions occurred between CILs and lipase and to understand the performance of CILCE as catalyst.

REFERENCES

- Abbot, A. P., Capper, G. and Gray, S. (2006). Design of Improved Deep Eutectic Solvents using Hole Theory. *ChemPhysChem* 7: 803–806.
- Abdul Rahman, M. B., Yap, C. L., Dzulkefly, K., Abdul Rahman, R. N. Z., Salleh, A. B. and Basri, M. (2003). Synthesis of Palm Kernel Oil Alkanolamide using Lipase. *Journal of Oleo Science* 52: 65–72.
- Abdul Rahman, M. B., Jumbri, K., Sirat, K., Kia, R. and Fun, H.-K. (2008). Tetraethylammonium L-tartrate dihydrate. *Acta Crystallography Section E* 64: 2343.
- Abdul Rahman, M. B., Jumbri, K., Sirat, K., Kia, R. and Fun, H.-K. (2009). Tetraethylammonium L-malate 1.36-hydrate. *Acta Crystallography Section E* 65: 49–50.
- Abraham, M. H., Zissimos, A. M., Huddleston, J. G. Willauer, H. D., Rogers, R. D. and Acree, W. E. Jr. (2003). Some Novel Liquid Partitioning Systems: Water-Ionic Liquids and Aqueous Biphasic Systems, *Industrial and Engineering Chemistry Research* 42: 413–418.
- Ajam, M. (2005). Metathesis and Hydroformylation Reactions in Ionic Liquids., MSc Thesis, University of Johannesburg, Auckland Park, South Africa.
- Aki, S. N. V. K., Brennecke, J. F. and Samanta, A. (2001). How Polar are Room-temperature Ionic Liquids?. *Chemical Communications* 413–414.
- Allen, F. H., Kennard, O., Watson, D. G., Brammer, L., Orpen, A. G. and Taylor, R. (1987). Tables of Bond Lengths Determined by X-ray and Neutron Diffraction. Part 1. Bond Lengths in Organic Compounds. *Journal of the Chemical Society, Perkin Transactions 2*: S1–19.



- Allen, C. R., Richard, P. L., Ward, A. J., van de Water, L. G. A., Masters, A. F. and Maschmeyer, T. (2006). Facile Synthesis of Ionic Liquids Possessing Chiral Carboxylates. *Tetrahedron Letters* 47: 7367–7370.
- Anouti, M., Caillon-Caravanier, M., Le Floch, C. and Lemordant, D. (2008). Alkylammonium-Based Protic Ionic Liquids Part I: Preparation and Physicochemical Characterization. *Journal of Physical Chemistry B* 112: 9406–9411.
- Awad, W. H., Gilman, J. W., Nyden, M., Harris Jr., R. H., Sutto, T. E., Callahan, J., Trulove, P. C., DeLong, H. C. and Fox, D. M. (2004). Thermal Degradation Studies of Alkyl-imidazolium Salts and Their Application in Nanocomposites. *Thermochimica Acta* 409: 3–11.
- Bao, W., Wang and Z., Li, Y. (2003). Synthesis of Chiral Ionic Liquids from Natural Amino Acids. *Journal of Organic Chemistry*. 68: 591–593.
- Basri, M., Salleh, A. B., Abdul Rahman, R. N. Z. and Abdul Rahman, M. B. (2005). Lipase-Catalyzed Syntheses of Palm-Based Specialty Oleochemicals. *Current Topics in Catalysis* 4: 23–41.
- Baudequin, C., Baudoux, J., Levillain, J., Cahard, D., Gaumontb, A. and Plaquevent, J. (2003). Ionic Liquids and Chirality: Opportunities and Challenges. *Tetrahedron Asymmetry* 14: 3081–3093.
- Baudequin, C., Brégeon, D., Levillain, J., Guillen, F., Plaquevent, J. and Gaumont, A. (2005). Chiral Ionic Liquids, A Renewal for the Chemistry of Chiral Solvents? Design, Synthesis and Applications for Chiral Recognition and Asymmetric Synthesis. *Tetrahedron Asymmetry* 16: 3921–3945.
- Bernstein, J., Davis, R. E., Shimoni, L. and Chang, N.-L. (1995). Patterns in Hydrogen Bonding: Functionality and Graph Set Analysis in Crystals. *Angewandte Chemie (International Edition in English)* 34: 1555–1573.



- Boon, J. A., Levisky, J. A., Pflug, J. L. and Wilkes, J. S. (1986). Friedel-Crafts Reactions in Ambient-temperature Molten Salts. *Journal of Organic Chemistry* 51: 480–483.
- Bonhôte, P., Dias, A. P., Papageorgiou, N., Kalyanasundaram, K. and Gratzel, M. (1996). Hydrophobic, Highly Conductive Ambient-Temperature Molten Salts. *Inorganic Chemistry* 35: 1168–1178.
- Bornscheur, U. T. and Kazlauskas, R. J. (1999). *Hydrolases in Organic Synthesis*, Weinheim: Wiley-VCH.
- Brauer, D. J., Kottsieper, K. W., Liek, C., Stelzer, O., Waffenschmidt, H., Wasserscheid, P. (2001). Phosphines with 2-imidazolium and para-phenyl-2-imidazolium moieties - Synthesis and Application in Two-phase Catalysis. *Journal of Organometallic Chemistry* 630:2, 177–184.
- Brausch, N., Metlen, A. and Wasserscheid, P. (2004). New, Highly Acidic Ionic Liquid Systems and Their Application in the Carbonylation of Toluene. *Chemical Communications* 1552–1553.
- Cao, L., van Rantwijk, F. and Sheldon, R. A. (2000). Cross-Linked Enzyme Aggregates: A Simple and Effective Method for the Immobilization of Penicillin Acylase. *Organic Letters* 2: 1361-1364.
- Carlin, R. T. and Wilkes, J. S. (1990). Complexation of Cp_2MCl_2 in a Chloroaluminate Molten Salt: Relevance to Homogeneous Ziegler-Natta Catalysis. *Journal of Molecular Catalysis* 63: 125–129.
- Chauvin, Y., Gilbert, B. and Guibard, I. (1990). Catalytic Dimerization of Alkenes by Nickel Complexes in Organochloroaluminate Molten Salts. *Journal of the Chemical Society, Chemical Communications* 1715–1716.



- Chauvin, Y., Einloft, S., Olivier, H. (1995). Catalytic Dimerization of Propene by Nickel-phosphine Complexes in 1-Butyl-3-Methylimidazolium Chloride/ $\text{AlEt}_x\text{Cl}_{3-x}$ ($x = 0, 1$) Ionic Liquids. *Industrial and Engineering Chemistry Research* 34: 1149–1155.
- Cope, A. C. and Trumbull, E. R. (1960). Olefins from Amines: The Hofmann Elimination Reaction and Amine Oxide Pyrolysis. *Organic Reactions* 11: 317–493.
- Crowhurst, L., Lancaster, N. L., Arlandis, J. M. P. and Welton, T. (2004). Manipulating Solute Nucleophilicity with Room Temperature Ionic Liquids. *Journal of the American Chemical Society* 126: 11549–11555.
- Dai, S., Ju, Y. H. and Barnes, C. E. (1999). Solvent Extraction of Strontium Nitrate by a Crown Ether using Room-Temperature Ionic Liquids. *Journal of the Chemical Society: Dalton Transactions* 1201-1208.
- Ding, J. and Armstrong, D. W. (2005). Chiral Ionic Liquids: Synthesis and Applications. *Chirality* 17: 281–292.
- Doherty, S., Goodrich, P., Hardacre, C., Luo, H., Rooney, D. W., Seddon, K. R. and Styring, P. (2004). Marked Enantioselectivity Enhancements for Diels-Alder Reactions in Ionic Liquids Catalyzed by Platinum Diphosphine Complexes. *Green Chemistry* 6: 63–67.
- Earle, M. J. and Seddon K. R. (2000). Ionic Liquids. Green Solvents for the Future. *Pure and Applied Chemistry* 72: 1391–1398.
- Earle, M. J., Katdare, S. P. and Seddon, K. R. (2004). Paradigm Confirmed: The First Use of Ionic Liquids to Dramatically Influence the Outcome of Chemical Reactions. *Organic Letters* 6: 707–710.
- Ellis, B., Keim, W. and Wasserscheid, P. (1999). Linear Dimerisation of But-1-ene in Biphasic Mode using Buffered Chloroaluminate Ionic Liquid Solvents. *Chemical Communications* 337–338.



- Erbeldinger, M., Mesiano, A. J. and Russel, A. J. (2000). Enzymatic Catalysis of Formation of Z-aspartame in Ionic Liquid an Alternative to Enzymatic Catalysis in Organic Solvents. *Biotechnology Progress* 16: 1129–1131.
- Fadeev, A. G. and Meagher, M. M. (2001). Opportunities for Ionic Liquid in Recovery of Biofuels. *Chemical Communications* 295–296.
- Fagain, C. O. (1997). Manipulating Protein Stability in: Stabilizing Protein Functions. *Springer, Berlin* 67–191.
- Fannin, Jr. A. A., Loreani, D. A., King, L. A., Landers, J. S., Piersma, B. J., Stech, D. J., Vaughn, R. L., Wilkes, J. S. and William, J. L. (1984). Properties of 1,3-dialkylimidazolium chloride-aluminum chloride Ionic Liquids. 2. Phase Transitions, Densities, Electrical Conductivities and Viscosities. *Journal of Physical Chemistry* 88: 2614–2621.
- Fredlake, C. P., Crosthwaite, J. M., Hert, D. G., Aki, S. N. V. K. and Brennecke, J. F. (2004). Thermophysical Properties of Imidazolium-based Ionic Liquids. *Journal of Chemical and Engineering Data* 49: 954–964.
- Fukumoto, K., Yoshizawa, M. and Ohno, H. (2005). Room Temperature Ionic Liquids from 20 Natural Amino Acids. *Journal of the American Chemical Society* 127: 2398–2399.
- Fukumoto, K. and Ohno, H. (2006). Design and Synthesis of Hydrophobic and Chiral Anions from Amino Acids as Precursor for Functional Ionic Liquids. *Chemical Communications* 3081–3083.
- Fuller, J., Carlin, R. T., De Long, H. C., Haworth, D. (1994). Structure of 1-Ethyl-3-Methylimidazolium Hexafluorophosphate – Model for Room Temperature Molten-Salts. *Journal of Chemical Society, Chemical Communications* 299–300.
- Galinski, M., Lewandowski, A. and Stepniak, I. (2006). Ionic Liquids as Electrolytes. *Electrochimica Acta* 51: 5567–5580.



- Gandhi, N. N., Sawant, S. B. and Joshi, J. B. (1995). Specificity of a Lipase in Ester Synthesis: Effect of Alcohol. *Biotechnology Progress* 11: 282–287.
- Geldbach, T. J., Dyson, P. J. (2004). A Versatile Ruthenium Precursor for Biphasic Catalysis and its Application in Ionic Liquid Biphasic Transfer Hydrogenation: Conventional vs Task-specific Catalysts. *Journal of the American Chemical Society* 126: 8114–8115.
- Holbrey, J. D. and Seddon, K. R. (1999). The Phase Behaviour of 1-alkyl-3-Methylimidazolium Tetrafluoroborates: Ionic liquids and Ionic Liquid Crystals. *Journal of the Chemical Society Dalton Transactions* 2133–2139.
- Holbrey, J. D., Seddon, K. R. and Wareing, R. (2001). A Simple Colorimetric Method for the Quality Control of 1-alkyl-3-methylimidazolium Ionic Liquid Precursors. *Green Chemistry* 3: 33–36.
- Huddleston, J. G., Visser, A. E., Reichert, W. M., Willauer, H. D., Broker, G. A. and Rogers, R. D. (2001). Characterization and Comparison of Hydrophilic and Hydrophobic Room Temperature Ionic Liquids Incorporating the Imidazolium Cation. *Green Chemistry* 3: 156-164.
- Jiang, Y-Y., Wang, G-N., Zhou, Z., Wu, Y-T., Geng, J. and Zhang, Z-B. (2008). Tetraalkylammonium Amino Acids as Functionalized Ionic Liquids of Low Viscosity. *Chemical Communications* 505–507.
- Kagimoto, J., Fukumoto, K. and Ohno, H. (2007). Effect of Tetrabutylphosphonium Cation on the Physico-chemical Properties of Amino-acid Ionic Liquids. *Chemical Communications* 21: 2254–2256.
- Kim, K.-W., Song, B., Choi, M.-Y. and Kim, M.-J. (2001). Biocatalysis in Ionic Liquids: Markedly Enhanced Enantioselectivity of Lipase. *Organic Letters* 3: 1507
- Ke, T. and Klibanov, A. M. (1998). Enzymatic Activity in Organic Solvents as a Function of Enzyme History. *Biotechnology and Bioengineering* 57: 46-50.



- Klar, U., Röhr, B., Kuczynski, F., Schwede, W., Berger, M., Skuballa, W. and Buchmann, B. (2005). Efficient Chiral Pool Synthesis of the C1-C6 Fragment of Epothilones. *Synthesis* 301-305.
- Klibanov, A. M. (1997). Why Are Enzymes Less Active in Organic Solvents than in Water?. *Trends in Biotechnology* 15: 97-101.
- Kölle, P. and Dronskowski, R. (2004). Hydrogen Bonding on the Crystal Structures of Ionic Liquid Compounds Butyl-Dimethylimidazolium Hydrogen Sulfate Chloride and Chloroferrate (II, III). *Inorganic Chemistry* 43: 2803-2809.
- Kreiner, M., Moore, B. D. and Parker, M. C. (2001). Enzyme-Coated Micro-Crystals: A 1-Step Method for High Activity Biocatalyst Preparation. *Chemical Communications* 12: 1096-1097.
- Lancaster, N. L., Welton, T. and Young, G. B. (2001). A Study of Halide Nucleophilicity in Ionic Liquids. *Journal of the Chemical Society, Perkin Transactions 2*: 2267–2270.
- Laszlo, J. A. and Compton, D. L. (2001). α -chymotrypsin Catalysis in Imidazolium-based Ionic Liquids. *Biotechnology and Bioengineering* 75: 181–186.
- Law, G. and Watson, P. R. (2001). Surface Tension Measurements of *N*-Alkylimidazolium Ionic Liquids. *Langmuir* 17: 6138–6141.
- Lee, J. K. and Kim, M. J. (2002). Ionic Liquid-Coated Enzyme for Biocatalysis in Organic Solvent. *Journal of Organic Chemistry* 67: 6845–6847.
- Levillain, J., Dubant, G., Abrunhosa, I., Gulea, M. and Gaumont, A. (2003). Synthesis and Properties of Thiazoline Based Ionic Liquids Derived from the Chiral Pool. *Chemical Communications* 2914–2915.



- Liao, Q. and Hussey, C. L. (1996). Densities, Viscosities and Conductivities of Mixtures of Benzene with the Lewis Acidic Aluminum chloride + 1-methyl-3-ethylimidazolium chloride Molten Salt. *Journal of Chemical and Engineering Data* 41: 1126–1130.
- Lide, D. R. (1992). CRC Handbook of Chemistry and Physics, 73th Ed (ed.), CRC Press, Boca Raton.
- Lozano, P., de Deigo, T., Guegan, J.-P., Vaultier, M. and Iborra, J. L. (2001). Stabilization of α -chymotrypsin by Ionic Liquids in Transesterification Reactions. *Biotechnology and Bioengineering* 75: 563–569.
- McFarlane, D. R., Pringle, J. M., Johanson, K. M., Forsyth, S. A. and Forsyth, M. (2006). Lewis Base Ionic Liquids. *Chemical Communications* 1905–1917.
- Madeira Lau, R., van Rantwijk, F., Sedddon, K. R. and Sheldon, R. A. (2000). Lipase-catalyzed Reactions in Ionic Liquids. *Organic Letters* 2: 4189–4191.
- Mat Radzi, S., Basri, M., Salleh, A. B., Ariff, A., Mohammad, R., Abdul Rahman, M. B. and Abdul Rahman, R. N. Z. (2005). High Performance Enzymatic Synthesis of Oleyl Oleate using Immobilised Lipase from *Candida antarctica*. *Electronic Journal of Biotechnology* 8: 291-298.
- Mo, J., Xu, L. and Xiao, J. (2005). Ionic Liquid-promoted Highly Regioselective Heck Arylation of Electron-rich Olefins by Aryl Halides. *Journal of the American Chemical Society* 127: 751–760.
- Muldoon, M. J., Gordon, C. M. and Dunkin, I. R. (2001). Investigations of Solvent-solute Interactions in Room Temperature Ionic Liquids using Solvatochromic Dyes. *Journal of the Chemical Society, Perkin Transactions* 2: 433–435.
- Ng, S. H. (2008). Synthesis, Characterization and Biocatalysis Application of Imidazolium-based Chiral Ionic Liquids. MSc Thesis, Universiti Putra Malaysia, Serdang, Malaysia.



- Ngo, H. L., LeCompte, K., Hargens, L. and McEwan, A. B. (2000). Thermal Properties of Imidazolium Ionic Liquids. *Thermochimica Acta* 357–358: 97–102.
- Obliosca, J. M., Arco, S. D., Huang, M. H. J. (2007). Synthesis and Optical Properties of 1-Alkyl-3-Methylimidazolium Lauryl Sulfate Ionic Liquids. *Fluorescence* 17: 613–618.
- Ohno, H. (2005). *Electrochemical Aspects of Ionic Liquids*. New York: Wiley-Interscience.
- Ohno, H. (2006). Functional Design of Ionic Liquids. *Bulletin of the Chemical Society of Japan* 79: 1665–1680.
- Ohno, H. and Fukumoto, K. (2007). Amino Acid Ionic Liquids. *Accounts of Chemical Research* 40: 1122–1129.
- Okahata, Y. and Mori, T. (1997). Lipid-Coated Enzymes as Efficient Catalysts in Organic Media. *Trends in Biotechnology* 15: 50–54.
- Park, S. and Kazlauskas, R. J. (2001). Improved Preparation and use of Room-temperature Ionic Liquids in Lipase-catalyzed Enantio- and Regioselective Acylations. *Journal of Organic Chemistry* 66: 8395–8401.
- Park, S. and Kazlauskas, R. J. (2003). Biocatalysis in Ionic Liquids – Advantages Beyond Green Technology. *Current Opinion in Biotechnology* 14: 432–437.
- Parshall, G. W. (1972). Catalysis in Molten Salt Media. *Journal of the American Chemical Society* 94: 8716–8719.
- Pecul, M., Ruud, K., Rizzo, A. and Helgaker, T. (2004). Conformational Effects on the Optical Rotation of Alanine and Proline. *Journal of Physical Chemistry A* 108: 4269–4276.



- Pecul, M. (2006). Conformational Structures and Optical Rotation of Serine and Cysteine. *Chemical Physics Letters* 418: 1–10.
- Pomaville, R. M. and Poole, C. F. (1990). Gas Chromatographic Study of the Solution Thermodynamics of Organic Solutes in Tetraalkylammonium Alkanesulfonate and Perfluoroalkanesulfonate Solvent. *Journal of Chromatography* 499: 749–759.
- Pringle, J. M., Golding, J., Baranyai, K., Forsyth, C. M., Deacon, G. B., Scott, J. L. and MacFarlane, D. R. (2003). The Effect of Anion Fluorination in Ionic Liquids - Physical Properties of a Range of Bis(methanesulfonyl)amide Salts. *New Journal of Chemistry* 27: 1504–1510.
- Seddon, K. R. (1997). Ionic Liquids for Clean Technology. *Journal of Chemical Technology and Biotechnology* 68: 351–356.
- Seddon, K. R., Stark, A. and Torres, M.-J. (2000). Influence of Chloride, Water, and Organic Solvents on the Physical Properties of Ionic Liquids. *Pure and Applied Chemistry* 72: 2275–2287.
- Seddon, K. R. (2002). Ionic liquids: Designer Solvents for Green Synthesis. *Chemical Engineer* 33–35.
- Schöfer, S., Kaftzik, N., Wassercheid, P. and Kragl, U. (2001). Enzyme Catalysis in Ionic Liquids: Lipase Catalysed Kinetic Resolution of 1-phenylethanol with Improved Enantioselectivity. *Chemical Communications* 425–426.
- Summers, C. A. and Flowers II, R. A. (2000). Protein Renaturation by the Liquid Organic Salt ethylammonium nitrate. *Protein Science* 9: 2001–2008.
- Sun, I-W., Ward, E. H., Hussey, C. L. (1988). Electrochemistry of Osmium (III) and -(IV) Chloride Complexes in the Basic Aluminum Chloride-1-Methyl-3-Ethylimidazolium Chloride Ionic Liquid. *Journal of the Electrochemical Society* 135: 3035–3038.



- Swartling, D., Ray, L., Compton, S. and Ensor, D. (2000). Temperature Dependence of Viscosity for Room Temperature Ionic Liquids. *Bulletin Biochemistry and Biotechnology* 13: 145–151.
- Swatloski, R. P., Visser, A. E., Reichert, W. M., Broker, G. A., Farina, L. M., Holbrey, J. D and Rogers, R. D. (2001). Solvation of 1-butyl-3-Methylimidazolium Hexafluorophosphate in Aqueous Ethanol Green Solution for Dissolving ‘Hydrophobic’ Ionic Liquids. *Chemical Communications* 2070–2071.
- Tamar, K., Salanne, M., Simon, C., Turq, P., Madden, P.A. (2006). Conductivity-Viscosity-Structure: Unpicking the Relationship in an Ionic Liquid. *Journal of Physical Chemistry B* 111: 4678–4684.
- Tao, G., He, L., Sun, N. and Kou, Y. (2005). New Generation Ionic Liquids: Cations derived from Amino Acids. *Chemical Communications* 3562–3564.
- Tokuda, H., Hayamizu, K., Ishii, K., Susan, M. A. B. H. and Watanabe, M. (2005). Physicochemical Properties and Structures of Room Temperature Ionic Liquids. 2. Variation of Alkyl Chain Length in Imidazolium Cation. *Journal of Physical Chemistry B* 109: 6103–6110.
- Tran, C. D., Oliveira, D. and Yu, S. (2006). Chiral Ionic Liquid that Function as Both Solvent and Chiral Selector for the Determination of Enantiomeric Compositions of Pharmaceutical Products. *Analytical Chemistry* 78: 1349–1356.
- van Rantwijk, F., Lau, R. M. and Sheldon, R. A. (2003). Biocatalytic Transformations in Ionic Liquids. *Trends in Biotechnology* 21: 131–138.
- Vidugiris, G.-J. A., Razumas, V. J., Drungiliene, A. A., Kulys, J. J. (1988). Complex Formation of Amino Acids and Proteins with Silver Ions. *Biochemistry and Bioenergetic* 19: 513–520.
- Vogel, A. I. (1961). *A Textbook of Quantitative Inorganic Analysis*, 3rd ed, London: Longmans, Green and Co.



- Wang, Z., Wang, Q., Zhang, Y. and Bao, W. (2005). Synthesis of New Chiral Ionic Liquids from Natural Acids and Their Applications in Enantioselective Michael Addition. *Tetrahedron Letters* 46: 4657–4660.
- Wasserscheid, P. and Keim, W. (2000). Ionic liquids – New 'Solutions' for Transition Metal Catalysis. *Angewandte Chemie – International Edition* 39: 3773–3789.
- Wasserscheid, P., Gordon, C. M., Hilgers, C., Maldoon, M. J. and Dunkin, I. R. (2001). Ionic liquids: Polar, but Weakly Coordinating Solvents for the First Biphasic Oligomerization of Ethene to Higher α -olefins with Cationic Ni Complexes. *Chemical Communications* 1186–1187.
- Wasserscheid, P.; van Hal, R. and Bösmann, A. (2002). 1-n-butyl-3-methylimidazolium ([bmim]) octylsulfate - An even 'Greener' Ionic Liquid. *Green Chemistry* 4: 400–404.
- Wasserscheid, P. and Welton, T. (2003). *Ionic Liquids in Synthesis*, eds. Weinheim, Germany: Wiley- VCH.
- Wei, P., Gu C. and Su W. (2002). Enzymatic Reaction for Glycoside Lactate Synthesis in Organic Solvent. *Enzyme Microbiology Technology* 33: 508–512.
- Wei, G. T. and Yang, C. J. (2003). Room Temperature Ionic Liquid as a Novel Medium for Liquid/ Liquid Extraction of Metal Ions. *Journal of Analytica Chimica Acta* 488: 183–186.
- Welton, T. (1999). Room-Temperature Ionic Liquids. Solvents for Synthesis and Catalysis. *Chemical Reviews* 99: 2071–2083.
- Wilkes, J. S., Levisky, J. A., Wilson, R. A. and Hussey, C. L. (1982). Dialkylimidazolium Chloroaluminate Melts: A New Class of Room-temperature Ionic Liquids for Electrochemistry, Spectroscopy and Synthesis. *Inorganic Chemistry* 21: 1263–1264.



- Wilkes, J. S. and Zaworotko, M. J. (1992). Air and Water Stable 1-ethyl-3-methylimidazolium based Ionic Liquids. *Chemical Communications* 965–967.
- Wilkes, J. S. (2004). Properties of Ionic Liquid Solvents for Catalysis. *Journal of Molecular Catalysis A: Chemical* 214: 11–17.
- Xiao, J.-C. and Shreeve, J. M. (2005). Synthesis of 2,2'-biimidazolium-based Ionic Liquids: Use as a New Reaction Medium and Ligand for Palladium-catalyzed Suzuki Cross-coupling Reactions. *Journal of Organic Chemistry* 70: 3072–3078.
- Yamaguchi, K., Yoshida, C., Uchida, S., Mizuno, N. (2005). Peroxotungstate Immobilized on Ionic Liquid-modified Silica as a Heterogeneous Epoxidation Catalyst with Hydrogen Peroxide. *Journal of the American Chemical Society* 127: 530–531.



APPENDIX A

Calculation for Esterification Reaction of Oleyl Alcohol with Various Fatty Acids

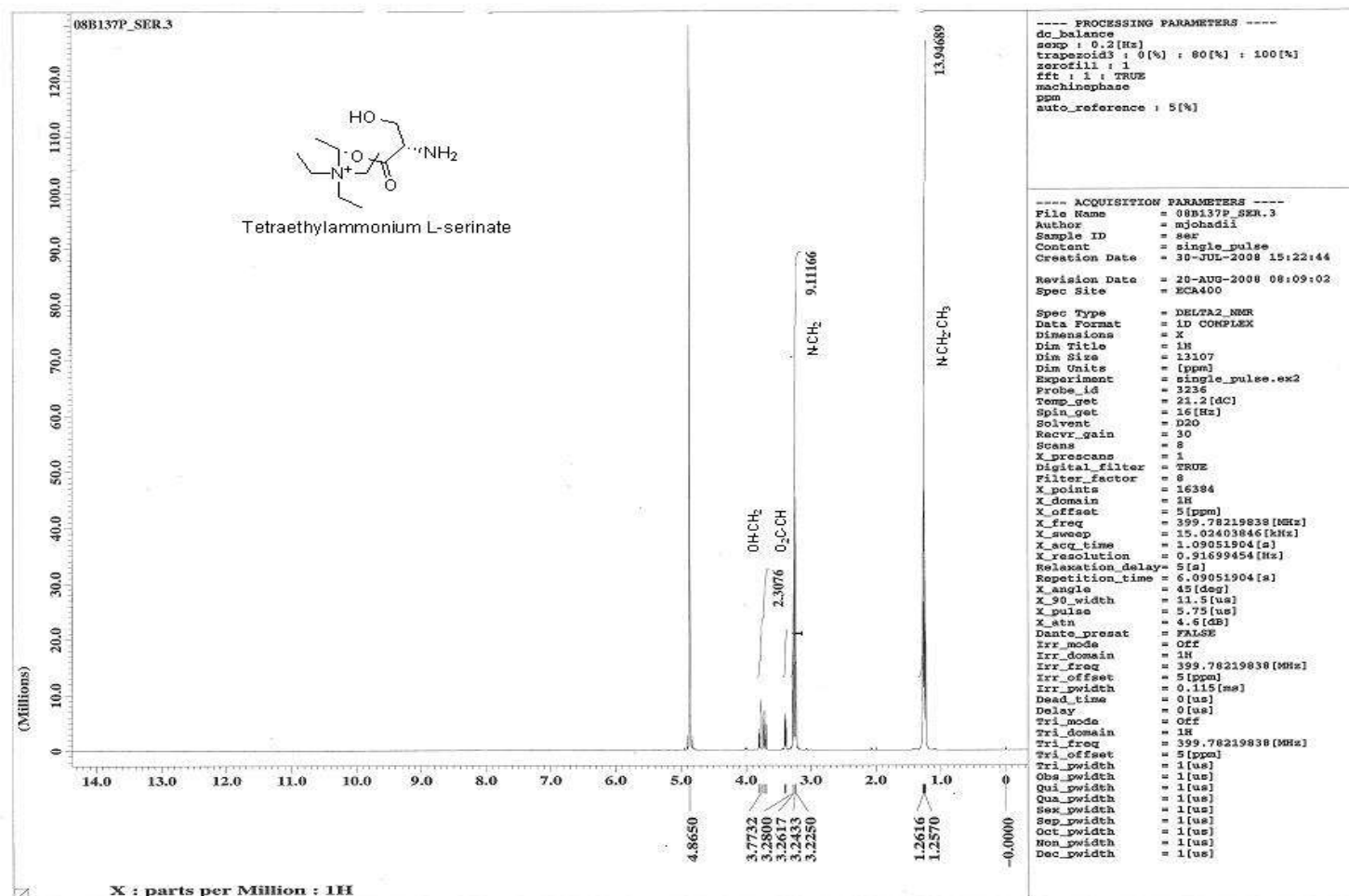
The percentage of conversion (%) was calculated based on the following equation:

$$\text{Percentage of Conversion (\%)} = \frac{(V_{\text{control}} - V_{\text{sample}})}{V_{\text{control}}} \times 100 \%$$

V_{control} = Volume of 0.1 M NaOH needed to titrate the control

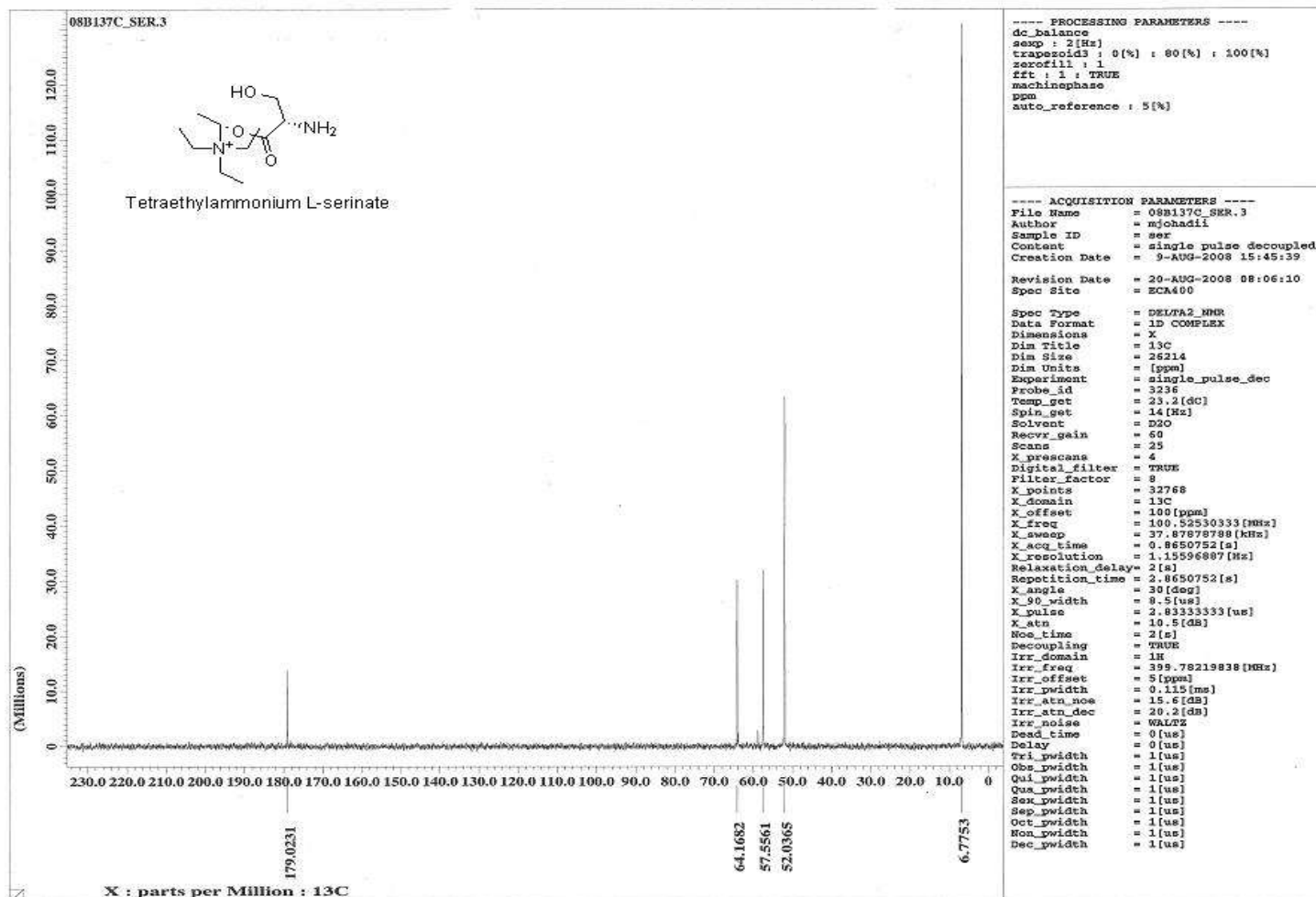
V_{sample} = Volume of 0.1 M NaOH needed to titrate the sample

APPENDIX B-1 (¹H NMR)



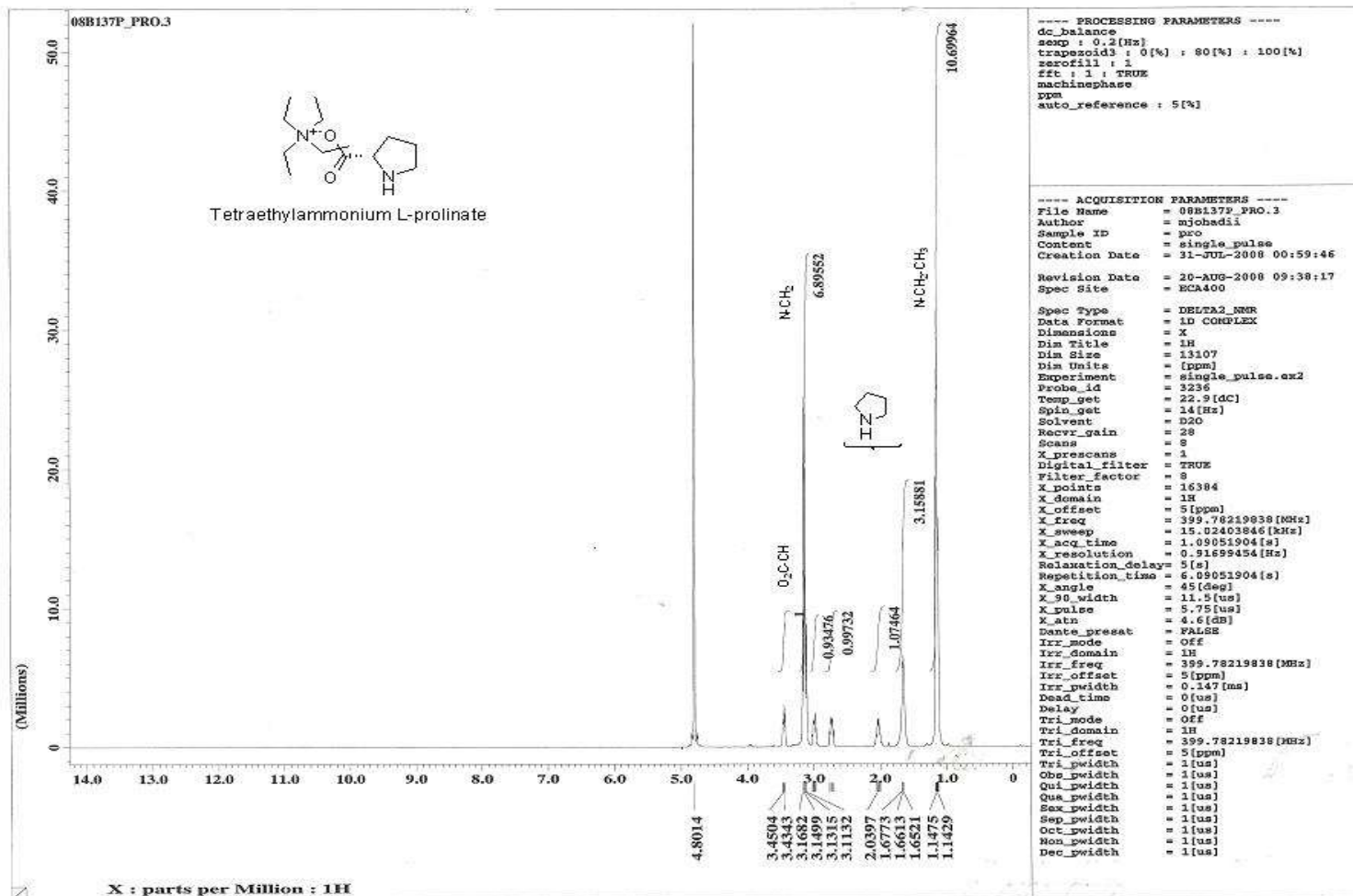
¹H NMR spectrum of tetraethylammonium L-serinate

APPENDIX B-1 (¹³C NMR)



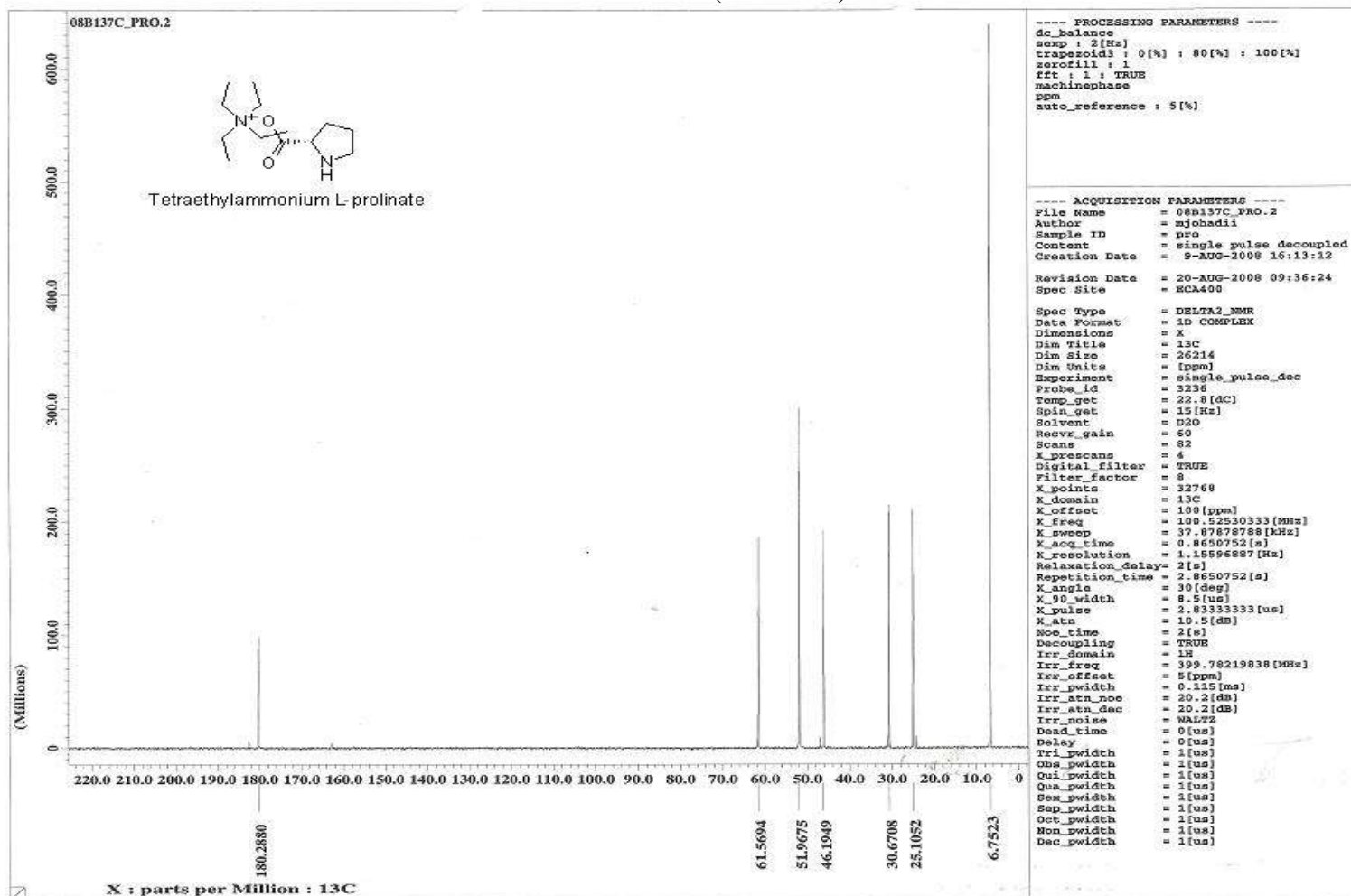
¹³C NMR spectrum of tetraethylammonium L-serinate

APPENDIX B-2 (¹H NMR)



¹H NMR spectrum of tetraethylammonium L-prolinate

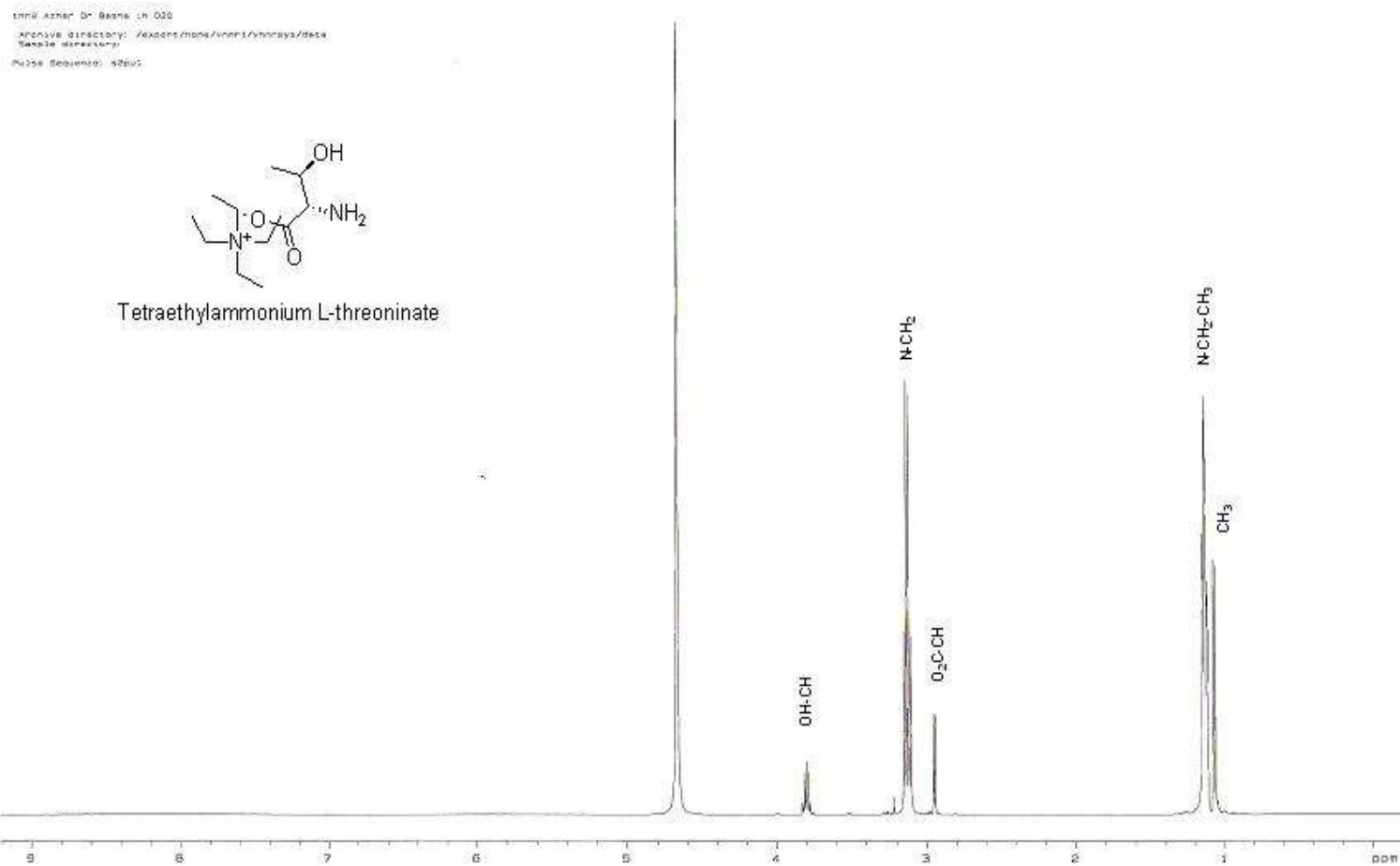
APPENDIX B-2 (¹³C NMR)



¹³C NMR spectrum of tetraethylammonium L-prolinate

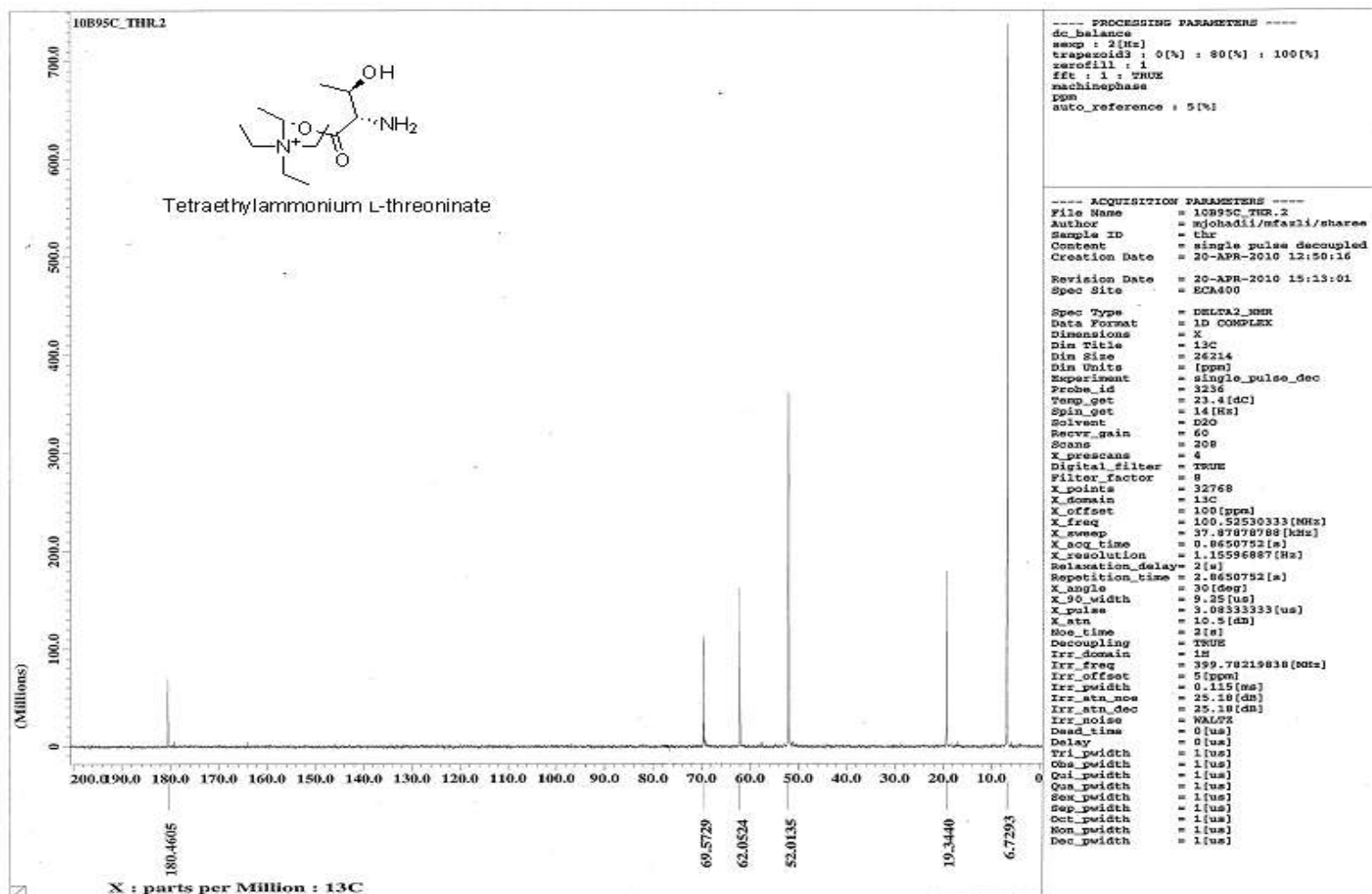


APPENDIX B-3 (^1H NMR)



^1H NMR spectrum of tetraethylammonium L-threoninate

APPENDIX B-3 (¹³C NMR)

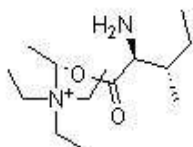


¹³C NMR spectrum of tetraethylammonium L-threoninate

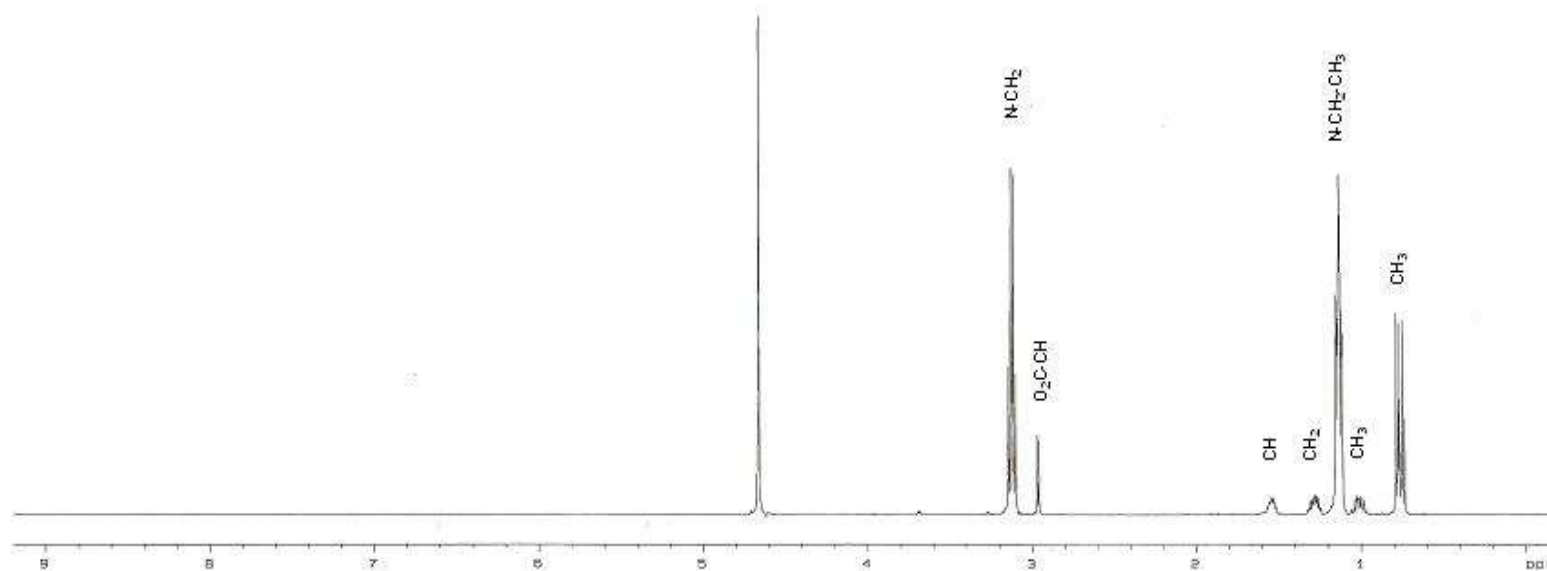


APPENDIX B-4 (^1H NMR)

130 Azhar Dr. Becha Ln. 030
Archive directory: /axaris/nmr/nmr1/analysis/data
Sample directory:
Pulse Sequence: zgpg30

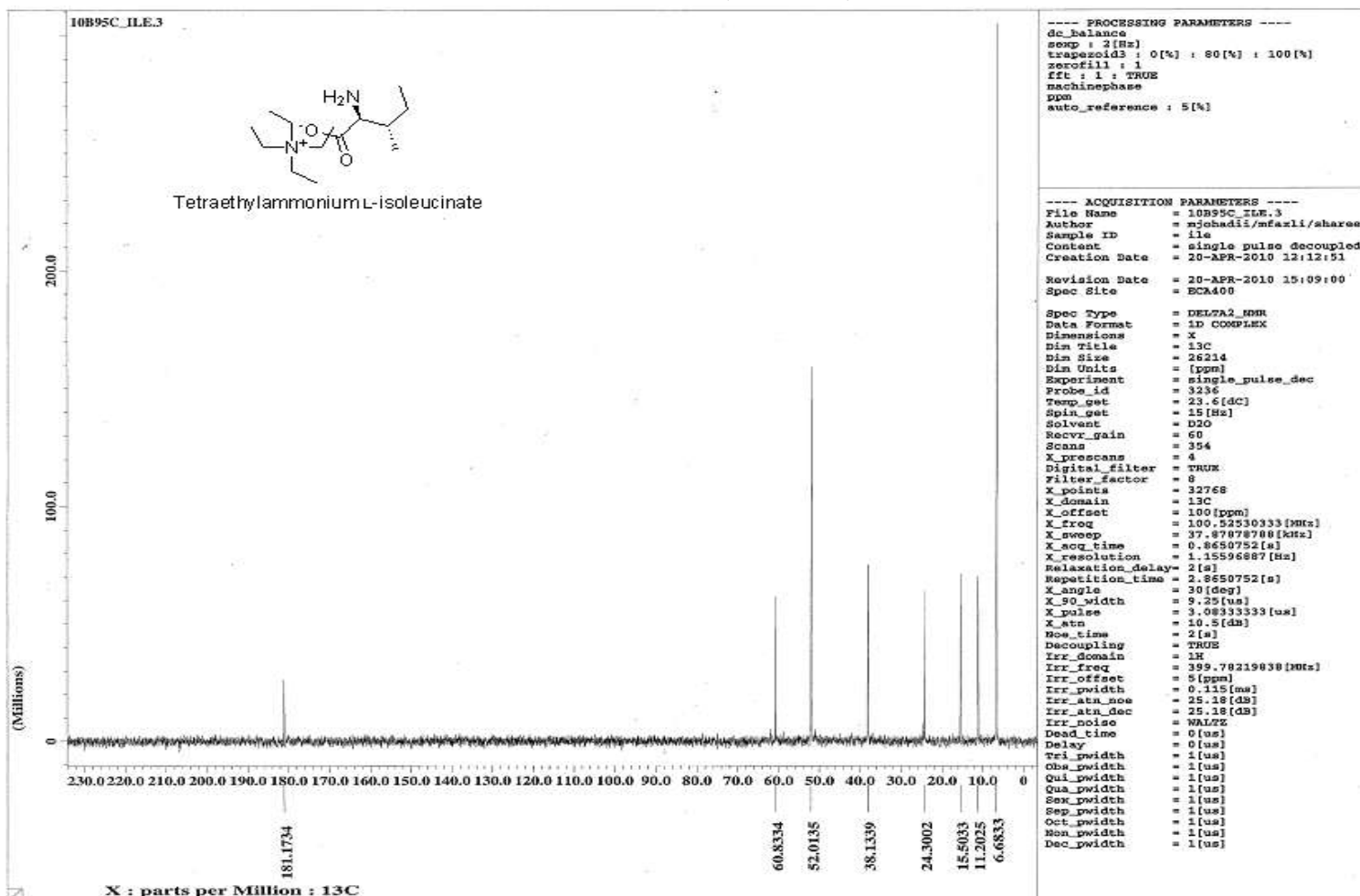


Tetraethylammonium L-isoleucinate



^1H NMR spectrum of tetraethylammonium L-isoleucinate

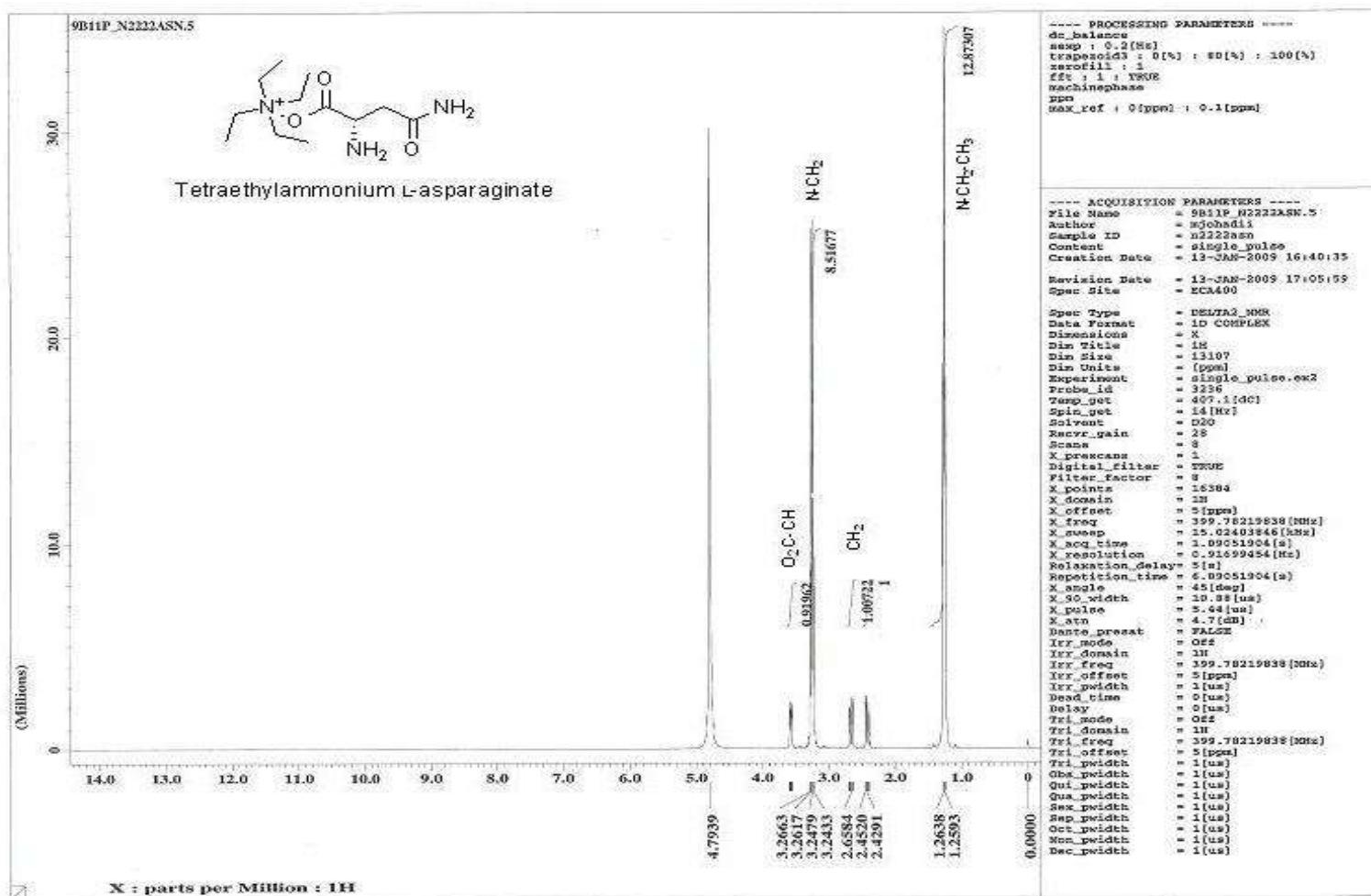
APPENDIX B-4 (¹³C NMR)



¹³C NMR spectrum of tetraethylammonium L-isoleucinate

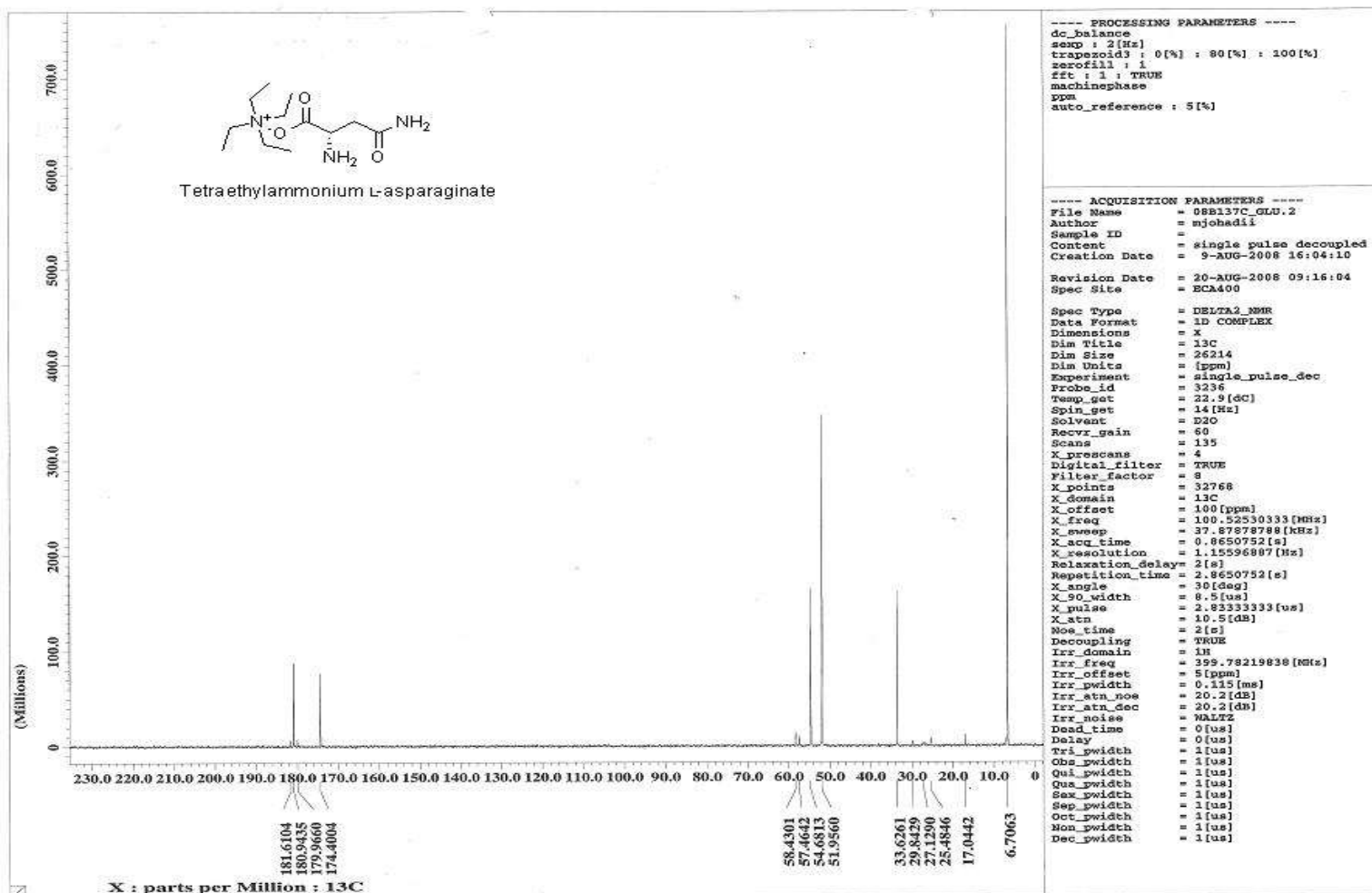


APPENDIX B-5 (¹H NMR)



¹H NMR spectrum of tetraethylammonium L-asparaginate

APPENDIX B-5 (¹³C NMR)



¹³C NMR spectrum of tetraethylammonium L-asparaginate



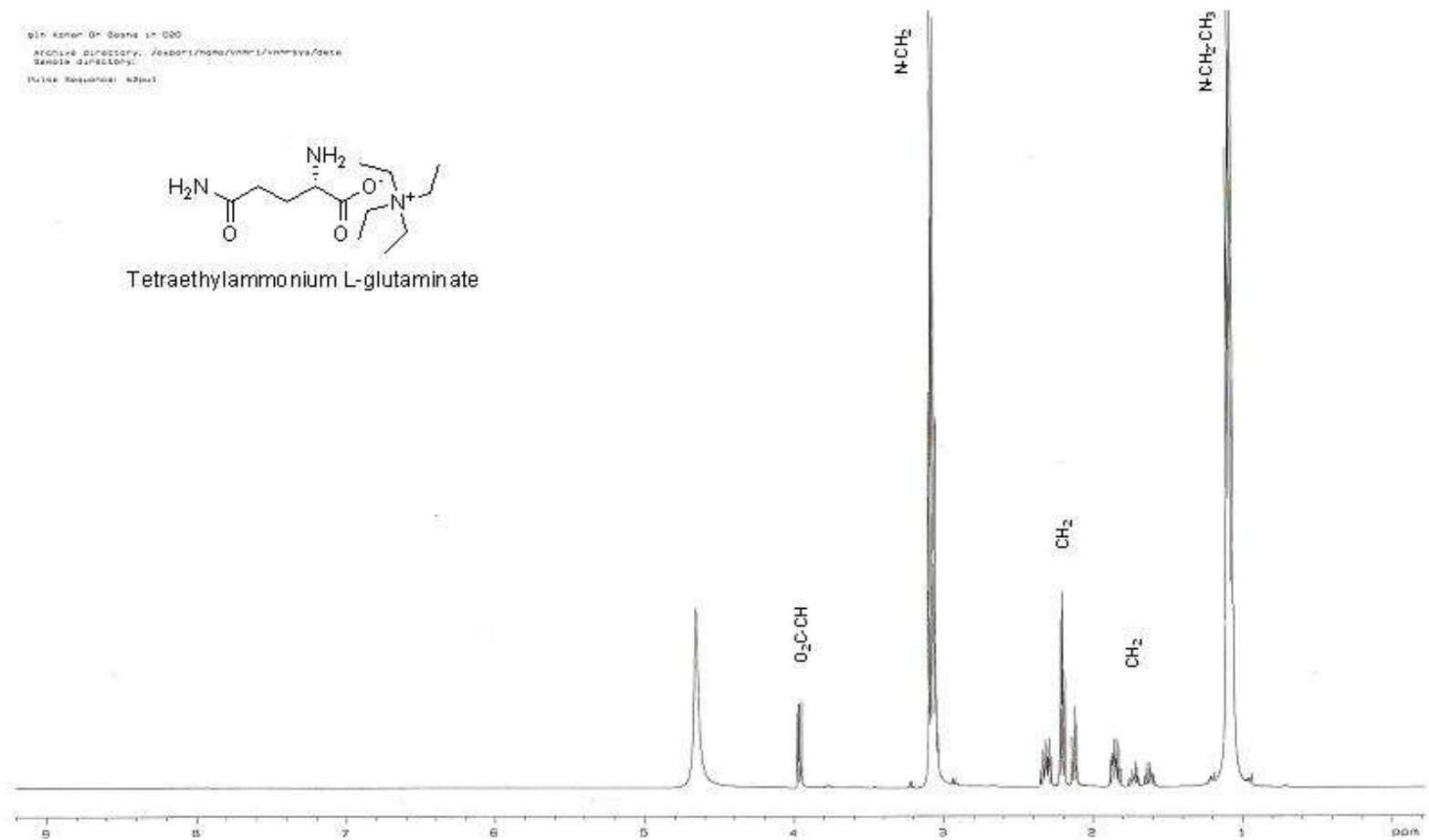
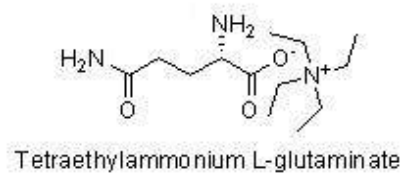
APPENDIX B-6 (^1H NMR)

gln-komen-01-08-04-14-020

Archive directory: /experiments/vnmr1/vnmr14/020/

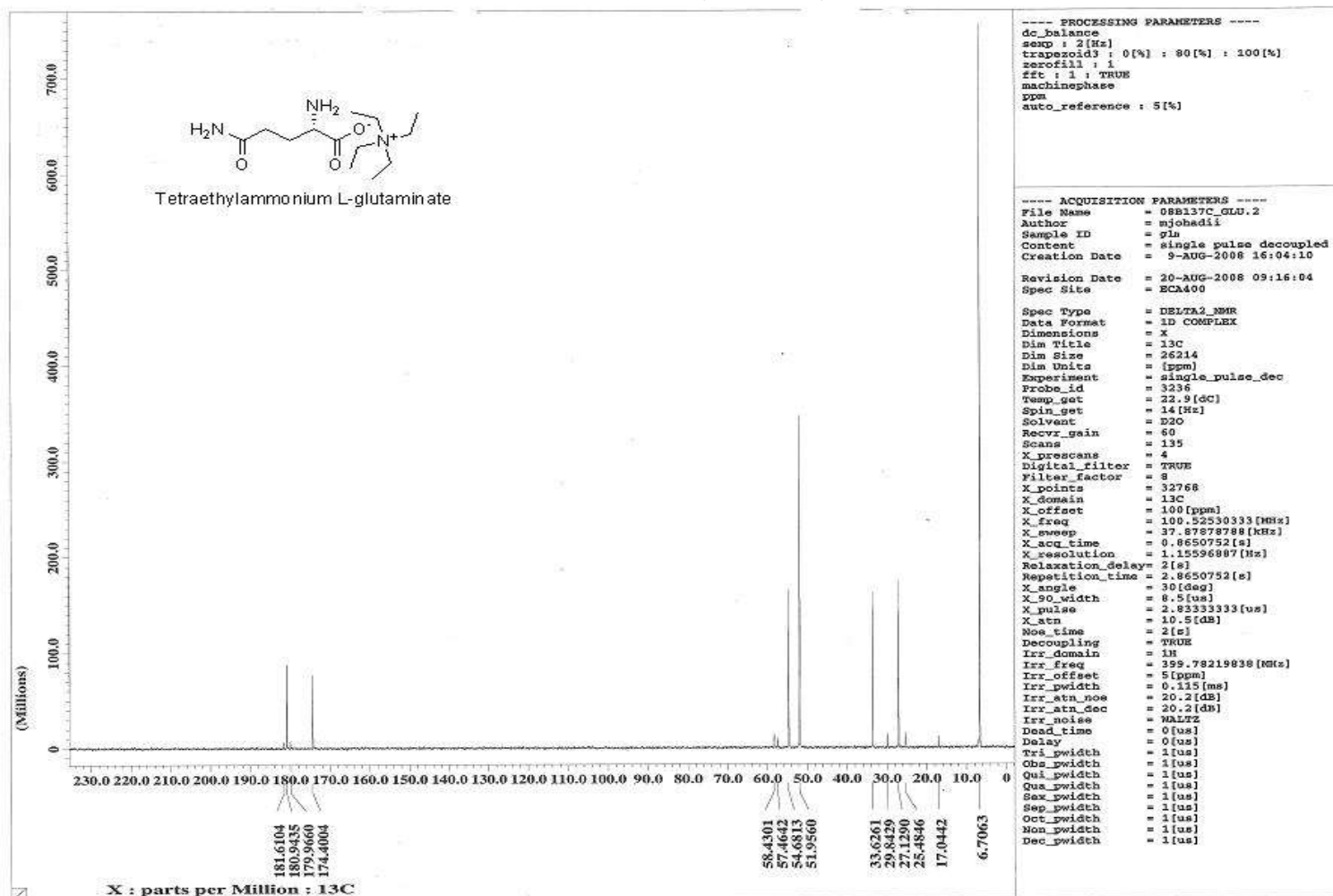
Sample directory: /

File: kq00001_020.f2



^1H NMR spectrum of tetraethylammonium L-glutamate

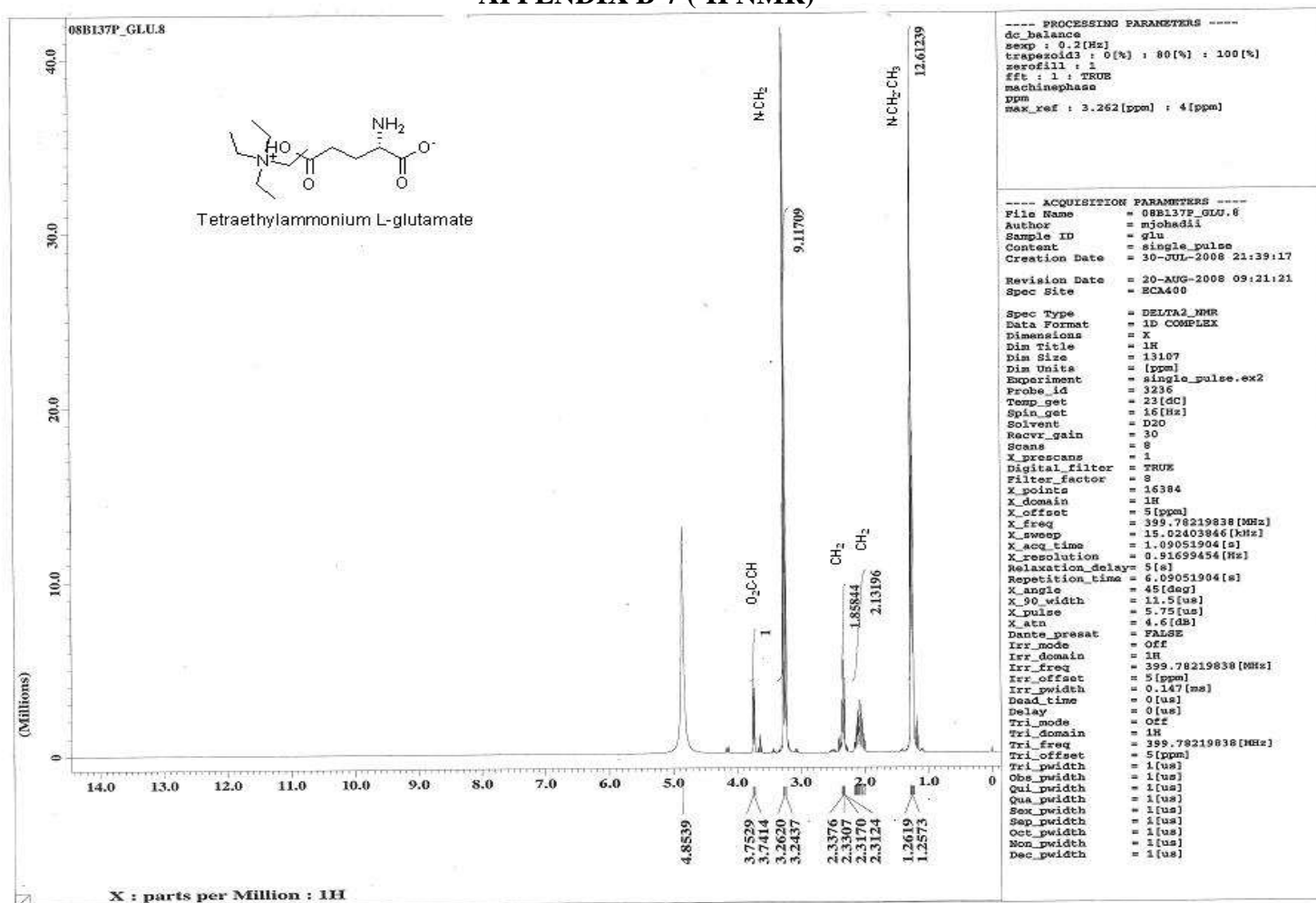
APPENDIX B-6 (¹³C NMR)



¹³C NMR spectrum of tetraethylammonium L-glutamate



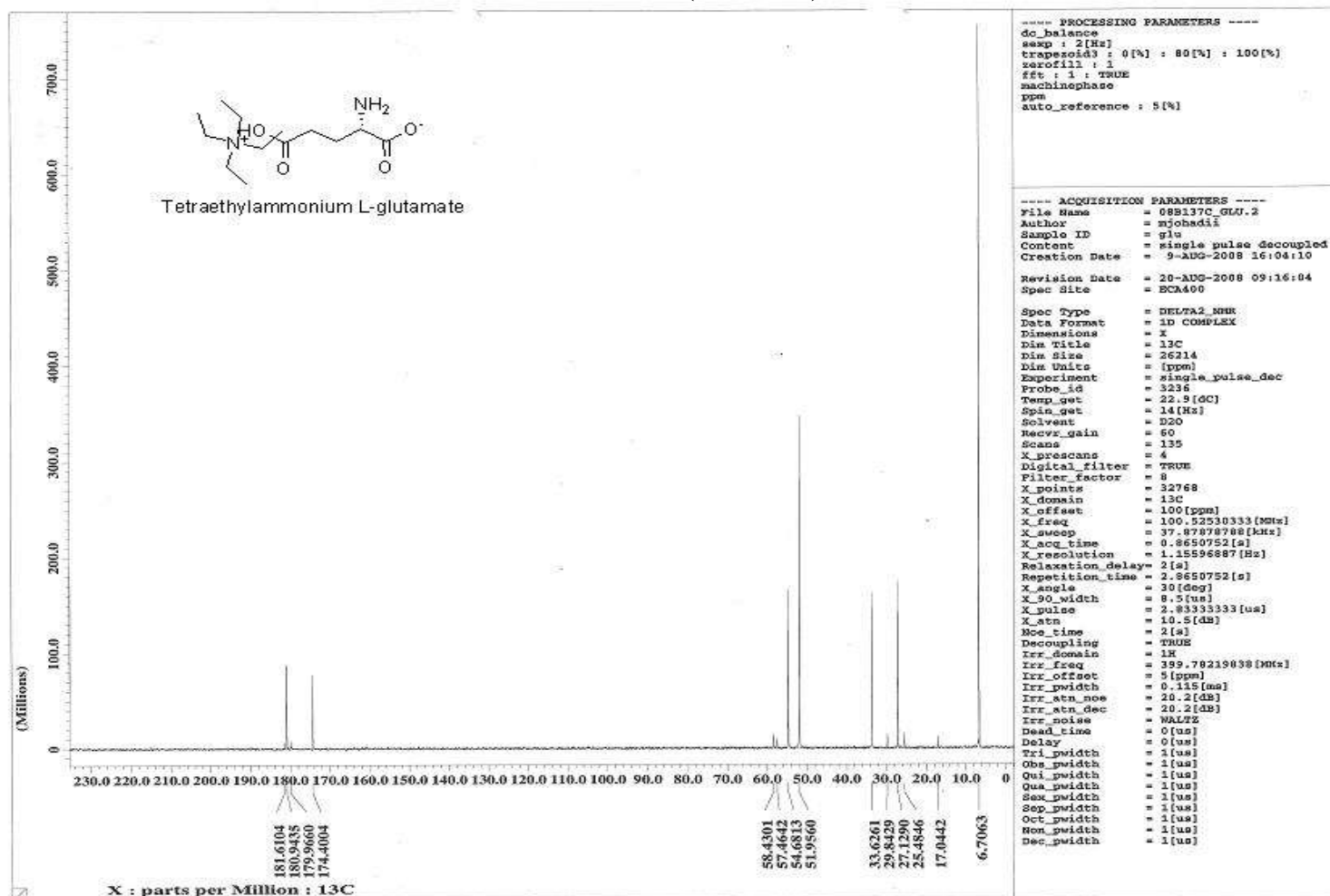
APPENDIX B-7 (¹H NMR)



¹H NMR spectrum of tetraethylammonium L-glutamate

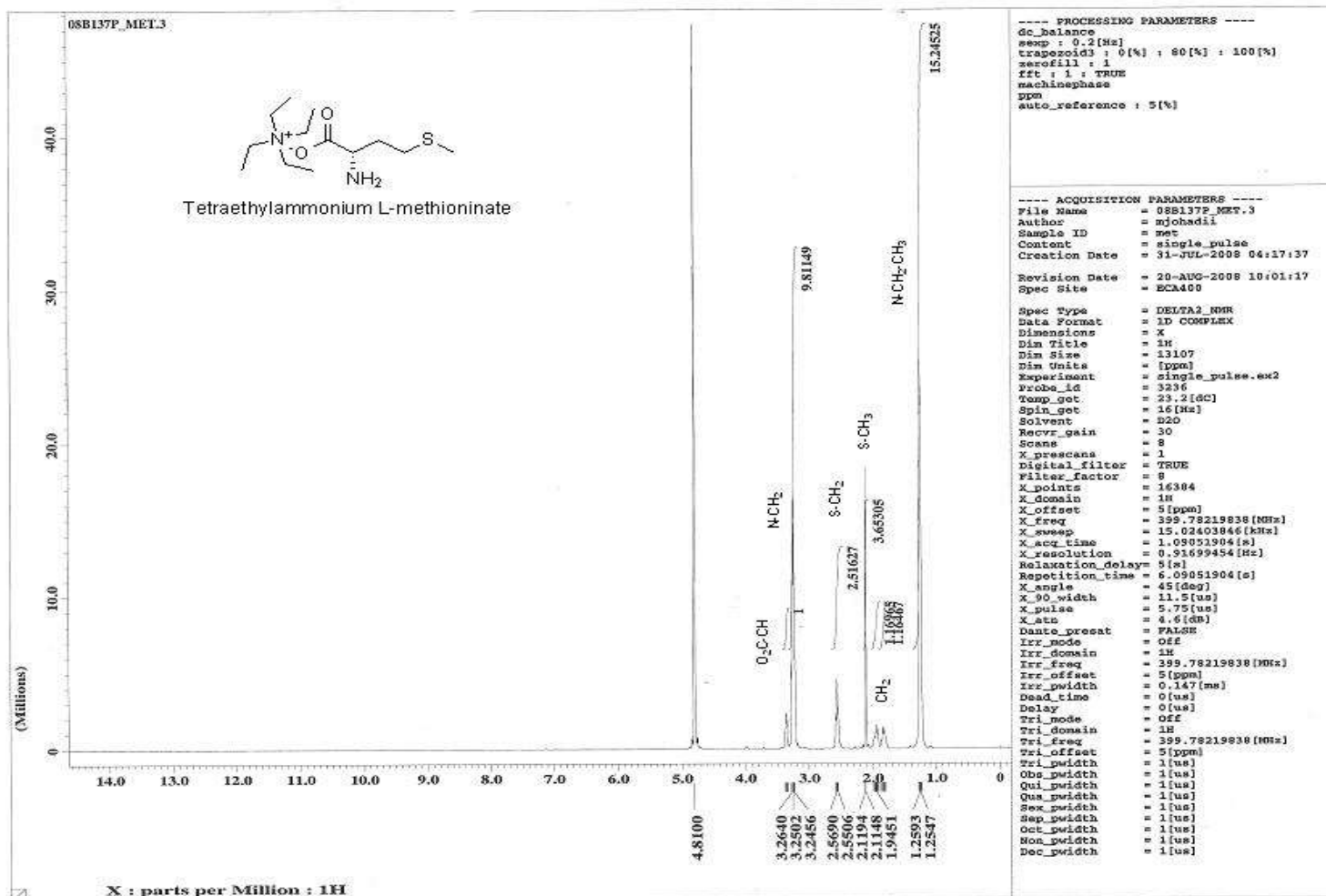


APPENDIX B-7 (¹³C NMR)



¹³C NMR spectrum of tetraethylammonium L-glutamate

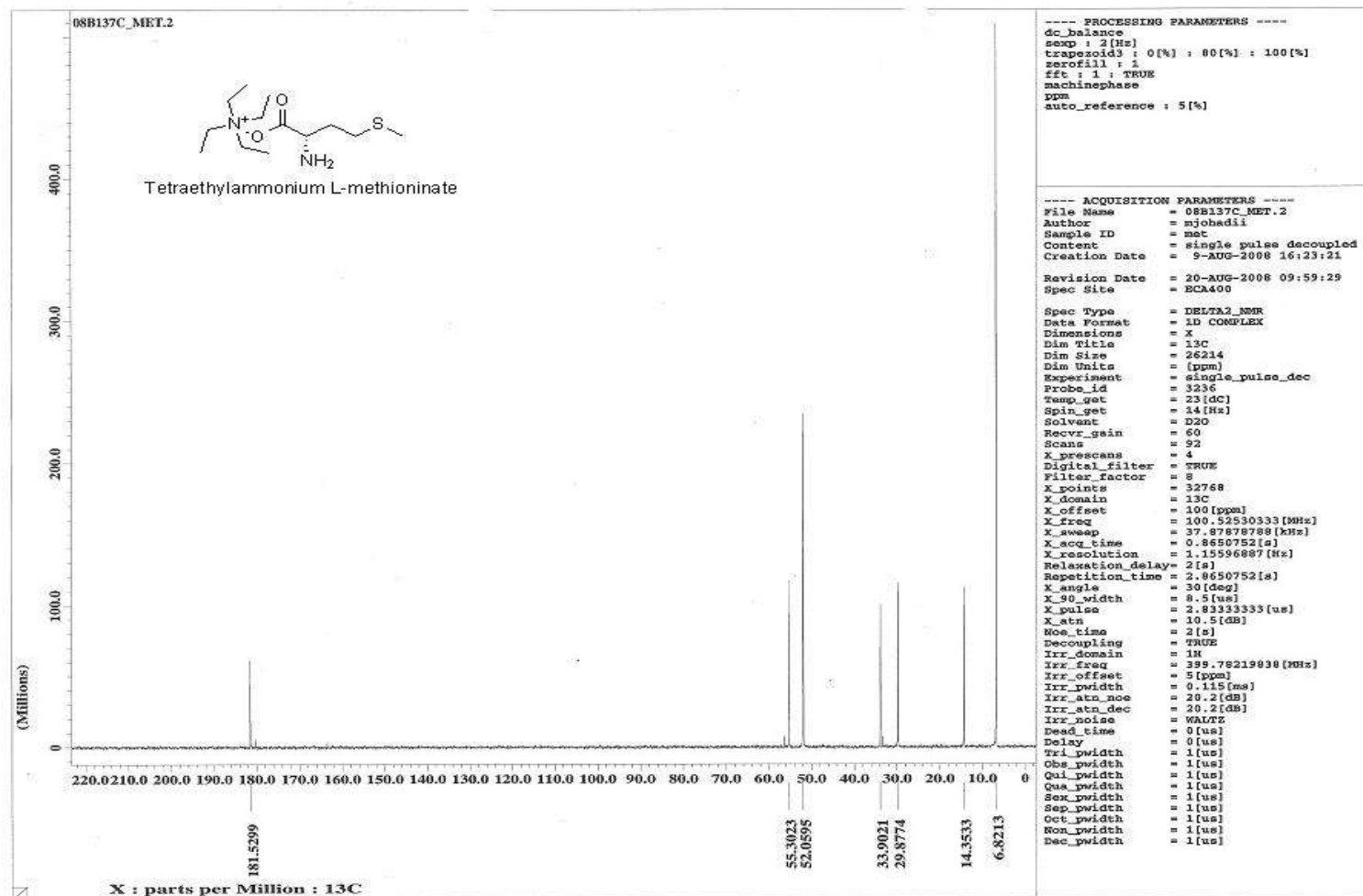
APPENDIX B-8 (¹H NMR)



¹H NMR spectrum of tetraethylammonium L-methioninate

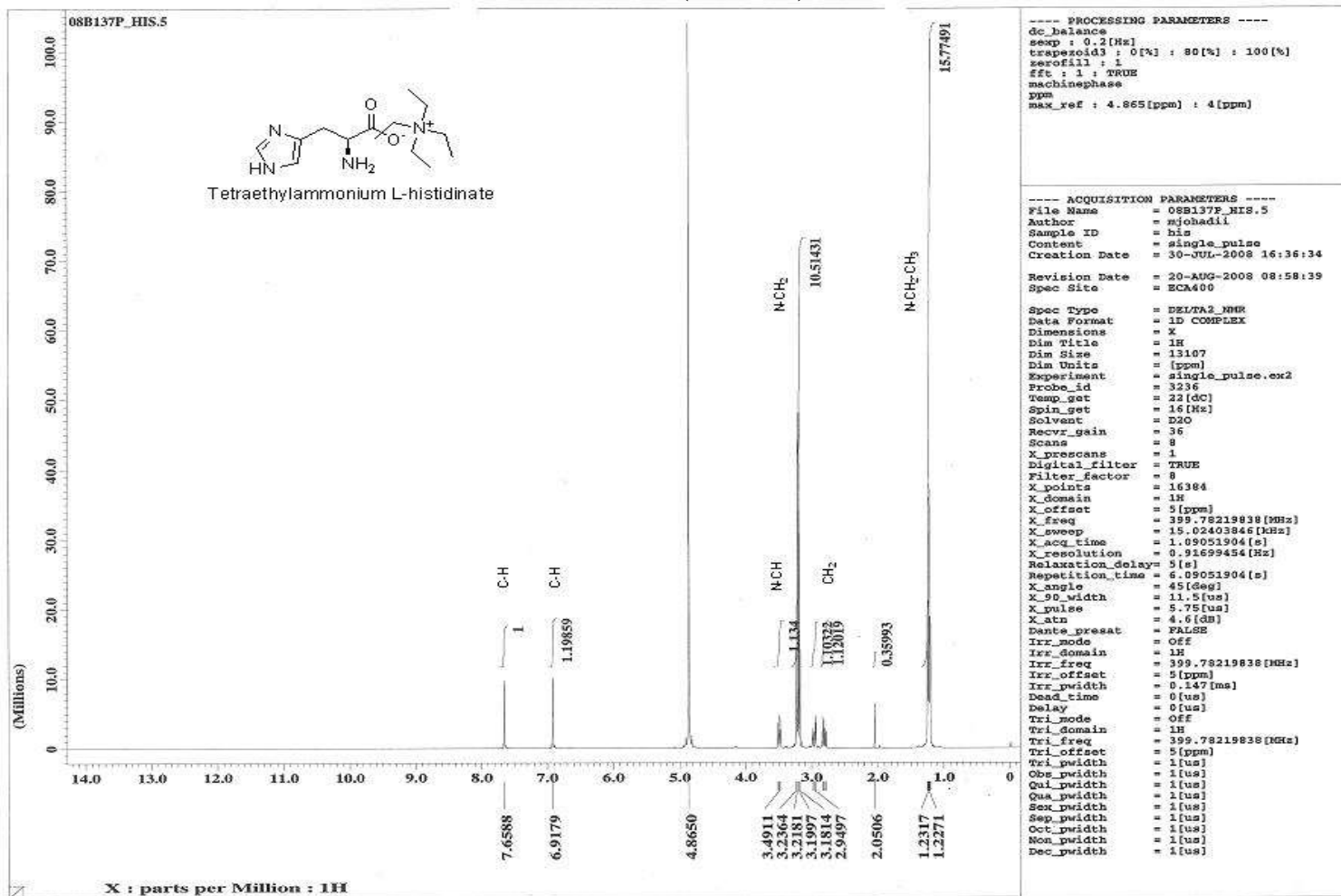


APPENDIX B-8 (¹³C NMR)



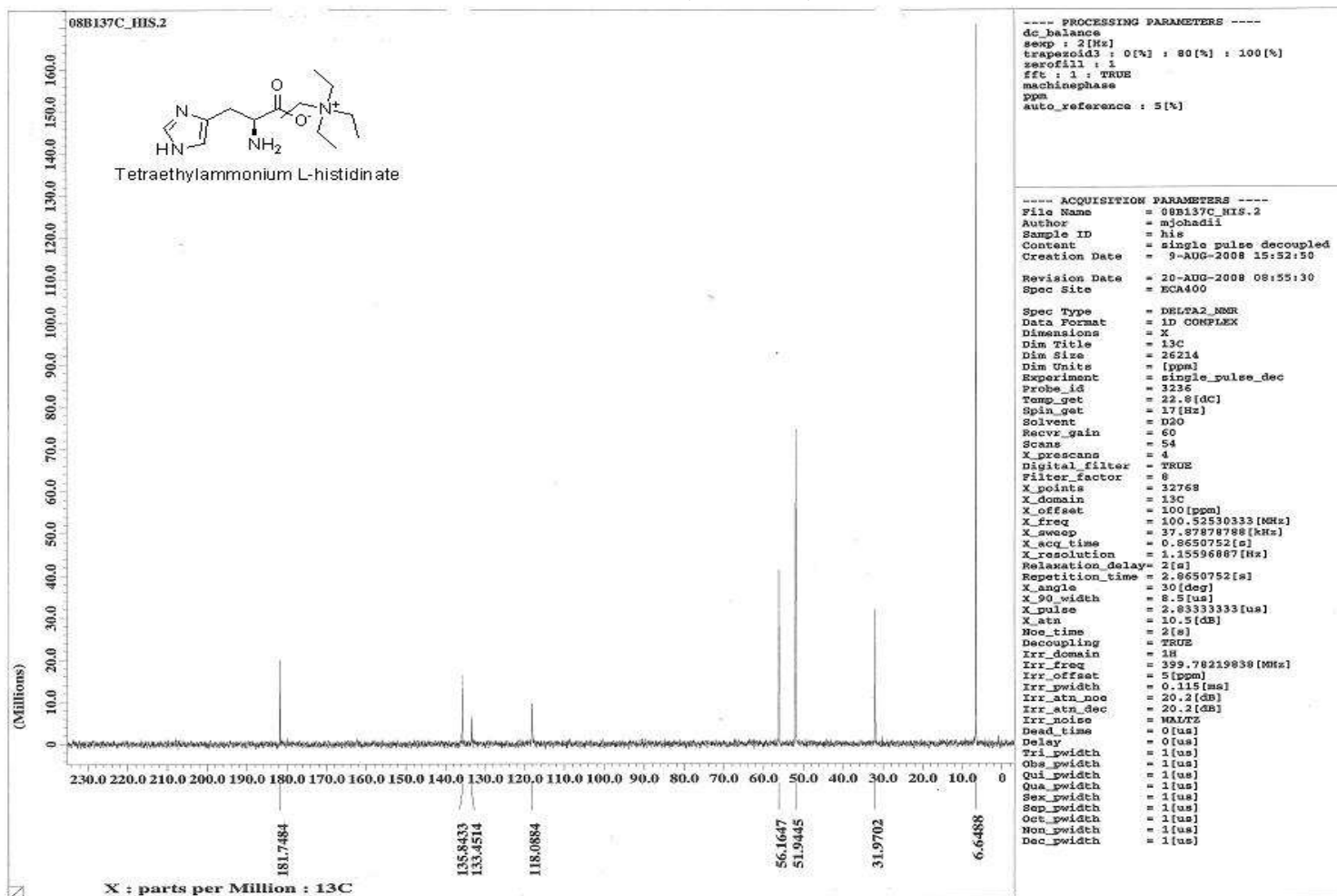
¹³C NMR spectrum of tetraethylammonium L-methioninate

APPENDIX B-9 (¹H NMR)



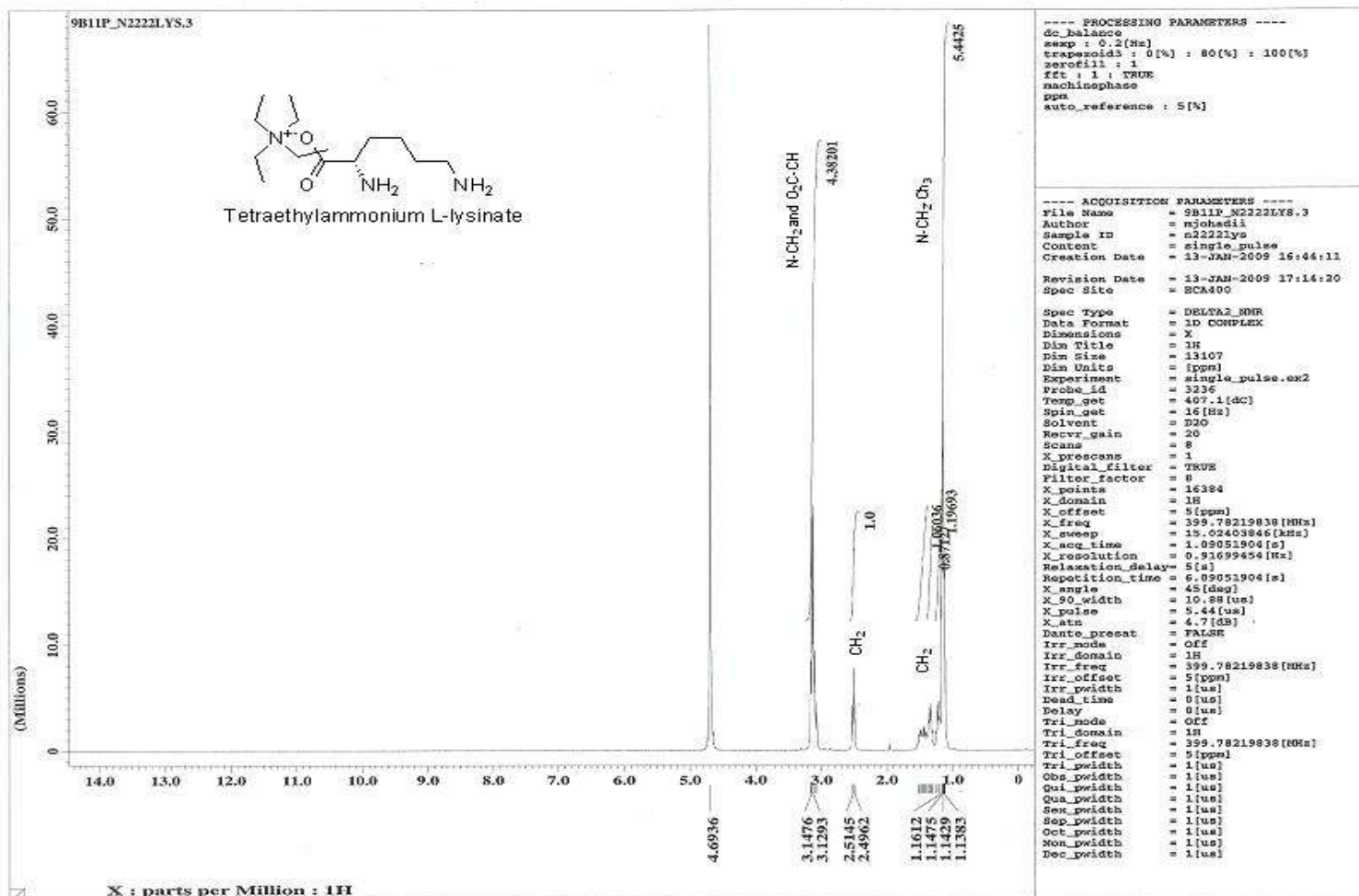
¹H NMR spectrum of tetraethylammonium L-histidinate

APPENDIX B-9 (¹³C NMR)



¹³C NMR spectrum of tetraethylammonium L-histidinate

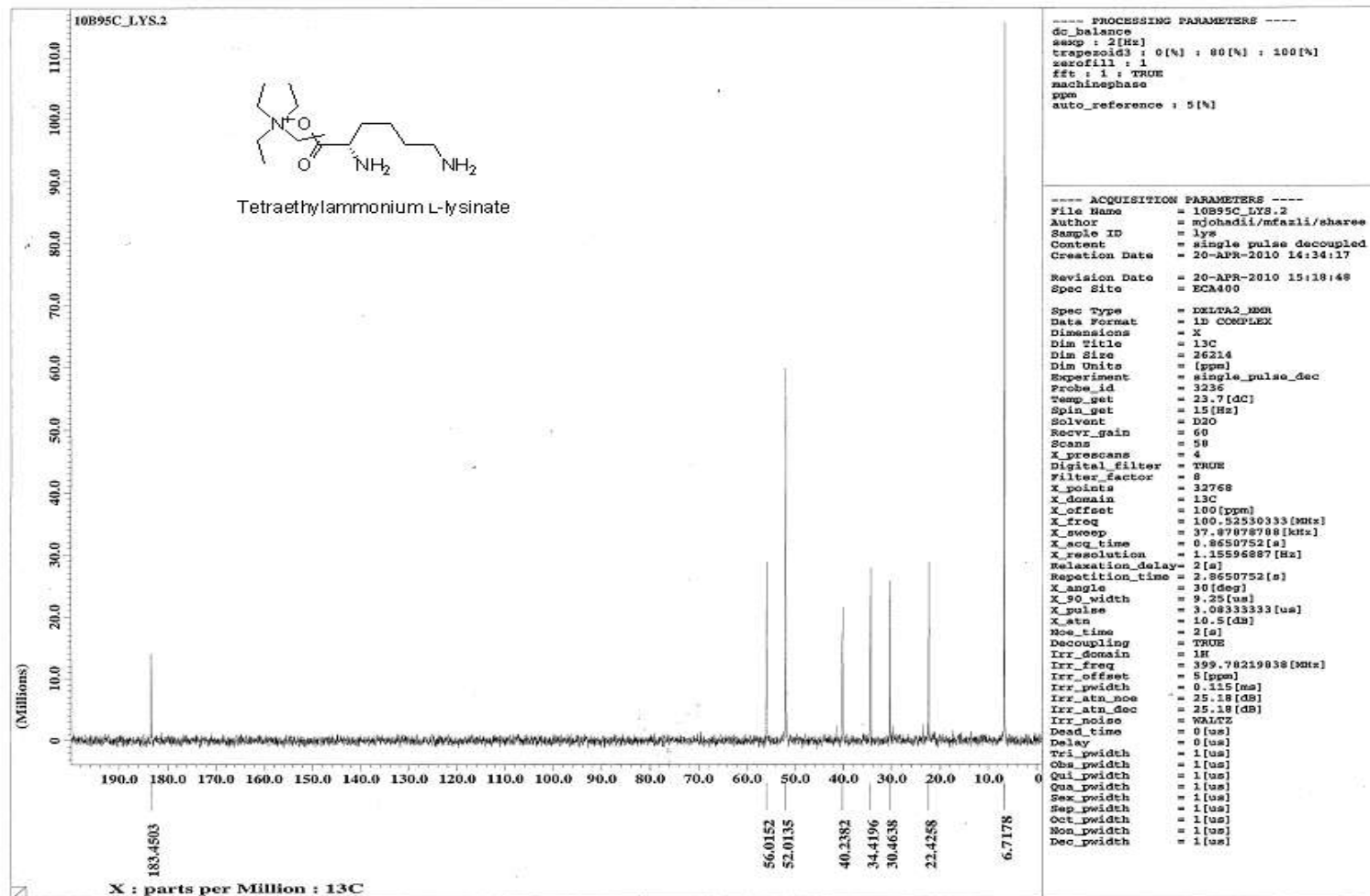
APPENDIX B-10 (¹H NMR)



¹H NMR spectrum of tetraethylammonium L-lysinate

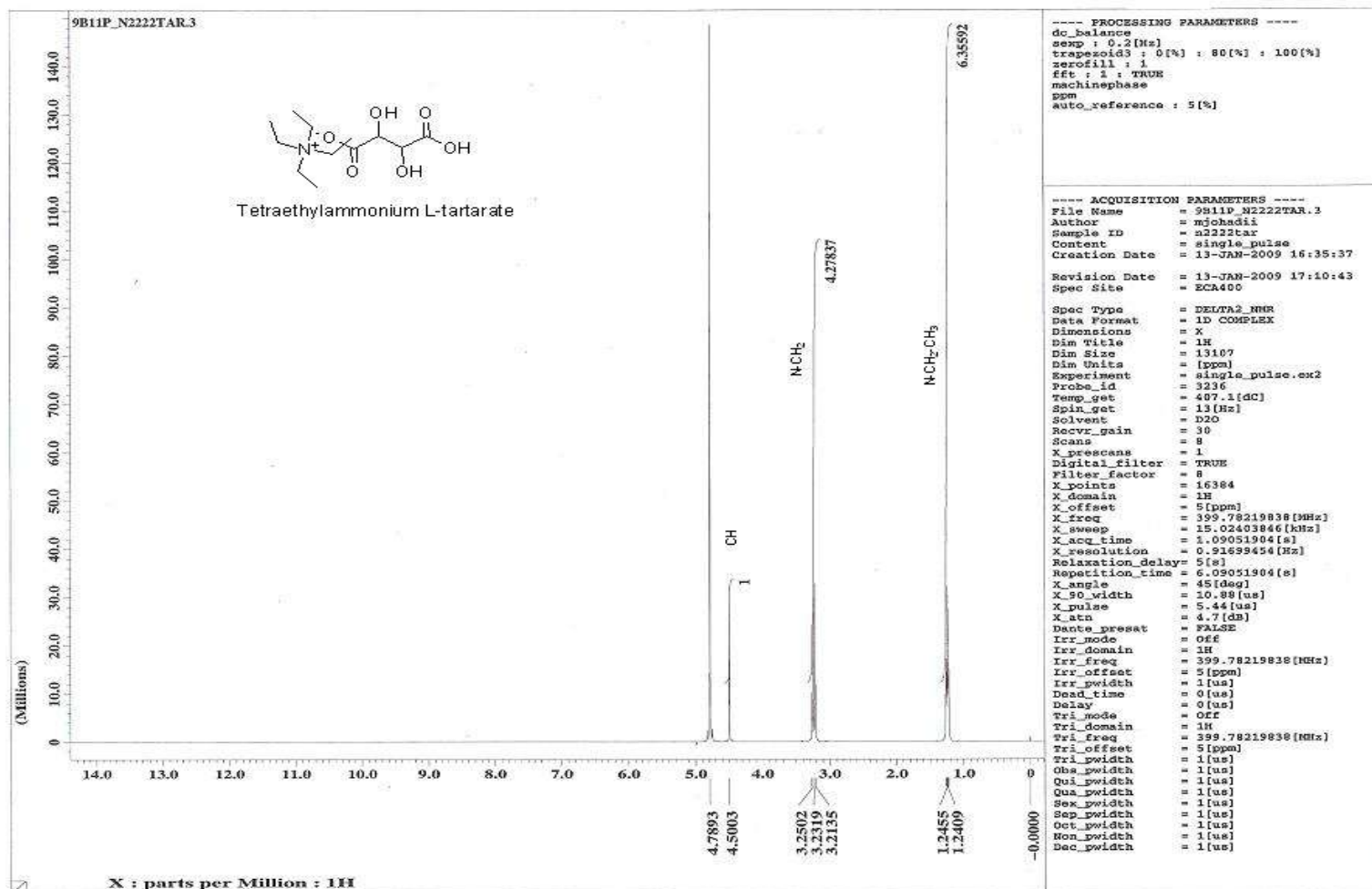


APPENDIX B-10 (¹³C NMR)



¹³C NMR spectrum of tetraethylammonium L-lysinate

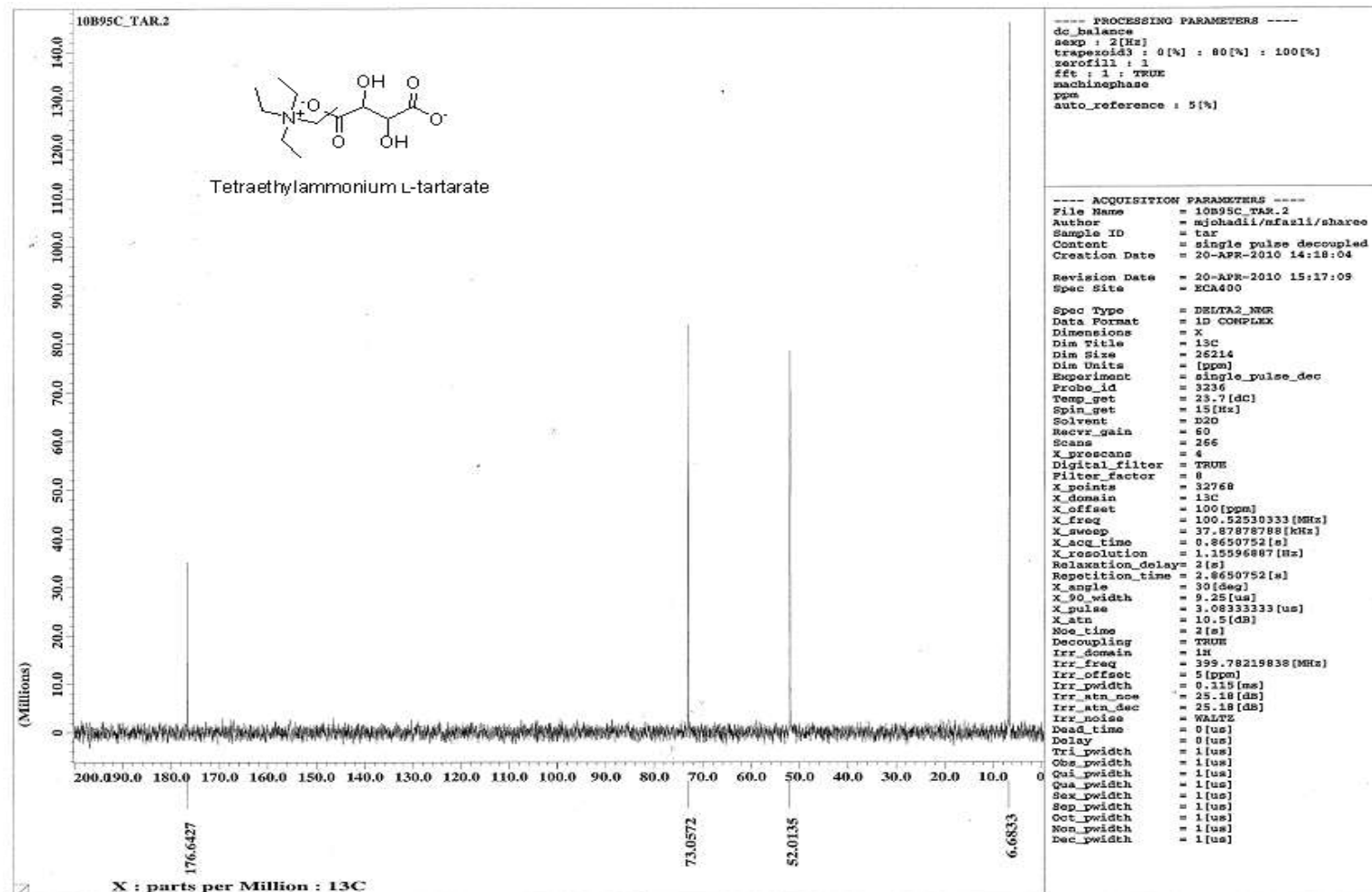
APPENDIX B-11 (¹H NMR)



¹H NMR spectrum of tetraethylammonium L-tartrate

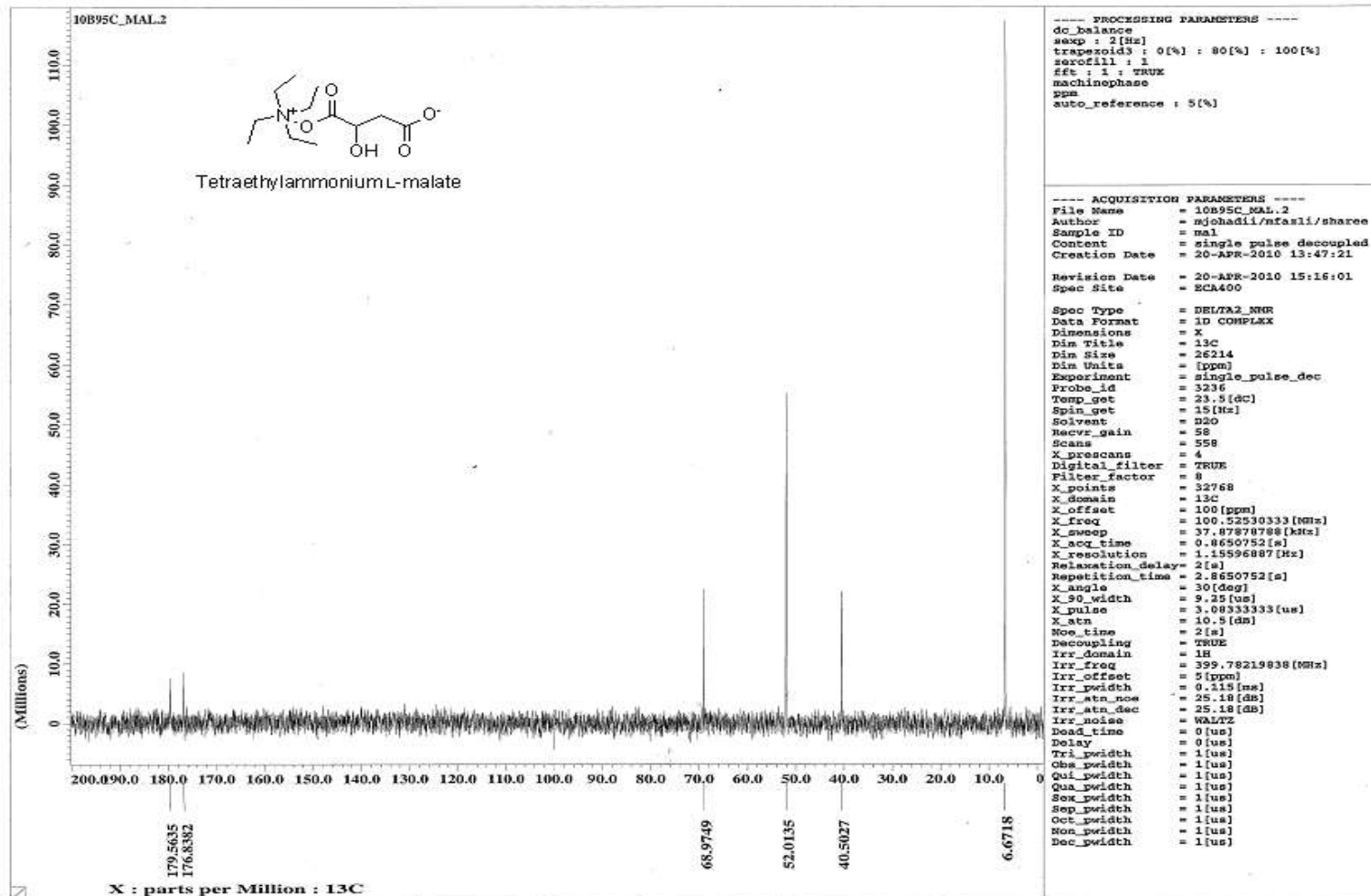


APPENDIX B-11 (¹³C NMR)



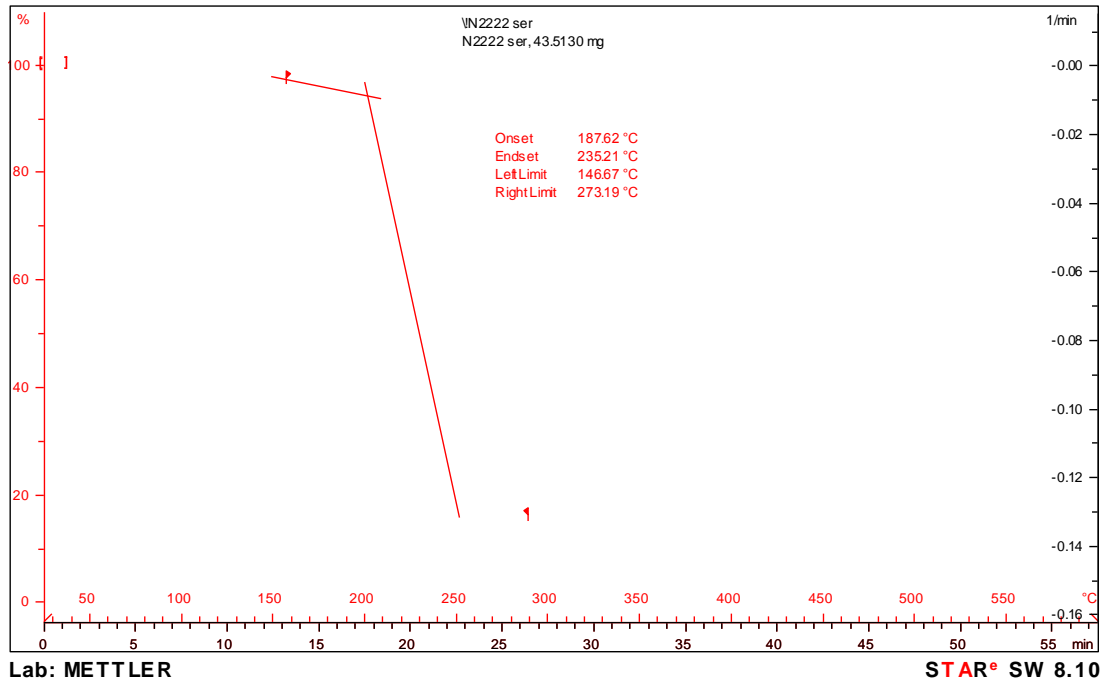
¹³C NMR spectrum of tetraethylammonium L-tartrate

APPENDIX B-12 (¹³C NMR)



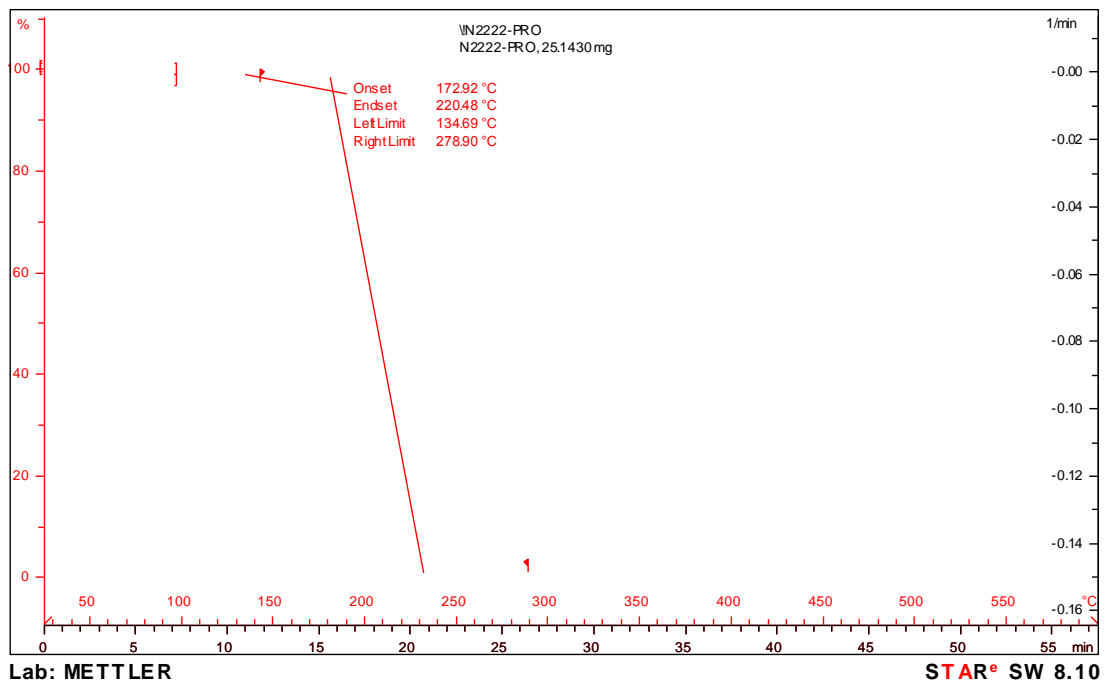
¹³C NMR spectrum of tetraethylammonium L-malate

APPENDIX C-1



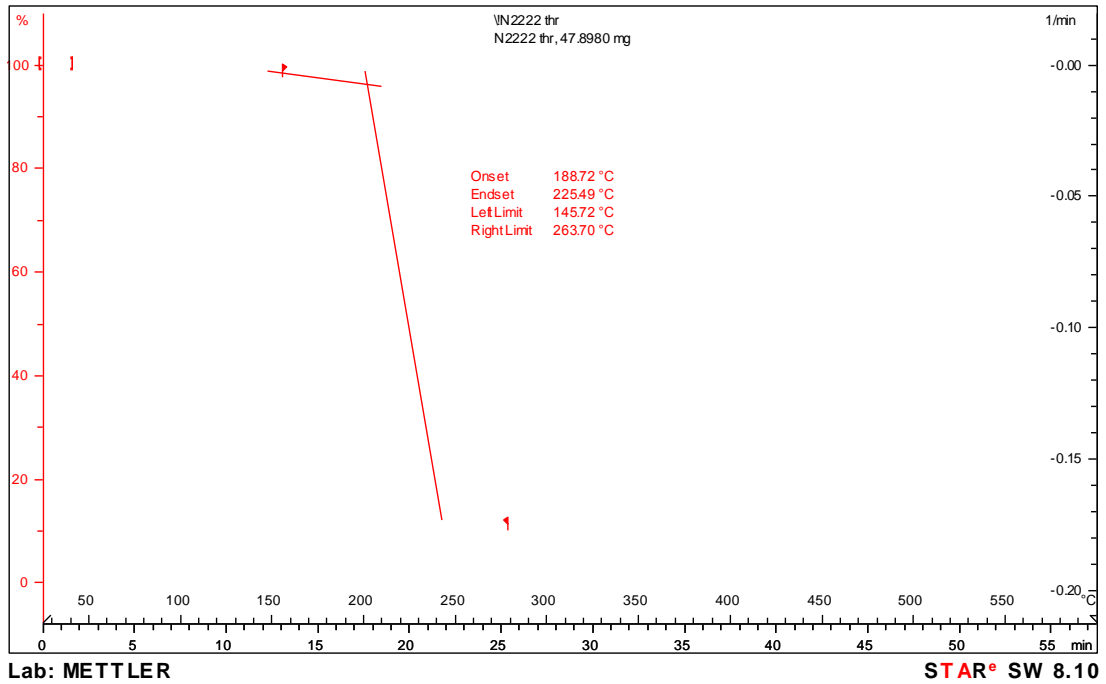
TGA and DTG curves for tetraethylammonium L-serinate ([N₂₂₂₂][ser])

APPENDIX C-2



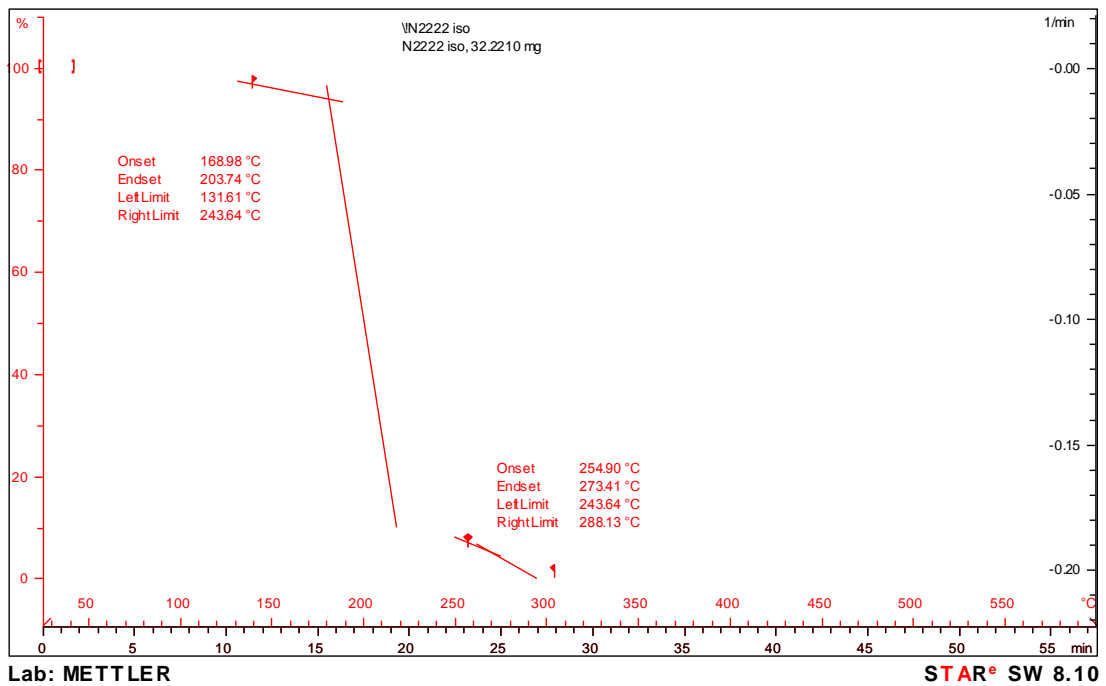
TGA and DTG curves for tetraethylammonium L-prolinate ([N₂₂₂₂][pro])

APPENDIX C-3



TGA and DTG curves for tetraethylammonium L-threoninate ([N₂₂₂₂][thr])

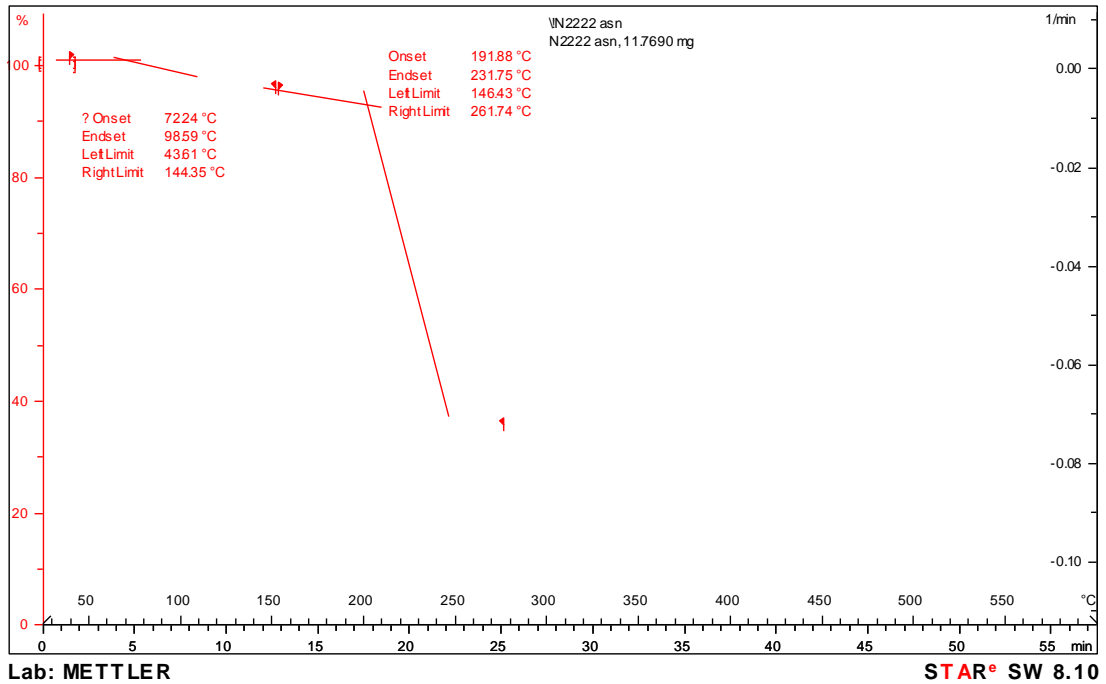
APPENDIX C-4



TGA and DTG curves for tetraethylammonium L-isoleucinate ([N₂₂₂₂][ile])

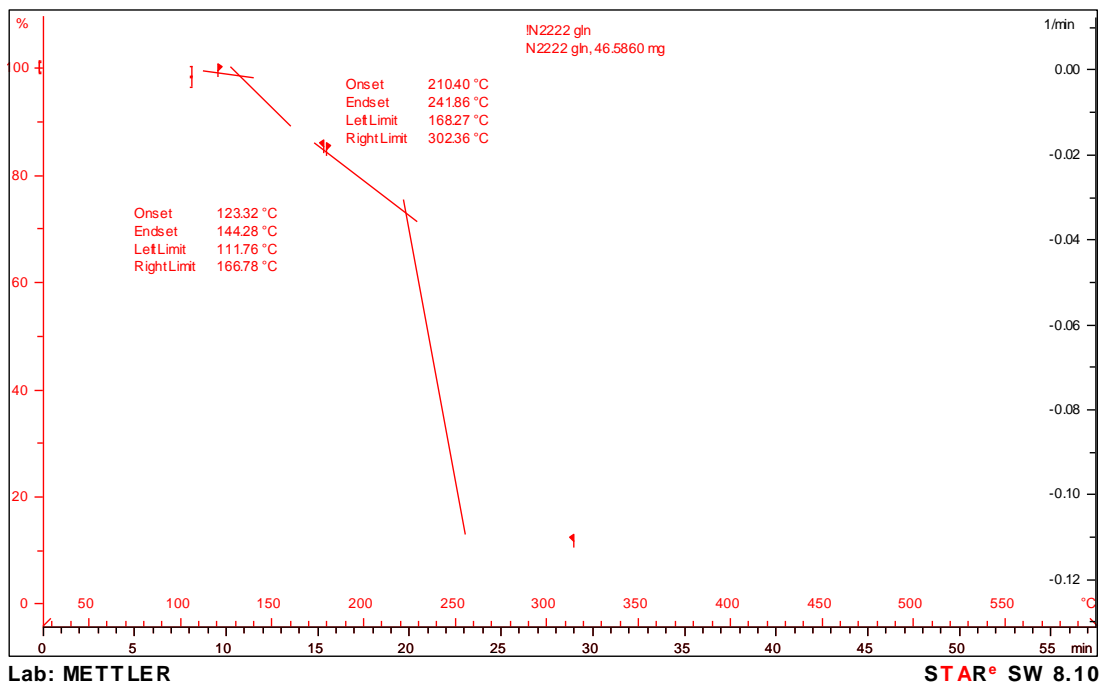


APPENDIX C-5



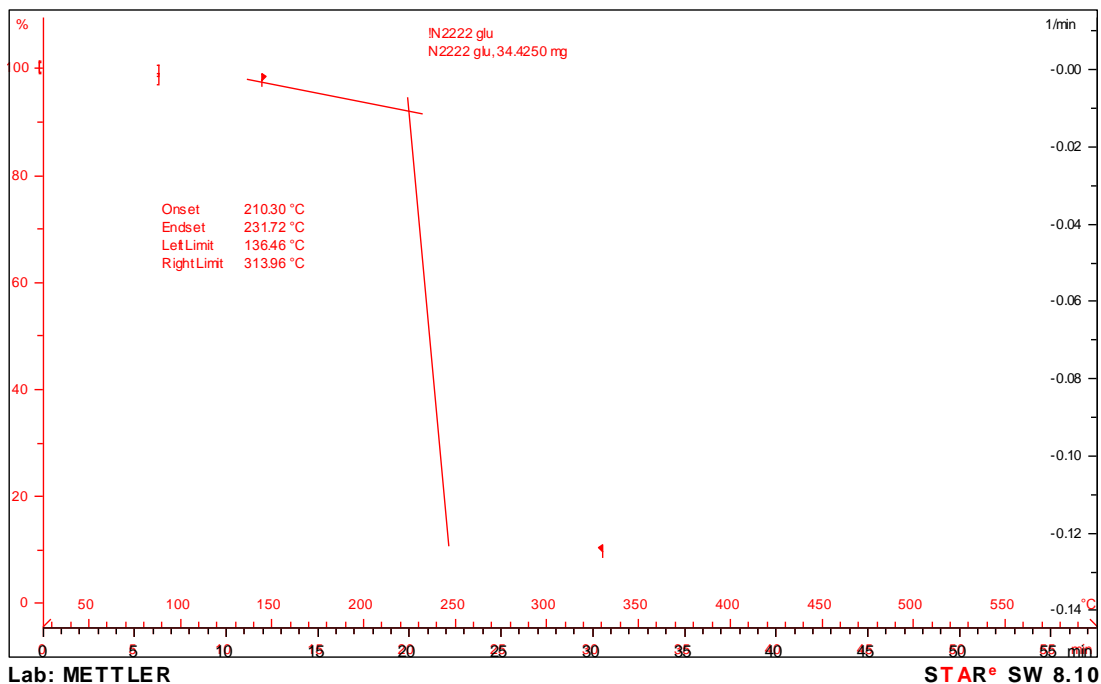
TGA and DTG curves for tetraethylammonium L-asparaginate ($[N_{2222}][asn]$)

APPENDIX C-6



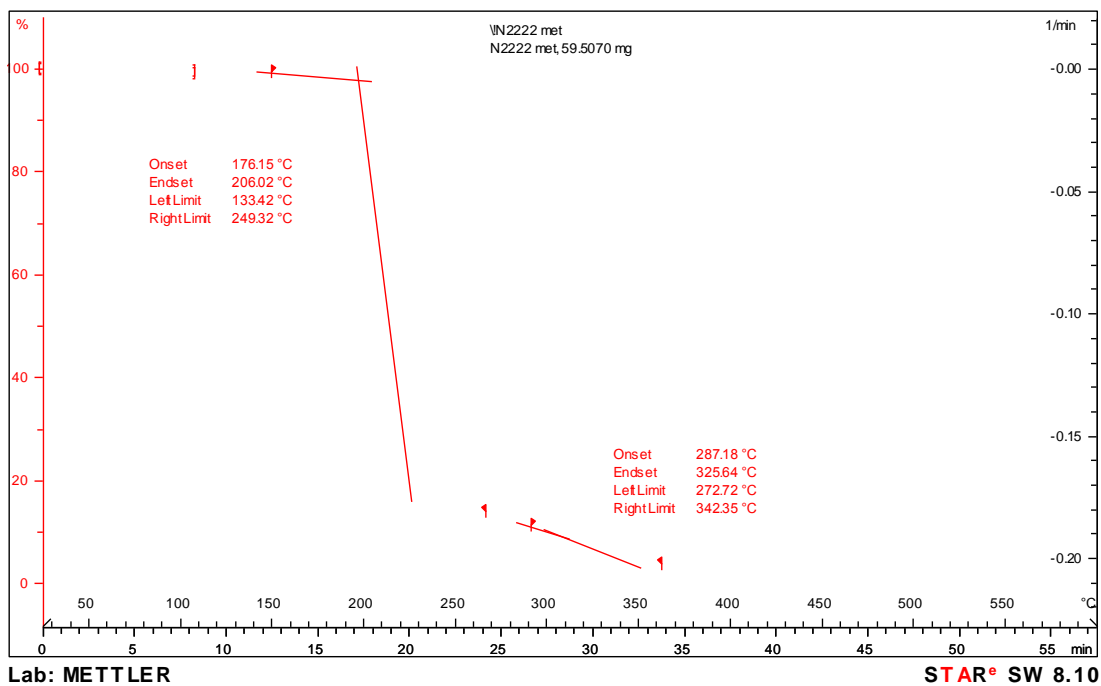
TGA and DTG curves for tetraethylammonium L-glutamate ($[N_{2222}][gln]$)

APPENDIX C-7



TGA and DTG curves for tetraethylammonium L-glutamate ([N₂₂₂₂][glu])

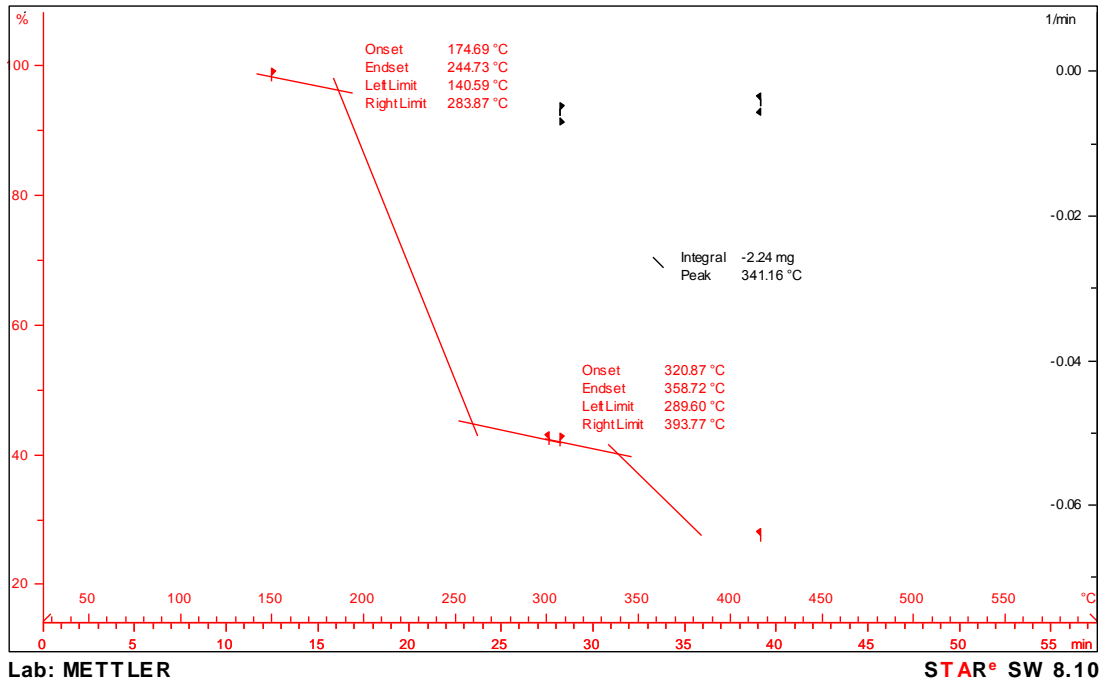
APPENDIX C-8



TGA and DTG curves for tetraethylammonium L-methioninate ([N₂₂₂₂][met])

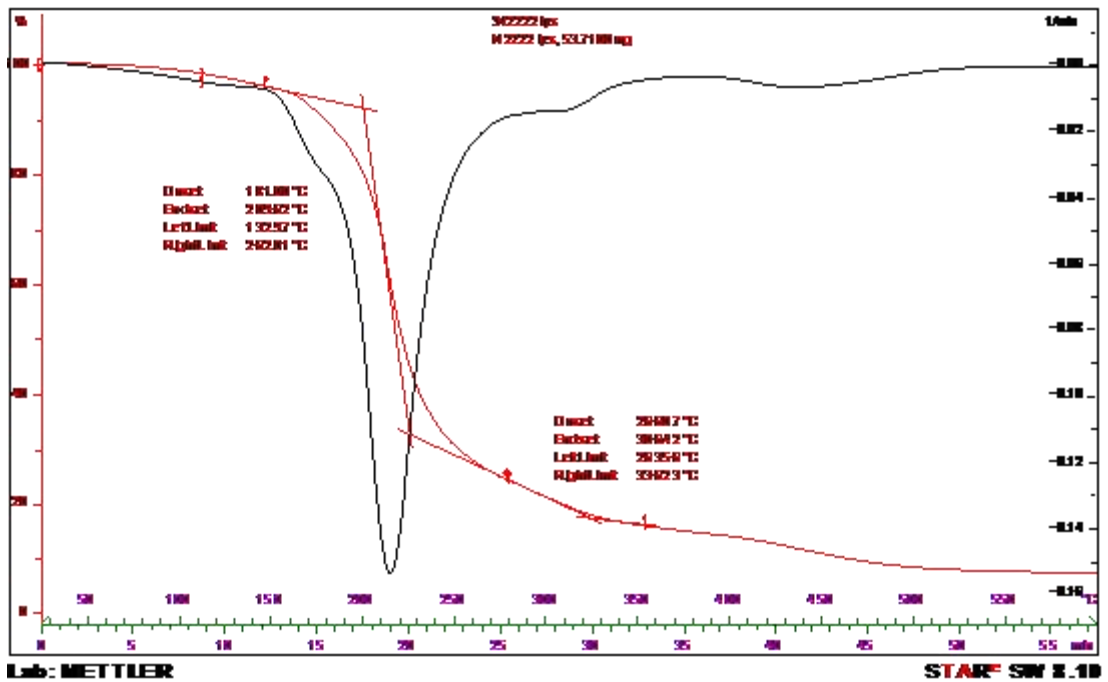


APPENDIX C-9



TGA and DTG curves for tetraethylammonium L-histidinate ([N₂₂₂₂][his])

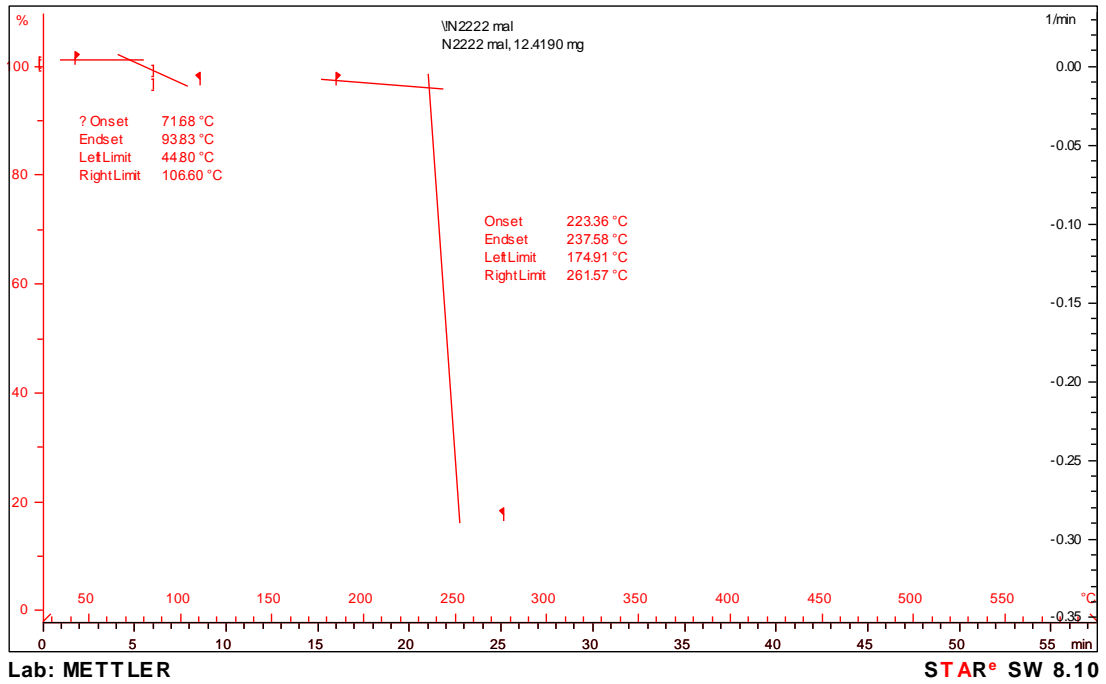
APPENDIX C-10



TGA and DTG curves for tetraethylammonium L-lysinate ([N₂₂₂₂][lys])

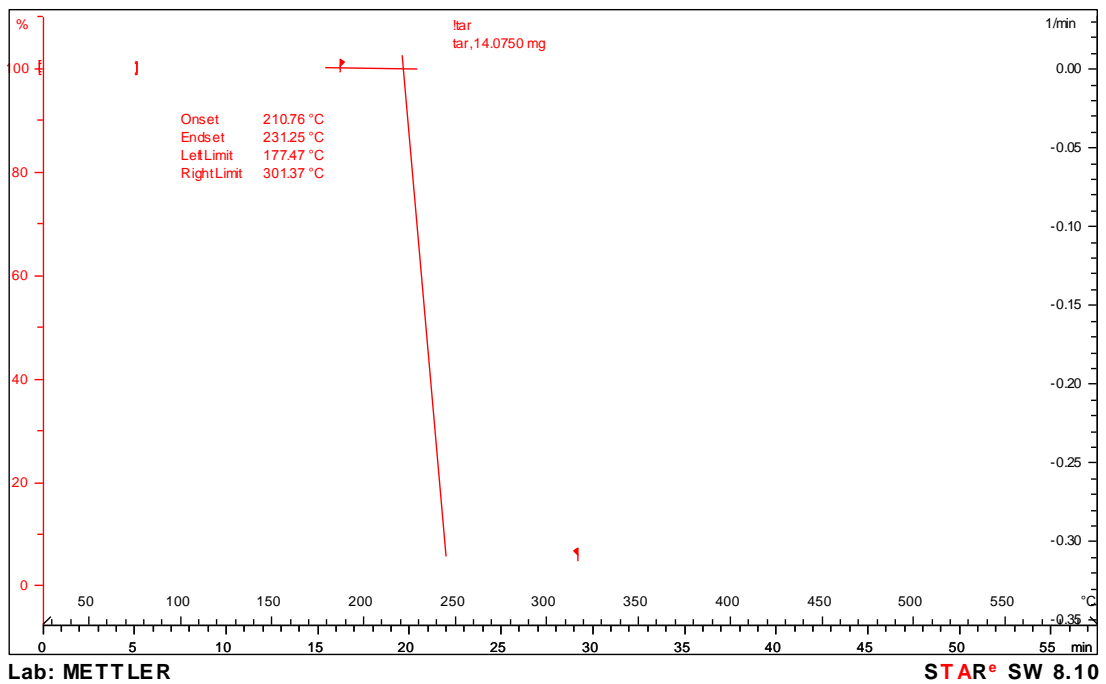


APPENDIX C-11



TGA and DTG curves for tetraethylammonium L-malate ([N₂₂₂₂][mal])

APPENDIX C-12



TGA and DTG curves for tetraethylammonium L-tartrate ([N₂₂₂₂][tar])

APPENDIX D

Table D1. Crystal data and structure refinement for tetraethylammonium L-tartarate ([N₂₂₂₂][tar])

Empirical formula	C ₁₂ H ₂₉ N ₁ O ₈
Formula weight	315.36
Temperature	100.0(1) K
Wavelength	0.71073 Å
Crystal system, space group	Monoclinic, P2 ₁
Unit cell dimensions	$a = 7.4074(1) \text{ \AA}$ $\alpha = 90^\circ$ $b = 13.8989(2) \text{ \AA}$ $\beta = 106.553^\circ (1)$ $c = 8.0546(1) \text{ \AA}$ $\gamma = 90^\circ$
Volume (Å ³)	794.891(19)
Z, Calculated density (Mg/m ³)	2, 1.318
Absorption coefficient (mm ⁻¹)	0.110
F(000)	344
Crystal size (mm)	0.47 x 0.45 x 0.17
Theta range for data collection (°)	2.64 to 35.00
Limiting indices	-9 ≤ h ≤ 11, -22 ≤ k ≤ 17, -12 ≤ l ≤ 12
Reflections collected / unique	10518 / 3579 [R(int) = 0.0307]
Completeness to theta = 35.00 (%)	99.4
Absorption correction	Semi-empirical from equivalents
Max. and min. transmission	0.9811 and 0.8614
Refinement method	Full-matrix least-squares on F ²
Data / restraints / parameters	3579 / 1 / 218
Goodness-of-fit on F ²	1.049
Final R indices [I > 2σ(I)]	R1 = 0.0371, wR2 = 0.0886
R indices (all data)	R1 = 0.0426, wR2 = 0.0922
Largest diff. peak and hole (e.Å ⁻³)	0.292 and -0.231



Table D2. Atomic coordinates ($\times 10^4$) and equivalent isotropic displacement parameters ($\text{Å}^2 \times 10^3$) for [N₂₂₂₂][tar]. U(eq) is defined as one third of the trace of the orthogonalized U_{ij} tensor.

	x	y	z	U (eq)
O (1)	7144 (1)	1923 (1)	-357 (1)	18 (1)
O (2)	10201 (1)	2326 (1)	445 (1)	20 (1)
O (3)	6193 (1)	3682 (1)	-1876 (1)	17 (1)
O (4)	6846 (2)	3911 (1)	1793 (1)	19 (1)
C (1)	8385 (2)	2511 (1)	-182 (2)	14 (1)
C (2)	7987 (2)	3567 (1)	-687 (2)	13 (1)
C (3)	8193 (2)	4184 (1)	945 (2)	14 (1)
C (4)	8070 (2)	5255 (1)	461 (2)	16 (1)
N (1)	6178 (2)	1358 (1)	4453 (1)	14 (1)
C (5)	6807 (2)	568 (1)	3433 (2)	17 (1)
C (6)	8153 (2)	-164 (1)	4516 (2)	25 (1)
C (7)	7851 (2)	1880 (1)	5644 (2)	17 (1)
C (8)	9195 (2)	2332 (1)	4760 (2)	23 (1)
C (9)	5073 (2)	948 (1)	5618 (2)	19 (1)
C (10)	3270 (2)	428 (1)	4690 (2)	22 (1)
C (11)	4973 (2)	2033 (1)	3107 (2)	16 (1)
C (12)	4121 (2)	2871 (1)	3829 (2)	21 (1)
O (1W)	3085 (2)	2756 (1)	8465 (2)	24 (1)
O (2W)	6983 (2)	9760 (1)	9557 (2)	25 (1)
O (5)	9367 (1)	5548 (1)	-173 (2)	22 (1)
O (6)	6774 (2)	5747 (1)	704 (1)	23 (1)



Table D3. Bond lengths [Å] and angles [deg] for [N₂₂₂₂][tar]

O (1) -C (1)	1.2084 (16)
O (2) -C (1)	1.3203 (15)
O (2) -H (1O2)	1.01 (3)
O (3) -C (2)	1.4085 (16)
O (3) -H (1O3)	0.90 (3)
O (4) -C (3)	1.4124 (17)
O (4) -H (1O4)	0.84 (3)
C (1) -C (2)	1.5292 (17)
C (2) -C (3)	1.5400 (17)
C (2) -H (2A)	0.9800
C (3) -C (4)	1.5356 (18)
C (3) -H (3A)	0.9800
C (4) -O (6)	1.2382 (17)
C (4) -O (5)	1.2763 (17)
N (1) -C (11)	1.5178 (16)
N (1) -C (7)	1.5183 (17)
N (1) -C (9)	1.5205 (16)
N (1) -C (5)	1.5209 (17)
C (5) -C (6)	1.515 (2)
C (5) -H (5A)	0.9700
C (5) -H (5B)	0.9700
C (6) -H (6A)	0.9600
C (6) -H (6B)	0.9600
C (6) -H (6C)	0.9600
C (7) -C (8)	1.516 (2)
C (7) -H (7A)	0.9700
C (7) -H (7B)	0.9700
C (8) -H (8A)	0.9600
C (8) -H (8B)	0.9600
C (8) -H (8C)	0.9600
C (9) -C (10)	1.516 (2)
C (9) -H (9A)	0.9700
C (9) -H (9B)	0.9700
C (10) -H (10A)	0.9600
C (10) -H (10B)	0.9600
C (10) -H (10C)	0.9600
C (11) -C (12)	1.516 (2)
C (11) -H (11A)	0.9700
C (11) -H (11B)	0.9700
C (12) -H (12A)	0.9600
C (12) -H (12B)	0.9600
C (12) -H (12C)	0.9600
O (1W) -H (1W1)	0.83 (3)
O (1W) -H (2W1)	0.88 (3)
O (2W) -H (1W2)	0.91 (3)
O (2W) -H (2W2)	0.85 (3)
C (1) -O (2) -H (1O2)	110.3 (15)
C (2) -O (3) -H (1O3)	110.7 (16)
C (3) -O (4) -H (1O4)	101.3 (17)
O (1) -C (1) -O (2)	124.88 (12)
O (1) -C (1) -C (2)	122.38 (11)

O(2)-C(1)-C(2)	112.74(11)
O(3)-C(2)-C(1)	111.28(10)
O(3)-C(2)-C(3)	111.23(10)
C(1)-C(2)-C(3)	110.06(10)
O(3)-C(2)-H(2A)	108.0
C(1)-C(2)-H(2A)	108.0
C(3)-C(2)-H(2A)	108.0
O(4)-C(3)-C(4)	112.59(11)
O(4)-C(3)-C(2)	110.58(10)
C(4)-C(3)-C(2)	109.84(10)
O(4)-C(3)-H(3A)	107.9
C(4)-C(3)-H(3A)	107.9
C(2)-C(3)-H(3A)	107.9
O(6)-C(4)-O(5)	126.43(13)
O(6)-C(4)-C(3)	119.17(12)
O(5)-C(4)-C(3)	114.40(11)
C(11)-N(1)-C(7)	111.31(10)
C(11)-N(1)-C(9)	111.21(10)
C(7)-N(1)-C(9)	105.96(9)
C(11)-N(1)-C(5)	105.62(9)
C(7)-N(1)-C(5)	111.49(10)
C(9)-N(1)-C(5)	111.36(10)
C(6)-C(5)-N(1)	115.24(11)
C(6)-C(5)-H(5A)	108.5
N(1)-C(5)-H(5A)	108.5
C(6)-C(5)-H(5B)	108.5
N(1)-C(5)-H(5B)	108.5
H(5A)-C(5)-H(5B)	107.5
C(5)-C(6)-H(6A)	109.5
C(5)-C(6)-H(6B)	109.5
H(6A)-C(6)-H(6B)	109.5
C(5)-C(6)-H(6C)	109.5
H(6A)-C(6)-H(6C)	109.5
H(6B)-C(6)-H(6C)	109.5
C(8)-C(7)-N(1)	115.36(10)
C(8)-C(7)-H(7A)	108.4
N(1)-C(7)-H(7A)	108.4
C(8)-C(7)-H(7B)	108.4
N(1)-C(7)-H(7B)	108.4
H(7A)-C(7)-H(7B)	107.5
C(7)-C(8)-H(8A)	109.5
C(7)-C(8)-H(8B)	109.5
H(8A)-C(8)-H(8B)	109.5
C(7)-C(8)-H(8C)	109.5
H(8A)-C(8)-H(8C)	109.5
H(8B)-C(8)-H(8C)	109.5
C(10)-C(9)-N(1)	115.34(10)
C(10)-C(9)-H(9A)	108.4
N(1)-C(9)-H(9A)	108.4
C(10)-C(9)-H(9B)	108.4
N(1)-C(9)-H(9B)	108.4
H(9A)-C(9)-H(9B)	107.5
C(9)-C(10)-H(10A)	109.5
C(9)-C(10)-H(10B)	109.5
H(10A)-C(10)-H(10B)	109.5
C(9)-C(10)-H(10C)	109.5



H (10A) -C (10) -H (10C)	109.5
H (10B) -C (10) -H (10C)	109.5
C (12) -C (11) -N (1)	115.18 (10)
C (12) -C (11) -H (11A)	108.5
N (1) -C (11) -H (11A)	108.5
C (12) -C (11) -H (11B)	108.5
N (1) -C (11) -H (11B)	108.5
H (11A) -C (11) -H (11B)	107.5
C (11) -C (12) -H (12A)	109.5
C (11) -C (12) -H (12B)	109.5
H (12A) -C (12) -H (12B)	109.5
C (11) -C (12) -H (12C)	109.5
H (12A) -C (12) -H (12C)	109.5
H (12B) -C (12) -H (12C)	109.5
H (1W1) -O (1W) -H (2W1)	106 (3)
H (1W2) -O (2W) -H (2W2)	106 (2)

Symmetry transformations used to generate equivalent atoms

Table D4. Anisotropic displacement parameters ($\text{Å}^2 \times 10^3$) for $[\text{N}_{2222}][\text{tar}]$. The anisotropic displacement factor exponent takes the form: $-2 \pi^2 [h^2 a^{*2} U_{11} + \dots + 2 h k a^* b^* U_{12}]$.

	U11	U22	U33	U23	U13	U12
O (1)	17 (1)	12 (1)	26 (1)	1 (1)	7 (1)	-2 (1)
O (2)	15 (1)	12 (1)	31 (1)	-2 (1)	3 (1)	1 (1)
O (3)	17 (1)	14 (1)	17 (1)	2 (1)	1 (1)	-1 (1)
O (4)	24 (1)	16 (1)	19 (1)	2 (1)	9 (1)	1 (1)
C (1)	16 (1)	11 (1)	15 (1)	-1 (1)	5 (1)	1 (1)
C (2)	15 (1)	10 (1)	16 (1)	1 (1)	4 (1)	-1 (1)
C (3)	16 (1)	10 (1)	16 (1)	-1 (1)	2 (1)	0 (1)
C (4)	16 (1)	10 (1)	18 (1)	-1 (1)	1 (1)	0 (1)
N (1)	15 (1)	14 (1)	13 (1)	0 (1)	4 (1)	-1 (1)
C (5)	19 (1)	13 (1)	19 (1)	-3 (1)	6 (1)	0 (1)
C (6)	23 (1)	16 (1)	35 (1)	3 (1)	7 (1)	3 (1)
C (7)	17 (1)	18 (1)	16 (1)	-1 (1)	1 (1)	-2 (1)
C (8)	19 (1)	22 (1)	26 (1)	1 (1)	4 (1)	-5 (1)
C (9)	20 (1)	21 (1)	16 (1)	3 (1)	7 (1)	-2 (1)
C (10)	20 (1)	22 (1)	25 (1)	2 (1)	9 (1)	-3 (1)
C (11)	17 (1)	15 (1)	14 (1)	1 (1)	2 (1)	1 (1)
C (12)	21 (1)	16 (1)	24 (1)	-2 (1)	6 (1)	3 (1)
O (1W)	20 (1)	27 (1)	26 (1)	2 (1)	8 (1)	0 (1)
O (2W)	25 (1)	19 (1)	32 (1)	-4 (1)	9 (1)	-5 (1)
O (5)	19 (1)	12 (1)	36 (1)	1 (1)	10 (1)	-2 (1)
O (6)	25 (1)	16 (1)	29 (1)	2 (1)	10 (1)	7 (1)



Table D5. Hydrogen coordinates ($\times 10^4$) and isotropic displacement parameters ($\text{\AA}^2 \times 10^3$) for [N₂₂₂₂][tar]

	x	y	z	U (eq)
H (2A)	8929	3785	-1246	16
H (3A)	9446	4064	1739	17
H (5A)	5698	232	2745	20
H (5B)	7406	866	2638	20
H (6A)	8474	-632	3769	37
H (6B)	7563	-481	5285	37
H (6C)	9275	156	5181	37
H (7A)	7381	2382	6249	21
H (7B)	8550	1428	6507	21
H (8A)	10203	2644	5609	34
H (8B)	8532	2797	3926	34
H (8C)	9703	1841	4183	34
H (9A)	5880	505	6428	22
H (9B)	4763	1471	6286	22
H (10A)	2674	194	5523	33
H (10B)	3558	-104	4047	33
H (10C)	2437	864	3910	33
H (11A)	5737	2288	2411	19
H (11B)	3959	1665	2344	19
H (12A)	3389	3259	2891	31
H (12B)	5110	3253	4562	31
H (12C)	3325	2630	4489	31
H (1O2)	10430 (40)	1610 (20)	450 (30)	45 (7)
H (1O3)	5340 (30)	3304 (19)	-1590 (30)	36 (6)
H (1O4)	5900 (30)	4220 (20)	1220 (30)	33 (6)
H (1W1)	2600 (40)	3060 (20)	9110 (40)	55 (8)
H (2W1)	3160 (40)	2160 (20)	8840 (30)	43 (7)
H (1W2)	8180 (40)	9985 (19)	9800 (30)	37 (6)
H (2W2)	6300 (40)	10250 (20)	9620 (30)	39 (6)



Table D6. Torsion angles (°) for [N₂₂₂₂][tar]

O (1) -C (1) -C (2) -O (3)	-20.73 (16)
O (2) -C (1) -C (2) -O (3)	159.12 (10)
O (1) -C (1) -C (2) -C (3)	103.04 (13)
O (2) -C (1) -C (2) -C (3)	-77.11 (13)
O (3) -C (2) -C (3) -O (4)	60.68 (13)
C (1) -C (2) -C (3) -O (4)	63.12 (13)
O (3) -C (2) -C (3) -C (4)	-64.19 (13)
C (1) -C (2) -C (3) -C (4)	172.01 (10)
O (4) -C (3) -C (4) -O (6)	-5.84 (16)
C (2) -C (3) -C (4) -O (6)	117.86 (13)
O (4) -C (3) -C (4) -O (5)	174.27 (11)
C (2) -C (3) -C (4) -O (5)	62.03 (14)
C (11) -N (1) -C (5) -C (6)	175.99 (11)
C (7) -N (1) -C (5) -C (6)	54.95 (15)
C (9) -N (1) -C (5) -C (6)	-63.16 (15)
C (11) -N (1) -C (7) -C (8)	-60.40 (15)
C (9) -N (1) -C (7) -C (8)	178.57 (12)
C (5) -N (1) -C (7) -C (8)	57.25 (15)
C (11) -N (1) -C (9) -C (10)	56.22 (15)
C (7) -N (1) -C (9) -C (10)	177.31 (12)
C (5) -N (1) -C (9) -C (10)	-61.29 (15)
C (7) -N (1) -C (11) -C (12)	-60.88 (14)
C (9) -N (1) -C (11) -C (12)	57.02 (14)
C (5) -N (1) -C (11) -C (12)	177.97 (12)

Symmetry transformations used to generate equivalent atoms

Table D7. Hydrogen bonds for [N₂₂₂₂][tar] ([A and deg.]

D-H---A	D-H	H---A	D---A	D-H---A
O2-H1O2---O5 ⁱ	1.00 (2)	1.52 (2)	2.5108 (13)	173 (2)
O3-H1O3---O1W ⁱⁱ	0.91 (2)	1.85 (2)	2.7191 (14)	162 (2)
O4-H1O4---O2W ⁱⁱⁱ	0.84 (2)	2.18 (2)	2.9780 (16)	160 (2)
O1W-H1W1---O2 ^{iv}	0.82 (2)	2.56 (2)	3.0668 (14)	122 (2)
O1W-H1W1---O2W ^{iv}	0.82 (2)	2.57 (2)	3.2155 (16)	137 (2)
O1W-H2W1---O6 ⁱⁱⁱ	0.88 (3)	2.00 (3)	2.8672 (15)	171 (2)
O2W-H2W2---O1 ^{vi}	0.84 (2)	2.40 (2)	3.0082 (14)	129 (2)
C5-H5A---O3 ^{vii}	0.97	2.56	3.4344 (15)	151
C8-H8B---O4	0.96	2.38	3.3447 (16)	178
C10-H10B---O3 ^{vii}	0.96	2.47	3.4195 (16)	168
C11-H11A---O4	0.97	2.50	3.2693 (15)	136

Symmetry codes: (i) $-x + 2, y - \frac{1}{2}, -z$; (ii) $x, y, z - 1$; (iii) $-x + 1, y - \frac{1}{2}, -z + 1$; (iv) $x - 1, y, z + 1$; (v) $-x + 1, y - \frac{1}{2}, -z + 2$; (vi) $x, y + 1, z + 1$; (vii) $-x + 1, y - \frac{1}{2}, -z$.



APPENDIX E

Table E1. Crystal data and structure refinement for [N₂₂₂₂][mal]

Empirical formula	C ₂₄ H ₅₆ N ₂ O ₁₃
Formula weight	580.71
Temperature (K)	100.0(1)
Wavelength (Å)	0.71073
Crystal system, space group	Monoclinic, P 2 ₁
Unit cell dimensions	a = 7.4724(2)Å alpha = 90° b = 19.9721(5)Å beta = 92.481° (1) c = 10.2726(3)Å gamma = 90°
Volume (Å ³)	1531.64(7)
Z, Calculated density (Mg/m ³)	2, 1.259
Absorption coefficient (mm ⁻¹)	0.101
F(000)	636
Crystal size (mm)	0.45 x 0.35 x 0.32
Theta range for data collection (°)	2.23 to 38.06
Limiting indices	-12<=h<=12, -34<=k<=29, -15<=l<=17
Reflections collected / unique	36497 / 8479 [R(int) = 0.0291]
Completeness to theta = 38.06 (%)	99.1
Absorption correction	Semi-empirical from equivalents
Max. and min. transmission	0.9685 and 0.9560
Refinement method	Full-matrix least-squares on F ²
Data / restraints / parameters	8479 / 1 / 372
Goodness-of-fit on F ²	1.039
Final R indices [I>2sigma(I)]	R1 = 0.0456, wR2 = 0.1197
R indices (all data)	R1 = 0.0527, wR2 = 0.1247
Largest diff. peak and hole (e.Å ⁻³)	0.625 and -0.804



Table E2. Atomic coordinates ($\times 10^4$) and equivalent isotropic displacement parameters ($\text{Å}^2 \times 10^3$) for $[\text{N}_{2222}][\text{mal}]$. $U(\text{eq})$ is defined as one third of the trace of the orthogonalized U_{ij} tensor.

	x	y	z	$U(\text{eq})$
O (1A)	6458 (1)	6846 (1)	10952 (1)	17 (1)
O (2A)	5515 (1)	6177 (1)	9303 (1)	20 (1)
O (3A)	2755 (1)	7363 (1)	8417 (1)	20 (1)
O (4A)	-385 (1)	6564 (1)	10463 (1)	19 (1)
O (5A)	-748 (1)	7347 (1)	8899 (1)	17 (1)
N (1A)	6029 (2)	6735 (1)	5175 (1)	16 (1)
C (1A)	5223 (1)	6583 (1)	10160 (1)	14 (1)
C (2A)	3359 (1)	6821 (1)	10446 (1)	16 (1)
C (3A)	2136 (1)	6847 (1)	9225 (1)	14 (1)
C (4A)	167 (1)	6940 (1)	9552 (1)	14 (1)
C (5A)	7321 (2)	6657 (1)	4091 (1)	23 (1)
C (6A)	8686 (3)	7217 (1)	4015 (2)	42 (1)
C (7A)	4655 (2)	6182 (1)	4985 (1)	18 (1)
C (8A)	3250 (2)	6157 (1)	6002 (2)	30 (1)
C (9A)	5129 (2)	7421 (1)	5138 (2)	23 (1)
C (10A)	4094 (3)	7579 (1)	3869 (2)	30 (1)
C (11A)	7000 (2)	6688 (1)	6507 (1)	19 (1)
C (12A)	7974 (2)	6034 (1)	6771 (1)	22 (1)
O (1B)	10276 (1)	9994 (1)	5734 (1)	21 (1)
O (2B)	11058 (1)	9310 (1)	4133 (1)	17 (1)
O (3B)	7671 (1)	8809 (1)	6707 (1)	22 (1)
O (4B)	4241 (1)	9551 (1)	4625 (1)	19 (1)
O (5B)	4110 (1)	8800 (1)	6248 (1)	18 (1)
N (1B)	1188 (2)	9390 (1)	22 (1)	19 (1)
C (1B)	9902 (2)	9572 (1)	4895 (1)	14 (1)
C (2B)	8001 (2)	9319 (1)	4638 (1)	16 (1)
C (3B)	6929 (1)	9308 (1)	5862 (1)	14 (1)
C (4B)	4920 (1)	9197 (1)	5564 (1)	14 (1)
C (5B)	-219 (2)	9916 (1)	276 (2)	26 (1)
C (6B)	-1906 (3)	9876 (1)	-579 (3)	51 (1)
C (7B)	2657 (2)	9496 (1)	1070 (1)	21 (1)
C (8B)	4142 (3)	8983 (1)	1094 (2)	33 (1)
C (9B)	392 (2)	8692 (1)	80 (1)	23 (1)
C (10B)	-470 (3)	8512 (1)	1345 (2)	30 (1)
C (11B)	1899 (2)	9453 (1)	-1342 (1)	22 (1)
C (12B)	2867 (2)	10102 (1)	-1615 (2)	23 (1)
O (1W)	1293 (2)	6036 (1)	2888 (2)	40 (1)
O (2W)	963 (1)	8060 (1)	6482 (1)	21 (1)
O (3W)	6117 (1)	8104 (1)	8653 (1)	20 (1)



Table E3. Bond lengths [Å] and angles [deg] for [N₂₂₂₂][mal].

O (1A) -C (1A)	1.3136 (14)
O (1A) -H (10A)	0.8200
O (2A) -C (1A)	1.2238 (16)
O (3A) -C (3A)	1.4148 (16)
O (3A) -H (30A)	0.8200
O (4A) -C (4A)	1.2806 (15)
O (5A) -C (4A)	1.2400 (15)
N (1A) -C (5A)	1.5128 (19)
N (1A) -C (7A)	1.5150 (17)
N (1A) -C (11A)	1.5233 (16)
N (1A) -C (9A)	1.5255 (18)
C (1A) -C (2A)	1.5120 (16)
C (2A) -C (3A)	1.5206 (16)
C (2A) -H (2AA)	0.9700
C (2A) -H (2AB)	0.9700
C (3A) -C (4A)	1.5345 (15)
C (3A) -H (3AA)	0.9800
C (5A) -C (6A)	1.517 (2)
C (5A) -H (5AA)	0.9700
C (5A) -H (5AB)	0.9700
C (6A) -H (6AA)	0.9600
C (6A) -H (6AB)	0.9600
C (6A) -H (6AC)	0.9600
C (7A) -C (8A)	1.514 (2)
C (7A) -H (7AA)	0.9700
C (7A) -H (7AB)	0.9700
C (8A) -H (8AA)	0.9600
C (8A) -H (8AB)	0.9600
C (8A) -H (8AC)	0.9600
C (9A) -C (10A)	1.519 (2)
C (9A) -H (9AA)	0.9700
C (9A) -H (9AB)	0.9700
C (10A) -H (10A)	0.9600
C (10A) -H (10B)	0.9600
C (10A) -H (10C)	0.9600
C (11A) -C (12A)	1.514 (2)
C (11A) -H (11A)	0.9700
C (11A) -H (11B)	0.9700
C (12A) -H (12A)	0.9600
C (12A) -H (12B)	0.9600
C (12A) -H (12C)	0.9600
O (1B) -C (1B)	1.2294 (16)
O (2B) -C (1B)	1.3011 (15)
O (2B) -H (20B)	0.8200
O (3B) -C (3B)	1.4179 (16)
O (3B) -H (30B)	0.8200
O (4B) -C (4B)	1.2827 (15)
O (5B) -C (4B)	1.2354 (15)
N (1B) -C (5B)	1.517 (2)
N (1B) -C (9B)	1.5172 (18)
N (1B) -C (7B)	1.5187 (18)
N (1B) -C (11B)	1.5256 (19)

C (1B) -C (2B)	1.5198 (15)
C (2B) -C (3B)	1.5200 (16)
C (2B) -H (2BA)	0.9700
C (2B) -H (2BB)	0.9700
C (3B) -C (4B)	1.5350 (15)
C (3B) -H (3BA)	0.9800
C (5B) -C (6B)	1.507 (3)
C (5B) -H (5BA)	0.9700
C (5B) -H (5BB)	0.9700
C (6B) -H (6BA)	0.9600
C (6B) -H (6BB)	0.9600
C (6B) -H (6BC)	0.9600
C (7B) -C (8B)	1.510 (2)
C (7B) -H (7BA)	0.9700
C (7B) -H (7BB)	0.9700
C (8B) -H (8BA)	0.9600
C (8B) -H (8BB)	0.9600
C (8B) -H (8BC)	0.9600
C (9B) -C (10B)	1.519 (2)
C (9B) -H (9BA)	0.9700
C (9B) -H (9BB)	0.9700
C (10B) -H (10D)	0.9600
C (10B) -H (10E)	0.9600
C (10B) -H (10F)	0.9600
C (11B) -C (12B)	1.516 (2)
C (11B) -H (11C)	0.9700
C (11B) -H (11D)	0.9700
C (12B) -H (12D)	0.9600
C (12B) -H (12E)	0.9600
C (12B) -H (12F)	0.9600
O (1W) -H (1W1)	0.9230
O (1W) -H (2W1)	0.9242
O (2W) -H (1W2)	0.8398
O (2W) -H (2W2)	0.6475
O (3W) -H (2W3)	0.75 (3)
O (3W) -H (1W3)	0.87 (3)
C (1A) -O (1A) -H (10A)	109.5
C (3A) -O (3A) -H (30A)	109.5
C (5A) -N (1A) -C (7A)	106.29 (10)
C (5A) -N (1A) -C (11A)	111.09 (10)
C (7A) -N (1A) -C (11A)	111.35 (10)
C (5A) -N (1A) -C (9A)	111.67 (12)
C (7A) -N (1A) -C (9A)	110.82 (11)
C (11A) -N (1A) -C (9A)	105.71 (10)
O (2A) -C (1A) -O (1A)	124.62 (11)
O (2A) -C (1A) -C (2A)	122.85 (11)
O (1A) -C (1A) -C (2A)	112.50 (10)
C (1A) -C (2A) -C (3A)	112.09 (10)
C (1A) -C (2A) -H (2AA)	109.2
C (3A) -C (2A) -H (2AA)	109.2
C (1A) -C (2A) -H (2AB)	109.2
C (3A) -C (2A) -H (2AB)	109.2
H (2AA) -C (2A) -H (2AB)	107.9
O (3A) -C (3A) -C (2A)	108.00 (10)
O (3A) -C (3A) -C (4A)	112.44 (10)

C (2A) -C (3A) -C (4A)	111.81 (10)
O (3A) -C (3A) -H (3AA)	108.1
C (2A) -C (3A) -H (3AA)	108.1
C (4A) -C (3A) -H (3AA)	108.1
O (5A) -C (4A) -O (4A)	126.27 (11)
O (5A) -C (4A) -C (3A)	118.14 (11)
O (4A) -C (4A) -C (3A)	115.55 (10)
N (1A) -C (5A) -C (6A)	114.43 (14)
N (1A) -C (5A) -H (5AA)	108.7
C (6A) -C (5A) -H (5AA)	108.7
N (1A) -C (5A) -H (5AB)	108.7
C (6A) -C (5A) -H (5AB)	108.7
H (5AA) -C (5A) -H (5AB)	107.6
C (5A) -C (6A) -H (6AA)	109.5
C (5A) -C (6A) -H (6AB)	109.5
H (6AA) -C (6A) -H (6AB)	109.5
C (5A) -C (6A) -H (6AC)	109.5
H (6AA) -C (6A) -H (6AC)	109.5
H (6AB) -C (6A) -H (6AC)	109.5
C (8A) -C (7A) -N (1A)	114.95 (12)
C (8A) -C (7A) -H (7AA)	108.5
N (1A) -C (7A) -H (7AA)	108.5
C (8A) -C (7A) -H (7AB)	108.5
N (1A) -C (7A) -H (7AB)	108.5
H (7AA) -C (7A) -H (7AB)	107.5
C (7A) -C (8A) -H (8AA)	109.5
C (7A) -C (8A) -H (8AB)	109.5
H (8AA) -C (8A) -H (8AB)	109.5
C (7A) -C (8A) -H (8AC)	109.5
H (8AA) -C (8A) -H (8AC)	109.5
H (8AB) -C (8A) -H (8AC)	109.5
C (10A) -C (9A) -N (1A)	114.50 (12)
C (10A) -C (9A) -H (9AA)	108.6
N (1A) -C (9A) -H (9AA)	108.6
C (10A) -C (9A) -H (9AB)	108.6
N (1A) -C (9A) -H (9AB)	108.6
H (9AA) -C (9A) -H (9AB)	107.6
C (9A) -C (10A) -H (10A)	109.5
C (9A) -C (10A) -H (10B)	109.5
H (10A) -C (10A) -H (10B)	109.5
C (9A) -C (10A) -H (10C)	109.5
H (10A) -C (10A) -H (10C)	109.5
H (10B) -C (10A) -H (10C)	109.5
C (12A) -C (11A) -N (1A)	114.92 (11)
C (12A) -C (11A) -H (11A)	108.5
N (1A) -C (11A) -H (11A)	108.5
C (12A) -C (11A) -H (11B)	108.5
N (1A) -C (11A) -H (11B)	108.5
H (11A) -C (11A) -H (11B)	107.5
C (11A) -C (12A) -H (12A)	109.5
C (11A) -C (12A) -H (12B)	109.5
H (12A) -C (12A) -H (12B)	109.5
C (11A) -C (12A) -H (12C)	109.5
H (12A) -C (12A) -H (12C)	109.5
H (12B) -C (12A) -H (12C)	109.5
C (1B) -O (2B) -H (2OB)	109.5



C (3B) -O (3B) -H (3OB)	109.5
C (5B) -N (1B) -C (9B)	110.71 (11)
C (5B) -N (1B) -C (7B)	105.41 (11)
C (9B) -N (1B) -C (7B)	111.96 (11)
C (5B) -N (1B) -C (11B)	111.81 (12)
C (9B) -N (1B) -C (11B)	105.35 (10)
C (7B) -N (1B) -C (11B)	111.73 (11)
O (1B) -C (1B) -O (2B)	124.16 (11)
O (1B) -C (1B) -C (2B)	122.17 (11)
O (2B) -C (1B) -C (2B)	113.66 (10)
C (1B) -C (2B) -C (3B)	112.55 (10)
C (1B) -C (2B) -H (2BA)	109.1
C (3B) -C (2B) -H (2BA)	109.1
C (1B) -C (2B) -H (2BB)	109.1
C (3B) -C (2B) -H (2BB)	109.1
H (2BA) -C (2B) -H (2BB)	107.8
O (3B) -C (3B) -C (2B)	108.07 (10)
O (3B) -C (3B) -C (4B)	111.97 (10)
C (2B) -C (3B) -C (4B)	112.50 (9)
O (3B) -C (3B) -H (3BA)	108.0
C (2B) -C (3B) -H (3BA)	108.0
C (4B) -C (3B) -H (3BA)	108.0
O (5B) -C (4B) -O (4B)	126.43 (11)
O (5B) -C (4B) -C (3B)	118.57 (11)
O (4B) -C (4B) -C (3B)	114.98 (10)
C (6B) -C (5B) -N (1B)	115.57 (15)
C (6B) -C (5B) -H (5BA)	108.4
N (1B) -C (5B) -H (5BA)	108.4
C (6B) -C (5B) -H (5BB)	108.4
N (1B) -C (5B) -H (5BB)	108.4
H (5BA) -C (5B) -H (5BB)	107.4
C (5B) -C (6B) -H (6BA)	109.5
C (5B) -C (6B) -H (6BB)	109.5
H (6BA) -C (6B) -H (6BB)	109.5
C (5B) -C (6B) -H (6BC)	109.5
H (6BA) -C (6B) -H (6BC)	109.5
H (6BB) -C (6B) -H (6BC)	109.5
C (8B) -C (7B) -N (1B)	115.11 (13)
C (8B) -C (7B) -H (7BA)	108.5
N (1B) -C (7B) -H (7BA)	108.5
C (8B) -C (7B) -H (7BB)	108.5
N (1B) -C (7B) -H (7BB)	108.5
H (7BA) -C (7B) -H (7BB)	107.5
C (7B) -C (8B) -H (8BA)	109.5
C (7B) -C (8B) -H (8BB)	109.5
H (8BA) -C (8B) -H (8BB)	109.5
C (7B) -C (8B) -H (8BC)	109.5
H (8BA) -C (8B) -H (8BC)	109.5
H (8BB) -C (8B) -H (8BC)	109.5
N (1B) -C (9B) -C (10B)	115.57 (12)
N (1B) -C (9B) -H (9BA)	108.4
C (10B) -C (9B) -H (9BA)	108.4
N (1B) -C (9B) -H (9BB)	108.4
C (10B) -C (9B) -H (9BB)	108.4
H (9BA) -C (9B) -H (9BB)	107.4
C (9B) -C (10B) -H (10D)	109.5



C (9B) -C (10B) -H (10E)	109.5
H (10D) -C (10B) -H (10E)	109.5
C (9B) -C (10B) -H (10F)	109.5
H (10D) -C (10B) -H (10F)	109.5
H (10E) -C (10B) -H (10F)	109.5
C (12B) -C (11B) -N (1B)	115.39 (11)
C (12B) -C (11B) -H (11C)	108.4
N (1B) -C (11B) -H (11C)	108.4
C (12B) -C (11B) -H (11D)	108.4
N (1B) -C (11B) -H (11D)	108.4
H (11C) -C (11B) -H (11D)	107.5
C (11B) -C (12B) -H (12D)	109.5
C (11B) -C (12B) -H (12E)	109.5
H (12D) -C (12B) -H (12E)	109.5
C (11B) -C (12B) -H (12F)	109.5
H (12D) -C (12B) -H (12F)	109.5
H (12E) -C (12B) -H (12F)	109.5
H (1W1) -O (1W) -H (2W1)	122.4
H (1W2) -O (2W) -H (2W2)	107.0
H (2W3) -O (3W) -H (1W3)	99 (3)

Symmetry transformations used to generate equivalent atoms

Table E4. Anisotropic displacement parameters ($\text{Å}^2 \times 10^3$) for $[\text{N}_{2222}][\text{mal}]$. The anisotropic displacement factor exponent takes the form: $-2 \pi^2 [h^2 a^{*2} U_{11} + \dots + 2 h k a^* b^* U_{12}]$

	U11	U22	U33	U23	U13	U12
O(1A)	11(1)	25(1)	16(1)	0(1)	0(1)	-1(1)
O(2A)	19(1)	24(1)	18(1)	-2(1)	0(1)	5(1)
O(3A)	12(1)	27(1)	22(1)	11(1)	0(1)	-2(1)
O(4A)	12(1)	5(1)	22(1)	8(1)	2(1)	0(1)
O(5A)	13(1)	20(1)	19(1)	2(1)	-1(1)	1(1)
N(1A)	21(1)	14(1)	12(1)	-1(1)	-3(1)	-1(1)
C(1A)	13(1)	17(1)	12(1)	4(1)	0(1)	1(1)
C(2A)	12(1)	24(1)	14(1)	0(1)	0(1)	1(1)
C(3A)	10(1)	18(1)	14(1)	1(1)	0(1)	0(1)
C(4A)	10(1)	16(1)	16(1)	-1(1)	0(1)	-2(1)
C(5A)	24(1)	30(1)	15(1)	2(1)	2(1)	-3(1)
C(6A)	36(1)	57(1)	33(1)	4(1)	6(1)	-22(1)
C(7A)	20(1)	17(1)	18(1)	-3(1)	-1(1)	-2(1)
C(8A)	26(1)	4(1)	31(1)	-4(1)	7(1)	-6(1)
C(9A)	35(1)	15(1)	19(1)	-1(1)	-8(1)	3(1)
C(10A)	42(1)	24(1)	24(1)	0(1)	-13(1)	7(1)
C(11A)	27(1)	17(1)	13(1)	-1(1)	-5(1)	1(1)
C(12A)	26(1)	22(1)	18(1)	0(1)	-5(1)	5(1)
O(1B)	18(1)	24(1)	21(1)	-8(1)	3(1)	-5(1)
O(2B)	11(1)	24(1)	16(1)	-3(1)	2(1)	-2(1)
O(3B)	12(1)	29(1)	24(1)	11(1)	2(1)	1(1)
O(4B)	12(1)	23(1)	21(1)	6(1)	0(1)	-1(1)
O(5B)	14(1)	20(1)	21(1)	4(1)	4(1)	2(1)
N(1B)	23(1)	16(1)	16(1)	-5(1)	1(1)	-3(1)
C(1B)	13(1)	17(1)	12(1)	1(1)	1(1)	-2(1)
C(2B)	12(1)	20(1)	15(1)	-1(1)	2(1)	-3(1)
C(3B)	11(1)	17(1)	16(1)	2(1)	2(1)	0(1)
C(4B)	12(1)	14(1)	16(1)	-2(1)	2(1)	0(1)
C(5B)	23(1)	21(1)	34(1)	-8(1)	1(1)	0(1)
C(6B)	32(1)	39(1)	78(2)	-16(1)	-21(1)	6(1)
C(7B)	24(1)	25(1)	14(1)	-4(1)	1(1)	-3(1)
C(8B)	30(1)	38(1)	32(1)	0(1)	-3(1)	6(1)
C(9B)	33(1)	17(1)	19(1)	-5(1)	5(1)	-8(1)
C(10B)	38(1)	29(1)	24(1)	-6(1)	8(1)	-13(1)
C(11B)	35(1)	18(1)	14(1)	3(1)	2(1)	-5(1)
C(12B)	27(1)	20(1)	21(1)	-1(1)	2(1)	-6(1)
O(1W)	33(1)	47(1)	40(1)	11(1)	-4(1)	-6(1)
O(2W)	17(1)	20(1)	26(1)	6(1)	1(1)	-1(1)
O(3W)	16(1)	20(1)	23(1)	5(1)	2(1)	0(1)



Table E5. Hydrogen coordinates (x 10⁴) and isotropic displacement parameters (Å² x 10³) for [N₂₂₂₂][mal].

	x	y	z	U (eq)
H (10A)	7450	6722	10740	26
H (30A)	1900	7537	8020	31
H (2AA)	3433	7263	10834	20
H (2AB)	2847	6521	11073	20
H (3AA)	2244	6421	8762	17
H (5AA)	6640	6633	3267	27
H (5AB)	7954	6236	4211	27
H (6AA)	9461	7129	3314	62
H (6AB)	9383	7241	4821	62
H (6AC)	8076	7634	3862	62
H (7AA)	4055	6237	4135	22
H (7AB)	5277	5756	4984	22
H (8AA)	2405	5808	5786	46
H (8AB)	2638	6579	6025	46
H (8AC)	3817	6068	6841	46
H (9AA)	4314	7447	5846	28
H (9AB)	6040	7761	5289	28
H (10A)	3550	8012	3929	45
H (10B)	3181	7247	3712	45
H (10C)	4898	7576	3166	45
H (11A)	7860	7051	6587	22
H (11B)	6134	6752	7172	22
H (12A)	8418	6023	7661	33
H (12B)	8958	5996	6205	33
H (12C)	7163	5667	6613	33
H (20B)	12073	9421	4380	26
H (30B)	6891	8663	7167	32
H (2BA)	8045	8870	4281	19
H (2BB)	7397	9603	3993	19
H (3BA)	7079	9742	6297	17
H (5BA)	-542	9879	1178	31
H (5BB)	312	10354	166	31
H (6BA)	-2739	10209	-312	76
H (6BB)	-2431	9440	-500	76
H (6BC)	-1623	9952	-1469	76
H (7BA)	3177	9935	949	25
H (7BB)	2118	9495	1913	25
H (8BA)	5080	9120	1705	50
H (8BB)	4610	8947	241	50
H (8BC)	3680	8557	1351	50
H (9BA)	1332	8370	-70	27
H (9BB)	-503	8646	-628	27
H (10D)	-826	8050	1322	45
H (10E)	-1503	8789	1451	45
H (10F)	375	8583	2063	45
H (11C)	2711	9084	-1481	27
H (11D)	900	9408	-1971	27
H (12D)	3107	10126	-2524	34



H(12E)	3976	10116	-1107	34
H(12F)	2131	10474	-1385	34
H(1W1)	585	6170	2176	60
H(2W1)	955	5698	3439	60
H(1W2)	1780	8322	6271	31
H(2W2)	254	8239	6558	31
H(2W3)	5270 (40)	7904 (14)	8570 (30)	29 (6)
H(1W3)	6860 (30)	7777 (13)	8800 (20)	24 (5)

Table E6. Torsion angles [deg] for [N₂₂₂₂][mal]

O (2A) -C (1A) -C (2A) -C (3A)	-32.73 (17)
O (1A) -C (1A) -C (2A) -C (3A)	149.15 (11)
C (1A) -C (2A) -C (3A) -O (3A)	-68.04 (14)
C (1A) -C (2A) -C (3A) -C (4A)	167.74 (10)
O (3A) -C (3A) -C (4A) -O (5A)	14.54 (16)
C (2A) -C (3A) -C (4A) -O (5A)	136.23 (12)
O (3A) -C (3A) -C (4A) -O (4A)	-167.70 (11)
C (2A) -C (3A) -C (4A) -O (4A)	-46.00 (15)
C (7A) -N (1A) -C (5A) -C (6A)	173.16 (14)
C (11A) -N (1A) -C (5A) -C (6A)	-65.56 (17)
C (9A) -N (1A) -C (5A) -C (6A)	52.19 (17)
C (5A) -N (1A) -C (7A) -C (8A)	178.29 (13)
C (11A) -N (1A) -C (7A) -C (8A)	57.17 (16)
C (9A) -N (1A) -C (7A) -C (8A)	-60.20 (16)
C (5A) -N (1A) -C (9A) -C (10A)	58.20 (17)
C (7A) -N (1A) -C (9A) -C (10A)	-60.10 (18)
C (11A) -N (1A) -C (9A) -C (10A)	179.14 (14)
C (5A) -N (1A) -C (11A) -C (12A)	-59.77 (16)
C (7A) -N (1A) -C (11A) -C (12A)	58.50 (15)
C (9A) -N (1A) -C (11A) -C (12A)	178.92 (13)
O (1B) -C (1B) -C (2B) -C (3B)	-32.10 (17)
O (2B) -C (1B) -C (2B) -C (3B)	149.06 (11)
C (1B) -C (2B) -C (3B) -O (3B)	-68.03 (14)
C (1B) -C (2B) -C (3B) -C (4B)	167.84 (10)
O (3B) -C (3B) -C (4B) -O (5B)	14.26 (16)
C (2B) -C (3B) -C (4B) -O (5B)	136.20 (12)
O (3B) -C (3B) -C (4B) -O (4B)	-167.51 (11)
C (2B) -C (3B) -C (4B) -O (4B)	-45.57 (15)
C (9B) -N (1B) -C (5B) -C (6B)	-53.8 (2)
C (7B) -N (1B) -C (5B) -C (6B)	-175.06 (19)
C (11B) -N (1B) -C (5B) -C (6B)	63.3 (2)
C (5B) -N (1B) -C (7B) -C (8B)	174.49 (14)
C (9B) -N (1B) -C (7B) -C (8B)	54.04 (17)
C (11B) -N (1B) -C (7B) -C (8B)	-63.86 (17)
C (5B) -N (1B) -C (9B) -C (10B)	-57.06 (18)
C (7B) -N (1B) -C (9B) -C (10B)	60.25 (18)
C (11B) -N (1B) -C (9B) -C (10B)	78.11 (14)
C (5B) -N (1B) -C (11B) -C (12B)	63.10 (16)
C (9B) -N (1B) -C (11B) -C (12B)	-176.58 (13)
C (7B) -N (1B) -C (11B) -C (12B)	-54.79 (17)

Symmetry transformations used to generate equivalent atoms:



Table E7. Hydrogen bonds for [N₂₂₂₂][mal] ([A and deg])

D-H---A	D-H	H---A	D---A	D-H---A
O1A-1OA---O4A ⁱ	0.82	1.68	2.4968 (12)	171.0
O3A-3OA---O2W	0.82	2.00	2.7292 (15)	149.0
O3A-3OA---O5A	0.82	2.24	2.6850 (13)	114.0
O3B-3OB---O3W	0.82	2.00	2.7438 (16)	151.0
O3B-3OB---O5B	0.82	2.26	2.6827 (13)	112.0
O1W-1W1---O4A ⁱⁱ	0.92	2.03	2.9359 (19)	166.0
O1W-2W1---O1B ⁱⁱⁱ	0.92	1.90	2.8020 (2)	165.0
O2W-1W2---O5B	0.84	1.99	2.7962 (14)	162.0
O2W-2W2---O3B ^{iv}	0.65	2.25	2.8969 (14)	175.0
O3W-2W3---O3A	0.75 (3)	2.17 (3)	2.9163 (14)	176.6 (19)
O3W-1W3---O5A ⁱ	0.87 (2)	1.98 (2)	2.7907 (14)	155.0 (2)
C2A-2AB---O1W ^v	0.97	2.44	3.3850 (2)	165.0
C5A-5AA---O1A ⁱⁱ	0.97	2.41	3.2826 (16)	149.0
C7A-7AA---O1W	0.97	2.42	3.2510 (2)	144.0
C11A-11B---O2A	0.97	2.53	3.2863 (16)	135.0
C7A-7AB---O4B ⁱⁱⁱ	0.97	2.46	3.3810 (17)	157.0
C5B-5BB---O4A ^{vi}	0.97	2.50	3.4140 (2)	156.0
C7B-7BB---O2B ^{iv}	0.97	2.47	3.4332 (16)	170.0

Symmetry codes: (i) $x + 1, y, z$; (ii) $x, y, z - 1$; (iii) $-x + 1, y - \frac{1}{2}, -z + 1$; (iv) $x - 1, y, z$; (v) $x, y, z + 1$; (vi) $-x, y + \frac{1}{2}, -z + 1$; (vii) $-x, y + \frac{1}{2}, -z$.

APPENDIX F

Publications

1. Published Paper

Abdul Rahman, M. B., **Jumbri, K.**, Basri, M., Abdmalek, E., Sirat, K. and Salleh, A. B. (2010). Synthesis and Physico-Chemical Properties of New Tetraethylammonium-Based Amino Acids Chiral Ionic Liquids”, *Molecules*, 15: 2388-2397; doi:10.3390/molecules15042388.

Abdul Rahman, M. B., **Jumbri, K.**, Sirat, K., Kia, R. and Fun, H.-K. (2009). Tetraethylammonium L-malate 1.36-hydrate. *Acta Cryst.* E65: o49-o50.

Abdul Rahman, M. B., **Jumbri, K.**, Sirat, K., Kia, R. and Fun, H.-K. (2008). Tetraethylammonium L-tartrate dihydrate. *Acta Cryst.* E64: o2343.

2. Seminars/Conferences/Exhibitions

Abdul Rahman, M. B., **Jumbri, K.**, Abdulmalek, M., Tejo, B. A., Basri, M., Abd Rahman, R. N. Z. R. and Salleh, A. B. “EverGREEN Frontier Solvents for Bespoke Biocatalysis”. *Pameran Anugerah Inovasi Cemerlang Selangor 2009, Sempena Festival Sains, Teknologi dan Inovasi Selangor (FESTiS 2009)*, 12-14th Jun 2009, Kompleks PKNS Shah Alam.

Abdul Rahman, M. B., Majidi, K., Arumugam, M., Khairuddin, N. S. K., Hanafiah, N. M. A., Omar, E. M., **Jumbri, K.** and Basri, M. “Innovative Chiral Ionic Liquids in Sustainable Enzymology”, *13th Industrial Chemistry Seminar*, 11th April 2009, Palm Garden Hotel, Putrajaya. (*Winner of Best Poster Content*).

Abdul Rahman, M. B., **Jumbri, K.**, Ng, S. L., Seddon, K., Basri, M., Abd Rahman, R. N. Z. R. and Salleh, A. B. “Innovative Chiral Ionic Liquids in Nonaqueous Enzymology”, *Malaysia Technology Expo (MTE 2008)*, 27-29th November 2008, PWTC. (*Winner of Silver Medal*).

Jumbri, K., Abdul Rahman, M. B., Basri, M., Sirat, K. and Salleh, A. B. “Functional Synthesis of New Chiral Ionic Liquids (CILs) for Use in Enzymatic Production of Ester”. *Simposium Kimia Analisis Malaysia 21*, 25-27th November 2008, UMS, Sabah.



Jumbri, K., Abdul Rahman, M. B., Basri, M., Sirat, K. And Salleh, A. B. “Functional Synthesis of New Chiral Ionic Liquids (CILs) for Use in Enzymatic Production of Ester”. *National Science Fellowship (NSF) Seminar, Ministry of Science, Technology and Innovation (MOSTI)*, 14-16th November 2008, UPM.

Abdul Rahman, M. B., **Jumbri, K.**, Ng, S. L., Seddon, K., Basri, M., Abd Rahman, R. N. Z. R. and Salleh, A. B.. “Innovative Application of Green Engineering Liquids of Facile Imidazolium-based Chiral Ionic Liquids”, *Exhibition of Invention, Research & Innovation (PRPI 2007)*, 27-29th November 2007, UPM. (*Winner of Gold Medal*).



Article

Synthesis and Physico-Chemical Properties of New Tetraethylammonium-Based Amino Acid Chiral Ionic Liquids

Mohd Basyaruddin Abdul Rahman ^{1,2,*}, Khairulazhar Jumbri ¹, Mahiran Basri ¹, Emilia Abdulmalek ¹, Kamaliah Sirat ¹ and Abu Bakar Salleh ³

¹ Department of Chemistry, Faculty of Science, Universiti Putra Malaysia, 43400 UPM Serdang, Selangor, Malaysia; E-Mails: khairulazhar_evo@yahoo.com (K.J.); mahiran@science.upm.edu.my (M.B.); emilia@science.upm.edu.my (E.A.); kamaliah@fsas.upm.edu.my (K.S.)

² Structural Biology Research Centre, Malaysia Genome Institute, UKM-MTDC Smart Technology Centre, 43600 UKM Bangi, Selangor, Malaysia

³ Laboratory of Industrial Biotechnology, Institute of Bioscience, Universiti Putra Malaysia, 43400 UPM Serdang, Selangor, Malaysia; E-Mail: abubakar@biotech.upm.edu.my (A.B.S.)

* Author to whom correspondence should be addressed; E-Mail: basya@science.upm.edu.my; Tel.: +603 8946 6798; Fax: +603 8943 2508.

Received: 12 February 2010; in revised form: 15 March 2010 / Accepted: 22 March 2010 /

Published: 5 April 2010

Abstract: This paper reports the synthesis of a series of new tetraethylammonium-based amino acid chiral ionic liquids (CILs). Their physico-chemical properties, including melting point, thermal stability, viscosity and ionic conductivity, have been comprehensively studied. The obtained results indicated that the decomposition for these salts proceeds in one step and the temperature of decomposition (T_{onset}) is in the range of 168–210 °C. Several new CILs prepared in this work showed high ionic conductivity compared to the amino acid ionic liquids (AAILs) found in the literature.

Keywords: chiral ionic liquids; tetraethylammonium; amino acids; viscosity; ionic conductivity

Abbreviations: [N₂₂₂₂]: tetraethylammonium; [ser]: serinate; [pro]: proline; [thr]: threoninate; [ile]: isoleucinate; [asn]: asparaginate; [gln]: glutamine; [glu]: glutamate; [met]: methioninate; [his]: histidinate.

1. Introduction

Ionic liquids (ILs), molten salts below 100 °C, have gained a lot of attention in the science and industry communities as reaction media, extraction solvents, electrolytes and biocatalysts [1]. These liquids contain ions which show good and tunable solubility properties combined with negligible vapour pressure and excellent thermal stability. At the same time, they have found a place of choice as valuable substitutes for many volatile solvents [2,3], which can dissolve polar to non-polar substrates and almost anything including coal, plastics, woods and even rocks [4]. They are not as flammable as classical volatile organic solvents (VOSs), therefore making the processes safer and environmental concerns less of an issue. Thermodynamic and kinetics of reactions carried out in these liquids could be different to those in traditional solvents, which has led to great interest in their potential use as solvents and co-solvents amongst chemists.

In the last few years, researchers have turned their interest to synthesis of chiral ionic liquids (CILs). Many CILs have been designed, synthesized and used in organic reactions. For example, a few researchers have reported that CILs have great potential applications as reaction media in chiral discrimination, asymmetric synthesis, and optical resolution of racemates [5–7]. Chiral ionic liquids can be synthesized from readily available starting materials containing chiral anions/cations or by using modification of non-chiral materials to produce chiral products. However, the modification reactions are usually more complicated and many steps are required to complete the whole reaction. By using starting materials such as lactates, sugars, sugar substitutes, plant acids and amino acids, a variety of CILs can be produced.

Recently, we have reported the synthesis of new tetraethylammonium-based CILs derived from plant acids [8,9]. As part of our ongoing study, amino acids have now been selected as starting material to produce CILs since they have a carboxylic acid residue, an amino group and a side chain that varies between different amino acids. Until now, a fairly large number of novel CILs based on amino acid cations or anions have been prepared [10–16], but most of them have relatively low ionic conductivities, higher viscosities and melting points. This viscous characteristic of amino acid ionic liquids (AAILs) limits many of their potential applications as fluids and electrolyte materials. The strong intermolecular interactions especially H-bonding in the AAILs was supposed to be the key point for the high melting points and viscosities [14,17]. Some literatures have reported that AAILs containing longer alkyl chains such as tetrabutylammonium, tetrabutylphosphonium and dialkyl-imidazolium show high viscosity and low conductivity at room temperature [13,19]. In this work, we aimed to study the effect of shorter alkyl chain of the tetraethylammonium cation, especially with regard to their thermodynamic properties of the resulting AAILs. We expect that the shorter alkyl chain of this cation will reduce the viscosity and increase the ionic conductivity.

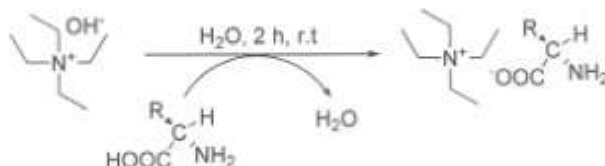
2. Results and Discussion

2.1. Synthesis and Characterization

New tetraethylammonium-based amino acids CILs were prepared according to a method modified from literature [16]. A simple and straightforward synthetic pathway involved neutralization of

commercially available starting materials that gave CILs in good overall yield (>85%), as shown in Scheme 1.

Scheme 1. Synthetic pathway to tetraethylammonium-based chiral ionic liquids.



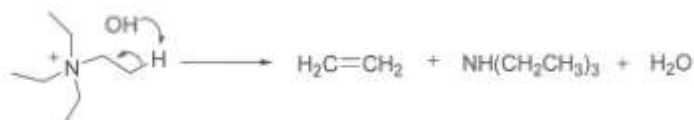
This method has an advantage since the by-product is only water, thus avoiding the use of metal salts and ion-exchange. Therefore, the purification of the CILs only required the removal of water. Most of the IL preparations have been carried out by formation of an organic halide salts which result in halide contamination. Subsequent separation of the halide can also post difficulties and give impurities that can change the properties of the desired ILs [18]. Therefore, in this work, halide contamination and extensive of purification procedures were avoided. The reactions were carried out at room temperature because tetraethylammonium hydroxide can readily deprotonate the carboxylic acid moiety of amino acids.

2.2. Thermal Stability and Physico-Chemical Properties

The melting point (T_m), decomposition temperature (T_{onset}), viscosity (η) and ionic conductivity (κ) data of the prepared CILs are summarized in Table 1. They are thermally stable up to 160–210 °C (Figure 1), which is low compared to alkylimidazolium based-ILs (general $T_d > 300$ °C). Interestingly, the decomposition temperature of these salts was a little lower than those of 1-ethyl-3-methylimidazolium-based ([emim][amino acids]) ILs (T_d around 220 °C) [13] and tetrabutylphosphonium-based ([TBP][amino acids]; T_d 210–320 °C) [19]. Although it had not been proven, we suspect that, the lower observed T_{onset} of our CILs are the result of *Hoffman* elimination reaction of tetraethylammonium salt.

A schematic presentation of this decomposition path is shown in Scheme 2. As it was discussed previously by MacFarlane *et al.*, [20], quaternary ammonium salts in a basic environment (ionized amino acids are slightly basic) are subject to a decomposition mechanism related to *Hoffman* elimination. Meanwhile, changing the amino acids anions had little effect on thermal stability.

Scheme 2. *Hoffman* elimination reaction.



All of these new compounds can be classified as ILs since their T_m are below 100 °C. The main factor that influences the T_m of these CILs is the structure of the corresponding anions. The two solid CILs, which are [N₂₂₂₂][asn] and [N₂₂₂₂][his], show T_m values of 58 °C and 54 °C, respectively. In

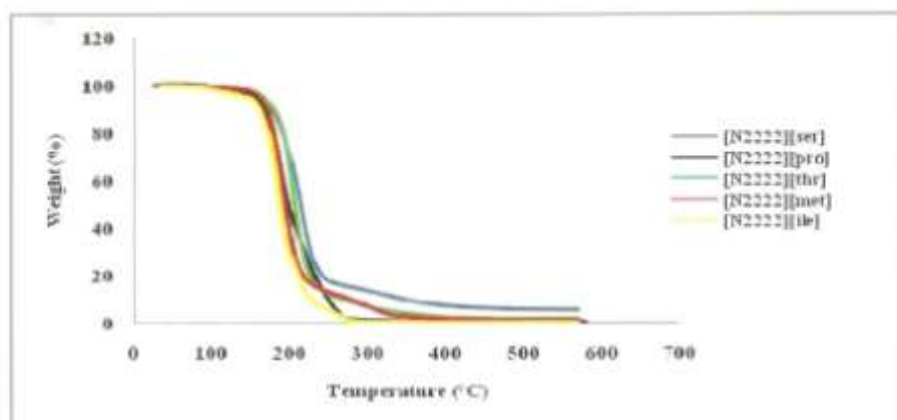
comparison to [his], [asn] has a more symmetrical structure that may have attributed to its higher T_m . As reported by Jiang *et al.* [16], the high degree of asymmetric structure of amino acids contributed to the low T_m values of tetraalkylammonium-based amino acids ILs. However, the higher T_m of these two solid CILs than the rest of CILs prepared cannot be fully explained. We are currently in the process of obtaining the corresponding crystal structure data to ascertain the packing structure of the salts.

Table 1. The physico-chemical properties of tetraethylammonium-based chiral ionic liquids.

No	CILs	T_m (°C)	T_{onset} (°C)	η (cP)	κ (mS cm ⁻¹)
1	[N ₂₂₂₂][ser]	ND	187	1763	0.16
2	[N ₂₂₂₂][pro]	ND	172	438	0.46
3	[N ₂₂₂₂][thr]	ND	188	1002	0.24
4	[N ₂₂₂₂][ile]	ND	168	526	0.35
5	[N ₂₂₂₂][asn]	58 ± 1.0	191	a	a
6	[N ₂₂₂₂][gln]	ND	210	a	a
7	[N ₂₂₂₂][glu]	ND	210	a	a
8	[N ₂₂₂₂][met]	ND	176	462	0.45
9	[N ₂₂₂₂][his]	54 ± 1.0	174	a	a

ND: not detected; a: solid or glass at 25 °C, hence the property was not determined

Figure 1. Thermogravimetric analysis of several new tetraethylammonium-based amino acids chiral ionic liquids.

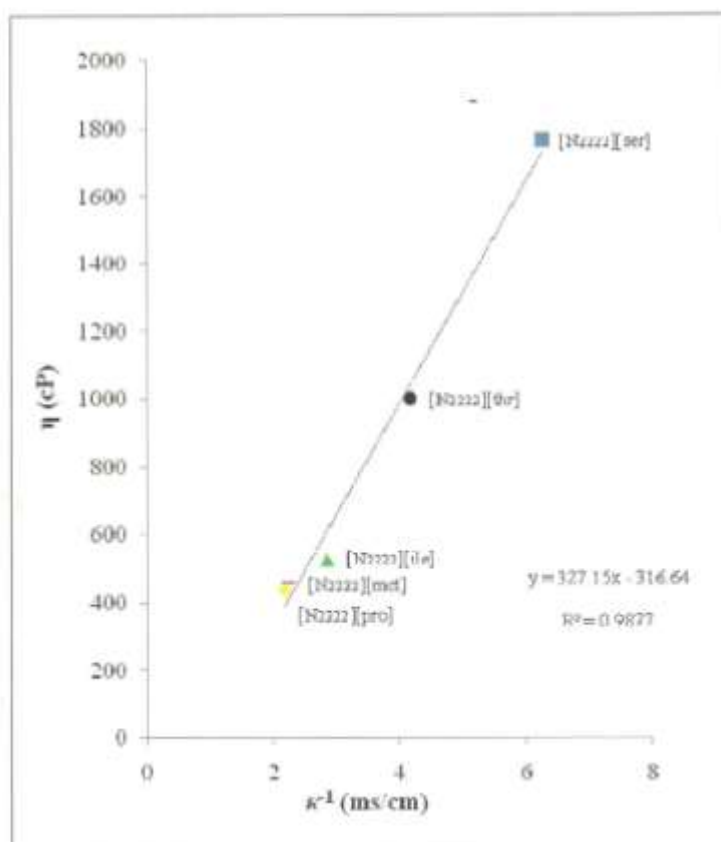


2.3. Viscosity (η) and Ionic Conductivity (κ)

Thermodynamic properties such as viscosity (η) and ionic conductivity (κ) of these new salts which are liquids at room temperature were measured and the corresponding data are presented in Table 1. According to the results, these salts showed conductivity values ranged from 0.16–0.54 ms cm⁻¹, were much higher than those of similar ILs, [emim][amino acids] ($\kappa = 9.1 \times 10^{-6}$ to 0.65 ms cm⁻¹) [13]. In this work, [N₂₂₂₂][pro] displayed the highest ionic conductivity (0.46 ms cm⁻¹) – three times higher than [emim][pro] (0.16 ms cm⁻¹) – while [N₂₂₂₂][ser] (0.16 ms cm⁻¹) showed the lowest ionic conductivity among [N₂₂₂₂][amino acids]. The lower conductivity of [emim] was due to the protons at

the 2, 4 and 5 positions that contribute to the H-bonding interaction [13]. This interaction becomes the reason of low ionic conductivity of [emim][amino acids] as compared to our CILs. For the same cation, the ionic conductivities values of anion are in the following order: [ser] < [thr] < [ile] < [met] < [pro]. We found that the ionic conductivity of these salts closely related to the viscosity. In this study, the salts followed the linear relationship between ionic conductivity and viscosity (Figure 2).

Figure 2. Relationship between ionic conductivity (κ^{-1}) and viscosity (η) for five tetraethylammonium-based chiral ionic liquids at 25 °C.



This linear correlation indicated that at 25 °C, the conductivity value is strongly affected by viscosity, and thus the salts with low viscosity showed high ionic conductivities. This may be due to an increase in the ion mobility of the salts. The cation structure strongly influences the viscosity, which is governed essentially by *van der Waals* interactions and H-bonding ability. It can be seen that, the [N2222] structure has a much small molecular weight as well as short and flexible alkyl chain. The short alkyl chains made the salts less viscous due to a decrease in *van der Waals* interactions and increase rate of ion mobility of the salts ensuing the high ionic conductivity.

However, these new salts still showed higher viscosity than conventional ILs. This phenomenon happens due to the symmetry properties of the cation structure. Generally, symmetric cations usually bring high viscosity of aliphatic ammonium-based ILs [21,22]. Furthermore, the side chain of the

corresponding amino acids and H-bonding interaction in the structure of ILs were also affect the viscosity and ionic conductivity [13]. H-bonding interaction should increase the solution viscosity as well as decrease the ionic conductivity. Especially in the case of amino acids as anion, most of them contain functional group such as not only amino group, but also carboxyl, hydroxyl and so on. This implies some intra- and inter-molecular interaction influenced in the packing structure of CILs. In others word, introduction of functional groups such as H-bonding donor or acceptor increased the viscosity and decreased the ionic conductivity through intra/intermolecular interaction [1].

For example, the salts [N₂₂₂₂][ser] ($\eta = 1763$ cP) and [N₂₂₂₂][thr] ($\eta = 1002$ cP) have relatively high viscosity that may be due to H-bonding or some other interaction which were expected through the side chains. The presence of hydroxyl group in both anions allowed the molecule to form H-bonding through inter/intramolecular interaction. Thus, the existences of strong H-bonding cause high viscosity and low ionic conductivity of these CILs. However, the relationship between the component ion structures with viscosity and ionic conductivity is not fully understood probably because there are several parameters, such as shape of ions, charge density and conformational changes of alkyl chain that involve in the structure of ILs [23].

3. Experimental

3.1. General

All chemicals were commercially available and of analytical grade unless otherwise specified. ¹H- and ¹³C-NMR spectra were recorded with JEOL JNM-ECA 400 MHz and chemical shifts δ (in ppm) were related to residual solvent signal (D₂O). Coupling constant J is expressed in Hz. Decomposition temperatures were measured with a Mettler-Toledo TGA/SDTA 851^e Thermal Gravimetric Analyzer (TGA) instrument under N₂ atmosphere. The Mettler-Toledo STAR^e software version 8.10 was used to determine the onset temperature (T_{onset}). All samples were run in alumina pan at heating rate 10 °C min⁻¹ and the temperature was programmed from 25–600 °C. Melting points (T_m) were determined by using Mettler-Toledo Differential Scanning Calorimeter (DSC), model DSC822^e and data were evaluated using Mettler-Toledo STAR^e software version 9.01. Measurement was carried out at a scan rate of 10 °C min⁻¹ by heating and cooling the samples from –60–130 °C. Viscosity (η) was measured at 25 °C using Brookfield LVDV-II+Pro cone/plate viscometer equipped with CPE-52 spindle. The instrument was connected to computer with Rheocalc32 software version 3.1. Ionic conductivity (κ) was determined at 25 °C by using SevenGo Conductivity Meter. Measurements of optical rotation were carried out using Jasco P-200 Polarimeter equipped with a 100 mm standard glass tube with bulb at 25 °C. The data were recorded on instruments which use the sodium lamp as a radiation source and wavelength is constant and standard. The data was then recorded three times and the average was taken as an observed optical rotation value (α). The value was then used in the formula (1) to calculate the specific optical rotation value, $[\alpha]_D^{25}$:

$$[\alpha]_D^{25} = \frac{\alpha}{lc} \quad (1)$$

where $[\alpha]$ = specific optical rotation; α = value of optical rotation observed; l = length of cell (dm); c = concentration in g/100 mL.

3.2. Typical Synthetic Procedure for Tetraethylammonium-Based Amino Acids

An aqueous solution of tetraethylammonium hydroxide (20% w/w, 50 mmol) was added to a solution of excess amino acid (50 mmol). The reaction mixture was stirred for 2 h at room temperature. Then, the crude products were obtained after being dried at 70 °C under vacuum for 1 day. Since the crude product was miscible with EtOH and amino acid was nearly insoluble in EtOH, the crude product was added into EtOH (50 mL) to precipitate the excess of amino acid. After filtration, the solvent was evaporated and the product was obtained after being dried *in vacuo* for 1 day at 65 °C.

Tetraethylammonium L-serinate ($[N_{2222}][ser]$): Yield 96%; $[\alpha]_D^{25} = -1.5$ (c 1, H₂O); ¹H-NMR δ 3.82–3.77 (m, 2H, HO-CH₂), 3.39–3.20 (m, 1H, O₂C-CH), 3.25 (q, ³J_{HH} = 7.3 Hz, 8H, N-CH₂), 1.25 (t, ³J_{HH} = 7.3 Hz, 12H, N-CH₂-CH₃); ¹³C-NMR δ 6.77, 52.03, 57.55, 64.16, 179.02; Anal. calcd. for C₁₁H₂₆N₂O₃: C 56.38, H 11.18, N 11.95; found: C 56.00, H 11.01, N 11.48.

Tetraethylammonium L-prolinate ($[N_{2222}][pro]$): Yield 90%; $[\alpha]_D^{25} = -42.9$ (c 1, H₂O); ¹H-NMR δ 3.45 (dd, 1H, ³J_{HHα} = 7.3 Hz, ³J_{HHβ} = 12.12 Hz, O₂C-CH), 3.12–3.09 (m, 1H, N-CH(α)), 3.21 (q, ³J_{HH} = 7.3 Hz, 8H, N-CH₂), 2.99–2.74 (m, 1H, N-CH(β)), 2.17–2.03 (m, 1H, HC-CH(α)), 1.72 to 1.61 (m, 3H, HC-CH(β) and H₂N-CH₂-CH₂), 1.14 (t, ³J_{HH} = 7.3 Hz, 12H, N-CH₂-CH₃); ¹³C-NMR δ 6.75, 25.10, 30.67, 46.19, 51.96, 61.56, 180.28; Anal. calcd. for C₁₃H₂₈N₂O₂: C 63.89, H 11.55, N 11.46; found: C 63.53, H 11.23, N 11.07.

Tetraethylammonium L-threoninate ($[N_{2222}][thr]$): Yield 94%; $[\alpha]_D^{25} = -3.8$ (c 1, H₂O); ¹H-NMR δ 3.82–3.77 (m, 1H, OH-CH), 3.14 (q, ³J_{HH} = 7.5 Hz, 8H, N-CH₂), 2.94 (d, ³J_{HH} = 5.5 Hz, 1H, O₂C-CH), 1.13 (t, ³J_{HH} = 7.5 Hz, 12H, N-CH₂-CH₃), 1.06 (d, ³J_{HH} = 6.0 Hz, 3H, OH-C-CH₃); ¹³C-NMR δ 6.58, 19.33, 57.73, 68.16, 70.54, 180.32; Anal. calcd. for C₁₂H₂₈N₂O₃: C 58.03, H 11.36, N 11.28; found: C 57.90, H 11.14, N 10.97.

Tetraethylammonium L-isoleucinate ($[N_{2222}][ile]$): Yield 87%; $[\alpha]_D^{25} = +4.9$ (c 1, H₂O); ¹H-NMR δ 3.13 (q, ³J_{HH} = 7.3 Hz, 8H, N-CH₂), 2.96 (d, ³J_{HH} = 5.0 Hz, 1H, O₂C-CH), 1.65–1.54 (m, 1H, H₂N-CH-CH), 1.30–1.28 (m, 2H, CH-CH₂), 1.13 (t, ³J_{HH} = 7.3 Hz, 12H, N-CH₂-CH₃), 1.17–1.01 (m, 3H, CHCH₃), 0.82–0.76 (m, 3H, CH₂CH₃); ¹³C-NMR δ: 6.63, 11.38, 15.61, 25.19, 39.74, 60.43, 57.81, 179.27; Anal. calcd. for C₁₄H₃₂N₂O₂: C 64.57, H 12.39, N 9.89; found: C 64.25, H 12.24, N 9.76.

Tetraethylammonium L-asparaginate ($[N_{2222}][asn]$): Yield 92%; $[\alpha]_D^{25} = -5.1$ (c 1, H₂O); ¹H-NMR δ 3.69–3.57 (m, 1H, O₂C-CH), 3.25 (q, ³J_{HH} = 7.5 Hz, 8H, N-CH₂), 2.64 (dd, ²J_{HHβ} = 12.5 Hz, ³J_{HH} = 5.5 Hz, 1H, OOC-C-CH(α)), 2.42 (dd, ²J_{HHβ} = 12.5 Hz, ³J_{HH} = 8.0 Hz, 1H, OOC-C-CH(β)), 1.26 (t, ³J_{HH} = 7.5 Hz, 12H, N-CH₂-CH₃); ¹³C-NMR δ 6.75, 40.20, 55.21, 57.10, 176.32, 179.90; Anal. calcd. for C₁₂H₂₇N₃O₃: C 55.15, H 10.41, N 16.08; found: C 54.93, H 10.16, N 15.83.

Tetraethylammonium L-glutaminat ($[N_{2222}][gln]$): Yield 91%; $[\alpha]_D^{25} = -7.4$ (c 1, H₂O); ¹H-NMR δ 3.96 (t, ³J_{HH} = 7.3 Hz, 1H, O₂C-CH), 3.05 (q, ³J_{HH} = 7.3 Hz, 8H, N-CH₂), 2.35 to 2.14 (m, 2H, CH-CH₂-CH₂), 1.88 to 1.61 (m, 2H, CH-CH₂-), 1.08 (t, ³J_{HH} = 7.3 Hz, 12H, N-CH₂-CH₃); ¹³C-NMR δ

6.72, 30.39, 33.84, 56.75, 58.51, 176.43, 181.95; Anal. calcd. for $C_{13}H_{29}N_3O_3$: C 56.70, H 10.61, N 15.26; found: C 56.38, H 10.34, N 15.04.

Tetraethylammonium L-glutamate ($[N_{2222}][glu]$): Yield 89%; $[\alpha]_D^{25} = -2.1$ (c 1, H_2O); 1H -NMR δ 3.74–3.58 (m, 1H, O_2C-CH), 3.24 (q, $^3J_{HH} = 7.3$ Hz, 8H, $N-CH_2$), 2.57–2.33 (m, 2H, O_2-CH_2), 2.16–1.99 (m, 2H, $O_2-CH_2-CH_2$), 1.25 (t, $^3J_{HH} = 7.3$ Hz, 12H, $N-CH_2-CH_3$); ^{13}C -NMR δ 6.70, 27.12, 33.62, 51.95, 54.68, 174.40, 180.94; Anal. calcd. for $C_{13}H_{28}N_2O_4$: C 56.50, H 10.21, N 10.14; found: C 56.27, H 10.04, N 9.96.

Tetraethylammonium L-methioninate ($[N_{2222}][met]$): Yield 95%; $[\alpha]_D^{25} = +1.1$ (c 1, H_2O); 1H -NMR δ 3.49–3.36 (m, 1H, O_2C-CH), 3.25 (q, $^3J_{HH} = 7.3$ Hz, 8H, $N-CH_2$), 2.51 (t, $^3J_{HH} = 8$ Hz, 2H, $S-CH_2$), 2.11 (s, 3H, $S-CH_3$), 1.82 to 1.99 (m, 2H, $CH-CH_2$), 1.25 (t, $^3J_{HH} = 7.3$ Hz, 12H, $N-CH_2-CH_3$); ^{13}C -NMR δ 6.82, 14.35, 29.87, 33.90, 52.05, 55.30, 181.52; Anal. calcd. for $C_{13}H_{30}N_2O_2S$: C 56.07, H 10.86, N 10.06, S 11.49; found: C 55.87, H 10.64, N 9.88, S 11.18.

Tetraethylammonium L-histidinate ($[N_{2222}][his]$): Yield 86%; $[\alpha]_D^{25} = -5.2$ (c 1, H_2O); 1H -NMR δ 7.65 (s, 1H, $N=CH-NH$), 6.91 (s, 1H, $HN-CH=C$), 3.49 (t, $^3J_{HH} = 7.3$ Hz, 1H, O_2C-CH), 3.19 (q, $^3J_{HH} = 7.3$ Hz, 8H, $N-CH_2$), 2.97 (dd, $^2J_{HH\beta} = 12.5$ Hz, $^3J_{HH} = 5.5$ Hz, 1H, $O_2C-CH-CH(\alpha)$), 2.83 (dd, $^2J_{HH\beta} = 12.5$ Hz, $^3J_{HH} = 7.0$ Hz, 1H, $O_2C-CH-CH(\beta)$), 1.22 (t, $^3J_{HH} = 7.3$ Hz, 12H, $N-CH_2-CH_3$); ^{13}C -NMR δ 6.64, 31.97, 51.94, 56.16, 118.08, 133.45, 135.84, 181.74; Anal. calcd. for $C_{14}H_{28}N_4O_2$: C 59.12, H 9.92, N 19.70; found: C 58.92, H 9.73, N 19.45.

4. Conclusions

Nine new tetraethylammonium-based amino acid chiral ionic liquids (CILs) have been synthesized and characterized. All of them showed lower decomposition temperatures but were stable up to 210 °C. By changing the anions, the thermal stability of the CILs is slightly affected due to the configurational and functional groups present in the structure. Although these salts were thermally less stable, they showed much improved viscosity and ionic conductivity compared to similar AAILs. From the trend found in this study, cation structure, ion mobility, *van der Waals* and H-bonding interaction influenced the viscosity and ionic conductivity. Some of these new CILs showed higher ionic conductivity than similar AAILs reported until now. To our knowledge, this paper is the first to report the existence of tetraethylammonium-based amino acids CILs having a high ionic conductivity. These finding should be useful for designing suitable CILs for specific application such as in chiral discrimination, biocatalysis and electrochemical field as electrolyte.

Acknowledgements

This research was supported by Ministry of Higher Education Malaysia for the research grant 05-10-07-377FR (Fundamental Research Grant Scheme-FRGS).

References

1. Ohno, H.; Fukumoto, K. Amino acid ionic liquids. *Acc. Chem. Res.* **2007**, *40*, 1122–1129.
2. Welton, T. Room-temperature ionic liquids. Solvents for synthesis and catalysis. *Chem. Rev.* **1999**, *99*, 2071–2083.
3. Van Rantwijk, F.; Lau, R.M.; Sheldon, R.A. Biocatalytic transformations in ionic liquids. *Trends Biotech.* **2003**, *21*, 131–138.
4. Obliosca, J.M.; Arco, S.D.; Huang, M.H. Synthesis and optical properties of 1-alkyl-3-methylimidazolium lauryl sulfate ionic liquids. *J. Fluoresc.* **2007**, *17*, 613–618.
5. Baudequin, C.; Baudoux, J.; Levillain, J.; Cahard, D.; Gaumont, A.-C.; Plaquevent, J.-C. Ionic liquids and chirality: Opportunities and challenges. *Tetrahedron Asymmetry* **2003**, *14*, 3081–3093.
6. Ding, J.; Armstrong, D.W. Chiral ionic liquids: Synthesis and applications. *Chirality* **2005**, *17*, 281–292.
7. Baudequin, C.; Brégeon, D.; Levillain, J.; Guillen, F.; Plaquevent, J.-C.; Gaumont, A.-C. Chiral ionic liquids, a renewal for the chemistry of chiral solvents? Design, synthesis and applications for chiral recognition and asymmetric synthesis. *Tetrahedron Asymmetry* **2005**, *16*, 3921–3945.
8. Abdul Rahman, M.B.; Jumbri, K.; Sirat, K.; Kia, R.; Fun, H.-K. Tetraethylammonium L-malate 1.36-hydrate. *Acta Cryst.* **2009**, *E65*, 49–50.
9. Abdul Rahman, M.B.; Jumbri, K.; Sirat, K.; Kia, R.; Fun, H.-K. Tetraethylammonium L-tartrate dihydrate. *Acta Cryst.* **2008**, *E64*, 2343.
10. Bao, W.; Wang, Z.; Li, Y. Synthesis of chiral ionic liquids from natural amino acids. *J. Org. Chem.* **2003**, *68*, 591–593.
11. Wasserscheid, P.; Bösmann, A.; Bolm, C. Synthesis and properties of ionic liquids derived from the 'chiral pool'. *Chem. Commun.* **2002**, 200–201.
12. Clavier, H.; Boulanger, L.; Audic, N.; Toupet, L.; Mauduit, M.; Guillemin, J.-C. Design and synthesis of imidazolium salts derived from (L)-valine, Investigation of their potential in chiral molecular recognition. *Chem. Commun.* **2004**, 1224–1225.
13. Fukumoto, K.; Yoshizawa, M.; Ohno, H. Room temperature ionic liquids from 20 natural amino acids. *J. Am. Chem. Soc.* **2005**, *127*, 2398–2399.
14. Tao, G.-H.; He, L.; Sun, N.; Kou, Y. New generation ionic liquids: Cations derived from amino acids. *Chem. Commun.* **2005**, 3562–3564.
15. Allen, C.R.; Richard, P.L.; Ward, A.J.; van de Water, L.G.A.; Masters, A.F.; Maschmeyer, T. Facile synthesis of ionic liquids possessing chiral carboxylates. *Tetrahedron Lett.* **2006**, *47*, 7367–7370.
16. Jiang, Y.-Y.; Wang, G.-N.; Zhou, Z.; Wu, Y.-T.; Geng, J.; Zhang, Z.-B. Tetraalkylammonium amino acids as functionalized ionic liquids of low viscosity. *Chem. Commun.* **2008**, 505–507.
17. Shirota, H.; Castner, E.W., Jr. Why are viscosities lower for ionic liquids with -CH₂Si(CH₃)₃ vs -CH₂C(CH₃)₃ substitutions on the imidazolium cations?. *J. Phys. Chem. B* **2005**, *109*, 21576–21585.
18. Seddon, K.R.; Stark, A.; Torres, M.J. Influence of chloride, water, and organic solvents on the physical properties of ionic liquids. *Pure Appl. Chem.* **2000**, *72*, 2775–2287.



19. Kagimoto, J.; Fukumoto, K.; Ohno, H. Effect of tetrabutylphosphonium cation on the physico-chemical properties of amino-acid ionic liquids. *Chem. Commun.* **2006**, 2254–2256.
20. MacFarlane, D.R.; Pringle, J.M.; Johansson, K.M.; Forsyth, S.A.; Forsyth, M. Lewis base ionic liquids. *Chem. Commun.* **2006**, 1905–1917.
21. MacFarlane, D.R.; Sun, J.; Golding, J.; Meakin, P.; Forsyth, M. High conductivity molten salts based on the imide ion. *Electrochim. Acta* **2000**, *45*, 1271–1278.
22. Matz, R.A.; Trulove, P.C. *Ionic Liquids in Synthesis*; Wasserscheid, P.; Welton, T., Eds.; Wiley-VCH Verlag: Weinheim, Germany, 2003; Chapter 3, p. 56.
23. Ohno, H. Functional design of ionic liquids. *Bull Chem. Soc. Jpn.* **2006**, *79*, 1665–1680.

Sample Availability: All samples are available from the authors.

© 2010 by the authors; licensee Molecular Diversity Preservation International, Basel, Switzerland. This article is an open-access article distributed under the terms and conditions of the Creative Commons Attribution license (<http://creativecommons.org/licenses/by/3.0/>).

Acta Crystallographica Section E

Structure Reports

Online

ISSN 1600-5368

Tetraethylammonium L-malate 1.36-hydrate

Mohd Basyaruddin Abdul Rahman,^a Khairulazhar
Jumbri,^a Kamaliah Sirat,^a Reza Kia^b and Hoong-Kun Fun^{b*}

^aDepartment of Chemistry, Faculty of Science, Universiti Putra Malaysia, 43400 UPM Serdang, Selangor, Malaysia, and ^bX-ray Crystallography Unit, School of Physics, Universiti Sains Malaysia, 11800 USM, Penang, Malaysia
Correspondence e-mail: hkf@upm.edu.my

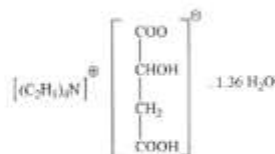
Received 12 November 2008; accepted 1 December 2008

Key indicators: single-crystal X-ray study; T = 100 K; mean $\sigma(\text{C}-\text{C}) = 0.002 \text{ \AA}$; disorder in main residue; R factor = 0.041; wR factor = 0.103; data-to-parameter ratio = 22.7.

The asymmetric unit of the title compound, $\text{C}_8\text{H}_{20}\text{N}^+ \cdot \text{C}_2\text{H}_3\text{O}_5^- \cdot 1.36\text{H}_2\text{O}$, contains two independent ion pairs, with similar conformations, and three water molecules of crystallization, one water molecule having a site-occupancy factor of 0.721 (5). Intramolecular $\text{O}-\text{H} \cdots \text{O}$ hydrogen bonds, involving the hydroxy groups and an O atom of each carboxylate anion, generate five-membered rings involving *S*(5) ring motifs. In the crystal structure, molecules are linked together by water molecules through four-membered $\text{O}-\text{H} \cdots \text{O} \cdots \text{H} \cdots \text{O}-\text{H}$ interactions to form one-dimensional infinite chains along the *a* axis. Since the molecules are also linked into one-dimensional infinite chains along the *b* axis, molecular sheets parallel to the (001) plane are created. Overall, the crystal structure is stabilized by two intramolecular $\text{O}-\text{H} \cdots \text{O}$ hydrogen bonds, nine intermolecular $\text{O}-\text{H} \cdots \text{O}$ and ten $\text{C}-\text{H} \cdots \text{O}$ hydrogen bonds.

Related literature

For hydrogen-bond motifs, see: Bernstein *et al.* (1995). For bond-length data, see: Allen *et al.* (1987). For related compounds, see, for example: Rahman *et al.* (2008); Allen *et al.* (2006); Jiang *et al.* (2008). For related literature, see: Anandha *et al.* (2008).



* Additional correspondence author; Laboratory of Industrial Biotechnology, Institute of Bioscience, Universiti Putra Malaysia, 43400 UPM Serdang, Selangor, Malaysia. E-mail: basya@science.upm.edu.my

Experimental

Crystal data

$\text{C}_8\text{H}_{20}\text{N}^+ \cdot \text{C}_2\text{H}_3\text{O}_5^- \cdot 1.36\text{H}_2\text{O}$
 $M_r = 287.83$
Monoclinic, $P2_1$
 $a = 7.4724 (2) \text{ \AA}$
 $b = 19.9721 (5) \text{ \AA}$
 $c = 10.2726 (3) \text{ \AA}$
 $\beta = 92.481 (1)^\circ$

$V = 1531.64 (7) \text{ \AA}^3$
 $Z = 4$
Mo $K\alpha$ radiation
 $\mu = 0.10 \text{ mm}^{-1}$
 $T = 100.0 (1) \text{ K}$
 $0.45 \times 0.35 \times 0.32 \text{ mm}$

Data collection

Bruker SMART APEXII CCD
area-detector diffractometer
Absorption correction: multi-scan
(SADABS; Bruker, 2005)
 $T_{\text{min}} = 0.950$, $T_{\text{max}} = 0.969$

36497 measured reflections
8479 independent reflections
7551 reflections with $I > 2\sigma(I)$
 $R_{\text{int}} = 0.029$

Refinement

$R[F^2 > 2\sigma(F^2)] = 0.041$
 $wR(F^2) = 0.103$
 $S = 1.03$
8479 reflections
373 parameters
1 restraint

H atoms treated by a mixture of
independent and constrained
refinement
 $\Delta\rho_{\text{max}} = 0.51 \text{ e \AA}^{-3}$
 $\Delta\rho_{\text{min}} = -0.47 \text{ e \AA}^{-3}$

Table 1
Hydrogen-bond geometry (\AA , $^\circ$).

<i>D</i> — <i>H</i> — <i>A</i>	<i>D</i> — <i>H</i>	<i>H</i> — <i>A</i>	<i>D</i> — <i>A</i>	<i>D</i> — <i>H</i> — <i>A</i>
O3A—H10A—O4A ⁱ	0.82	1.68	2.4977 (11)	171
O3A—H30A—O2W	0.82	1.98	2.7296 (14)	151
O3A—H30A—O5A	0.82	2.27	2.6853 (11)	112
O3B—H30B—O3W	0.82	2.00	2.7435 (13)	151
O3B—H30B—O5B	0.82	2.26	2.6837 (12)	112
O1W—H1W1—O4A ⁱⁱ	0.92	2.03	2.9354 (17)	166
O1W—H2W1—O1B ⁱⁱⁱ	0.92	1.90	2.8018 (10)	165
O2W—H1W2—O5B	0.84	1.99	2.7969 (13)	162
O2W—H2W2—O5B ^{iv}	0.72	2.18	2.8961 (13)	176
O3W—H2W3—O5A	0.80 (2)	2.13 (2)	2.9109 (13)	173 (2)
O3W—H1W3—O5A ⁱ	0.89 (2)	1.94 (2)	2.7894 (12)	160 (2)
C2A—H2AB—O1W ^v	0.97	2.44	3.3852 (18)	165
C5A—H5AA—O1A ^{vi}	0.97	2.41	3.2814 (15)	149
C6A—H6AA—O1W ^{vii}	0.96	2.59	3.296 (2)	131
C6A—H6AB—O2W ^{viii}	0.96	2.60	3.434 (2)	146
C7A—H7AA—O1W	0.97	2.42	3.2511 (10)	144
C11A—H11B—O2A	0.97	2.53	3.2884 (15)	135
C7A—H7AB—O4B ^{ix}	0.97	2.46	3.3796 (16)	158
C5B—H5BB—O4A ^x	0.97	2.51	3.4141 (17)	156
C6B—H6BC—O1W ^{xi}	0.96	2.58	3.350 (3)	137
C7B—H7BB—O2B ^{xii}	0.97	2.47	3.4325 (15)	170

Symmetry codes: (i) $x+1, y, z$; (ii) $x, y, z-1$; (iii) $-x+1, y-\frac{1}{2}, -z+1$; (iv) $x-1, y, z$; (v) $x, y, z+1$; (vi) $-x, y+\frac{1}{2}, -z+1$; (vii) $-x, y+\frac{1}{2}, -z$.

Data collection: APEX2 (Bruker, 2005); cell refinement: APEX2; data reduction: SAINT (Bruker, 2005); program(s) used to solve structure: SHELXTL (Sheldrick, 2008); program(s) used to refine structure: SHELXTL; molecular graphics: SHELXTL; software used to prepare material for publication: SHELXTL and PLATON (Spek, 2003).

The authors thank the Ministry of Higher Education, Malaysia, for the research grant 05-10-07-377FR (Fundamental Research Grant Scheme-FRGS). H-KF and RK thank the Malaysian Government and Universiti Sains Malaysia for the Science Fund grant No. 305/PFIZIK/613312. RK thanks Universiti Sains Malaysia for a postdoctoral research fellow-

organic compounds

ship. H-KF also thanks Universiti Sains Malaysia for the Research University Golden Goose grant No. 1001/PFIZIK/811012.

Supplementary data and figures for this paper are available from the IUCr electronic archives (Reference: FJ2170).

References

- Allen, C. R., Richard, P. L., Ward, A. J., van de Water, L. G. A., Masters, A. F. & Maschmeyer, T. (2006). *Tetrahedron Lett.* **47**, 7367–7370.
- Allen, F. H., Kennard, O., Watson, D. G., Brummer, L., Orpen, A. G. & Taylor, R. (1987). *J. Chem. Soc. Perkin Trans. 2*, pp. S1–19.
- Anandha Babu, G., Bhagavannarayana, G. & Ramasamy, P. (2008). *J. Cryst. Growth*, **310**, 1228–1238.
- Bernstein, J., Davis, R. E., Shimoni, L. & Chang, N.-L. (1995). *Angew. Chem. Int. Ed. Engl.* **34**, 1555–1573.
- Bruker (2005). *APEX2, SAINT and SADABS*. Bruker AXS Inc., Madison, Wisconsin, USA.
- Jiang, Y.-Y., Wang, G.-N., Zhou, Z., Wu, Y.-T., Geng, J. & Zhong, Z.-B. (2008). *Chem. Commun.* pp. 505–507.
- Rahman, M. B. A., Jambri, K., Sirat, K., Kin, R. & Fun, H.-K. (2008). *Acta Cryst. E* **64**, o2343.
- Sheldrick, G. M. (2008). *Acta Cryst. A* **64**, 112–122.
- Spek, A. L. (2003). *J. Appl. Cryst.* **36**, 7–13.



supplementary materials

electronic reprint

Acta Cryst. (2009). E65, o49-o50 [doi:10.1107/S1600536808040348]

Tetraethylammonium L-malate 1.36-hydrate

M. B. Abdul Rahman, K. Jumbri, K. Sirat, R. Kia and H.-K. Fun

Comment

Previously, we have reported the formation of the tetraethylammonium L-tartrate crystal (Rahman *et al.*, 2008). In this study, we used a different anion in order to compare the interaction between the tartrate and malate ions. Generally, organic molecules contain substituents with the ability to form inter- and intramolecular hydrogen bonding. In this work, tetraethylammonium L-malate $[\text{C}_2\text{H}_5)_4\text{N}]^+[\text{C}_4\text{H}_5\text{O}_5]^-$, was synthesized by neutralization reaction of tetraethylammonium hydroxide with L-malic acid. Related compounds containing the same anion have been prepared (Allen *et al.*, 2006, Ying-Ying *et al.*, 2007). Tetraethylammonium hydroxide is a strong base, which easily deprotonates the carboxylic acid moiety of L-malic acid to form carboxylate anion and water as a by-product (Allen *et al.*, 2006). The reaction between tetraethylammonium hydroxide and L-malic acid forms a weak bond. It seems that the bond formed between tetraethylammonium and L-malic acid is weaker than a covalent bond but may still contribute to the achieved minimum energy configuration (Anandha *et al.*, 2008).

In the title compound I, Fig. 1, the asymmetric unit is composed of two crystallographically independent ion pairs (A and B), with similar conformations and three water molecules of crystallization. One of the water molecule (O1W) is partially occupied with a site-occupancy factor of 0.721 (5). The bond lengths (Allen *et al.* 1987) and angles are within normal ranges. Intramolecular O3A—H3OA...O5A and O3B—H3OB...O5B hydrogen bonds form *S*(5) ring motifs (Table 1) (Bernstein *et al.*, 1995). In the crystal structure, the molecules are linked together by water molecules through directed four-membered O—H...O—H...O—H interactions to form 1-D infinite chains along the *a*-axis (Fig. 2). Since the molecules are also linked into 1-D infinite chains along the *b*-axis, molecular sheets parallel to the (001)-plane are created (Fig. 2). The crystal structure is stabilized by intramolecular O—H...O (*x* 2) hydrogen bonds, intermolecular O—H...O (*x* 9) and C—H...O (*x* 10) hydrogen bonds (Table 1).

Experimental

The synthetic procedure is similar to the previous one (Abdul Rahman *et al.*, 2008) except that L-malic acid (6.704 g, 0.05 mole) was used. Single crystals suitable for *X*-ray diffraction were obtained by slow evaporation at room temperature.

Refinement

The H atoms bound to O1W and O2W were located from the difference Fourier map and constrained to ride on the parent atom. The hydrogen atoms of O3W were also located from the difference Fourier map and refined freely. The hydrogen of the hydroxy groups were positioned using a freely rotating O—H bond and constrained with a fixed distance of 0.82 Å. The rest of the hydrogen atoms were positioned geometrically and refined as a riding model. A rotating group model was used for the methyl group. One of the water molecule (O1W) is partially occupied with a site-occupancy factor of 0.721 (5). In the absence of significant anomalous dispersion effects, the Friedel pairs (6331) were averaged. Only the relative configuration

sup-1

electronic reprint



supplementary materials

is known. The highest peak (0.51 e. \AA^{-3}) is located 0.35 \AA from H6BC and the deepest hole (-0.46 \AA^{-3}) is located 0.67 \AA from O1W.

Figures

Fig. 1. The molecular structure of (I) with atom labels and 40% probability ellipsoids for non-H atoms. The hydrogen atoms of the cations were omitted for clarity. Intramolecular interactions are shown as dashed lines.

Fig. 2. The crystal packing of (I), viewed down the c -axis showing infinite 1-D chains along the a and b -axes of the unit cell. Intermolecular interactions are shown as dashed lines.

Tetraethylammonium L-malate 1.36-hydrate

Crystal data

$\text{C}_8\text{H}_{20}\text{N}^+ \cdot \text{C}_4\text{H}_5\text{O}_5^- \cdot 1.36\text{H}_2\text{O}$	$F_{000} = 630$
$M_r = 287.83$	$D_x = 1.248 \text{ Mg m}^{-3}$
Monoclinic, $P2_1$	Melting point: 360 K
Hall symbol: $P 2_1yb$	Mo $K\alpha$ radiation
$a = 7.4724 (2) \text{ \AA}$	$\lambda = 0.71073 \text{ \AA}$
$b = 19.9721 (5) \text{ \AA}$	Cell parameters from 9898 reflections
$c = 10.2726 (3) \text{ \AA}$	$\theta = 2.2\text{--}37.3^\circ$
$\beta = 92.481 (1)^\circ$	$\mu = 0.10 \text{ mm}^{-1}$
$V = 1531.64 (7) \text{ \AA}^3$	$T = 100.0 (1) \text{ K}$
$Z = 4$	Block, colourless
	$0.45 \times 0.35 \times 0.32 \text{ mm}$

Data collection

Bruker SMART APEXII CCD area-detector diffractometer	8479 independent reflections
Radiation source: fine-focus sealed tube	7551 reflections with $I > 2\sigma(I)$
Monochromator: graphite	$R_{int} = 0.029$
$T = 100.0(1) \text{ K}$	$\theta_{max} = 38.1^\circ$
φ and ω scans	$\theta_{min} = 2.2^\circ$
Absorption correction: multi-scan (SADABS, Bruker, 2005)	$h = -12 \rightarrow 12$
$T_{min} = 0.950$, $T_{max} = 0.969$	$k = -34 \rightarrow 29$
36497 measured reflections	$l = -15 \rightarrow 17$

Refinement

Refinement on F^2	Secondary atom site location: difference Fourier map
Least-squares matrix: full	Hydrogen site location: inferred from neighbouring sites
$R[F^2 > 2\sigma(F^2)] = 0.041$	H atoms treated by a mixture of independent and constrained refinement

sup-2

electronic reprint

$wR(F^2) = 0.103$	$w = 1/[\sigma^2(F_o^2) + (0.0604P)^2 + 0.0914P]$
$S = 1.03$	where $P = (F_o^2 + 2F_c^2)/3$
8479 reflections	$(\Delta/\sigma)_{\max} = 0.001$
373 parameters	$\Delta\rho_{\max} = 0.51 \text{ e } \text{Å}^{-3}$
1 restraint	$\Delta\rho_{\min} = -0.46 \text{ e } \text{Å}^{-3}$
Primary atom site location: structure-invariant direct methods	Extinction correction: none

Special details

Experimental. The low-temperature data was collected with the Oxford Cryosystem Cobra low-temperature attachment.

Geometry. All e.s.d.'s (except the e.s.d. in the dihedral angle between two l.s. planes) are estimated using the full covariance matrix. The cell e.s.d.'s are taken into account individually in the estimation of e.s.d.'s in distances, angles and torsion angles; correlations between e.s.d.'s in cell parameters are only used when they are defined by crystal symmetry. An approximate (isotropic) treatment of cell e.s.d.'s is used for estimating e.s.d.'s involving l.s. planes.

Refinement. Refinement of F^2 against ALL reflections. The weighted R -factor wR and goodness of fit S are based on F^2 , conventional R -factors R are based on F , with F set to zero for negative F^2 . The threshold expression of $F^2 > \sigma(F^2)$ is used only for calculating R -factor(gt) etc. and is not relevant to the choice of reflections for refinement. R -factors based on F^2 are statistically about twice as large as those based on F , and R -factors based on ALL data will be even larger.

Fractional atomic coordinates and isotropic or equivalent isotropic displacement parameters (Å^2)

	<i>x</i>	<i>y</i>	<i>z</i>	U_{110}^*/U_{eq}	Occ. (<1)
O1A	0.64573 (10)	0.68458 (5)	1.09523 (8)	0.01788 (15)	
H1OA	0.7451	0.6730	1.0728	0.027*	
O2A	0.55148 (12)	0.61775 (5)	0.93035 (9)	0.02041 (16)	
O3A	0.27550 (11)	0.73628 (5)	0.84168 (9)	0.02079 (16)	
H3OA	0.1916	0.7510	0.7962	0.031*	
O4A	-0.03849 (11)	0.65649 (5)	1.04627 (9)	0.01975 (16)	
O5A	-0.07483 (10)	0.73468 (4)	0.88984 (9)	0.01767 (14)	
N1A	0.60300 (13)	0.67357 (5)	0.51749 (9)	0.01637 (15)	
C1A	0.52222 (13)	0.65830 (6)	1.01586 (10)	0.01443 (16)	
C2A	0.33579 (13)	0.68207 (6)	1.04454 (10)	0.01670 (18)	
H2AA	0.3433	0.7263	1.0833	0.020*	
H2AB	0.2846	0.6521	1.1072	0.020*	
C3A	0.21347 (12)	0.68474 (6)	0.92261 (10)	0.01460 (16)	
H3AA	0.2243	0.6421	0.8763	0.018*	
C4A	0.01667 (12)	0.69397 (5)	0.95518 (10)	0.01428 (16)	
C5A	0.73206 (17)	0.66565 (7)	0.40899 (12)	0.0230 (2)	
H5AA	0.6638	0.6633	0.3266	0.028*	
H5AB	0.7951	0.6235	0.4209	0.028*	
C6A	0.8688 (2)	0.72149 (11)	0.40131 (18)	0.0421 (4)	
H6AA	0.9500	0.7115	0.3340	0.063*	
H6AB	0.9346	0.7253	0.4833	0.063*	
H6AC	0.8085	0.7629	0.3817	0.063*	
C7A	0.46547 (15)	0.61822 (6)	0.49843 (12)	0.01862 (19)	

supplementary materials

H7AA	0.4056	0.6237	0.4134	0.022*
H7AB	0.5276	0.5756	0.4985	0.022*
C8A	0.3248 (2)	0.61578 (9)	0.60028 (16)	0.0308 (3)
H8AA	0.2389	0.5815	0.5778	0.046*
H8AB	0.2652	0.6583	0.6037	0.046*
H8AC	0.3812	0.6060	0.6839	0.046*
C9A	0.5129 (2)	0.74197 (6)	0.51372 (13)	0.0238 (2)
H9AA	0.4314	0.7445	0.5845	0.029*
H9AB	0.6039	0.7760	0.5289	0.029*
C10A	0.4094 (2)	0.75780 (8)	0.38697 (15)	0.0307 (3)
H10A	0.3576	0.8016	0.3922	0.046*
H10B	0.3161	0.7253	0.3723	0.046*
H10C	0.4892	0.7565	0.3162	0.046*
C11A	0.70013 (17)	0.66878 (6)	0.65050 (11)	0.01895 (19)
H11A	0.7861	0.7051	0.6585	0.023*
H11B	0.6135	0.6752	0.7171	0.023*
C12A	0.79772 (18)	0.60338 (7)	0.67707 (12)	0.0225 (2)
H12A	0.8461	0.6031	0.7652	0.034*
H12B	0.8933	0.5988	0.6182	0.034*
H12C	0.7156	0.5667	0.6647	0.034*
O1B	1.02736 (12)	0.99945 (5)	0.57343 (9)	0.02120 (16)
O2B	1.10569 (10)	0.93091 (5)	0.41324 (8)	0.01761 (14)
H20B	1.2073	0.9416	0.4385	0.026*
O3B	0.76722 (11)	0.88088 (5)	0.67077 (9)	0.02200 (17)
H30B	0.6892	0.8663	0.7168	0.033*
O4B	0.42411 (10)	0.95514 (5)	0.46248 (9)	0.01896 (15)
O5B	0.41095 (11)	0.87999 (5)	0.62477 (9)	0.01882 (15)
N1B	0.11875 (14)	0.93897 (5)	0.00228 (10)	0.01887 (17)
C1B	0.99015 (13)	0.95720 (6)	0.48948 (10)	0.01417 (16)
C2B	0.80012 (13)	0.93187 (6)	0.46378 (10)	0.01577 (17)
H2BA	0.8044	0.8870	0.4281	0.019*
H2BB	0.7397	0.9604	0.3993	0.019*
C3B	0.69307 (12)	0.93078 (6)	0.58625 (10)	0.01484 (16)
H3BA	0.7080	0.9742	0.6296	0.018*
C4B	0.49200 (13)	0.91967 (5)	0.55639 (10)	0.01426 (16)
C5B	-0.02184 (18)	0.99158 (7)	0.02759 (15)	0.0264 (2)
H5BA	-0.0549	0.9877	0.1175	0.032*
H5BB	0.0315	1.0354	0.0172	0.032*
C6B	-0.1902 (3)	0.98789 (11)	-0.0588 (3)	0.0523 (6)
H6BA	-0.2759	1.0197	-0.0293	0.078*
H6BB	-0.2396	0.9436	-0.0549	0.078*
H6BC	-0.1621	0.9980	-0.1469	0.078*
C7B	0.26558 (17)	0.94955 (7)	0.10709 (12)	0.0215 (2)
H7BA	0.3175	0.9935	0.0951	0.026*
H7BB	0.2117	0.9493	0.1913	0.026*
C8B	0.4142 (2)	0.89834 (9)	0.10931 (17)	0.0337 (3)
H8BA	0.5074	0.9117	0.1711	0.051*
H8BB	0.4619	0.8951	0.0242	0.051*
H8BC	0.3678	0.8556	0.1340	0.051*

sup-4

electronic reprint

C9B	0.03916 (19)	0.86912 (6)	0.00799 (13)	0.0232 (2)	
H9BA	-0.0503	0.8646	-0.0627	0.028*	
H9BB	0.1332	0.8369	-0.0070	0.028*	
C10B	-0.0468 (2)	0.85122 (8)	0.13452 (15)	0.0305 (3)	
H10D	-0.0843	0.8053	0.1317	0.046*	
H10E	-0.1488	0.8795	0.1459	0.046*	
H10F	0.0385	0.8576	0.2061	0.046*	
C11B	0.18992 (19)	0.94528 (6)	-0.13422 (12)	0.0224 (2)	
H11C	0.2713	0.9083	-0.1479	0.027*	
H11D	0.0901	0.9407	-0.1972	0.027*	
C12B	0.28672 (18)	1.01017 (7)	-0.16150 (13)	0.0229 (2)	
H12D	0.3146	1.0118	-0.2518	0.034*	
H12E	0.3955	1.0124	-0.1084	0.034*	
H12F	0.2113	1.0474	-0.1416	0.034*	
O1W	0.12929 (18)	0.60364 (8)	0.28868 (14)	0.0250 (4)	0.721 (5)
H1W1	0.0585	0.6171	0.2175	0.037*	0.721 (5)
H2W1	0.0955	0.5698	0.3439	0.037*	0.721 (5)
O2W	0.09626 (12)	0.80596 (5)	0.64819 (10)	0.02132 (16)	
H1W2	0.1780	0.8322	0.6271	0.032*	
H2W2	0.0171	0.8259	0.6557	0.032*	
O3W	0.61177 (12)	0.81035 (5)	0.86527 (9)	0.01997 (16)	
H2W3	0.521 (3)	0.7902 (13)	0.852 (2)	0.035 (6)*	
H1W3	0.695 (3)	0.7793 (11)	0.882 (2)	0.025 (5)*	

Atomic displacement parameters (\AA^2)

	U^{11}	U^{22}	U^{33}	U^{12}	U^{13}	U^{23}
O1A	0.0113 (3)	0.0259 (4)	0.0164 (3)	-0.0009 (3)	0.0000 (2)	-0.0004 (3)
O2A	0.0190 (3)	0.0241 (4)	0.0180 (4)	0.0048 (3)	-0.0005 (3)	-0.0020 (3)
O3A	0.0122 (3)	0.0276 (4)	0.0226 (4)	-0.0015 (3)	0.0004 (2)	0.0107 (3)
O4A	0.0126 (3)	0.0249 (4)	0.0219 (4)	-0.0003 (3)	0.0021 (2)	0.0073 (3)
O5A	0.0131 (3)	0.0198 (4)	0.0199 (4)	0.0003 (3)	-0.0010 (2)	0.0014 (3)
N1A	0.0214 (4)	0.0148 (4)	0.0126 (4)	-0.0008 (3)	-0.0025 (3)	-0.0010 (3)
C1A	0.0128 (3)	0.0178 (4)	0.0126 (4)	0.0006 (3)	0.0002 (3)	0.0041 (3)
C2A	0.0118 (3)	0.0243 (5)	0.0140 (4)	0.0007 (3)	0.0003 (3)	-0.0003 (4)
C3A	0.0105 (3)	0.0188 (4)	0.0144 (4)	-0.0002 (3)	0.0004 (3)	0.0012 (3)
C4A	0.0109 (3)	0.0161 (4)	0.0158 (4)	-0.0020 (3)	-0.0002 (3)	-0.0015 (3)
C5A	0.0242 (5)	0.0301 (6)	0.0149 (4)	-0.0030 (4)	0.0019 (3)	0.0016 (4)
C6A	0.0367 (8)	0.0565 (11)	0.0334 (8)	-0.0218 (8)	0.0063 (6)	0.0035 (8)
C7A	0.0206 (4)	0.0170 (5)	0.0181 (5)	-0.0019 (3)	-0.0010 (3)	-0.0033 (4)
C8A	0.0261 (6)	0.0350 (7)	0.0320 (7)	-0.0060 (5)	0.0072 (5)	-0.0040 (6)
C9A	0.0357 (6)	0.0156 (5)	0.0194 (5)	0.0034 (4)	-0.0079 (4)	-0.0012 (4)
C10A	0.0425 (8)	0.0240 (6)	0.0242 (6)	0.0068 (5)	-0.0126 (5)	-0.0001 (5)
C11A	0.0268 (5)	0.0171 (5)	0.0125 (4)	0.0009 (3)	-0.0044 (3)	-0.0010 (3)
C12A	0.0267 (5)	0.0221 (5)	0.0183 (5)	0.0044 (4)	-0.0045 (4)	-0.0001 (4)
O1B	0.0184 (3)	0.0239 (4)	0.0214 (4)	-0.0047 (3)	0.0029 (3)	-0.0072 (3)
O2B	0.0115 (3)	0.0249 (4)	0.0165 (3)	-0.0017 (3)	0.0019 (2)	-0.0030 (3)
O3B	0.0127 (3)	0.0291 (5)	0.0244 (4)	0.0010 (3)	0.0026 (3)	0.0111 (3)

supplementary materials

O4B	0.0120 (3)	0.0229 (4)	0.0219 (4)	-0.0011 (3)	0.0002 (2)	0.0063 (3)
O5B	0.0144 (3)	0.0203 (4)	0.0219 (4)	-0.0018 (3)	0.0037 (2)	0.0042 (3)
N1B	0.0236 (4)	0.0164 (4)	0.0166 (4)	-0.0034 (3)	0.0015 (3)	-0.0052 (3)
C1B	0.0129 (3)	0.0169 (4)	0.0128 (4)	-0.0018 (3)	0.0012 (3)	0.0017 (3)
C2B	0.0121 (3)	0.0202 (5)	0.0151 (4)	-0.0029 (3)	0.0021 (3)	-0.0013 (4)
C3B	0.0108 (3)	0.0179 (4)	0.0160 (4)	0.0000 (3)	0.0015 (3)	0.0014 (3)
C4B	0.0125 (3)	0.0144 (4)	0.0160 (4)	-0.0002 (3)	0.0024 (3)	-0.0017 (3)
C5B	0.0233 (5)	0.0215 (6)	0.0342 (7)	0.0000 (4)	0.0009 (4)	-0.0083 (5)
C6B	0.0329 (8)	0.0401 (10)	0.0819 (16)	0.0063 (7)	-0.0226 (9)	-0.0168 (10)
C7B	0.0243 (5)	0.0253 (5)	0.0150 (4)	-0.0036 (4)	0.0010 (3)	-0.0036 (4)
C8B	0.0309 (7)	0.0379 (8)	0.0318 (7)	0.0054 (6)	-0.0033 (5)	0.0003 (6)
C9B	0.0333 (6)	0.0172 (5)	0.0195 (5)	-0.0076 (4)	0.0046 (4)	-0.0051 (4)
C10B	0.0391 (7)	0.0288 (7)	0.0243 (6)	-0.0134 (5)	0.0080 (5)	-0.0060 (5)
C11B	0.0346 (6)	0.0185 (5)	0.0143 (5)	-0.0048 (4)	0.0018 (4)	-0.0028 (4)
C12B	0.0278 (5)	0.0203 (5)	0.0206 (5)	-0.0057 (4)	0.0026 (4)	-0.0012 (4)
O1W	0.0206 (6)	0.0304 (7)	0.0235 (7)	-0.0050 (4)	-0.0031 (4)	0.0084 (5)
O2W	0.0170 (3)	0.0205 (4)	0.0265 (4)	-0.0009 (3)	0.0011 (3)	0.0063 (3)
O3W	0.0168 (3)	0.0201 (4)	0.0231 (4)	-0.0002 (3)	0.0020 (3)	0.0046 (3)

Geometric parameters (\AA , $^\circ$)

O1A—C1A	1.3141 (13)	O3B—C3B	1.4187 (14)
O1A—H10A	0.8200	O3B—H30B	0.8200
O2A—C1A	1.2215 (14)	O4B—C4B	1.2835 (14)
O3A—C3A	1.4140 (14)	O5B—C4B	1.2350 (14)
O3A—H30A	0.8200	N1B—C5B	1.5161 (17)
O4A—C4A	1.2804 (13)	N1B—C7B	1.5184 (15)
O5A—C4A	1.2407 (13)	N1B—C9B	1.5186 (16)
N1A—C5A	1.5134 (16)	N1B—C11B	1.5262 (16)
N1A—C7A	1.5162 (15)	C1B—C2B	1.5197 (14)
N1A—C11A	1.5223 (14)	C2B—C3B	1.5200 (15)
N1A—C9A	1.5228 (16)	C2B—H2BA	0.9700
C1A—C2A	1.5127 (14)	C2B—H2BB	0.9700
C2A—C3A	1.5193 (14)	C3B—C4B	1.5366 (13)
C2A—H2AA	0.9700	C3B—H3BA	0.9800
C2A—H2AB	0.9700	C5B—C6B	1.509 (2)
C3A—C4A	1.5333 (13)	C5B—H5BA	0.9700
C3A—H3AA	0.9800	C5B—H5BB	0.9700
C5A—C6A	1.517 (2)	C6B—H6BA	0.9600
C5A—H5AA	0.9700	C6B—H6BB	0.9600
C5A—H5AB	0.9700	C6B—H6BC	0.9600
C6A—H6AA	0.9600	C7B—C8B	1.509 (2)
C6A—H6AB	0.9600	C7B—H7BA	0.9700
C6A—H6AC	0.9600	C7B—H7BB	0.9700
C7A—C8A	1.5158 (19)	C8B—H8BA	0.9600
C7A—H7AA	0.9700	C8B—H8BB	0.9600
C7A—H7AB	0.9700	C8B—H8BC	0.9600
C8A—H8AA	0.9600	C9B—C10B	1.517 (2)
C8A—H8AB	0.9600	C9B—H9BA	0.9700

sup-6

electronic reprint

supplementary materials

C8A—H8AC	0.9600	C9B—H9BB	0.9700
C9A—C10A	1.5185 (18)	C10B—H10D	0.9600
C9A—H9AA	0.9700	C10B—H10E	0.9600
C9A—H9AB	0.9700	C10B—H10F	0.9600
C10A—H10A	0.9600	C11B—C12B	1.5163 (18)
C10A—H10B	0.9600	C11B—H11C	0.9700
C10A—H10C	0.9600	C11B—H11D	0.9700
C11A—C12A	1.5150 (17)	C12B—H12D	0.9600
C11A—H11A	0.9700	C12B—H12E	0.9600
C11A—H11B	0.9700	C12B—H12F	0.9600
C12A—H12A	0.9600	O1W—H1W1	0.9230
C12A—H12B	0.9600	O1W—H2W1	0.9242
C12A—H12C	0.9600	O2W—H1W2	0.8398
O1B—C1B	1.2297 (14)	O2W—H2W2	0.7201
O2B—C1B	1.3011 (13)	O3W—H2W3	0.80 (3)
O2B—H2OB	0.8200	O3W—H1W3	0.89 (2)
C1A—O1A—H10A	109.5	C5B—N1B—C7B	105.47 (9)
C3A—O3A—H30A	109.5	C5B—N1B—C9B	110.76 (10)
C5A—N1A—C7A	106.18 (9)	C7B—N1B—C9B	111.87 (10)
C5A—N1A—C11A	111.11 (9)	C5B—N1B—C11B	111.84 (11)
C7A—N1A—C11A	111.36 (9)	C7B—N1B—C11B	111.72 (10)
C5A—N1A—C9A	111.72 (10)	C9B—N1B—C11B	105.31 (9)
C7A—N1A—C9A	110.76 (9)	O1B—C1B—O2B	124.28 (9)
C11A—N1A—C9A	105.80 (9)	O1B—C1B—C2B	122.10 (10)
O2A—C1A—O1A	124.62 (10)	O2B—C1B—C2B	113.61 (9)
O2A—C1A—C2A	122.90 (9)	C1B—C2B—C3B	112.47 (8)
O1A—C1A—C2A	112.45 (9)	C1B—C2B—H2BA	109.1
C1A—C2A—C3A	112.13 (9)	C3B—C2B—H2BA	109.1
C1A—C2A—H2AA	109.2	C1B—C2B—H2BB	109.1
C3A—C2A—H2AA	109.2	C3B—C2B—H2BB	109.1
C1A—C2A—H2AB	109.2	H2BA—C2B—H2BB	107.8
C3A—C2A—H2AB	109.2	O3B—C3B—C2B	108.12 (9)
H2AA—C2A—H2AB	107.9	O3B—C3B—C4B	111.92 (9)
O3A—C3A—C2A	108.03 (9)	C2B—C3B—C4B	112.45 (8)
O3A—C3A—C4A	112.50 (9)	O3B—C3B—H3BA	108.1
C2A—C3A—C4A	111.89 (8)	C2B—C3B—H3BA	108.1
O3A—C3A—H3AA	108.1	C4B—C3B—H3BA	108.1
C2A—C3A—H3AA	108.1	O5B—C4B—O4B	126.45 (9)
C4A—C3A—H3AA	108.1	O5B—C4B—C3B	118.59 (9)
O5A—C4A—O4A	126.25 (9)	O4B—C4B—C3B	114.93 (9)
O5A—C4A—C3A	118.17 (9)	C6B—C5B—N1B	115.56 (13)
O4A—C4A—C3A	115.55 (9)	C6B—C5B—H5BA	108.4
N1A—C5A—C6A	114.44 (12)	N1B—C5B—H5BA	108.4
N1A—C5A—H5AA	108.7	C6B—C5B—H5BB	108.4
C6A—C5A—H5AA	108.7	N1B—C5B—H5BB	108.4
N1A—C5A—H5AB	108.7	H5BA—C5B—H5BB	107.5
C6A—C5A—H5AB	108.7	C5B—C6B—H6BA	109.5
H5AA—C5A—H5AB	107.6	C5B—C6B—H6BB	109.5
C5A—C6A—H6AA	109.5	H6BA—C6B—H6BB	109.5

sup-7

electronic reprint



supplementary materials

C5A—C6A—H6AB	109.5	C5B—C6B—H6BC	109.5
H6AA—C6A—H6AB	109.5	H6BA—C6B—H6BC	109.5
C5A—C6A—H6AC	109.5	H6BB—C6B—H6BC	109.5
H6AA—C6A—H6AC	109.5	C8B—C7B—N1B	115.16 (11)
H6AB—C6A—H6AC	109.5	C8B—C7B—H7BA	108.5
C8A—C7A—N1A	114.88 (10)	N1B—C7B—H7BA	108.5
C8A—C7A—H7AA	108.5	C8B—C7B—H7BB	108.5
N1A—C7A—H7AA	108.5	N1B—C7B—H7BB	108.5
C8A—C7A—H7AB	108.5	H7BA—C7B—H7BB	107.5
N1A—C7A—H7AB	108.5	C7B—C8B—H8BA	109.5
H7AA—C7A—H7AB	107.5	C7B—C8B—H8BB	109.5
C7A—C8A—H8AA	109.5	H8BA—C8B—H8BB	109.5
C7A—C8A—H8AB	109.5	C7B—C8B—H8BC	109.5
H8AA—C8A—H8AB	109.5	H8BA—C8B—H8BC	109.5
C7A—C8A—H8AC	109.5	H8BB—C8B—H8BC	109.5
H8AA—C8A—H8AC	109.5	C10B—C9B—N1B	115.51 (11)
H8AB—C8A—H8AC	109.5	C10B—C9B—H9BA	108.4
C10A—C9A—N1A	114.62 (11)	N1B—C9B—H9BA	108.4
C10A—C9A—H9AA	108.6	C10B—C9B—H9BB	108.4
N1A—C9A—H9AA	108.6	N1B—C9B—H9BB	108.4
C10A—C9A—H9AB	108.6	H9BA—C9B—H9BB	107.5
N1A—C9A—H9AB	108.6	C9B—C10B—H10D	109.5
H9AA—C9A—H9AB	107.6	C9B—C10B—H10E	109.5
C9A—C10A—H10A	109.5	H10D—C10B—H10E	109.5
C9A—C10A—H10B	109.5	C9B—C10B—H10F	109.5
H10A—C10A—H10B	109.5	H10D—C10B—H10F	109.5
C9A—C10A—H10C	109.5	H10E—C10B—H10F	109.5
H10A—C10A—H10C	109.5	C12B—C11B—N1B	115.37 (10)
H10B—C10A—H10C	109.5	C12B—C11B—H11C	108.4
C12A—C11A—N1A	115.02 (10)	N1B—C11B—H11C	108.4
C12A—C11A—H11A	108.5	C12B—C11B—H11D	108.4
N1A—C11A—H11A	108.5	N1B—C11B—H11D	108.4
C12A—C11A—H11B	108.5	H11C—C11B—H11D	107.5
N1A—C11A—H11B	108.5	C11B—C12B—H12D	109.5
H11A—C11A—H11B	107.5	C11B—C12B—H12E	109.5
C11A—C12A—H12A	109.5	H12D—C12B—H12E	109.5
C11A—C12A—H12B	109.5	C11B—C12B—H12F	109.5
H12A—C12A—H12B	109.5	H12D—C12B—H12F	109.5
C11A—C12A—H12C	109.5	H12E—C12B—H12F	109.5
H12A—C12A—H12C	109.5	H1W1—O1W—H2W1	122.4
H12B—C12A—H12C	109.5	H1W2—O2W—H2W2	107.0
C1B—O2B—H2OB	109.5	H2W3—O3W—H1W3	105 (2)
C3B—O3B—H3OB	109.5		
O2A—C1A—C2A—C3A	-32.74 (15)	O1B—C1B—C2B—C3B	-32.15 (15)
O1A—C1A—C2A—C3A	149.15 (10)	O2B—C1B—C2B—C3B	149.04 (10)
C1A—C2A—C3A—O3A	-67.95 (12)	C1B—C2B—C3B—O3B	-68.04 (12)
C1A—C2A—C3A—C4A	167.69 (9)	C1B—C2B—C3B—C4B	167.90 (9)
O3A—C3A—C4A—O5A	14.42 (14)	O3B—C3B—C4B—O5B	14.28 (14)
C2A—C3A—C4A—O5A	136.25 (11)	C2B—C3B—C4B—O5B	136.21 (11)

sup-8

electronic reprint

supplementary materials

O3A—C3A—C4A—O4A	-167.72 (9)	O3B—C3B—C4B—O4B	-167.58 (10)
C2A—C3A—C4A—O4A	-45.90 (13)	C2B—C3B—C4B—O4B	-45.64 (13)
C7A—N1A—C5A—C6A	173.27 (12)	C7B—N1B—C5B—C6B	-175.46 (16)
C11A—N1A—C5A—C6A	-65.49 (15)	C9B—N1B—C5B—C6B	-54.24 (19)
C9A—N1A—C5A—C6A	52.41 (15)	C11B—N1B—C5B—C6B	62.89 (19)
C5A—N1A—C7A—C8A	178.34 (11)	C5B—N1B—C7B—C8B	174.61 (12)
C11A—N1A—C7A—C8A	57.26 (14)	C9B—N1B—C7B—C8B	54.12 (15)
C9A—N1A—C7A—C8A	-60.18 (14)	C11B—N1B—C7B—C8B	-63.67 (15)
C5A—N1A—C9A—C10A	58.05 (15)	C5B—N1B—C9B—C10B	-57.11 (16)
C7A—N1A—C9A—C10A	-60.11 (15)	C7B—N1B—C9B—C10B	60.26 (16)
C11A—N1A—C9A—C10A	179.09 (13)	C11B—N1B—C9B—C10B	-178.18 (13)
C5A—N1A—C11A—C12A	-59.67 (14)	C5B—N1B—C11B—C12B	63.04 (14)
C7A—N1A—C11A—C12A	58.48 (14)	C7B—N1B—C11B—C12B	-54.94 (15)
C9A—N1A—C11A—C12A	178.89 (11)	C9B—N1B—C11B—C12B	-176.59 (11)

Hydrogen-bond geometry (Å, °)

D—H...A	D—H	H...A	D...A	D—H...A
O1A—H10A...O4A ⁱ	0.82	1.68	2.4977 (11)	171
O3A—H30A...O2W	0.82	1.98	2.7296 (14)	151
O3A—H30A...O5A	0.82	2.27	2.6853 (11)	112
O3B—H30B...O3W	0.82	2.00	2.7435 (13)	151
O3B—H30B...O5B	0.82	2.26	2.6837 (12)	112
O1W—H1W1...O4A ⁱⁱ	0.92	2.05	2.9354 (17)	166
O1W—H2W1...O1B ⁱⁱⁱ	0.92	1.90	2.8018 (18)	165
O2W—H1W2...O5B	0.84	1.99	2.7969 (13)	162
O2W—H2W2...O3B ^{iv}	0.72	2.18	2.8961 (13)	176
O3W—H2W3...O3A	0.80 (2)	2.13 (2)	2.9169 (13)	173 (2)
O3W—H1W3...O5A ⁱ	0.89 (2)	1.94 (2)	2.7894 (12)	160 (2)
C2A—H2AB...O1W ^v	0.97	2.44	3.3852 (18)	165
C5A—H5AA...O1A ⁱⁱ	0.97	2.41	3.2814 (15)	149
C6A—H6AA...O1W ⁱ	0.96	2.59	3.296 (2)	131
C6A—H6AB...O2W ⁱ	0.96	2.60	3.434 (2)	146
C7A—H7AA...O1W	0.97	2.42	3.2511 (18)	144
C11A—H11B...O2A	0.97	2.53	3.2884 (15)	135
C7A—H7AB...O4B ⁱⁱⁱ	0.97	2.46	3.3796 (16)	158
C5B—H5BB...O4A ^{vi}	0.97	2.51	3.4141 (17)	156
C6B—H6BC...O1W ^{vii}	0.96	2.58	3.350 (3)	137
C7B—H7BB...O2B ^{iv}	0.97	2.47	3.4325 (15)	170

Symmetry codes: (i) $x+1, y, z$; (ii) $x, y, z-1$; (iii) $-x+1, y-1/2, -z+1$; (iv) $x-1, y, z$; (v) $x, y, z+1$; (vi) $-x, y+1/2, -z+1$; (vii) $-x, y+1/2, -z$.

sup-9

electronic reprint



Fig. 1

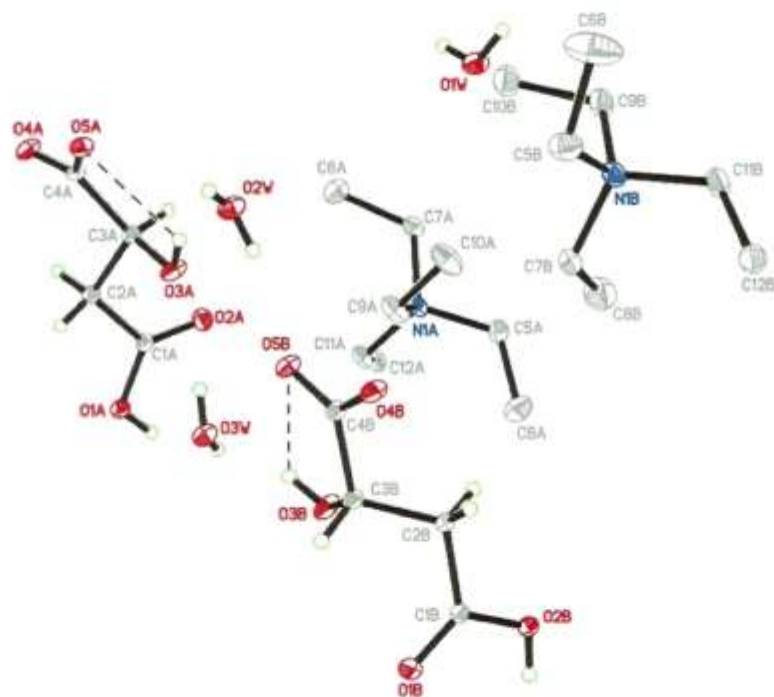
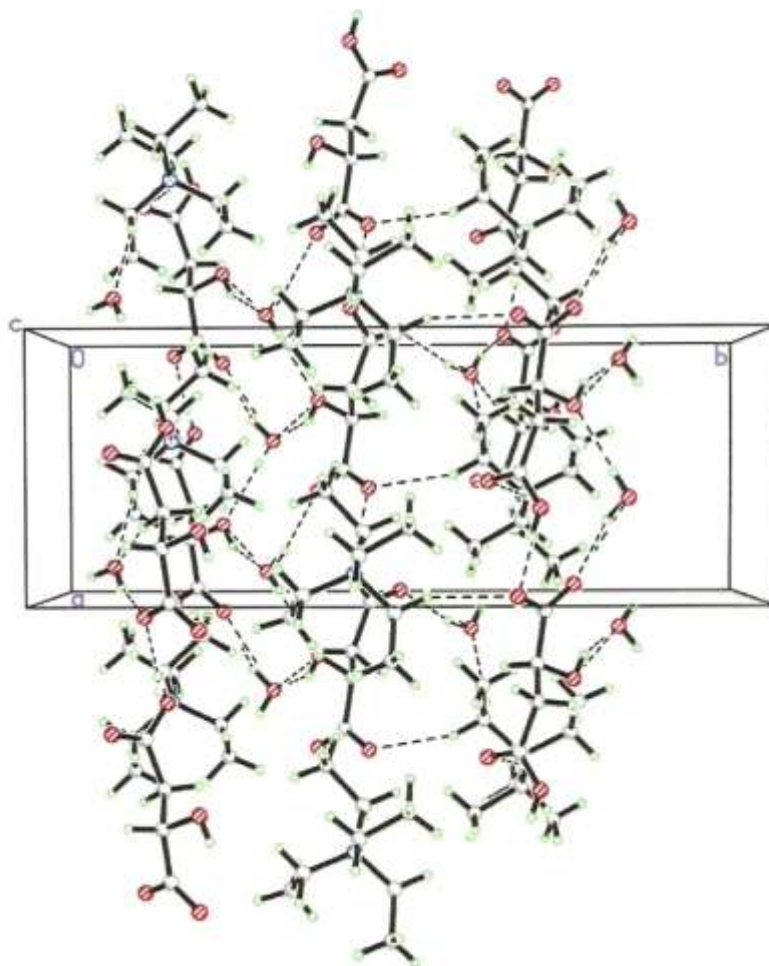


Fig. 2



Acta Crystallographica Section E

Structure Reports

Online

ISSN 1600-5368

Tetraethylammonium L-tartrate dihydrate

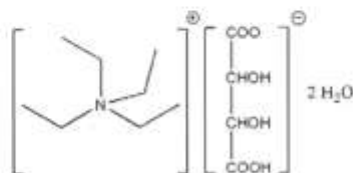
Mohd Basyaruddin Abdul Rahman,^{a,†} Khairulzhar Jumfri,^a Kamaliah Sirat,^a Reza Kia^b and Hoong-Kun Fun^{b*}^aDepartment of Chemistry, Faculty of Science, Universiti Putra Malaysia, 43400 UPM Serdang, Selangor, Malaysia, and ^bX-ray Crystallography Unit, School of Physics, Universiti Sains Malaysia, 11800 USM, Penang, Malaysia

Correspondence e-mail: hkfun@usm.my

Received 3 November 2008; accepted 10 November 2008

Key indicators: single-crystal X-ray study; $T = 100$ K; mean $\sigma(\text{C}-\text{C}) = 0.002$ Å; R factor = 0.037; wR factor = 0.092; data-to-parameter ratio = 16.4.In the crystal structure of the title compound, $\text{C}_8\text{H}_{20}\text{N}^+ \cdot \text{C}_4\text{H}_5\text{O}_6^- \cdot 2\text{H}_2\text{O}$, the ions and water molecules are linked via $\text{O}-\text{H} \cdots \text{O}$ and $\text{C}-\text{H} \cdots \text{O}$ hydrogen bonds, forming a two-dimensional network parallel to (001).

Related literature

For hydrogen-bond motifs, see: Bernstein *et al.* (1995). For related structures, see: Allen *et al.* (2006); Jiang *et al.* (2008); Mei *et al.* (2002).

Experimental

Crystal data

 $\text{C}_8\text{H}_{20}\text{N}^+ \cdot \text{C}_4\text{H}_5\text{O}_6^- \cdot 2\text{H}_2\text{O}$ $M_r = 315.36$ Monoclinic, $P2_1$ $a = 7.4074$ (1) Å $b = 13.8989$ (2) Å $c = 8.0546$ (1) Å $\beta = 106.553$ (1)° $V = 794.89$ (2) Å³ $Z = 2$ Mo K α radiation $\mu = 0.11$ mm⁻¹ $T = 100.0$ (1) K $0.47 \times 0.45 \times 0.17$ mm

Data collection

Bruker SMART APEXII CCD area-detector diffractometer

Absorption correction: multi-scan (SADABS; Bruker, 2005)

 $T_{\text{min}} = 0.861$, $T_{\text{max}} = 0.981$ 10518 measured reflections
3579 independent reflections

Refinement

 $R[F^2 > 2\sigma(F^2)] = 0.037$ $wR(F^2) = 0.092$ $S = 1.05$

3579 reflections

218 parameters

1 restraint

3240 reflections with $I > 2\sigma(I)$ $R_{\text{int}} = 0.031$

H atoms treated by a mixture of independent and constrained refinement

 $\Delta\rho_{\text{max}} = 0.29$ e Å⁻³ $\Delta\rho_{\text{min}} = -0.23$ e Å⁻³Table 1
Hydrogen-bond geometry (Å, °).

$D-H \cdots A$	$D-H$	$H \cdots A$	$D \cdots A$	$D-H \cdots A$
O2—H1O2—O5 ^a	1.00 (2)	1.52 (2)	2.5108 (13)	173 (2)
O3—H1O3—O1W ^b	0.91 (2)	1.85 (2)	2.7191 (14)	162 (2)
O4—H1O4—O2W ^b	0.84 (2)	2.18 (2)	2.9780 (16)	160 (2)
O1W—H1W1—O2 ^c	0.82 (2)	2.56 (2)	3.0668 (14)	172 (2)
O1W—H1W1—O2W ^c	0.82 (2)	2.57 (2)	3.2155 (16)	137 (2)
O1W—H2W1—O6 ^d	0.88 (3)	2.00 (3)	2.8672 (15)	171 (2)
O2W—H2W2—O1 ^d	0.84 (2)	2.40 (2)	3.0082 (14)	129 (2)
C3—H5A—O3 ⁱⁱⁱ	0.97	2.56	3.4344 (15)	151
C8—H8B—O4	0.96	2.38	3.3447 (16)	178
C10—H10B—O3 ⁱⁱⁱ	0.96	2.47	3.4195 (16)	168
C11—H11A—O4	0.97	2.50	3.2693 (15)	136

Symmetry codes: (i) $-x+2, y-\frac{1}{2}, -z$; (ii) $x, y, z-1$; (iii) $-x+1, y-\frac{1}{2}, -z+1$; (iv) $x-1, y, z+1$; (v) $-x+1, y-\frac{1}{2}, -z+2$; (vi) $x, y+1, z+1$; (vii) $-x+1, y-\frac{1}{2}, -z$.

Data collection: APEX2 (Bruker, 2005); cell refinement: SAINT (Bruker, 2005); data reduction: SAINT; program(s) used to solve structure: SHELXTL (Sheldrick, 2008); program(s) used to refine structure: SHELXTL; molecular graphics: SHELXTL; software used to prepare material for publication: SHELXTL and PLATON (Spek, 2003).

MBAR, KJ and KS thank the Ministry of Higher Education of Malaysia for the research grant 05-10-07-377FR (Fundamental Research Grant Scheme-FRGS). HKF and RK thank the Malaysian Government and Universiti Sains Malaysia for the Science Fund (grant No. 305/PFIZIK/613312). RK thanks Universiti Sains Malaysia for the award of a post-doctoral research fellowship.

Supplementary data and figures for this paper are available from the IUCr electronic archives (Reference: C12709).

References

- Allen, C. R., Richard, P. L., van de Ward, A. J., Water, L. G. A., Masters, A. E. & Maschmeyer, T. (2006). *Tetrahedron Lett.* **47**, 7367–7370.
- Bernstein, J., Davis, R. E., Shimoni, L. & Chang, N.-L. (1995). *Angew. Chem. Int. Ed. Engl.* **34**, 1555–1573.
- Bruker (2005). APEX2, SAINT and SADABS. Bruker AXS Inc., Madison, Wisconsin, USA.
- Jiang, Y.-Y., Wang, G.-N., Zhou, Z., Wu, Y.-T., Geng, J. & Zhang, Z.-B. (2008). *Chem. Commun.* **8**, 505–507.
- Mei, S., Jin-Nan, Z. & Qi, L. (2002). *Acta Chim. Sinica*, **60**, 1017–1024.
- Sheldrick, G. M. (2008). *Acta Cryst.* **A64**, 112–122.
- Spek, A. L. (2003). *J. Appl. Cryst.* **36**, 7–13.

† Additional correspondence author; Laboratory of Industrial Biotechnology, Institute of Bioscience, Universiti Putra Malaysia, 43400 UPM Serdang, Selangor, Malaysia; e-mail: basya@science.upm.edu.my



supplementary materials

Acta Cryst. (2008). E64, o2343 [doi:10.1107/S1600536808036969]

Tetraethylammonium L-tartrate dihydrate

M. B. A. Rahman, K. Jumbri, K. Sirat, R. Kia and H.-K. Fun

Comment

The crystal structures of chiral complexes of the plant acid (L-tartaric acid) with tetraethylammonium have been investigated in our laboratory in order to understand the nature of intramolecular and intermolecular interactions. The title compound was obtained by neutralization method at room temperature. Some other related compounds containing the same cation have been previously reported (Jiang *et al.*, 2008; Allen *et al.*, 2006). The crystal structure of bis(tetraethylammonium) tartrate bis(thiourea) dihydrate has also been reported (Mei *et al.*, 2002).

The asymmetric unit of the title compound (Fig. 1) contains a tartarate anion, a tetraethylammonium cation and two water molecules of crystallization. Two intermolecular C—H...O hydrogen bonds involving O4 as a bifurcated acceptor link anion and cation in the asymmetric unit to form a seven-membered ring, with $R^1_2(7)$ ring motif (Bernstein *et al.*, 1995). In the crystal structure, the ionic units and water molecules are linked via O—H...O and C—H...O hydrogen bonds (Table 1) forming a two-dimensional network parallel to the (001) [Fig. 2].

Experimental

L-Tartaric acid (7.504 g, 0.05 mol) was first dissolved in 20 ml of distilled water in a 50 ml beaker. An aqueous solution (20% in water) of tetraethylammonium hydroxide (36.59 ml, 0.05 mol) was added slowly into an aqueous solution of L-tartaric acid and the mixture was stirred with a magnetic stirrer for 2 h at room temperature. A white solid product was obtained after being dried at 343 K under vacuum for 2 d. The product was dissolved in methanol and then covered by aluminium foil to allow slow evaporation at room temperature. Clear crystalline solid was obtained after 3 d. Decomposition temperature range (471.35–472.6 K). Analysis calculated (%): C 51.60, H 9.02, N 5.01%; found: C 50.53, H 9.09, N 3.28%.

Refinement

O-bound H atoms were located in a difference Fourier map and refined freely [O—H = 0.83 (3)–1.01 (3) Å]. C-bound H atoms were positioned geometrically [C—H = 0.93–0.98 Å] and refined as a riding model, with $U_{iso}(H) = 1.2–1.5U_{eq}(C)$. A rotating group model was used for the methyl groups. In the absence of significant anomalous dispersion effects, Friedel pairs were merged before the final refinement.

supplementary materials

Figures

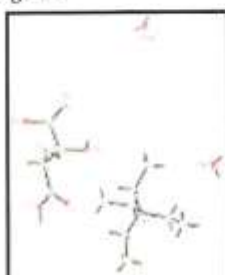


Fig. 1. The molecular structure of the title compound, showing 50% probability displacement ellipsoids and the atomic numbering. Hydrogen bonds are shown as dashed lines.

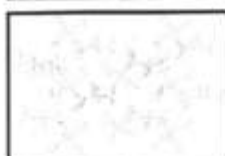


Fig. 2. The crystal packing of the title compound, viewed down the *c* axis. Hydrogen bonds are shown as dashed lines.

Tetraethylammonium L-tartrate dihydrate

Crystal data

$C_{12}H_{20}N^+C_4H_5O_6^- \cdot 2H_2O$

$M_r = 315.36$

Monoclinic, $P2_1$

Hall symbol: $P\ 2yb$

$a = 7.4074$ (1) Å

$b = 13.8989$ (2) Å

$c = 8.0546$ (1) Å

$\beta = 106.553$ (1)°

$V = 794.891$ (19) Å³

$Z = 2$

$F_{000} = 344$

$D_x = 1.318$ Mg m⁻³

Mo $K\alpha$ radiation

$\lambda = 0.71073$ Å

Cell parameters from 4555 reflections

$\theta = 2.6\text{--}33.5^\circ$

$\mu = 0.11$ mm⁻¹

$T = 100.0$ (1) K

Block, colourless

$0.47 \times 0.45 \times 0.17$ mm

Data collection

Bruker SMART APEXII CCD area-detector diffractometer

Radiation source: fine-focus sealed tube

Monochromator: graphite

$T = 100.0$ (1) K

φ and ω scans

Absorption correction: multi-scan (SADABS; Bruker, 2005)

$T_{\min} = 0.861$, $T_{\max} = 0.981$

10518 measured reflections

3579 independent reflections

3240 reflections with $I > 2\sigma(I)$

$R_{\text{int}} = 0.031$

$\theta_{\text{max}} = 35.0^\circ$

$\theta_{\text{min}} = 2.6^\circ$

$h = -9 \rightarrow 11$

$k = -22 \rightarrow 17$

$l = -12 \rightarrow 12$

sup-2

Refinement

Refinement on F^2	Secondary atom site location: difference Fourier map
Least-squares matrix: full	Hydrogen site location: inferred from neighbouring sites
$R[F^2 > 2\sigma(F^2)] = 0.037$	H atoms treated by a mixture of independent and constrained refinement
$wR(F^2) = 0.092$	$w = 1/[\sigma^2(F_o^2) + (0.0494P)^2 + 0.0426P]$
$S = 1.05$	where $P = (F_o^2 + 2F_c^2)/3$
3579 reflections	$(\Delta/\sigma)_{\max} = 0.001$
218 parameters	$\Delta\rho_{\max} = 0.29 \text{ e } \text{\AA}^{-3}$
1 restraint	$\Delta\rho_{\min} = -0.23 \text{ e } \text{\AA}^{-3}$
Primary atom site location: structure-invariant direct methods	Extinction correction: none

Special details

Experimental. The low-temperature data was collected with the Oxford Cryosystem Cobra low-temperature attachment.

Geometry. All e.s.d.'s (except the e.s.d. in the dihedral angle between two l.s. planes) are estimated using the full covariance matrix. The cell e.s.d.'s are taken into account individually in the estimation of e.s.d.'s in distances, angles and torsion angles; correlations between e.s.d.'s in cell parameters are only used when they are defined by crystal symmetry. An approximate (isotropic) treatment of cell e.s.d.'s is used for estimating e.s.d.'s involving l.s. planes.

Refinement. Refinement of F^2 against ALL reflections. The weighted R -factor wR and goodness of fit S are based on F^2 , conventional R -factors R are based on F , with F set to zero for negative F^2 . The threshold expression of $F^2 > \sigma(F^2)$ is used only for calculating R -factors(gt) etc. and is not relevant to the choice of reflections for refinement. R -factors based on F^2 are statistically about twice as large as those based on F , and R -factors based on ALL data will be even larger.

Fractional atomic coordinates and isotropic or equivalent isotropic displacement parameters (\AA^2)

	<i>x</i>	<i>y</i>	<i>z</i>	$U_{\text{iso}}^*/U_{\text{eq}}$
O1	0.71436 (14)	0.19227 (7)	-0.03566 (13)	0.01818 (18)
O2	1.02013 (14)	0.23261 (7)	0.04449 (14)	0.0201 (2)
O3	0.61932 (14)	0.36818 (7)	-0.18764 (12)	0.01677 (18)
O4	0.68458 (16)	0.39108 (7)	0.17930 (13)	0.0190 (2)
C1	0.83853 (18)	0.25107 (9)	-0.01824 (15)	0.0138 (2)
C2	0.79871 (18)	0.35668 (9)	-0.06869 (15)	0.0134 (2)
H2A	0.8929	0.3785	-0.1246	0.016*
C3	0.81928 (18)	0.41837 (9)	0.09447 (16)	0.0144 (2)
H3A	0.9446	0.4064	0.1739	0.017*
C4	0.80699 (19)	0.52553 (9)	0.04614 (16)	0.0156 (2)
N1	0.61784 (16)	0.13577 (8)	0.44527 (13)	0.01415 (19)
C5	0.68066 (19)	0.05680 (10)	0.34333 (17)	0.0169 (2)
H5A	0.5698	0.0232	0.2745	0.020*
H5B	0.7406	0.0866	0.2638	0.020*
C6	0.8153 (2)	-0.01643 (11)	0.4516 (2)	0.0249 (3)



supplementary materials

H6A	0.8474	-0.0632	0.3769	0.037*
H6B	0.7563	-0.0481	0.5285	0.037*
H6C	0.9275	0.0156	0.5181	0.037*
C7	0.78506 (19)	0.18803 (10)	0.56438 (16)	0.0174 (2)
H7A	0.7381	0.2382	0.6249	0.021*
H7B	0.8550	0.1428	0.6507	0.021*
C8	0.9195 (2)	0.23319 (12)	0.47596 (19)	0.0227 (3)
H8A	1.0203	0.2644	0.5609	0.034*
H8B	0.8532	0.2797	0.3926	0.034*
H8C	0.9703	0.1841	0.4183	0.034*
C9	0.50734 (19)	0.09482 (11)	0.56176 (16)	0.0186 (2)
H9A	0.5880	0.0505	0.6428	0.022*
H9B	0.4763	0.1471	0.6286	0.022*
C10	0.3270 (2)	0.04279 (11)	0.46895 (19)	0.0218 (3)
H10A	0.2674	0.0194	0.5523	0.033*
H10B	0.3558	-0.0104	0.4047	0.033*
H10C	0.2437	0.0864	0.3910	0.033*
C11	0.49727 (18)	0.20335 (10)	0.31067 (15)	0.0157 (2)
H11A	0.5737	0.2288	0.2411	0.019*
H11B	0.3959	0.1665	0.2344	0.019*
C12	0.4121 (2)	0.28706 (11)	0.38285 (18)	0.0205 (3)
H12A	0.3389	0.3259	0.2891	0.031*
H12B	0.5110	0.3253	0.4562	0.031*
H12C	0.3325	0.2630	0.4489	0.031*
O1W	0.30848 (16)	0.27561 (10)	0.84652 (15)	0.0243 (2)
O2W	0.69834 (18)	0.97603 (9)	0.95574 (16)	0.0252 (2)
O5	0.93673 (14)	0.55475 (7)	-0.01728 (15)	0.0218 (2)
O6	0.67739 (15)	0.57466 (8)	0.07043 (14)	0.0226 (2)
H1O2	1.043 (4)	0.161 (2)	0.045 (3)	0.045 (7)*
H1O3	0.534 (3)	0.3304 (19)	-0.159 (3)	0.036 (6)*
H1O4	0.590 (3)	0.422 (2)	0.122 (3)	0.033 (6)*
H1W1	0.260 (4)	0.306 (2)	0.911 (4)	0.055 (8)*
H2W1	0.316 (4)	0.216 (2)	0.884 (3)	0.043 (7)*
H1W2	0.818 (4)	0.9985 (19)	0.980 (3)	0.037 (6)*
H2W2	0.630 (4)	1.025 (2)	0.962 (3)	0.039 (6)*

Atomic displacement parameters (\AA^2)

	U^{11}	U^{22}	U^{33}	U^{12}	U^{13}	U^{23}
O1	0.0174 (4)	0.0115 (4)	0.0261 (4)	-0.0015 (3)	0.0070 (4)	0.0010 (4)
O2	0.0150 (4)	0.0121 (4)	0.0307 (5)	0.0009 (4)	0.0027 (4)	-0.0024 (4)
O3	0.0174 (4)	0.0135 (4)	0.0167 (4)	-0.0013 (3)	0.0006 (3)	0.0020 (3)
O4	0.0242 (5)	0.0155 (4)	0.0191 (4)	0.0013 (4)	0.0091 (4)	0.0022 (3)
C1	0.0164 (5)	0.0107 (5)	0.0146 (4)	0.0011 (4)	0.0050 (4)	-0.0005 (4)
C2	0.0151 (5)	0.0095 (5)	0.0156 (4)	-0.0007 (4)	0.0040 (4)	0.0005 (4)
C3	0.0161 (5)	0.0096 (5)	0.0162 (5)	0.0001 (4)	0.0024 (4)	-0.0005 (4)
C4	0.0164 (5)	0.0104 (5)	0.0180 (5)	-0.0001 (4)	0.0013 (4)	-0.0010 (4)
N1	0.0153 (5)	0.0138 (5)	0.0131 (4)	-0.0007 (4)	0.0037 (3)	0.0003 (3)

sup-4

supplementary materials

C5	0.0185 (5)	0.0134 (5)	0.0191 (5)	-0.0001 (5)	0.0057 (4)	-0.0026 (4)
C6	0.0232 (7)	0.0160 (6)	0.0349 (7)	0.0027 (5)	0.0071 (6)	0.0052 (5)
C7	0.0168 (5)	0.0175 (6)	0.0156 (5)	-0.0016 (5)	0.0007 (4)	-0.0013 (4)
C8	0.0191 (6)	0.0217 (7)	0.0256 (6)	-0.0052 (5)	0.0036 (5)	0.0012 (5)
C9	0.0200 (6)	0.0209 (6)	0.0162 (5)	-0.0018 (5)	0.0073 (4)	0.0025 (4)
C10	0.0196 (6)	0.0221 (7)	0.0254 (6)	-0.0029 (5)	0.0089 (5)	0.0024 (5)
C11	0.0171 (5)	0.0147 (5)	0.0140 (4)	0.0012 (4)	0.0024 (4)	0.0012 (4)
C12	0.0213 (6)	0.0161 (6)	0.0235 (6)	0.0025 (5)	0.0055 (5)	-0.0020 (5)
O1W	0.0200 (5)	0.0272 (6)	0.0262 (5)	-0.0003 (4)	0.0076 (4)	0.0019 (4)
O2W	0.0250 (6)	0.0191 (5)	0.0321 (5)	-0.0048 (4)	0.0094 (4)	-0.0044 (4)
O5	0.0187 (4)	0.0118 (4)	0.0361 (5)	-0.0022 (4)	0.0096 (4)	0.0006 (4)
O6	0.0245 (5)	0.0164 (5)	0.0286 (5)	0.0071 (4)	0.0102 (4)	0.0021 (4)

Geometric parameters (Å, °)

O1—C1	1.2084 (16)	C6—H6C	0.96
O2—C1	1.3203 (15)	C7—C8	1.516 (2)
O2—H1O2	1.01 (3)	C7—H7A	0.97
O3—C2	1.4085 (16)	C7—H7B	0.97
O3—H1O3	0.90 (3)	C8—H8A	0.96
O4—C3	1.4124 (17)	C8—H8B	0.96
O4—H1O4	0.84 (3)	C8—H8C	0.96
C1—C2	1.5292 (17)	C9—C10	1.516 (2)
C2—C3	1.5400 (17)	C9—H9A	0.97
C2—H2A	0.98	C9—H9B	0.97
C3—C4	1.5356 (18)	C10—H10A	0.96
C3—H3A	0.98	C10—H10B	0.96
C4—O6	1.2382 (17)	C10—H10C	0.96
C4—O5	1.2763 (17)	C11—C12	1.516 (2)
N1—C11	1.5178 (16)	C11—H11A	0.97
N1—C7	1.5183 (17)	C11—H11B	0.97
N1—C9	1.5205 (16)	C12—H12A	0.96
N1—C5	1.5209 (17)	C12—H12B	0.96
C5—C6	1.515 (2)	C12—H12C	0.96
C5—H5A	0.97	O1W—H1W1	0.83 (3)
C5—H5B	0.97	O1W—H2W1	0.88 (3)
C6—H6A	0.96	O2W—H1W2	0.91 (3)
C6—H6B	0.96	O2W—H2W2	0.85 (3)
C1—O2—H1O2	110.3 (15)	C8—C7—N1	115.36 (10)
C2—O3—H1O3	110.7 (16)	C8—C7—H7A	108.4
C3—O4—H1O4	101.3 (17)	N1—C7—H7A	108.4
O1—C1—O2	124.88 (12)	C8—C7—H7B	108.4
O1—C1—C2	122.58 (11)	N1—C7—H7B	108.4
O2—C1—C2	112.74 (11)	H7A—C7—H7B	107.5
O3—C2—C1	111.28 (10)	C7—C8—H8A	109.5
O3—C2—C3	111.23 (10)	C7—C8—H8B	109.5
C1—C2—C3	110.06 (10)	H8A—C8—H8B	109.5
O3—C2—H2A	108.0	C7—C8—H8C	109.5
C1—C2—H2A	108.0	H8A—C8—H8C	109.5

sup-5



supplementary materials

C3—C2—H2A	108.0	H8B—C8—H8C	109.5
O4—C3—C4	112.59 (11)	C10—C9—N1	115.34 (10)
O4—C3—C2	110.58 (10)	C10—C9—H9A	108.4
C4—C3—C2	109.84 (10)	N1—C9—H9A	108.4
O4—C3—H3A	107.9	C10—C9—H9B	108.4
C4—C3—H3A	107.9	N1—C9—H9B	108.4
C2—C3—H3A	107.9	H9A—C9—H9B	107.5
O6—C4—O5	126.43 (13)	C9—C10—H10A	109.5
O6—C4—C3	119.17 (12)	C9—C10—H10B	109.5
O5—C4—C3	114.40 (11)	H10A—C10—H10B	109.5
C11—N1—C7	111.31 (10)	C9—C10—H10C	109.5
C11—N1—C9	111.21 (10)	H10A—C10—H10C	109.5
C7—N1—C9	105.96 (9)	H10B—C10—H10C	109.5
C11—N1—C5	105.62 (9)	C12—C11—N1	115.18 (10)
C7—N1—C5	111.49 (10)	C12—C11—H11A	108.5
C9—N1—C5	111.36 (10)	N1—C11—H11A	108.5
C6—C5—N1	115.24 (11)	C12—C11—H11B	108.5
C6—C5—H5A	108.5	N1—C11—H11B	108.5
N1—C5—H5A	108.5	H11A—C11—H11B	107.5
C6—C5—H5B	108.5	C11—C12—H12A	109.5
N1—C5—H5B	108.5	C11—C12—H12B	109.5
H5A—C5—H5B	107.5	H12A—C12—H12B	109.5
C5—C6—H6A	109.5	C11—C12—H12C	109.5
C5—C6—H6B	109.5	H12A—C12—H12C	109.5
H6A—C6—H6B	109.5	H12B—C12—H12C	109.5
C5—C6—H6C	109.5	H1W1—O1W—H2W1	106 (3)
H6A—C6—H6C	109.5	H1W2—O2W—H2W2	106 (2)
H6B—C6—H6C	109.5		
O1—C1—C2—O3	-20.73 (16)	C11—N1—C5—C6	175.99 (11)
O2—C1—C2—O3	159.12 (10)	C7—N1—C5—C6	54.95 (15)
O1—C1—C2—C3	103.04 (13)	C9—N1—C5—C6	-63.16 (15)
O2—C1—C2—C3	-77.11 (13)	C11—N1—C7—C8	-60.40 (15)
O3—C2—C3—O4	60.68 (13)	C9—N1—C7—C8	178.57 (12)
C1—C2—C3—O4	-63.12 (13)	C5—N1—C7—C8	57.25 (15)
O3—C2—C3—C4	-64.19 (13)	C11—N1—C9—C10	56.22 (15)
C1—C2—C3—C4	172.01 (10)	C7—N1—C9—C10	177.31 (12)
O4—C3—C4—O6	-5.84 (16)	C5—N1—C9—C10	-61.29 (15)
C2—C3—C4—O6	117.86 (13)	C7—N1—C11—C12	-60.88 (14)
O4—C3—C4—O5	174.27 (11)	C9—N1—C11—C12	57.02 (14)
C2—C3—C4—O5	-62.03 (14)	C5—N1—C11—C12	177.97 (12)

Hydrogen-bond geometry (\AA , $^\circ$)

<i>D</i> — <i>H</i> ··· <i>A</i>	<i>D</i> — <i>H</i>	<i>H</i> ··· <i>A</i>	<i>D</i> ··· <i>A</i>	<i>D</i> — <i>H</i> ··· <i>A</i>
O2—H1O2···O5 ⁱ	1.00 (2)	1.52 (2)	2.5108 (13)	173 (2)
O3—H1O3···O1W ⁱⁱ	0.91 (2)	1.85 (2)	2.7191 (14)	162 (2)
O4—H1O4···O2W ⁱⁱⁱ	0.84 (2)	2.18 (2)	2.9780 (16)	160 (2)
O1W—H1W1···O2 ^{iv}	0.82 (2)	2.56 (2)	3.0668 (14)	122 (2)

sup-6

supplementary materials

O1W—H1W1—O2W ^v	0.82 (2)	2.57 (2)	3.2155 (16)	137 (2)
O1W—H2W1—O6 ⁱⁱⁱ	0.88 (3)	2.00 (3)	2.8672 (15)	171 (2)
O2W—H2W2—O1 ^{vi}	0.84 (2)	2.40 (2)	3.0082 (14)	129 (2)
C5—H15A—O3 ^{vii}	0.97	2.56	3.4344 (15)	151
C8—H8B—O4	0.96	2.38	3.3447 (16)	178
C10—H10B—O3 ⁱⁱⁱ	0.96	2.47	3.4195 (16)	168
C11—H11A—O4	0.97	2.50	3.2693 (15)	136

Symmetry codes: (i) $-x+2, y-1/2, -z$; (ii) $x, y, z-1$; (iii) $-x+1, y-1/2, -z+1$; (iv) $x-1, y, z+1$; (v) $-x+1, y-1/2, -z+2$; (vi) $x, y+1, z+1$; (vii) $-x+1, y-1/2, -z$.

sup-7



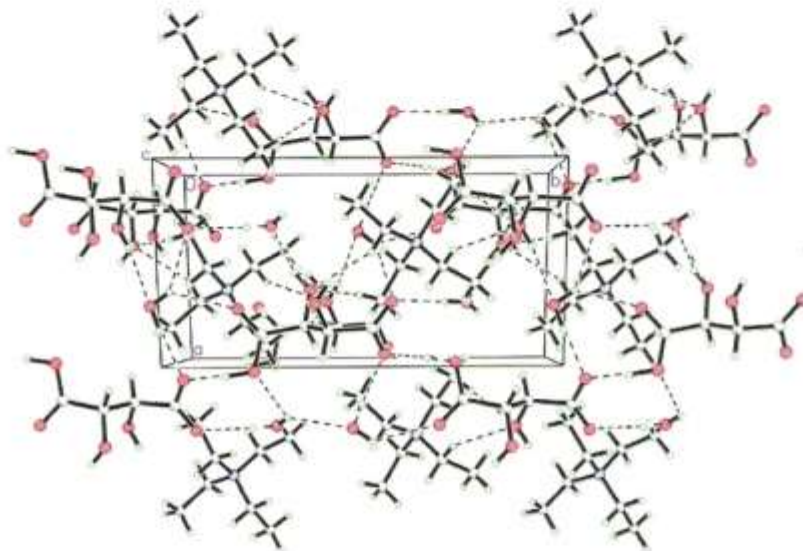
supplementary materials

Fig. 1



sup-8

Fig. 2



BIODATA OF STUDENT



Khairulazhar Jumbri was born in Kuala Kurau, Perak on 28th May 1984. He received his primary education at Sekolah Kebangsaan Kuala Kurau and then continued his secondary education at Sekolah Menengah Kebangsaan Alang Iskandar (SMKAI), Bagan Serai, Perak. He completed his Matriculation of Science under Ministry of Education Malaysia (KPM) at Trolak Country Resort in 2003. Then he was offered to pursue his studies at UPM and three years later in 2006 he obtained Bachelor of Science (Honours) degree in Petroleum Chemistry. Upon his graduation, he was offered as temporary teacher at his old school, SMKAI. During the period as temporary teacher, he was taught engineering drawing and mathematical subject. Starting of December 2006, he enrolled his Master of Science programme at Department of Chemistry, Faculty of Science, UPM under supervision Prof. Dr. Mohd. Basyaruddin Abdul Rahman. He was offered National Science Fellowship scholarship (NSF) from Ministry of Science, Technology and Innovation (MOSTI) Malaysia during his study.